Evaluation of Hand Lay-Up and Resin Transfer Molding in Composite Wind Turbine Blade Manufacturing

Douglas S. Cairns and Jon D. Skramstad

Sandia National Laboratories

Evaluation Of Hand Lay-Up And Resin Transfer Molding In Composite Wind Turbine Blade Manufacturing

Douglas S. Cairns and Jon D. Skramstad
Department of Mechanical and Industrial Engineering
Montana State University-Composites Technology Team
Bozeman, MT 59717

Abstract

The majority of the wind turbine blade industry currently uses low cost hand lay-up manufacturing techniques to process composite blades. While there are benefits to the hand lay-up process, drawbacks inherent to this process along with advantages of other techniques suggest that better manufacturing alternatives may be available.

Resin Transfer Molding (RTM) was identified as a processing alternative and shows promise in addressing the shortcomings of hand lay-up. This report details a comparison of the RTM process to hand lay-up of composite wind turbine blade structures.

Several lay-up schedules and critical turbine blade structures were chosen for comparison of their properties resulting from RTM and hand lay-up processing. The geometries investigated were flat plate, thin and thick flanged T-stiffener, I-beam, and root connection joint.

It was found that the manufacturing process played an important role in laminate thickness, fiber volume, and weight for the geometries investigated. RTM was found to reduce thickness and weight and increase fiber volumes for all substructures. RTM resulted in tighter material transition radii and eliminated the need for most secondary bonding operations. These results would significantly reduce the weight of wind turbine blades. Hand lay-up was consistently slower in fabrication times for the structures investigated. A comparison of mechanical properties showed no significant differences after employing fiber volume normalization techniques to account for geometry differences resulting from varying fiber volumes. The current root specimen design does not show significant mechanical property differences according to process and exceeds all static and fatigue requirements.

This page intentionally left blank.

TABLE OF CONTENTS

TABLE OF CONTENTS – <u>Continued</u>

LIST OF TABLES

LIST OF FIGURES

CHAPTER 1

INTRODUCTION

Low cost composites are gaining wider acceptance as a structural material. One form, commonly referred to as "fiberglass", consists of glass fabric reinforcement and a thermosetting or thermoplastic polymer matrix. The aerospace and automotive industries have proven that composites have superior strength-to-weight ratios and excellent fatigue resistance when compared to many traditional materials [1]. Another advantage of composites is their ability to be tailored for different properties using various reinforcement configurations, matrix materials, and manufacturing processes. In addition, fiberglass is relatively inexpensive when compared with other composites, such as the carbon-fiber/epoxy composites used in aerospace and sporting goods applications [2]. Fiberglass composites, which were once reserved for boat hulls, surfboards and other stiffness and cost dominated applications, are now being driven towards more complicated geometries and critical structures.

Hand Lay-up in Turbine Blade Fabrication

One industry advancing the structural implementation of fiberglass composites is the wind turbine blade industry. The standard method of blade manufacturing employs inexpensive E-glass fabric reinforcement and polyester resin to fabricate complex

composite wind turbine blades for electrical power generation. A typical composite wind turbine blade and its components are illustrated in Figure 1. This blade is the current, MSU blade design for the Atlantic Orient Company AOC 15/50 turbine [3]. From this figure it can be observed that the composite blade is composed of skin surface, spar cap, spar web, spar flange and root components. Each substructure provides a well-defined function to the wind turbine blade structure. The leading and trailing edge skin surfaces give the turbine blade its airfoil shape. The spar structures support the large wind induced bending moments on the blade. And the root section transmits the structural loads of the turbine blade to the rotating turbine hub. These turbine blade components vary in thickness and lay-up over the blade's length, as allowances must be made for the blade's tapered, twisted geometry. In Figure 1, Table (b) the lay-ups and thicknesses for the current design can be found for the different blade components at a variety of blade locations.

The majority of the turbine blade industry uses the low budget, hand lay-up manufacturing technique to combine resin and fabric components. In the hand lay-up process, fiber reinforcement is manually inserted into a single-sided mold, where resin is then forced through the thickness of the individual fiber mats using hand rollers. After the fabric is saturated, excess resin is removed with squeegees. Variations to this method include the use of "pre-preg" material, which is purchased with resin already saturated in the fiber mat. Other methods include individually wetting out each layer by hand, or using machines to wet each layer before placing them in the mold. The part is allowed to cure and is finally extracted from the mold. A primary advantage to the hand lay-up technique

2
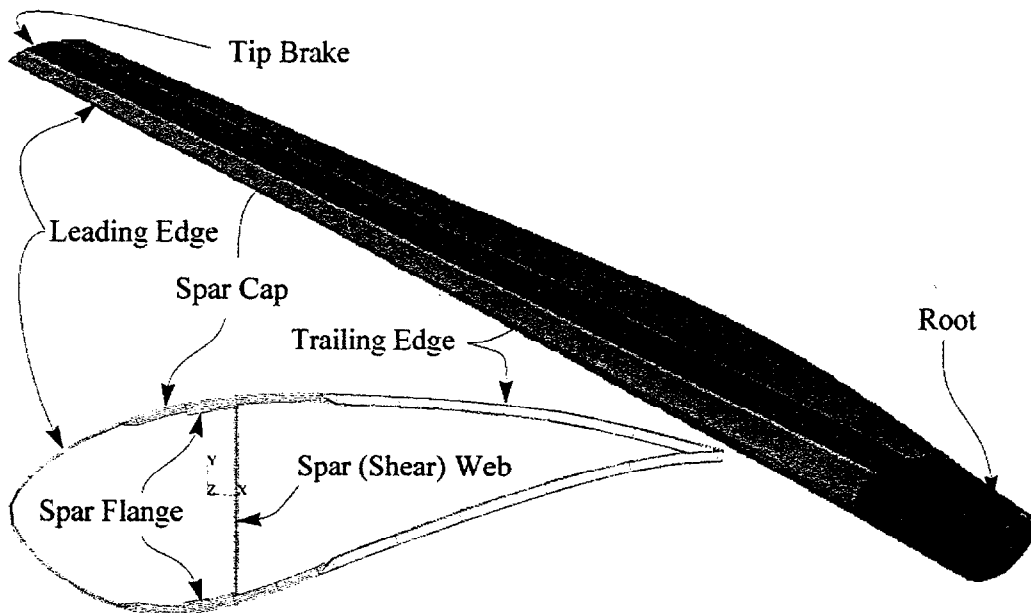
(a) graphic display of components in layup schedule

Component	Z Location (inches)	Layup Schedule	Thickness (inches)
Root	11 to 30.5	$[\pm 45/0_6/\pm 45/0_6/+45]_s$	0.620
	30.5 to 35	$[\pm 45/0_5/\pm 45/0_5/+45]_s$	0.530
	35 to 43	$[\pm 45/0_4/\pm 45/0_4/+45]_s$	0.440
Spar Cap	43 to 91	$[\pm 45/0_4/\pm 45/0_4/+45]_s$	0.440
	91 to 155	$[\pm 45/0_3/\pm 45/0_3/+45]_s$	0.350
	155 to 219	$[\pm 45/0_2/\pm 45/0_2/+45]_s$	0.260
	219 to 295	$[\pm 45/0/\pm 45/0/+45]_s$	0.170
Leading Edge	43 to 91	$[\pm 45/0_2/\pm 45]_s$	0.154
	91 to 295	$[\pm 45/0/\pm 45]_s$	0.109
Trailing Edge	43 to 250	$[\pm 45/0/balsa/0/\pm 45]$	0.452
	250 to 295	$[\pm 45/0]_s$	0.077
Spar (Shear) web	43 to 278	$[\pm 45/0_2/\pm 45]_s$	0.158
Spar Flange	43 to 295	$[\pm 45/0_2/\pm 45]_s$	0.154

(b) layup schedule

Figure 1. MSU composite blade design for AOC 15/50 turbine [3].

3

is its ability to fabricate very large, complex parts with a quick initial start-up. Additional benefits to the process are simple equipment and tooling that are relatively less expensive than required by other manufacturing options. Yet, the drawbacks of hand lay-up suggest that other methods of composites manufacturing may be more desirable in industrial-scale, wind turbine blade fabrication.

Drawbacks Inherent to Hand Lay-up

Hand lay-up's first disadvantage is that the process is labor intensive, which can result in high cycle times and a low volume output of parts. The nature of the hand lay-up process may also result in parts with inconsistent fiber orientations. In other words, the more the reinforcement is handled, the more likely strands will separate or distort from the preform and compromise the mechanical strength of the composite. For the wind turbine blade example, the open molding feature of the hand lay-up process requires one skin to be molded at a time and in the final step, skins, spars, and core are bonded together. Such a sequential process increases the amount of labor required, increases variability between blades, and slows the rate of production. In addition, the method generates a textured finish on the inner surface of the blade skin, which provides a poor condition for bonding between parts. Tight dimensional accuracy and smooth surfaces at the bonding interface are more desirable.

Another drawback inherent to hand lay-up is that it yields laminates of variable thickness. This raises concerns with bond line thicknesses, uniformity of composites, and blade weights. To allow for the larger deviations in thickness found in hand lay-up geometries, looser tolerances must be allowed at the bond lines where the blade

4

substructures are joined together. This allowance substitutes bonding materials for structural composite and increases blade weight. Variations in laminate thickness also present a problem in hand lay-up because large dimensional tolerances often yield composites of non-uniform fiber volume and mechanical strength. Maintaining fiber volumes higher than those found for hand lay-up significantly decreases blade mass. For example, a mass savings of approximately 6.3 kg or 10% would result in the current composite blade design for the AOC 15/50 turbine, if a single skin laminate thickness could be compressed by one millimeter over the length of the blade.

Lastly, this technique raises environmental and safety concerns with the amount of hazardous volatiles the open mold process releases.

Hand lay-up is a proven process for constructing composite turbine blades and other structures, but the method's limiting volume output and part inconsistencies motivates research into other manufacturing techniques.

The Potential of Resin Transfer Molding

There exists a wide variety of alternative techniques available for the manufacturing of composites. Compression molding, prepreging, vacuum molding, pultruding, filament winding, and resin transfer molding are just a few of the current options [4]. Candidates of interest to utility-grade wind turbine blade fabrication need to improve fiber volume, lower the blade weight, increase structural reliability, and decrease the overall cost of blade fabrication. Through previous work conducted by the Composites Technology Team at Montana State University and Sandia National Laboratories, resin transfer molding or RTM was identified as a viable process in blade

fabrication [5]. Resin transfer molding is a relatively new process that has received a significant amount of attention due to its potential in low budget applications. This process begins with the placement of the reinforcement mat, or preform, into a two-sided closed mold. The mold is then closed, and resin is forced through the length and width of the mold by applying pressure, drawing a vacuum, or a combination of the two. After the resin is applied, the part is cured and finally removed from the mold. Resin transfer molding is a very versatile process and can be performed with or without the influences of post-molding heat and pressure [6]. The method has had limited exposure to manufacturing turbine blades, but RTM has many advantages over the hand lay-up technique, even after consideration of RTM's limiting factors.

Concerns Associated with RTM

RTM's first limitation is initial cost. In comparison to hand lay-up, the equipment necessary for RTM is significantly more expensive. In hand lay-up, the minimal equipment required is a one-sided mold, resin applying rollers and resin removing squeegees, while RTM requires a relatively strong two-part closed mold, along with resin injection equipment. Another challenge facing RTM is that resin flow can be difficult to predict due to the nature of the closed mold process. Resin flow around corners and through joints is not easily predicted because locally high fiber volumes in these regions can drastically change mold fill behavior. Currently, RTM operators cannot accurately anticipate these effects, nor can they visually verify whether the part has reached full saturation before the injection process is shut down. If the part is not entirely "wetted out", dry spots or voids are introduced, which may require rework or part rejection.

Flaws in resin transfer moldings can also be introduced if the operator uses resin injection pressures or flow rates that are too high. In this instance, fibers can be distorted or possibly "washed out" resulting in a part of questionable mechanical strength.

The Advantages of RTM

Despite its limitations, RTM does have many advantages over other methods of turbine blade construction. When compared with hand lay-up methods, RTM has much lower cycle times and higher volume outputs. Resin transfer molding also produces parts with a higher degree of repeatability. The structural properties of a hand laid-up blade depend upon the pressure and speed at which the operator physically applies the resin, while in RTM, speeds and pressures remain constant and blades are removed from molds practically identical to one another [7]. RTM is unique in its potential for molding an entire blade in one step while producing smooth-surfaced parts on both inner and outer mold surfaces. Both methods generate an acceptable airfoil surface but only RTM'd skins have a good surface finish on the interior, which is ideal for secondary bonding. Lastly, RTM's closed mold feature is a more environmentally friendly process because fewer volatiles are released.

Research Evaluation Objectives

Worldwide, wind turbine designs have improved substantially due to the incorporation of composite technology [5]. As composite usage becomes more commonplace, manufacturing efforts will continue to focus on minimizing the time required to fabricate blades while increasing dimensional accuracy, repeatability, fiber

content, and affordability. These efforts include advancing current techniques, while exploring other available manufacturing options. The current evaluation between hand lay-up and RTM takes a twofold approach in answering how each process addresses potential improvements in blade fabrication.

First, the physical variables of composite samples were investigated and compared. Laminate thickness, fiber volume, cycle time, and porosity measurement, along with their variability, were measured for five geometries representative of turbine blade structures. These properties are important in a manufacturing comparison because they define the strength to weight ratios, manufacturing speeds, repeatability, and defect levels of composite materials. The geometries investigated were: flat plates (skin sections), thin flanged T-stiffeners with skin intersections, thick flanged T-stiffeners, I-beam load carriers, and sample root connection joints (Fig. 2). The RTM tools used in fabricating these five substructures were compared to determine their benefits and drawbacks in dimensional accuracy, cure time, and ease of manufacture.

a) Thin Flanged T   b) Thick Flanged T   c) I-beam   d) Root
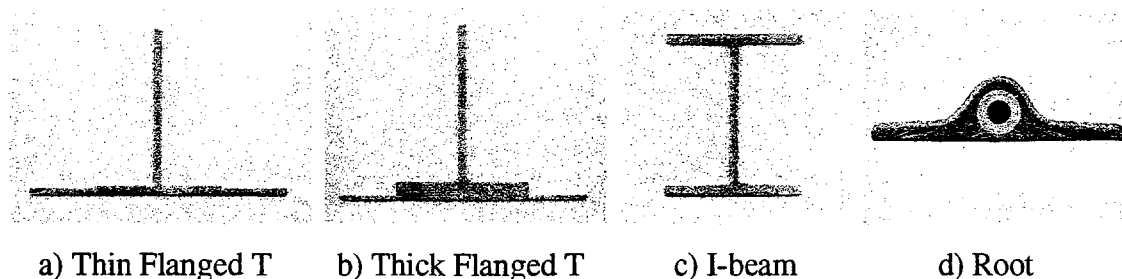
Figure 2. Composite T-stiffener, I-beam, and root critical structures.

Secondly, the mechanical performances of the five composite substructures were compared for each of the two methods of manufacturing. This component of the manufacturing evaluation helped to determine any differences between the strength to weight ratios and fatigue cycle lifetimes of hand laid-up and RTM'd structures. Flat plates were tested under five common loadings: transverse tension, compression, three-point bending, tension, and fatigue. Thick and thin flanged T-stiffeners were tested in a stiffener pull-off configuration, while I-beams were loaded under four-point bending in fatigue. The final mechanical tests involved the root specimen in tensile and fatigue loading to gauge differences in the structural performances of hand lay-up and RTM in a thick, complicated geometry.

CHAPTER 2

BACKGROUND

Resin Transfer Molding Technology

Resin transfer molding applications and the technologies being developed to enhance the process are increasing. As new industries adopt RTM, unique innovations are introduced that drive manufacturing methods toward stronger, more economical parts. These interests in RTM have required a closer look at the mechanics of the molding process and molded parts. This has motivated studies on RTM processing [8-16], methods of defect introduction [17-26], and resultant structural performance [27-30] in an attempt to enhance the understanding of RTM science. RTM models, porosity observations at different flow rates, strengths of various fabric reinforcements, temperature effects on cycle times, convergent flow fronts, and the impact of porosity on mechanical properties are topics that have been investigated and will be mentioned in prelude to the experimental investigations performed in this work.

Flow Modeling

An area that has been the focus of significant RTM research is the modeling of resin flow for the resin transfer molding process. Modeling is a critical topic in the advancement of RTM because it addresses a primary drawback – the insufficient

knowledge of closed mold resin flow. In parts with simple geometries and relatively short dimensions, proper mold fill is easily attained because resin flow paths are short and unimpeded by three-dimensional complexities. If the part is not wetted out, it is discarded and changes are made to the injection geometry until all dry spots are eliminated. Applying this trial and error methodology to the RTMing of a utility grade turbine blade, from 8 up to 25 meters in length, is inefficient and expensive. However, through the successful modeling of RTM flow, it is possible to predict the flow properties in a complex structure and eliminate the trial and error approach. Currently, there exists a wide variety of commercial and non-commercial modeling software for RTM flow [8, 9, 31, 32].

MSU RTM Flow Model. Under the MSU RTM studies, a basic model has been developed that is based on Darcy's law in fibrous bundle regions and channel flow equations between bundles [8]. The model incorporates a micro- and macro-approach to account for local architecture and structural geometry. The micro model is important to capture local nonhomogeneities as shown in Figure 3. In Figure 3, the edges of the fiber bundle tows with a resin-rich channel between them can be clearly seen. The analytical model predicts the wetting out of this cross-section using Equations 1 and 2:
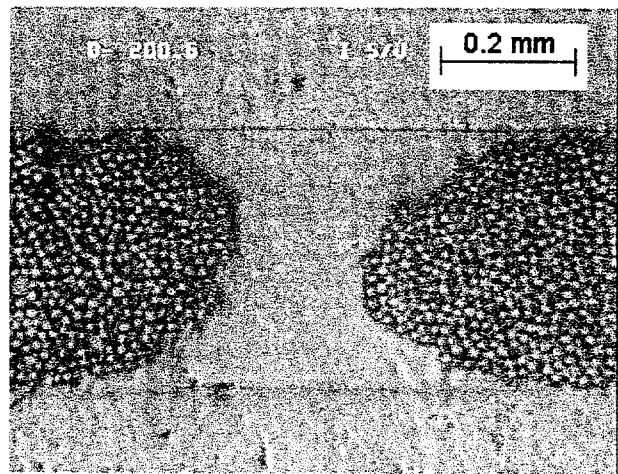
Figure 3. Composite cross-section.

Micro-model (Darcy's Law):
$$V_z = -\frac{k_z}{\mu} \cdot \frac{\Delta P}{\Delta z}$$
(1)

Where: V_z = velocity (in z direction) k_z = permeability (in z direction)

μ = viscosity of resin $\Delta P/\Delta z$ = local pressure gradient

Macro-model (Navier-Stokes):
$$\rho\left(\frac{\partial V_z}{\partial t}\right) = -\frac{\partial p}{\partial z} + \mu\left(\frac{\partial^2 V_z}{\partial x^2} + \frac{\partial^2 V_z}{\partial y^2}\right)$$
(2)

Where: ρ = density of resin V_z = velocity (in z direction)

t = time   p = pressure applied to resin

z = location along specimen length μ = viscosity of resin

x = location through width   y = location in thickness

Darcy's Law (Eq. 1) evaluates the flow through fibrous bundles while the Navier-Stokes equation (Eq. 2) acts as a field solver that incorporates flow through channels.

Results of model predictions for resin flow through unidirectional, stitched preforms, and multi-layer configurations (Fig. 4) have agreed well with experimental results [8]. These results have illustrated that incorporating channel flow is important for properly modeling the RTM process. Due to the large difference between permeabilities of the channels and bundle tows, the channels will fill much more rapidly than the fiber bundles (channels are the gaps illustrated in Figure 4). Pressure profiles, resin velocities,

12
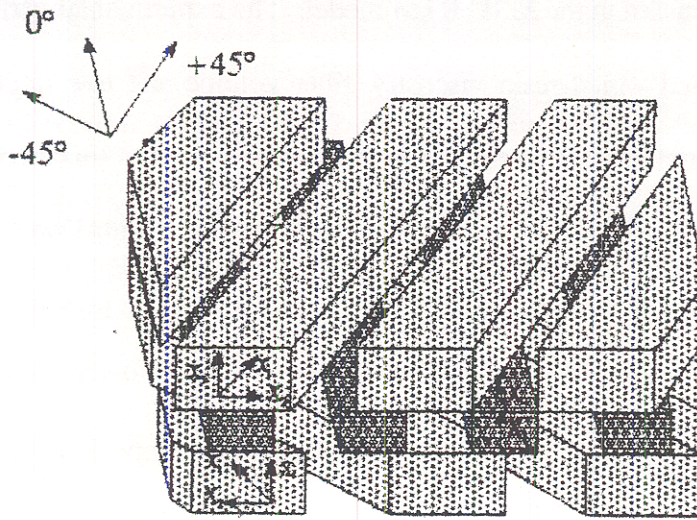
Figure 4. MSU RTM flow model with global and local coordinate orientations [8]

and resin flow fronts are predicted accurately and these topics continue to be explored at MSU. It should also be noted here that the model results were compared to experimental stitched preform injections. It was found that although the shapes for resin flow are similar between experimental and analytical results, the stitching affects the permeability such that unidirectional ply data does not accurately reflect resin flow velocity [p.8]. The fabric stitching was found to complicate the modeling of flow through glass reinforcement. At the location of the stitching, the fiber bundle is greatly constricted which impedes resin permeability and opens up a larger channel for flow between bundles. Consequently, the current MSU RTM model predicts a flow rate in this local region that is notably slower than found experimentally.

University of Surrey RTM Flow Model. Lekakou and Badger [9] have also developed a mathematical model which will predict flow fronts using the micro- and

macro-approach discussed in the MSU RTM model. The experimental verifications these two authors performed varied resin viscosity, fiber volume and tow radius to compare predicted and measured infiltration times. A noteworthy aspect of this model is its ability to accurately capture micro-infiltration times. In accordance with Darcy's law (Eq. 1), as the resin moves away from the injection port, local mechanical pressures will decrease and micro-infiltration times will increase. This behavior, predicted analytically, was also observed in the experimental procedures. Additional tests imposing viscosity changes were performed using Darcy's Law that verified proportional changes in macro- and micro-infiltration times. Fabrics of varying tow diameters were also included in this study. The results demonstrated the relationship of fiber tow diameter to macro-pore diameter, macro-permeability and macro-capillary pressure in resin transfer moldings. The last parameter Lekakou and Bader addressed was fiber volume. In their study, fiber volumes were varied between 30 and 58% which resulted in the macro-porosity changing from 0.48 to 0.034%, respectively, while micro-porosity was assumed constant. Their work was also able to repeat previous experiments where higher pressures and flow rates used in the RTM process determined a mold fill behavior that was macro-flow dominate. In addition, Lekakou and Bader found that higher fiber volumes lead to a decrease in macro-permeability. For experiments at a 58% fiber volume, the authors reported that micro- and macro-infiltration flow fronts were identical to one another and at this level of fiber content changes in pressure had no effect on changes in permeability.

Flow Rate and Porosity

The ideal composite would be free of porosity. Unfortunately, voids in composite materials are a real problem that stems from the mechanical combining of resin and fiber reinforcement. Pores inside a composite do not transfer stresses, act as stress concentrators, and degrade mechanical properties. They are introduced by a number of means in both hand lay-up and RTM: through air bubbles entrapped in the resin mixture, through the release of volatiles and dissolved air during cure, or through the application of resin. Hinrichs suggests that voids will raise concern only if they reach a level beyond 1% of a sample's volume [30]. Both hand lay-up and RTM may produce parts exceeding this allowable level of porosity and require further investigation to determine whether it is possible to consistently maintain void content under 1%.

Hand lay-up has not received a significant amount of attention with respect to porosity content. This is due to the inherent variability of the hand lay-up process and the many ways voids can be introduced. RTM on the other hand, is being studied extensively, and a particular area of investigation includes determining the factors of pore formation. One such study was performed by Hedley concerning flow rate versus resultant porosity [33]. His work looked at varying flow rates for the RTMing of a polyester/random mat system and then recording pore diameter, void content, entrapped air location and differences between macro- and micro-flow levels. The four flow rate tests performed illustrated that as volumetric flow rate was increased, percent porosity and the average pore diameter increased as well (Table 1). It is often observed in experiments and predicted by Darcy's Law that porosity has the tendency to increase as

the distance from the injection port increases (the pressure gradient becomes insufficient to drive entrapped air out of the mold). For the small plates Hedley molded, the distance from the injection port most likely did not play a significant role. However, for the larger specimens being fabricated in the current study, it will be important to note porosity contents with relation to injection location. Lastly, the current evaluation employs

Table 1. RTM flow rate versus percent porosity results by Hedley [33].

Flow Rate Test	Volumetric Flow Rate (mL/min)	Porosity (%)	Average Pore Diameter (mm)
1	3	0.22	0.015
2	6	0.27	0.022
3	24	0.39	0.026
4	54	0.53	0.028

industrial grade RTM machines with much higher volumetric flow rates than those listed in Table 1. The correlation between these higher flow rates and porosity levels will also be determined.

Fabric Reinforcements in RTM

Another RTM investigation was performed by Pearce, et al. on the effects of fabric architecture in composite processing and properties [34]. For RTM applications, industry maintains a wide range of fabrics, many of which cluster individual fiber strands into bundles to ease reinforcement manufacturing, to secure fiber orientation and to enhance resin permeability. However, reinforcement fabrics using fiber bundles generate

a composite of non-uniform construction on the micro-scale. Referring back to Figure 3 will demonstrate this more clearly. The fiber bundle halves shown contain the individual strands of glass that provide mechanical strength to the composite. At the circumference of these bundles, a large discontinuity exists where stresses are transmitted to the significantly weaker polymer matrix material. For mechanical performance, fibers that are distributed evenly over the entire cross-section (for example, prepregs) would yield little discontinuity and stronger materials. However, since channel flow and reinforcement integrity remain necessities of the RTM process, RTM'd parts continue to suffer from decreased mechanical performance due to the use of clustered tows [35].

The study conducted by Pearce, et al. compared degradations in strength to fabric weave type. Their work examined three widely used carbon fiber fabrics and rated them according to the resultant composite's mechanical properties so that observations could be made on which fabrics minimize the loss of strength in composites using fabrics with bundled reinforcement. The three fabrics examined were satin, twill and Injectex® weave reinforcement (Fig. 5 a-c). They were studied according to porosity content, resin permeability and inter-laminar shear strength (ILSS), the results of which are summarized in Table 2. In the permeability study, it was found that channel size had an important correlation to resin infiltration, void formation, and void volume fraction. Larger channels (in the twill and Injectex® fabrics) were found to increase macro-flow and consequently, propagate a quicker transverse micro-flow that filled the bundle tows. The study hypothesized that larger channels will determine the lead and lag time between capillary and channel flow, in addition to increased air entrapment and larger diameter

17

voids. The noteworthy aspect of this work was that Pearce, et al. confirmed that more permeable fabrics yield more porous composites, which in turn, lead to a degradation of ILSS and other mechanical properties.

a) Satin   b) Twill   c) Injectex®
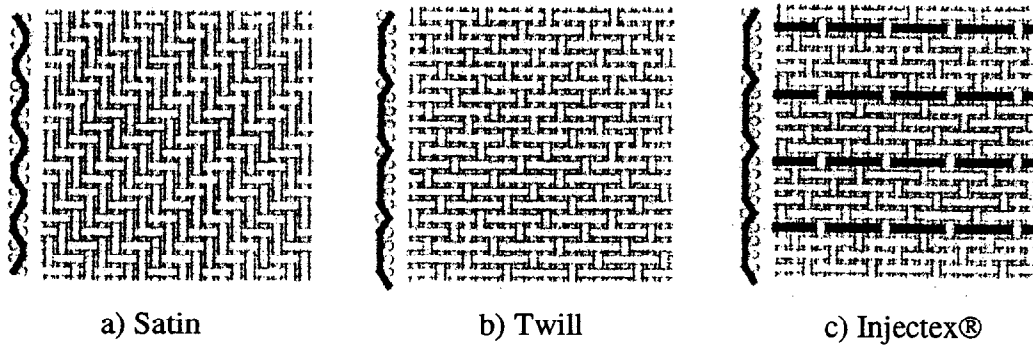
Figure 5. Satin, Twill, and Injectex® carbon fabric weaves.

Table 2. Summary of results on fabric investigation by Pearce, et al. [34].

Fabric	Permeability	Porosity	ILSS
Satin	lowest	lowest	greatest
Twill	greatest	greatest	lowest
Injectex®	average	average	average

Optimal Processing Temperatures

In any industrial application, minimizing manufacturing time is important to increase output while decreasing cost. Of all the processing parameters in the RTM process, processing temperature is the single most important when cycle times are concerned. Temperature is the easiest way to control resin viscosity, a first-order

18

variable in Darcy's Law (Equation 1). With RTM at ambient temperatures, injections can take only a few of minutes, while the curing procedure can consume an entire workday. Elevated injection and cure temperatures are the only variables that can greatly decrease the molding cure time for a given laminate.

The polyester resins used in typical, low-budget applications initiate cure through a natural, exothermic reaction. When catalyst and resin systems are combined, the catalyst will initiate cross-linking, then gelling, and finally, curing of the thermosetting resin. During curing, the matrix will generate a significant amount of heat as the composite reaches the final stages of the RTM process. A study performed by Yu and Young investigated the influences elevated temperatures had on reducing the time required for the RTM cycle [36]. Their work examined two resins, unsaturated polyester and epoxy, and found optimal conditions in which to elevate injection line temperature, mold temperature and cure temperature in order to minimize the time required for RTM'd parts to cure. Yu and Young recognized that minimizing mold filling time and cure time would reduce energy consumption over the complete RTM cycle. The challenge they faced was to develop an algorithm which found processing temperatures that would allow complete mold fill just short of gel conversion times while also not exceeding the resin's degradation temperature. The degradation temperature is a property that, when exceeded, will break down the structural integrity of the resin system. The work performed by Yu and Young also found that in an RTM mold during process cycling, the part being manufactured can have a wide distribution of temperatures which will result in a different thermal history for each point in the mold. This condition was found to yield varying

deformations and non-uniform properties for each specimen. The processing temperatures Yu and Young prescribe, through the development of a mathematical algorithm, will minimize the effects wide temperature ranges have on the RTM process. Their findings for RTM temperature ranges and optimal processing conditions for unsaturated polyester and epoxy resins are shown here in Tables 3 and 4, respectively.

Table 3. Suggested RTM cycle temperature ranges by Yu and Young [36]

Resin System	Injection Line Temperature	Mold Fill Temperature	Post-Fill Heating Rate	Cure Temperature
Unsaturated Polyester	20 - 40°C	20 - 40°C	1 - 7°C/min	60 - 120°C
Epoxy	20 – 40°C	20 - 60°C	1 - 7°C/min	100 - 180°C

Table 4. Optimal RTM cycle temperatures under Yu and Young [36]

Resin System	Injection Line Temperature	Mold Fill Temperature	Post-Fill Heating Rate	Cure Temperature
Unsaturated Polyester	25°C	24°C	7°C/min	91°C
Epoxy	39°C	31°C	3°C/min	159°C

Convergent Flows and Mechanical Properties

The detrimental effect of porosity on composite strength was discussed earlier in this section. A porosity initiating mechanism not mentioned at that time was convergent flow fronts. Because of their importance in molding very large parts, like wind turbine blade components, convergent flow fronts, and their resultant mechanical properties, deserve special attention.

Hand lay-up, like many other composites manufacturing techniques, permeates resin through the reinforcement fabric over very short distances. Resin is applied and forced through individual layers that are commonly less than 1 mm thick. RTM is faced with a very different challenge – the pressures being applied may have to drive resin over very large distances. For example, in the RTMing of a composite turbine blade skin, thicknesses may range between 2 – 20 mm, while lengths can exceed 9 meters. If such a part were to be injected with a single end port, areas of low pressure gradients would exist over the entire 9 meter span. The hypothetical injection would require an extremely large amount of time since resin infiltration is dependent upon localized pressure and flow rate. What is commonly suggested to alleviate this dilemma is an injection manifold. A manifold will inject resin, either simultaneously or at staged intervals, at multiple points in the mold. This procedure reduces filling times by greatly increasing local resin pressures and reducing the lengths in which resin must travel. The only concern multiple injection points raise is the porosity introduced by convergent flow fronts. On a micro-level, RTM'd parts can acquire porosity from the macro-flow racing ahead and then permeating the fiber bundles radially. As the microscopic flow fronts converge, air can become entrapped between individual fibers as flow front pressures cancel one another. On a macro-level, convergent flow fronts are also formed with the use of multiple injection ports. When two flow fronts confront one another, the pressure will equalize, resin flow will cease, and any air trapped in the fingers of the flow fronts will remain in this localized region. The level of void content found here can be quite high and was studied extensively by Pearce, et al. [37].

Vacuum applied to RTM molds is an excellent solution to void formation under convergent flow fronts [18, 19]. With vacuum drawn on the mold, voids will have insufficient internal pressure to support themselves and will eventually collapse [20]. Also, the pressure gradient provided by vacuum results in resin that can flow into areas of the mold without having to displace air or other gases during flow. Molds that are not vacuum tight, however, are a problem. Any leaks in the molding apparatus will draw air in and actually increase the porosity content [21]. Vacuum effects have also been known to cause detrimental effects in some vinylester and unsaturated polyester systems when used in heated molds. Lundstrom noted that pure styrene boils at 40°C with a 90% vacuum and at 140°C under atmospheric pressure [38]. However effective vacuum may be for certain RTM applications, there exists molding schemes where vacuum cannot feasibly be applied. Whether temperatures, geometries, or costs intervene, the majority of RTM applications remain unassisted by vacuum effects. For this reason, studies on convergent flow fronts and porosity entrapment are still an important development.

The study conducted by Pearce, et al. used an RTM flat plate mold, three carbon fiber reinforcement fabrics and a series of injection schemes to capture the outline of high porosity as flow fronts converge [37]. Their work also included a summary of porosity's effects on a range of mechanical properties. Reviewing these findings gives a clearer picture of porosity's role in mechanical performance:

- Voids reduce interlaminar shear strength (ILSS) [39], flexural modulus, longitudinal and transverse tensile strength and modulus, compressive strength and modulus, fatigue resistance and high temperature resistance [40].

22

- The first 1% of voids can decrease bending strength by 30%, tensile strength by 3%, torsional shear by 9% and impact performance by 8% [40].

- Regardless of resin type, fiber type and surface treatment, the ILSS of a composite will be reduced by 7% for each 1% of voids up to a total percent porosity of 4% [40].

- For carbon fiber/epoxy specimens each 1% of voids up to a sum of 5% reduced flexural modulus by 5%, flexural strength by 10% and ILSS by 10% [41].

- In carbon fiber reinforced plastics (CFRPs) with void percentages less than 1.5%, pores tend to be spherical with diameters ranging between 5 – 20 μm. At higher porosity contents, pores appear more cylindrical with lengths up to an order of magnitude greater than their diameters [42].

- Porosity profiles are important because areas with locally high porosities will have a greater probability of failure [42].

- Voids increase moisture absorption, which weakens the fiber/matrix interface [43].

- Voids can improve some properties such as tensile strain to failure [44].

These previous research topics in RTM were used for developing the experimental molding and testing procedures of this study.

CHAPTER 3

EXPERIMENTAL METHODS

Materials and Manufacturing

The materials, equipment, and manufacturing techniques employed in the current research were carefully chosen to represent, as realistically as possible, the practices of modern wind turbine blade manufacturers. Through each step of processing with hand lay-up and RTM, an effort was put forth to minimize cost, time, and difficulty of manufacture. This methodology assured that results made in the laboratory would be repeatable on an industrial scale.

Resin and Fabric Systems

As mentioned earlier, the primary components of the fiberglass composites or fiber reinforced plastics (FRPs) used in the wind turbine blade industry are polyester resin and E-glass fabric reinforcement. The unsaturated polyester resin processed in the current research was an Interplastic Corporation product, CoRezyn 63-AX-051. This resin, when combined with Lupersol DDM-9 methyl ethyl ketone peroxide (MEKP) at 2% by volume, yields a matrix material that is representative of the strength and cost characteristics of typcial resins used in blade fabrication.

The fabrics used in fabricating test specimens were also the same products utilized in industry, or close counterparts. Four different fabrics, supplied by two different manufacturers were used in the current work. The architecture of the four reinforcements are summarized in Table 5 and illustrated in Figure 6.

Table 5. E-glass fabric reinforcement summary.

Material Supplier	Fabric Designation	Ply Angle(s)	Fabric Architecture	Roll/Bundle Orientation	Mass/Area (g/m^2)
Owens-Corning/ Knytex	D155	0°	stitched	weft	526
	A130	0°	woven	warp	440
	DB120	±45°	stitched	double bias	407
CollinsCraft	UC1018/V	0°	veil/bonded	warp	640

D155   A130   UC1018V   DB120

a)   b)   c)   d)   2 cm
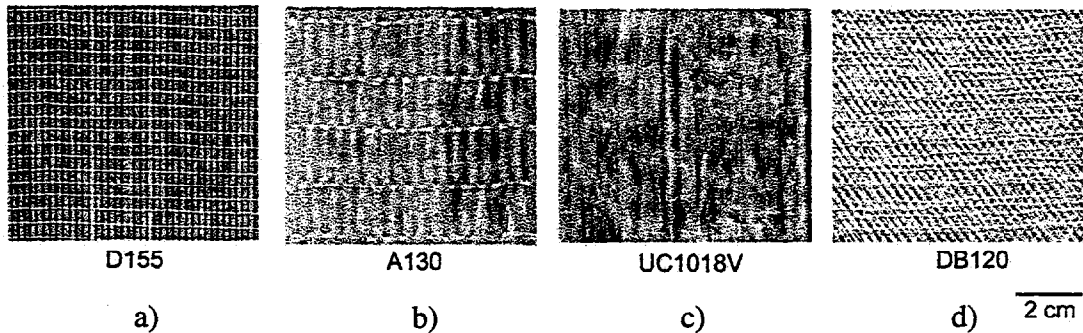
Figure 6. Stitched, woven, and adhered E-glass fabric architectures.

The first fabric noted is the Owens-Corning/Knytex D155, which is a unidirectional, zero degree fabric (Fig 6a). D155 was chosen for this study because it represents one of the best mechanically performing unidirectional E-glass fabrics currently available [5]. This reinforcement architecture contains bundles of individual

glass strands, stitched together with a thermoplastic polyester thread. The orientation of the zero degree bundles or tows is also in the weft direction, or more simply put, the length of the glass bundles run perpendicular to the length of the fabric roll. D155 fabric has excellent resin wet-out and compressive strength properties, but because the zero degree tows are only as long as the width of a fabric roll, currently 1.27 meters, the reinforcement cannot be used continuously in the blade length direction. Consequently, alternative zero degree fabrics are being investigated in an effort to borrow the advantages of D155 for a reinforcement that supports utility-grade blade length parts.

The second glass fiber reinforcement mentioned in Table 5 is the Knytex A130 illustrated in Figure 6b. This fabric is representative of the zero degree reinforcements currently being used by turbine blade manufacturers. The architecture of this fabric is comprised of zero degree glass bundles that are woven and adhered to one another with a perpendicular tow of glass fibers coated in thermoplastic polyester. The fabric weave compromises the ultimate compressive strength (the glass tows are initially wavy), but currently, the A130 fabric is the best option available for blade manufacturers requiring a weft, zero directional reinforcement [5].

UC1018/V is a CollinsCraft, glass fabric reinforcement that was selected for its potential in addressing the concerns of woven, warp zero directional fabrics (Fig 6c). The fabric architecture of this reinforcing material is notably different than those previously discussed. UC1018/V contains bundles of zero degree glass fibers, but unlike the other stitched or woven fabrics, the CollinsCraft product adheres its bundles to a light, random oriented, glass fiber veil. Potential advantages of this fabric are that the

unidirectional bundles of glass fibers are not woven through the thickness of the fabric nor are they stitched into confined bundles. These two factors may allow the load carrying fibers of a composite made from this material to perform better than the industrial standard A130 weaves. This fabric was studied for manufacturability in flat plates samples and strength performance in the I-beam geometry during the hand lay-up and RTM evaluation.

DB120 was the single $\pm45°$ double-bias fabric employed in this study and is shown in Figure 6d. This fabric contains both +45° and –45° (relative to the length of the fabric roll) layers stitched on top of one another with the same materials used in the D155 fabric. DB120 is a double bias fabric with glass bundles running perpendicular to one another, but it has been observed that the reinforcement has poor fiber orientation tolerances. The +45° and –45° individual plies tend to vary by $\pm5°$ due to variations in roll construction, material handling, and composite processing [5].

Hand Lay-up and RTM Equipment

Hand lay-up fabrications utilized very simple equipment and in most cases, the same tooling or molds as the RTM specimens. The hand lay-up methodology involved applying catalyzed resin to the tooling surface, placing an individual layer of fabric to the mold, permeating the resin through the fabric thickness with hand rollers and brushes (Fig. 7), and then repeating this procedure for the build-up of the remaining laminate. In the final step, excess resin is removed with a wet lay-up squeegee. The rollers used were typical of composite fabrication, were 25.4 mm in diameter and 89 mm in width, and are

readily available from most composite materials suppliers. The bristle brushes and thermoplastic squeegees were inexpensive items found at a local hardware store.
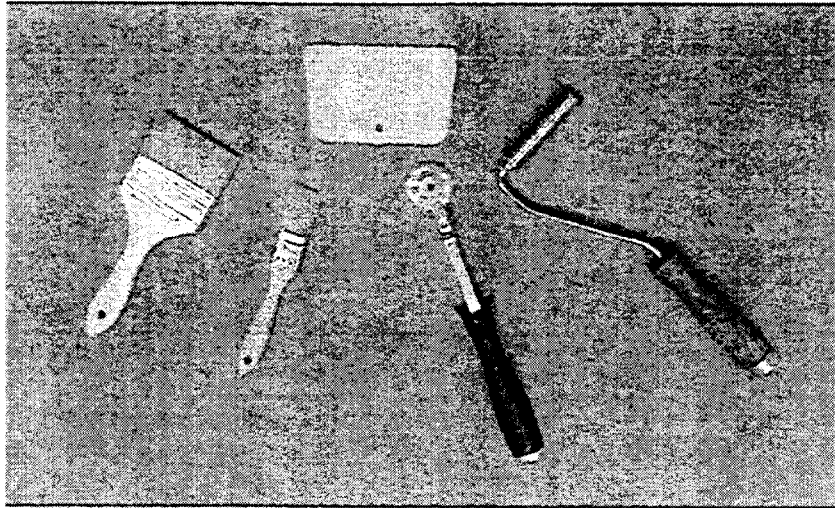
Figure 7. Hand lay-up brushes, rollers, and squeegees.

The resin transfer molding equipment used was more expensive and involved than that of the hand lay-up process. Before discussing the operation of the two RTM injectors, it should be mentioned that a Speedaire air compressor pneumatically powered both. The 75.7 liters of air that it supplies was regulated at a pressure of approximately 827 kPa and a flow rate of 283 liters per minute. This compressor was found to adequately meet the air requirements of both injection systems.

The first RTM machine used in manufacturing was a Glas-Craft Spartan VR3 injector (Fig. 8). This system operates a series of reciprocating pneumatic cylinders that force resin and catalyst through a static mixer and then into an RTM tool. Injection pressures and flow rates are fully adjustable, but for the mechanical test samples, the supply line pressures and injector regulator pressures were held constant at 827 kPa and

97 kPa, respectively. The Spartan is a highly automated machine that will recirculate materials to prime the system prior to injection, count the number of strokes per injection, dispense a given number of strokes for an injection, and force acetone solvent and air through the static mixer to clean the machine upon completion of the RTM process. An additional feature of the Glas-Craft system is vacuum assist. This option allows the Spartan RTM machine to be compatible with vacuum assisted resin transfer molding (VARTM) with a vacuum of up to 85 kPa. This injector lends well to the RTM of large parts, like turbine blade components, because it draws from a 208 liter source and delivers resin in large volumes (293 mL/stroke). For research applications however, the Spartan has its limitations. It does not come equipped with a data acquisition system that can record injection pressures, resin flow rates, and molding cycle times. To record this information for the current work, a pressure transducer and Hewlett-Packard data acquisition system were used. An example plot of the injection pressure data recorded with this equipment is shown in Figure 9. The varying injection pressures of the Spartan RTM machine are demonstrated in this figure. The up and down-strokes produce distinctly different pressures in the RTM tool during the course of an injection. Resin flow rates were calculated from Figure 9 by noting the number of strokes and then multiplying by the specified 293 mL per stroke.

The second resin transfer molding device used in research was the Radius 2100cc injector (Figs. 10 - 11). The Radius operates similarly to a large pneumatic syringe. The lower half of the injector is a long pneumatic cylinder that actuates a slave piston in the
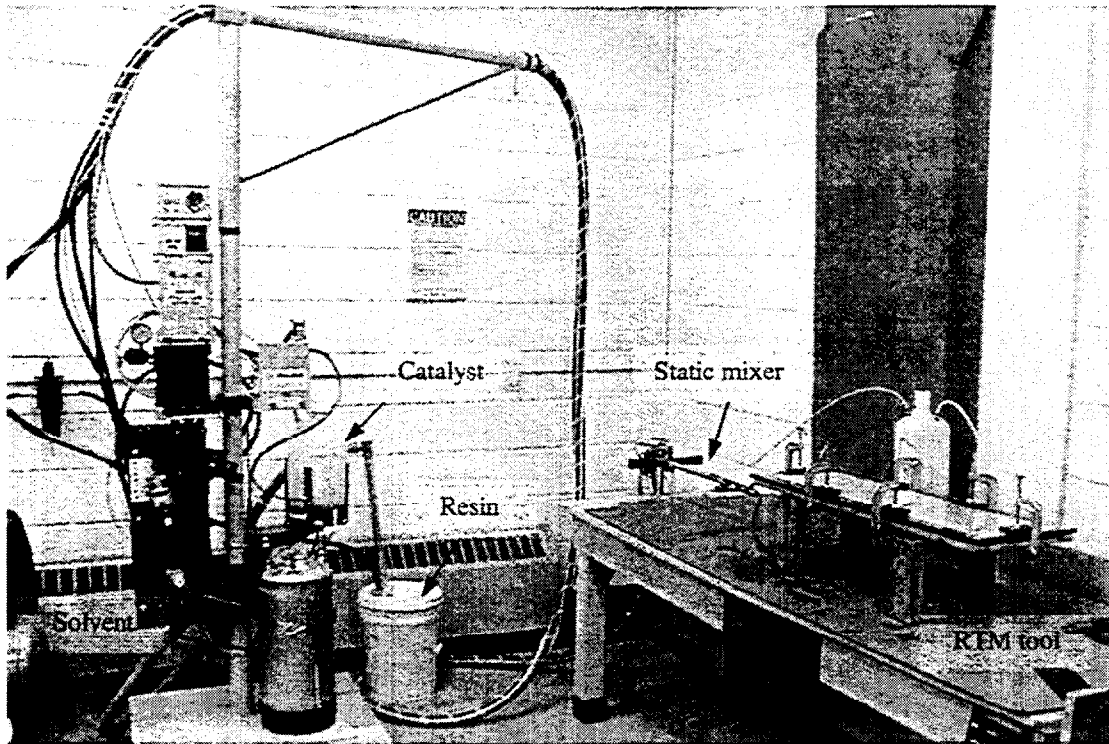
Figure 8. Spartan industrial grade RTM injection device
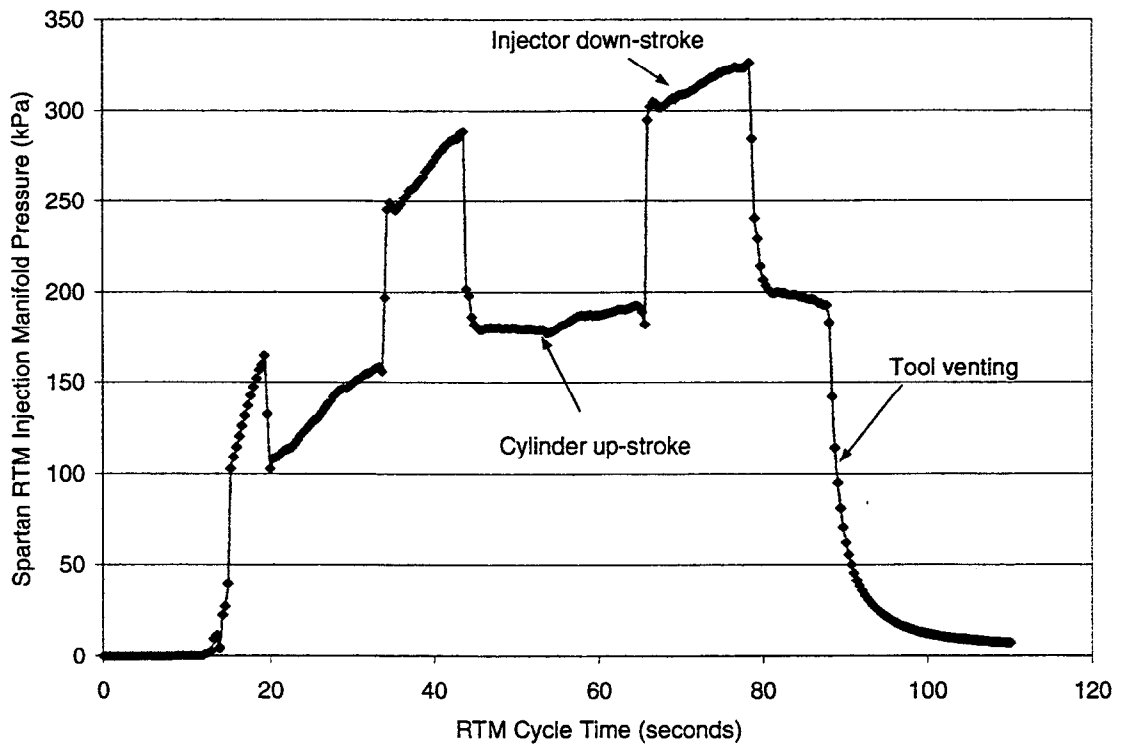
Figure 9. Spartan RTM injection pressure history.
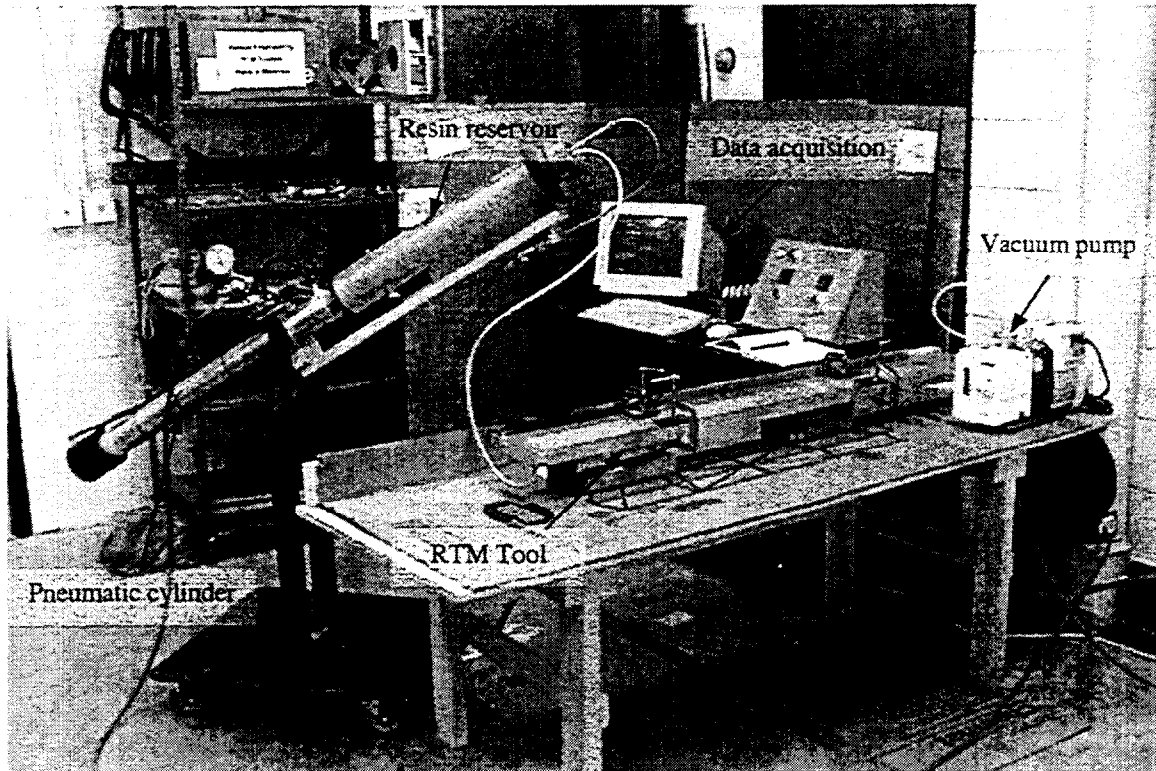
Figure 10. Radius 2100cc RTM injector with data acquisition.
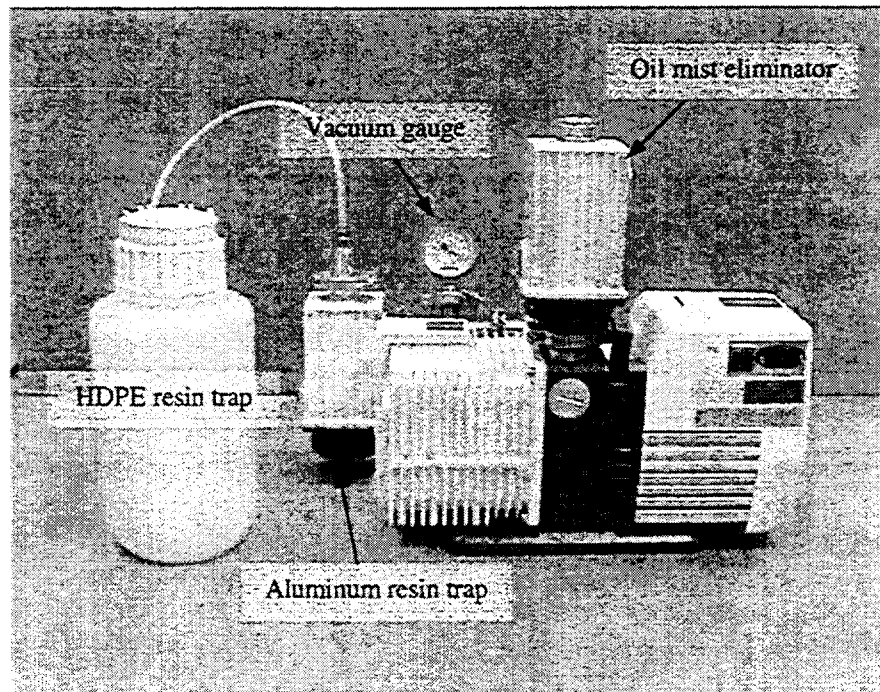
Figure 11. Alcatel rotary vane vacuum pump used in VARTM.

upper half, or resin reservoir side, of the Radius. Toggle controls manipulate the extension, retraction and location of the slave piston. This system is capable of a wide range of pressures and flow rates. The current work employed injection pressures between 414 and 827 kPa with flow rates set by an adjustment screw.

The Radius 2100cc injector's advantages do not lie with large moldings or automated processes. The injector can only move 2100cc's of resin in one stroke and then must be refilled for further injecting (it must be noted however, that this is the smallest injector manufactured by Radius Engineering). This process can be quite cumbersome when compared with the Spartan's method of operation. In addition, the Radius does not have the automation features of the other RTM machine. Resin mixing, injection control, and clean up must be performed manually. However, the Radius system excels in its ability to perform advanced RTM injections, and to record the RTM process with a complete data acquisition system. Advanced features available with the Radius are resin position sensing, resin reservoir heating, and injection line temperature elevation. These options allowed for the monitoring of convergent flow fronts and the use of elevated temperatures for optimal RTM processing as outlined in the Background. The data acquisition outfitted with the Radius 2100cc injector records all of the previous information in six second intervals, in addition to the basic RTM parameters of injection pressure, resin flow rate, tool pressure, and tool temperature. Though the Radius was limited in initial injection volume, a data acquisition system was found to be necessary in properly quantifying the RTM process. Examples of the injection pressure and flow rate

profiles recorded by the Radius data acquisition are shown in Figures 12 and 13, respectively. From these figures the constant pressure operation and varying flow rates of the Radius RTM system can be observed.

Radius Engineering Inc. highly recommended experimenting with vacuum assisted injections using the 2100cc injector. In the interest of quantifying the benefits of Vacuum-Assisted RTM or VARTM, an Alcatel 2005 SD, rotary vane vacuum pump (Fig. 11) was used in conjunction with the Radius injector. This pump worked to remove air molecules from the resin, fiber preforms, and tooling for flat plate moldings with a vacuum of 12-15 kPa. Additional components necessary for using the Alcatel pump in a VARTM setting were a 4 liter, Nalgene heavy duty polyethylene (HDPE) bottle resin trap, 0-100 kPa vacuum gauge, mechanical vacuum adjustment valve, and exhaust oil mist eliminator.

Hand Lay-up and RTM Tooling

The above fabrics, resins, and processes were put to work on five different molds during the course of this study. Flat plate, T-stiffener, I-beam, and Root mold materials as well as their cure times are summarized in Table 6. These geometries were chosen for their similarities to the leading edge, spar web, spar cap, and hub connection regions of a composite wind turbine blade (Fig. 1). The T-stiffener and I-beam molds were existing tools while the flat plate and root specimen molds were constructed during the course of this study. The tools and their seals were manufactured from a variety of materials and were selected because each has its own strengths and weaknesses. By employing a
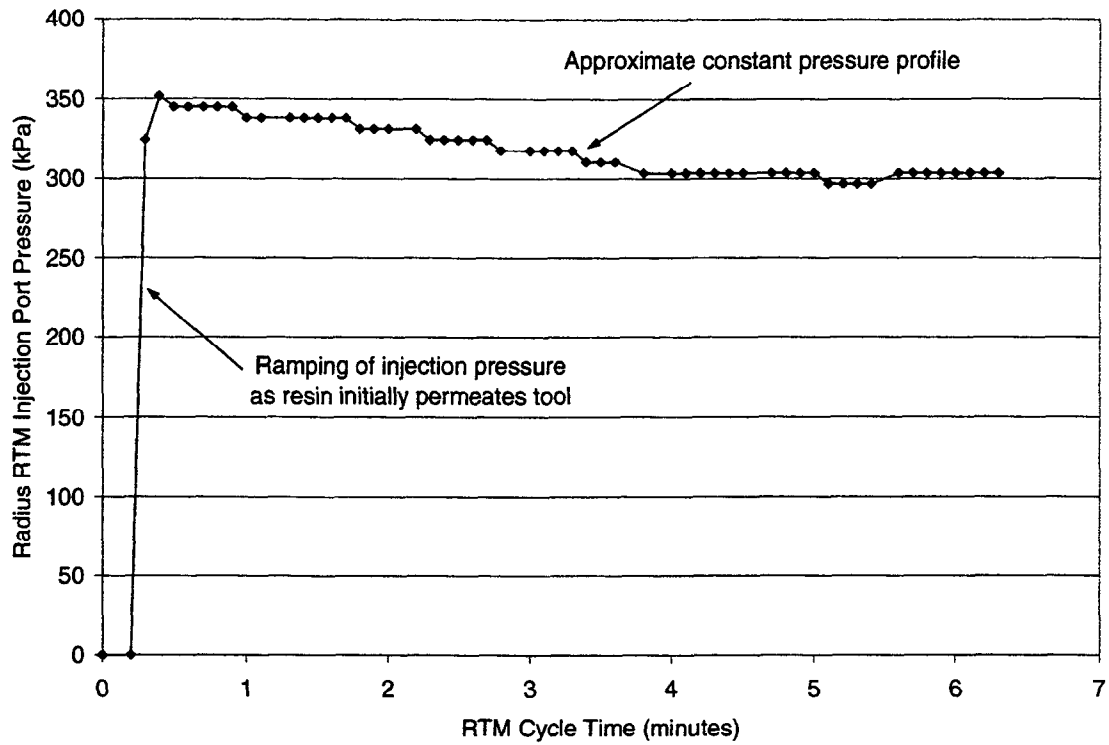
Figure 12. Radius RTM injection pressure profile.
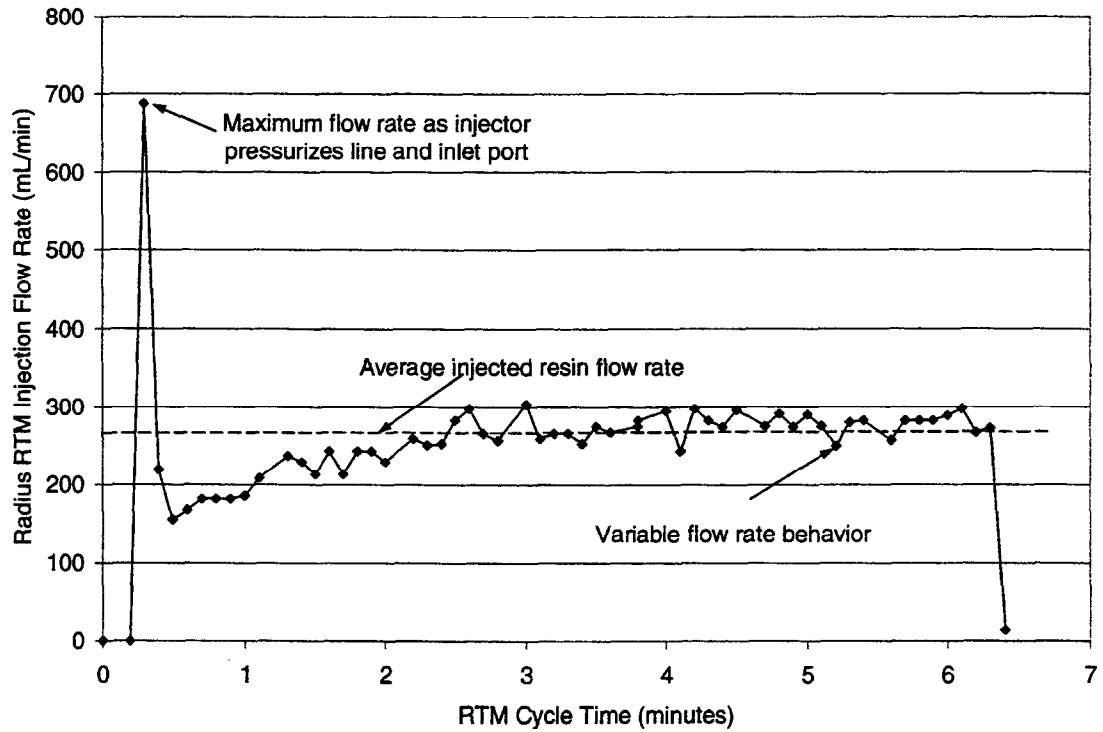
Figure 13. Radius RTM injection flow rate behavior.

variety of tooling and gasket materials for processing, observations could be made on their benefits or drawbacks in blade fabrication applications.

Table 6. Tooling materials and cure times.

Part Geometry	Tooling Materials	Gasket Material(s)	Cure Time (hours)
1) Flat Plate	Aluminum / glass face	Silicone O-ring	6 - 8
2) Thin Flanged T		Nitrile Rubber	
3) Thick Flanged T		Nitrile Rubber	
4) I-beam with Flanges	Steel	Rubber and Paper	6 - 8
5) Root Specimen	Composite / Steel back	Silicone and Rubber	3 - 4

510 x 810 mm Flat Plate Tools. The hand lay-up 510 x 810 mm flat plate moldings were performed with minimal tooling. A 610 x 914 mm, 12.7 mm thick steel plate provided the flat surface necessary for working resin into the glass fabric. The tool was prepped prior to processing with 6-8 coats of Frekote 700-NC mold release. Frekote was the mold release of choice for all of the tooling used in both hand lay-up and RTM procedures. It works very well with polyester/glass composite moldings and lasts for 20-50 parts before requiring further applications.

The RTM tooling for flat plate fabrications was a little more involved than its hand lay-up counterpart. The mold base consisted of a 25.4 mm thick aluminum plate with a 3.18 mm deep cavity and 4.78 mm silicone O-ring groove machined from it (Fig. 14). The cavity of the mold yielded parts 510 mm in width and 810 mm in length. Seven, 3.18 mm diameter ports were also machined into the mold base for a variety of injection, vacuum, and vent combinations. These ports allowed the usage of Parker
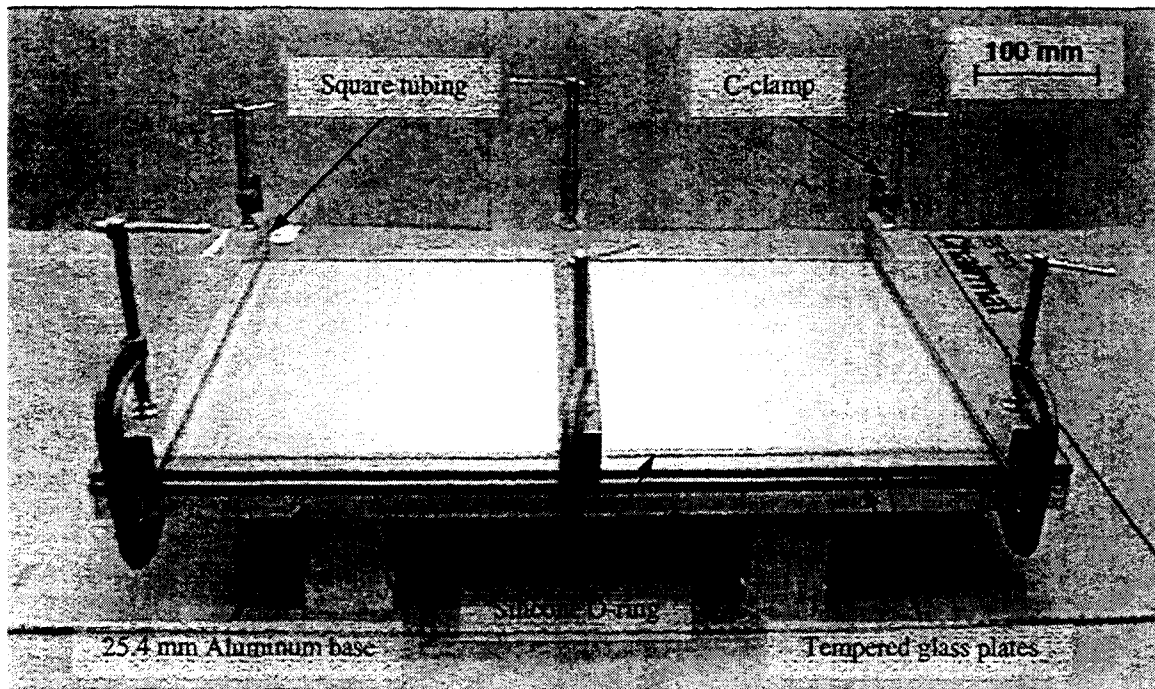
Figure 14. 510 x 810 mm aluminum flat plate RTM tool.

Presto-Lok® fittings that accepted 6.4 mm polyethylene tubes. Parker fittings and polyethylene tubes were used in all resin transfer moldings for their ease in clean-up and removal. The flat plate mold was topped by two 12.7 mm thick, tempered glass plates and a 4.78 mm thick sheet of Plexiglas® for protection in the event excessive resin pressures shattered the glass. The top glass plates were secured to the mold base and compressed the silicone O-ring using 16, 152 mm C-clamps. The forces of the individual C-clamps were distributed to the mold face via five rectangular tubes (51 x 51 mm in cross section) which alleviated any stress concentrations that might fracture the glass plates. For the flat plate wash-out study, to be discussed subsequently, a 19.1 mm thick aluminum plate was substituted for the tempered glass faces because the injection pressures were significantly higher than in the standard moldings.

Thin Flanged T-Stiffener Molds. The RTM thin flanged T-stiffener mold consists of two 19.1 mm thick aluminum, L-shaped halves and a 12.7 mm tempered glass top (Fig. 15). Both faces of the aluminum L-halves are machined out for mold cavities and the upper surface of the tool has a milled groove to allow for a square, 6.4 x 6.4 mm, nitrile rubber gasket/spacer. Unlike the flat plate mold where the tempered glass mated immediately to the aluminum tool, the T-section molds were manufactured with a combination gasket and spacer that allows more flexibility in the skin thickness. This can cause some concerns, which will be addressed later in the Experimental Results chapter. Between the web halves of the T-mold was another gasket/spacer made of nitrile rubber. This gasket was fabricated from a sheet of 3.18 mm thick rubber and was punched to allow 6.4 mm diameter bolts to secure the two L-shaped halves together. Mold filling was accomplished through two skin ports located at one end of the mold with venting allowed at the other. Two types of RTM T-stiffeners were molded from this tool. The first allowed the web, flange and skin to co-cure in one complete geometry, while the other included a piece of ReleaseEase®, a porous Teflon release film, between the flange and skin. The Airtech release film product allowed for the secondary bonding of the RTM'd part and the inclusion of this as a variable in investigating manufacturing techniques. Unfortunately, due to the complex sealing structure of this tool's geometry, and that of the remaining tools, vacuum assistance was not feasible. A series of attempts were made on the thin T-mold to seal it well enough to maintain a 15 kPa vacuum. All the experiments performed to meet this end were unsuccessful. Additional tests were performed on the thick flanged T and root molds, but these endeavors failed as
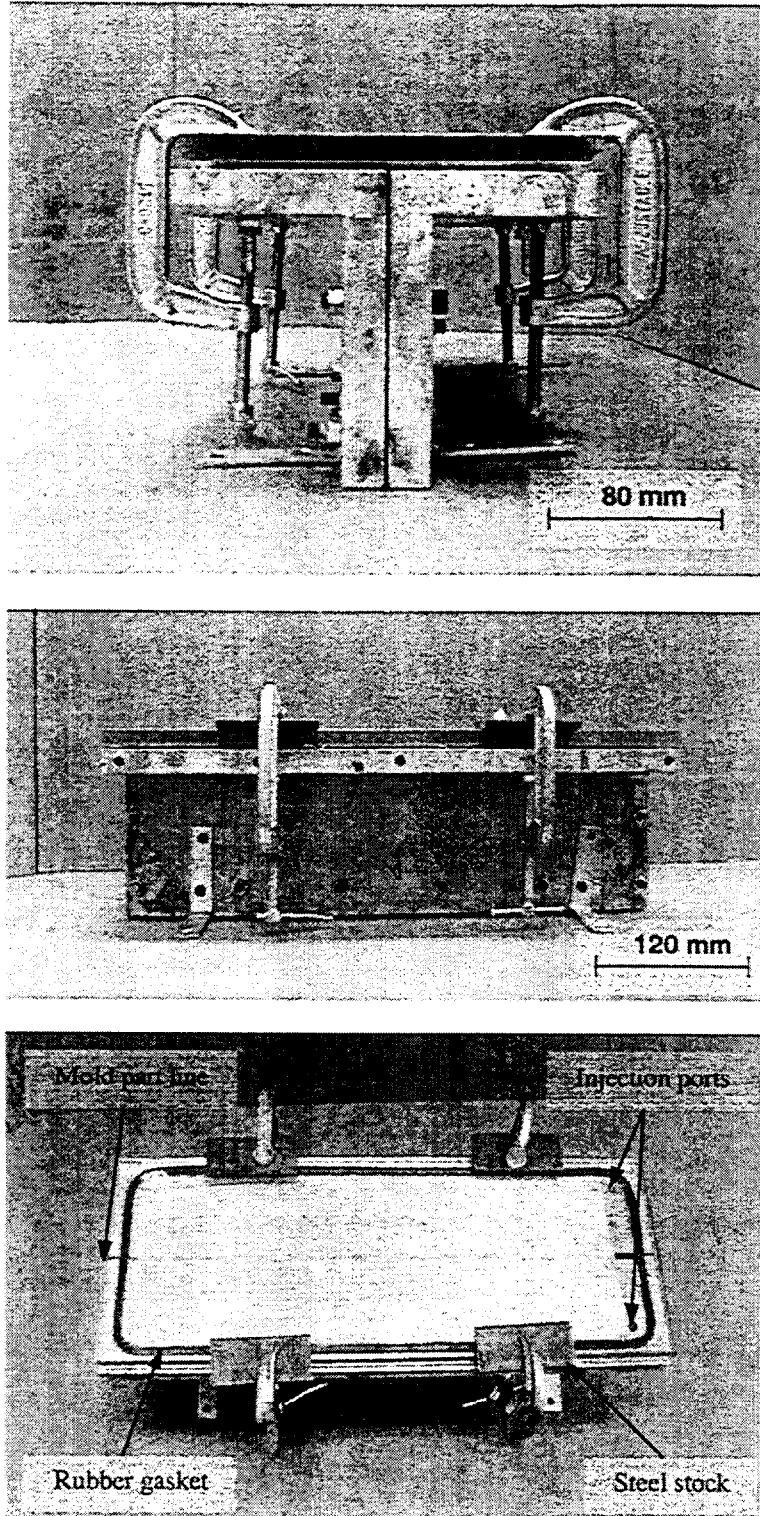
Figure 15. Thin flanged T-stiffener RTM mold (end, side, and top views).

well. Thus, flat plate moldings allowed for experimentation with VARTM, while the more complex composite structures were limited to RTM and hand lay-up comparisons. Similarities with the flat plate mold included the usage of 4.78 mm thick acrylic sheet, C-clamps and steel stock to secure the glass face and to protect the RTM operators. The dimensions of the resultant thin flanged T-stiffener geometry (Fig. 16) were as follows: skin and web thickness - 4.5 mm, length - 432 mm , width - 152 mm, and depth - 114 mm.
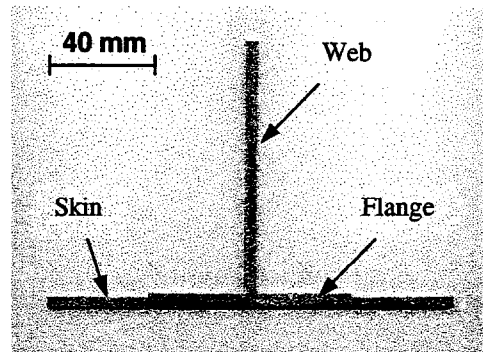
Figure 16. Thin flanged T-stiffener geometry.

Hand laid-up thin flanged T-stiffeners were manufactured three different ways. The first two processes were modified hand lay-up techniques. They involved wetting the reinforcement out in a hand lay-up fashion, but then securing all three components together in the RTM mold. This is not a common hand lay-up practice, but was chosen in an attempt to preserve the amount of porosity introduced by the hand lay-up process while maintaining the tight dimensional tolerances of RTM. Differences between the two modified hand lay-up techniques involved the flange bond surface. In one instance, skin and both web/flange pieces were allowed to cure in a single molding step, while in the other, the skin was cured separately from the web and flanges to facilitate secondary bonding of the surface later. The final hand lay-up technique remained true to the actual process; two web and flange halves in addition to a single skin, was hand wet-out, allowed to cure and then secondary bonded into the full T-stiffener geometry. Forming

the fabric lay-up of the web/flange halves proved to be very difficult with the very sharp radii (r = 1.8 mm) of the RTM mold. The reinforcement had the tendency to pull away from this radius and adopt a greater transition between the web and flange surfaces. This motivated the introduction of the modified hand lay-up technique already discussed.

Thick Flanged T-Stiffener Tooling. The RTM thick flanged T-stiffener mold parallels very closely with the thin flange T-stiffener tool (Fig. 17). However, differences between the two molds include flange lay-up, tool thickness, and injection/vent location. For thick flanged T-stiffener fabrications, a build-up of additional fabric was used between the flange and skin. These plies were added to simulate the spar cap scenario in actual turbine blades, and the inclusion of this fabric introduced some changes in mold design. One modification was thicker, 25.4 mm aluminum plates used in the L-halves to allow for more material at the flange/skin interface. Differences between the thin and thick flanged T-molds also included part length and injection geometry. Longer molds produce more specimens per injection, which is desirable for many manufacturing cases. However, longer tools yield slow mold fill times when injected from an end as a result of low pressure gradients away from the injection ports. To counter this problem, injection locations were chosen at the center of the mold and into both flange caps. This location also allowed resin to enter immediately into a high volume area and facilitate better wet-out of the part. Vents were located at both ends and performed well in letting displaced air and mixed air/resin to escape. Teflon release film was also employed for some specimens between the flange cap and skin to explore secondary bonding effects.
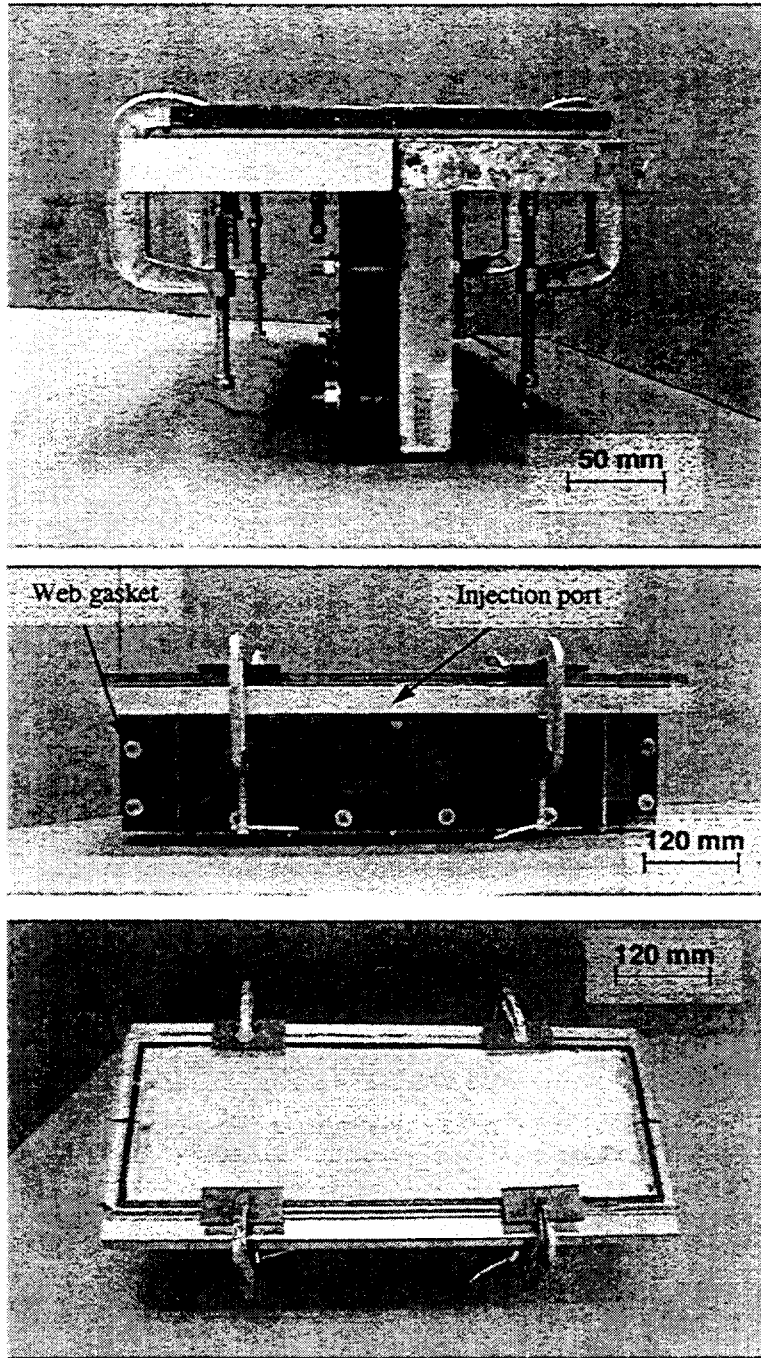
Figure 17. Thick flanged T-stiffener RTM tool (end, side, and top views).

In the thick T geometry (Fig. 18), skin and web thicknesses were not identical. The skin surface of this tool was shallower than in the thin flange T mold and consequently, two less zero plies were used in fabricating the thick flanged T-stiffeners. The average dimensions for skin and web thicknesses were 3.25 and 5.0 mm, respectively. The length, width, and depth were recorded at 533, 178, and 140 mm. The built up flange cap raised the overall thickness of the flange interface area from 7.75 to 13.0 mm.
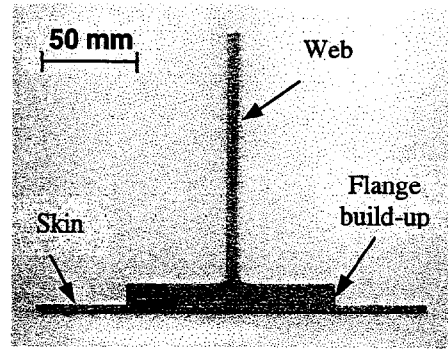
Figure 18. Thick flanged T-stiffener geometry

A fortunate discovery in the first hand lay-up attempts with the thick flanged T-mold was that the flange/web radii of 6.35 mm would allow the reinforcement to lay completely on the tool surface during processing. Consequently, there was no need to use the modified hand lay-up technique that was necessary with the thin flanged T-tool. Conventional hand lay-up thick flange T-stiffeners were fabricated, where webs were wet-out on the aluminum L-halves and the flat flange and skin components were molded on a prepped steel plate. In a secondary operation, these four parts were bonded together with Hysol EA 9309.2NA epoxy into the complete T-stiffener geometry.

Composite I-Beam Molds. The I-beam geometry was RTM'd with a six part match machined, steel mold (Fig. 19). Two identical halves constituted the web and flange cavities, two narrow plates sealed the flange surfaces (Fig. 20), and two additional plates capped the tool ends. Cap sealing was accomplished by 3.18 mm thick, nitrile
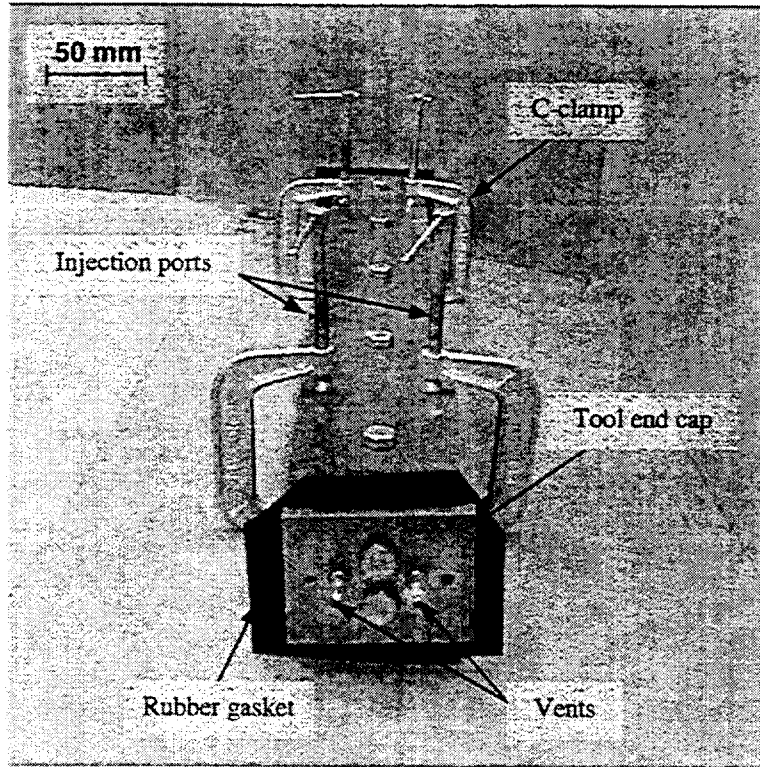
Figure 19. Composite I-beam RTM mold.
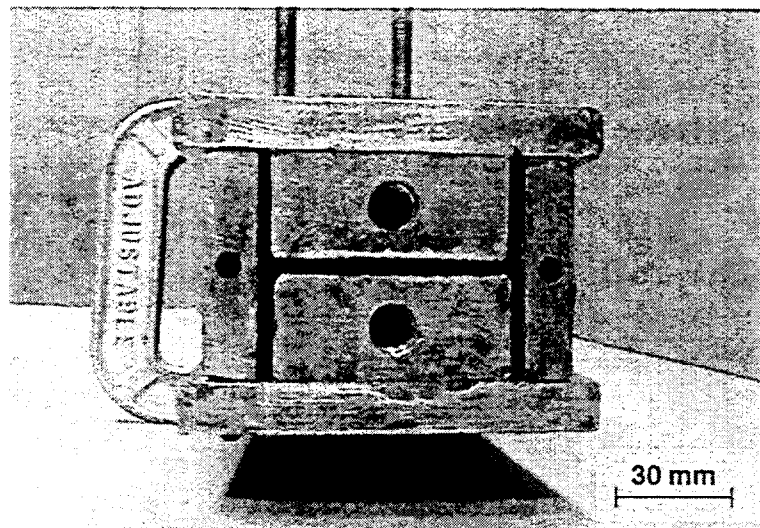
Figure 20. End view of I-beam RTM tool cavity.

rubber sheet and flange sealing was provided by plain paper strips. C-clamps were used to force the steel mold components together and 15.9 mm diameter bolts were used to secure the mold ends to the tool. Injection ports were centrally located on both flange caps and vents were located at each mold end. The steel I-beam tool yielded a geometry (Fig. 21) with an overall width of 57 mm, depth of 64 mm, and length of 838 mm. Flange and web thicknesses averaged 4.5 and 3.25 mm, respectively.
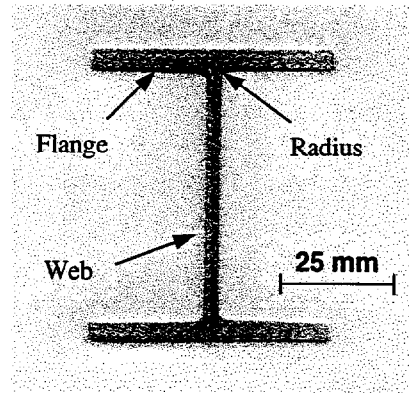
Figure 21. I-beam specimen cross-section

The sharp web to flange radius of the I-beam tool cavity presented hand lay-up problems for this geometry as well. The radius of 1.8 mm did not allow the glass reinforcement to conform to the sharp geometrical changes without additional "pinning" of the material. After the fabric had been adequately wet-out using the hand lay-up process, the entire length of the flanges on both ends required mechanical assistance in holding the U-shaped webs. Steel bars were set along the flange surfaces at equally spaced intervals to help the reinforcement hold the desired shape. Even with this "pinning", the hand lay-up I-beam reinforcement had difficulty maintaining a sharp radius between the flange and web. With this case being the best available option for hand lay-up comparisons, the two channels were bonded to two flange caps manufactured on flat molds and then tested against the RTM'd geometries.

Root Specimen Tooling. The RTM root specimen mold is a composite tool, reinforced with heavy gauge steel tubing, and closed via four toggle clamps (Fig. 22).

44

Headwaters Composites Inc. of Three Forks, MT. supplied this tool under MSU's DOE EPSCoR Program. Hedley molded the fiberglass composite tool from a hand laid-up template and used two seals, silicone and rubber, to contain resin flow within the cavity during injections (Fig. 23). Gel coat was applied prior to lamination, to form a smooth, protective surface on the mold that would allow for easy removal of the finished parts. Injection was achieved through a centrally located port in the skin side of the tool and vents were located at three of the tool's corners. Composite tooling is unique when compared to the other materials used in molding the previous four geometries. Greater care must be exercised because the metal equipment and acetone used to prep metal tooling can be detrimental to composite molds. A strong advantage to using this "softer" material is cure time, however. The root specimen is a relatively thick laminate and generates a large amount of heat during polymer crosslinking. The fiberglass composite tooling acts to insulate this reaction and it was found that the root specimens could be processed in half the time of the other geometries. It should be noted here that while some insulation assists in speeding along the curing process, a mold that does not dissipate the exothermic reaction could reach degradation and combustion temperatures. A final innovation worthy of mention concerning the RTM root molding is the combined RTM'ing with a steel insert. The root geometry has been an important investigation because of its unique role in transmitting large loads from the composite blade to the rotating turbine hub. The root specimen currently being researched is a single sample from an entire root section comprised of an oval geometry and ten inserts. It has been an innovation in composites research to explore the use of blade mounting steel inserts in
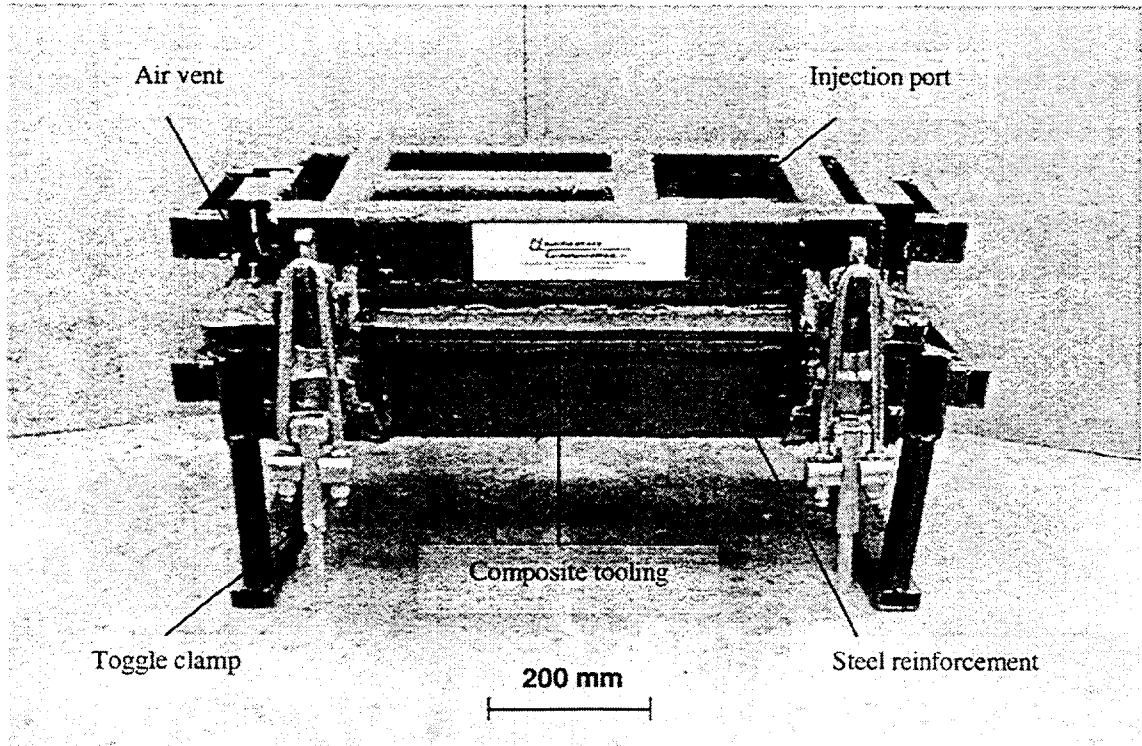
Figure 22. Root specimen RTM mold from Headwaters Composites Inc.
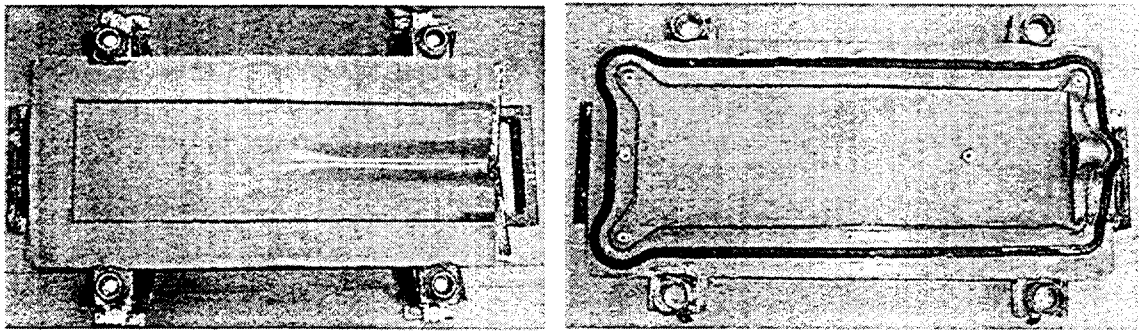
Figure 23. Seal, injection, and vent locations for root specimen tool halves.

RTM processing. The root specimen uses a tapered and ribbed cylindrical insert from a previous wooden turbine blade design for the AOC 15/50 turbine. These inserts were incorporated for the first time between two composite laminates in this study. The root RTM tool supports this insert during molding and is sealed with a rubber O-ring compressed by a 19.1 mm diameter insert-locating bolt.

The final width and length of an RTM root specimen was 203 and 635 mm, respectively (Fig 24). The laminate thickness, including the steel insert at the hub end, is 50 mm, while composite thickness towards the end of the laminate is 10 mm.
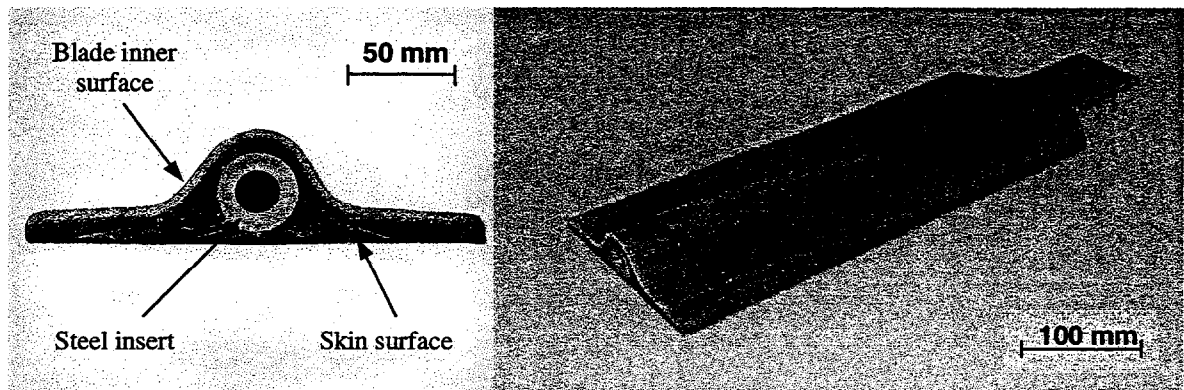
Figure 24. Root specimen geometry.

Hand lay-up root specimens were molded on the 12.7 mm thick flat plate used for components of the previous four geometries. A jig was fabricated from 3.18 mm thick angle iron to support the steel insert during fabrication and a 19.1 mm bolt was again used to locate the insert. The root specimen hand lay-up began with the wetting out of the skin laminate. Tapered insert pieces and strips were then placed and wet out in their appropriate locations. Next, the insert and darts were located and generous amounts of

resin were added in this difficult to wet-out area. Finally, the inner surface laminate was applied ply by ply and any excess resin was removed.

Safety Issues

There are inherent concerns when dealing with the materials that make up composite structures. Persons working with the molding and finishing of composites need to be well apprised on how to protect themselves from any potential safety concerns. For the fiber reinforced plastics (FRPs) manufactured in the current evaluation, serious risks were present if recommended safety equipment were not strictly used. Prior to processing in the laboratories, it was very important to review the Materials Safety and Data Sheets (MSDSs) for the chemicals and materials to be employed. A summary of the safety concerns and protective equipment available to guard against fiberglass processing dangers is presented in Table 7. These guidelines were rigidly followed for the present research and it is highly recommended that others involved with composites manufacturing remain well informed of the health risks and protective measures available for the materials they process.

Fiberglass Recycling

A fiberglass recycling program was initiated under this project in an effort to remain true to environmentally friendly, renewable wind energy developments. A composite recycler was located nearby in Sultan, WA. and they agreed to reuse the scrap product produced under this project. Amour Fiber Core Inc. accepted the mixed

Table 7. MSDS summary of safety concerns and protective equipment.

Material or Process	Potential Safety Concerns	Recommended Safety Equipment
Glass fabrics	Silica poisoning Eye, skin, and respiratory irritation	Ventilation, dust mask, gloves, safety glasses and protective clothing
Unsaturated polyester resin (styrene)	OSHA: 50 ppm for 8 hour work day Volatile, flammable Eye, skin, and respiratory irritation Possible carcinogenic effects	Ventilation, chemical goggles, protective clothing, respirator, and neoprene/nitrile rubber gloves
Methyl ethyl ketone peroxide (MEKP)	Flammable Fatal if swallowed Corrosive to eyes	Ventilation, chemical goggles, protective clothing, respirator, and neoprene/nitrile rubber gloves
Acetone	Volatile, flammable Eye, skin, and respiratory irritation High concentrations effect central nervous system	Ventilation, chemical goggles, protective clothing, and neoprene/ nitrile rubber gloves
Hysol epoxy adhesive	Eye, skin, and respiratory irritation	Ventilation, chemical goggles, protective clothing, and neoprene/ nitrile rubber gloves
Frekote 700-NC mold release	Volatile, flammable Eye, skin, and respiratory irritation	Ventilation, chemical goggles, protective clothing, respirator, and neoprene/nitrile rubber gloves
Super 77 spray adhesive	Flammable Eye, skin, and respiratory irritation	Ventilation, chemical goggles, protective clothing, and gloves
Fiberglass cutting and drilling operations	see Glass fabrics Hand entrapment	Ventilation, dust mask, safety glasses, and protective clothing No gloves
Resin transfer molding and hand lay-up	Chemical release under high pressure and/or potential chemical splashing	Ventilation, chemical goggles, protective clothing, respirator, and neoprene/nitrile rubber gloves

fiberglass scrap, cured polyester resin, and excess fabric to be used in their proprietary process of making recycled products. The Amour Fiber Core corporation assists in salvaging a small portion of the millions of tons of composite excess discarded every year to manufacture innovative planks, pilings, tables, benches, and roofing tiles from reclaimed materials. The assistance of Amour Fiber Core Inc. allowed for responsible action during fiberglass structure manufacturing, while providing a valuable material for further fabrications.

Physical and Mechanical Property Test Matrices

The experimental processes, lay-ups, fabrics, sample lots, and test types used in the composites manufacturing evaluation are shown in Tables 8 - 12. A variety of motives, rationale, and tests were considered in developing these experiments for the geometries under investigation. The objectives with all of the physical and mechanical investigations were to quantify any measurable differences between the hand lay-up and RTM processes.

Flat Plate Experiments

The flat plate geometry was chosen for evaluating hand lay-up and resin transfer molding because of its resemblance to the leading edge of the blade cross section illustrated in Figure 25. The T-stiffener and I-beam geometries were also critical components of the turbine blade cross-section (Figs. 26 - 27). Flat specimens were examined for physical qualities and mechanical properties to lay the groundwork for
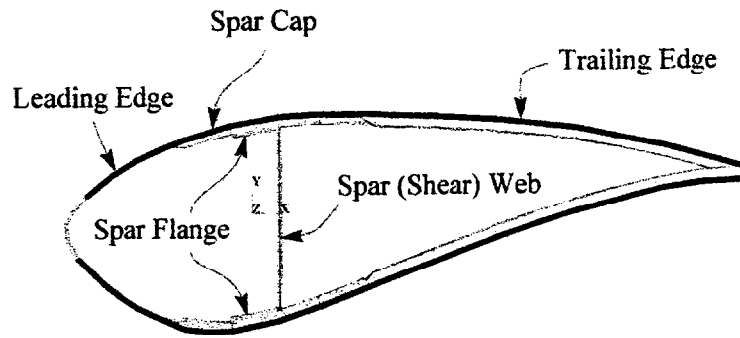
Figure 25. Skin (plate) surfaces in blade cross-section.
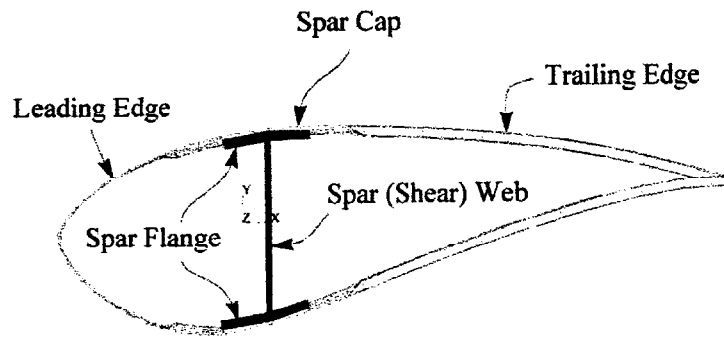
Figure 26. T-stiffener and skin interface in blade cross-section.
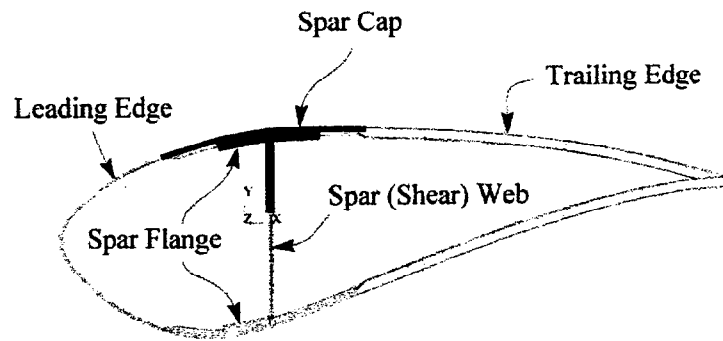
Figure 27. I-beam load carrier in blade cross-section.

51

investigating the more complicated geometries. Mechanical tests were necessary to define the moduli, ultimate strengths, damage initiations, and final failures for a variety of testing configurations. These properties helped to define the performance of more complicated composite substructures. Physical investigations with flat plate specimens provided the thickness, fiber volume fraction, weight, and cycle time data that were necessary in comparing the hand lay-up and RTM processes.

Transverse tensile, compressive, three-point bending, axial tensile, and fatigue testing configurations were chosen because they define the primary mechanical properties for composite materials (Table 8). These tests were also chosen because they have been conducted in previous research on carbon fiber reinforced plastics [40-44]. Though the materials and architectures are drastically different in the fiberglass composites studied herein, it was useful to define the mechanical performance for glass fiber reinforced plastics as they relate to different manufacturing processes. The background literature suggests that the transverse tension, compression, and bending tests will yield results that are heavily dependent on pore size and quantity [37]. These tests are anticipated to have significant differences between hand lay-up and RTM, and may be useful in distinguishing between processes on a mechanical performance basis. The strengths of composites in the uniaxial direction are largely dependent on the quantity of zero degree fibers, and are little influenced by matrix strength or void content [1]. Consequently, small deviations were expected for zero degree tensile results, but were performed because of the property's importance in composite analysis. Fatigue tests were

Table 8. Flat plate mechanical testing matrix.

Mechanical Test	Process	Lay-up Schedule	Zero Fabric	No. of Samples	Motivation
Bending	HL	[0/+45/0]s	D155	5	Pearce suggests a 30% reduction in bending strength for first 1% of porosity [37]. Will similar results be found for these glass-fiber composites and RTM equipment?
			A130	5	
		[0/0/+45/0]s	D155	5	
			A130	5	
	VARTM	[0/+45/0]s	D155	5	
			A130	5	
		[0/0/+45/0]s	D155	5	
			A130	5	
	RTM	[0/+45/0]s	D155	5	
			A130	5	
		[0/0/+45/0]s	D155	5	
			A130	5	
				60 total	
Transverse tension	HL	[0/+45/0]s	D155	5	Test that is heavily dependent on matrix strength and its reduction due to porosity.
			A130	5	
		[0/0/+45/0]s	D155	5	
			A130	5	
	VARTM	[0/+45/0]s	D155	5	
			A130	5	
		[0/0/+45/0]s	D155	5	
			A130	5	
	RTM	[0/+45/0]s	D155	5	
			A130	5	
		[0/0/+45/0]s	D155	5	
			A130	5	
				60 total	
Compression	HL	[0/+45/0]s	D155	5	Porosity effects should show up significantly with this test. Have compression test results been published before?
			A130	5	
		[0/0/+45/0]s	D155	5	
			A130	5	
	VARTM	[0/+45/0]s	D155	5	
			A130	5	
		[0/0/+45/0]s	D155	5	
			A130	5	
	RTM	[0/+45/0]s	D155	5	
			A130	5	
		[0/0/+45/0]s	D155	5	
			A130	5	
				60 total	

Table 8 (continued). Flat plate mechanical testing matrix.

Mechanical Test	Process	Lay-up Schedule	Zero Fabric	No. of Samples	Motivation
Tension	HL	[0/+45/0]s	D155	5	3% reduction in tensile strength for first 1% in porosity. Will this be notable between the methods of manufacturing?
			A130	5	
		[0/0/+45/0]s	D155	5	
			A130	5	
	VARTM	[0/+45/0]s	D155	5	
			A130	5	
		[0/0/+45/0]s	D155	5	
			A130	5	
				40 total	
Fatigue	HL	[0/+45/0]s	D155	5	Has the effects of porosity on fatigue between quantified and if not are the effects measurable?
			A130	5	
	VARTM	[0/+45/0]s	D155	5	
			A130	5	
				20 total	R: -1 approx. 100k cycles

performed with mixed tension and compression to reproduce the loadings found in typical wind turbine blade components.

VARTM, RTM and hand lay-up processes were varied for the transverse tensile, compressive, and bending tests. It was of interest to include VARTM in these tests because results could be found for nearly void free composites. Testing preparation and time constraints precluded comparisons in tension and fatigue, however.

For the mechanical testing of flat specimens fabricated from the three methods under investigation, lay-up schedule and unidirectional fabric were varied. Lay-up schedules were varied between [0/±45/0]s and [0/0/±45/0]s. The lay-up schedule denotes the fabric orientation and sequence for a given laminate. For example, the [0/±45/0]s lay-up suggests a six ply laminate that is symmetric about its midplane and contains four 0° plies and two ±45° plies. The first lay-up was chosen because it is the most frequently found in the MSU fatigue database. The second schedule includes two additional zero

degree plies and allowed for comparisons in fiber volume between RTM'd laminates of identical thickness and varying lay-up. This second schedule was also chosen because it is representative of turbine blade designs where a high percent of unidirectional fabrics are typically used (to resist large bending moments). Zero degree fabrics used in the preceding lay-ups were the A130 and D155 reinforcements. A130 was selected because it is the current fabric used in the MSU composite blade design. D155 was chosen because of its better unidirectional properties. UC1018/V was not used in the mechanical testing of flat plate specimens because of its difficulty in manufacturing and limited availability.

Lastly, statistical sample size requires mentioning. At a minimum, five samples of each configuration were tested for the different processes being studied. This sample size yielded reasonable confidence in the average resultant values found, and in many cases much larger groups were investigated. Actual sample lot sizes are presented along with their paired results in the Experimental Results chapter.

The physical property studies for flat plate specimens included thickness deviations, cycle times, porosity profiles, and wash-out thresholds. In preparing all of the aforementioned mechanical testing specimens, thicknesses were recorded and later compared according to fabric, lay-up, and process. This analysis provided evaluations between laminate thickness tolerances and fiber volume fraction variations. These two parameters are directly related to bond line tolerances, composite uniformities, blade weights, and strength. Cycle times were another parameter compared between hand lay-up and RTM in this study. This investigation assisted in quantifying the time required to

manufacture flat plate specimens using both processes. This information could then be reduced to find approximate daily volume outputs and costs of parts. Thickness variations and cycle times were measured for all of the composite substructures and are presented in the Experimental Results chapter under the Physical Property Comparisons section. The final topic under investigation with flat plate specimens was wash-out threshold for RTM injections. Fabric washout is undesirable distortion or movement of the glass fabric preform initiated by excessive pressure gradients in the RTM process. This condition compromises the mechanical strength of RTM'd substructures, and it is worthwhile to determine when washout occurs. Defining the general trends in washout behavior could also be beneficial to current research into RTM flow modeling [45]. Lay-up schedule, fabric type, and injection location were varied in the current plate washout study. The [0/±45/0]s and [0/0/±45/0]s lay-up schedules were used along with the A130, D155, and UC1018/V fabric reinforcement types, to gather a broad sampling of washout results. Injection location was another variable studied because it was suspected that it also plays a role in fiber washout behavior.

Thin Flanged T-Stiffener Investigations

The thin flanged T-stiffener geometry was chosen for the current study to represent the spar web to blade skin joint of composite wind turbine blades (Fig. 26). A critical mechanical test for this geometry is the stiffener pull-off test. This testing configuration demonstrates the behavior of spar flange and skin layer delamination, geometry stiffness, initial damage, and ultimate load capabilities of this structural detail [46]. The T-stiffener pull-off test is important to wind turbine blade substructures

because it quantifies a common failure mode in composite blades. It is also useful to study skin/stiffener delamination because this damage is difficult to detect for blades in service.

Comparisons between hand lay-up and RTM for this geometry investigated whether manufacturing process would have any effects on skin stiffness and consequently, the pull-off behavior of the thin flanged stiffener geometry. The pull off lay-up, fabric type, and bond interfaces were varied to investigate this concern (Table 9). The evaluation of hand lay-up and RTM for this geometry was made with only one fabric lay-up schedule. A $[\pm45/0_2/\pm45]s$ lay-up was chosen since it performed well in previous research [46]. The A130 and D155 fabrics were used based on the same rationale developed for flat plate testing. The last variable considered in the T-stiffener designs was bond interface. This variable was explored because it was unknown how the bonds between textured surfaces of hand lay-up laminates would compare to the adhesion of

Table 9. Thin-flanged stiffener testing matrix.

Mechanical Test	Process	Zero Fabric	Part Adhesion	No. of Samples	Motivation
Stiffener pull-off	HL	D155	co-cured	5	What effects might porosity and skin stiffness reduction have on the interface?
			secondary (2)	5	
			secondary (3)	5	
		A130	co-cured	5	
			secondary (2)	5	
	RTM	D155	co-cured	5	Is surface finish directly related to the bond strength at the stiffener?
			secondary (2)	5	
		A130	co-cured	5	
			secondary (2)	5	
				45 total	

Secondary (2) - Secondarily bonded in two components
Secondary (3) - Secondarily bonded from three components

smooth or co-cured RTM surfaces. To accommodate hand lay-ups for this geometry, the three different hand lay-up techniques were employed as described in the earlier T-tooling section. Five samples of each test listed in Table 9 were fabricated to produce a minimum sampling size for statistical comparisons.

Thick Flanged T-Stiffener Tests

The thick flanged T-stiffener geometry represents the spar web to blade skin intersections where a built-up spar cap is used (Fig. 26). The T-stiffener pull off test was used to quantify the mechanical behavior of this substructure. However, the results were anticipated to be quite different than those found with the thin flanged geometry. Haugen demonstrated that increased bending stiffness at the skin/stiffener interface would result in laminate failures initiating at the flange tip as opposed to the center of the flange halves in the thin flanged T-stiffener scenario [46]. Further details of these findings are presented later.

As in the case of the thin flanged T-stiffener tests, lay-up was not varied (Table 10). Web lay-ups were set at [±45/0₂/±45]s, skin lay-ups at [±45/0/±45]s, and flange cap lay-ups at [±45/0₂/±45/0₂/±45]s. As in previously mentioned tests, the A130 and D155 fabrics were used for comparisons. The sufficient radii of the thick flanged stiffener mold allowed for the wet lay-up of webs and flanges without additional support. Skin and spar cap laminates were also manufactured and in the final step all four components were secondary bonded to complete the T-stiffener geometry. Haugen's results showed that bond thicknesses of 0.15 mm or less did not play a role in the mechanical

performance of this geometry when manufactured by RTM [46]. Therefore, only co-cured RTM specimens were compared against hand lay-up stiffeners.

Table 10. Thick flanged stiffener mechanical testing matrix.

Mechanical Test	Process	Zero Fabric	Part Adhesion	No. of Samples	Motivation
Stiffener pull-off	HL	D155	secondary (4)	5	What effects might porosity and skin stiffness reduction have on the interface?
		A130	secondary (4)	5	
	RTM	D155	co-cured	5	
		A130	co-cured	5	
				20 total	

Secondary (4) - Secondarily bonded from four components

I-Beam Evaluations

The I-beam geometry represents the spar web and cap components of the current blade design (Fig. 27). This geometry is a primary structural segment of the total blade design, because it carries a significant portion of the bending loads generated by wind pressure and vibratory loading. Fatigue testing was conducted for this geometry because results could be compared with an existing database [47]. Further details on test preparation complexity are given in the next section. The mechanical testing of the I-beams was anticipated to quantify the effects of manufacturing process, porosity levels, and web to flange radii on structural performance.

The web and skin lay-ups of [±45/0/±45]s and [0/±45/0]s, respectively, were successful in previous fatigue research and were used for this manufacturing study [47]. The D155, A130, and UC1018/V zero degree fabrics were utilized for RTM vs. hand lay-up comparisons (Table 11). The beam structure was a much more complicated geometry than either the flat plates or T-stiffeners and required substantial manufacturing time.

Consequently, only three of each of the RTM specimens and two of the hand lay-up

beams were manufactured for this substructural comparison.

Table 11. I-beam fatigue testing matrix.

Mechanical Test	Process	Zero Fabric	No. of Samples	Motivation
Fatigue	HL	D155	2	What effects might porosity and sharp radii have on the strength of this complex geometry?
	RTM	D155	3	
		A130	3	
		UC1018	3	
			11 total	

Root Specimen Studies

The root specimen developed herein represents a single insert of a completed root

to hub joint (Fig. 24). This research laid the foundation for future studies into developing

the completed oval root substructure. Hand lay-up and RTM specimens were tested in

static tension and fatigue (Table 12). The comparison between processes determined

whether wet-out technique played a critical roll in the adhesion of the steel insert to the

composite laminates. Tensile tests measured the ultimate load of root specimens and how

they fared against the design limit load of 89 kN per insert, prescribed by McKittrick's

Finite Element Analysis results [3]. Fatigue tests determined the lifetimes and failure

modes of root specimens under repeated loading.

The root specimen was unlike the previous substructures in that previous work

had not been conducted and adequate material combinations had not been developed

prior to this study. Consequently, much of the work concerning the root involved finding

fabric and lay-up combinations that would fill the RTM mold with an adequate fiber

Table 12. Root testing matrix.

Mechanical Test	Process	Zero Fabric	No. of Samples	Motivation
Tensile	HL		2	What effects might porosity and fiber volume have on bonding between the insert and root assembly?
	RTM		2	
	HL	D155	1	
Fatigue	RTM		6	
			6 total	

volume content and with proper alignment. Difficulties arose from applying the same lay-up schedule as the original hand lay-up template. Low fiber volumes were found on either side of the insert and these were dealt with by adding triaxial fabric. Knytex CDB200 triaxial reinforcement is a heavy fabric (678 g/m^2) that works well in boosting fiber volume with few layers, and was incorporated into the root lay-up at either side of the insert.

The final lay-up for the root sample was [±45/0/±45/0$_2$/±45]s for the inner surface laminate (which follows the contoured root insert) and [±45/0$_2$/±45]s for the skin surface laminate. Small sections of fabric were added about the steel insert to address the low fiber volume issues that were encountered. An illustration of the reinforcement lay-up near the steel insert is given in Figure 28. Underneath the insert as it tapers down in diameter, 8 layers of CDB200 warp, triaxial fabric were included to assist in transitioning between the inner surface and outer skin laminates. These layers of fabric were cut 191 mm in length, with widths tapering down from 76.2 to 25.4 mm. Fabric plies were also carefully oriented such that no two layers were dropped at the same location. This technique assisted in minimizing undue stress concentrations [3,5]. Alongside the insert, two fabric build-ups were required to achieve satisfactory fiber volumes. First, fabric
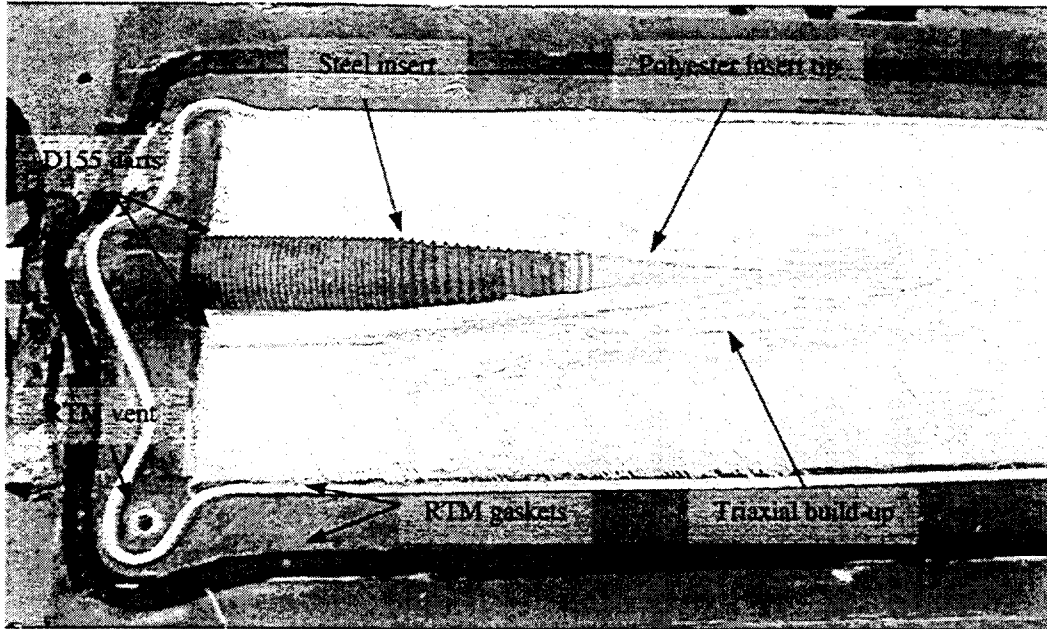
Figure 28. Example of root insert lay-up with dry fabric preform.

"darts" were inserted that had been used in the original hand lay-up template. The darts were fabricated from 356 mm wide sections of D155 fabric that were 305 mm long. These pieces were then cut at a 45° angle and rolled up to form a dart shaped reinforcement. Darts were included on both sides of the steel insert to assist in laminate transitioning. Through the iterative process of testing fiber volumes for the root specimens, it was found that fabric darts were not adequate for filling these areas with acceptable fiber volume fractions. Consequently, four additional strips of triaxial reinforcement were laid underneath the D155 darts (between the dart and skin surface) on either side of the steel insert. These narrow strips were 51 mm in width and tapered in length from 229 to 305 mm.

The addition of darts, strips, and small fabric pieces allowed for better uniformity in fiber volume over the total root geometry. But in the event similar geometries are

manufactured in the future, minimizing the number of these intricate pieces would be desirable. Fabric placement was cumbersome at times, variability was greatly increased, and time associated in fabric lay-up was magnified. For the current root mold, changes in fabric lay-up for a moderate number of specimens required less effort than changing mold geometry. However, from a manufacturing standpoint, it was observed that complicated lay-ups were more likely to introduce inconsistencies, and simplifying fabric lay-ups drastically reduced molding cycle times. The complicated lay-up also determined that the number of specimens for this geometry would be less than those manufactured for the flat plate and T-stiffener geometries. This observation underscores the need for preform research in RTM manufacturing.

Testing Equipment and Procedures

The wide variety of geometries evaluated for hand lay-up and RTM manufacturing necessitated a breadth of testing equipment and procedures. All of the flat plate, T-stiffener, I-beam, and root matrix burn-off experiments followed ASTM standard D2584 for fiber volume fraction calculations. Trimming and preparation of all samples was done with a 203 mm diameter, diamond blade circular saw. This table saw was equipped with a water system that provided cooling, flushed material away from the blade circumference, and minimized the number of particles released into the air. In addition, specimens less than 559 mm in length were cured in an oven at 60° C for two hours; samples longer than 559 mm were allowed to cure at ambient temperatures for at least seven days prior to testing.

Flat Plate Testing

The variety of mechanical tests performed on the flat plate specimens as well as the variables explored for each experiment was shown in Table 8. Specimen dimensions and testing specifications for these experiments are outlined in Table 13. All of the information contained in this table followed ASTM standards and Samborsky's recommendations [48]. For the mechanical tests, Instron 8562 servo-electric and 8501 servo-hydraulic universal testing machines were employed. The Instron 8562 was used for static testing, while the 8501 machine was used for fatigue testing. Instron extensometers 2620-524, 2620-525, and 2620-26 were used to measure strain during testing of axial and transverse tensile specimens (Fig. 29). Testing gage lengths for all of the above extensometers was 12.7 mm. For the bending tests, a Lebow model 3132,

Table 13. Flat plate mechanical testing specifications.

Test Type	Specimen Specifications		Testing Specifications		
	Length (cm)	Width (cm)	Gauge Length (cm)	Testing Rate (cm/min)	Sampling Rate (Hz)
Transverse Tension	20.3		12.7	0.3	5
Bending	15.2		12.7	1.3	4
Compression	10.2	2.8	1.3	76	--
Tension	8.3		12.7	0.3	10
Tensile Fatigue	8.3		1.3	–	6

2.2 kN load cell was run in series with the Instron 8562 load cell for greater precision. It should also be noted that fatigue samples were tested in reversed tension and compression loading (R value of –1, where R = maximum load/minimum load). This testing strategy was chosen because it represents the worst case, fully reversed wind

loading of turbine blades [3,5]. D155 and A130 fatigue samples were tested at $\pm$172 and $\pm$138 MPa, respectively, at 6 Hz. At these stresses the average fatigue lives approximated the target average of 100,000 cycles. For all of the mechanical tests summarized in Table 13, grip clamping pressures were chosen that would adequately hold the specimens without crushing them.

T-Stiffener Testing

Thin and thick flanged T-stiffeners were tested statically with the Instron 8562 and a T pull-off jig (Fig. 30). Loads were relatively low for stiffener pull-off, thus the Lebow 2.2 kN

Figure 29. Flat specimen testing with extensometer.

load cell was mounted "piggyback" to the standard 100 kN Instron load cell. The T-stiffener pull-off tests consisted of gripping the upper 38 mm of the T-web and applying a tensile load while the skin was debonded. The T-stiffener specimens and the dimensions of the testing supports are illustrated in Appendix B. The skin was simply supported at two locations with a spacing of 127 mm. Test specimens were approximately 28 mm in width. The T-stiffener testing jig also allowed for rotation at the points of contact with the skin. This condition did not bias the tensile pull-off loads with frictional forces. Secondary bonded specimens used Hysol EA 9309.2NA epoxy for the secondary

adhesive. They were cured for an additional 2 hours at 60° C to allow for the full cure of the adhesive prior to testing.
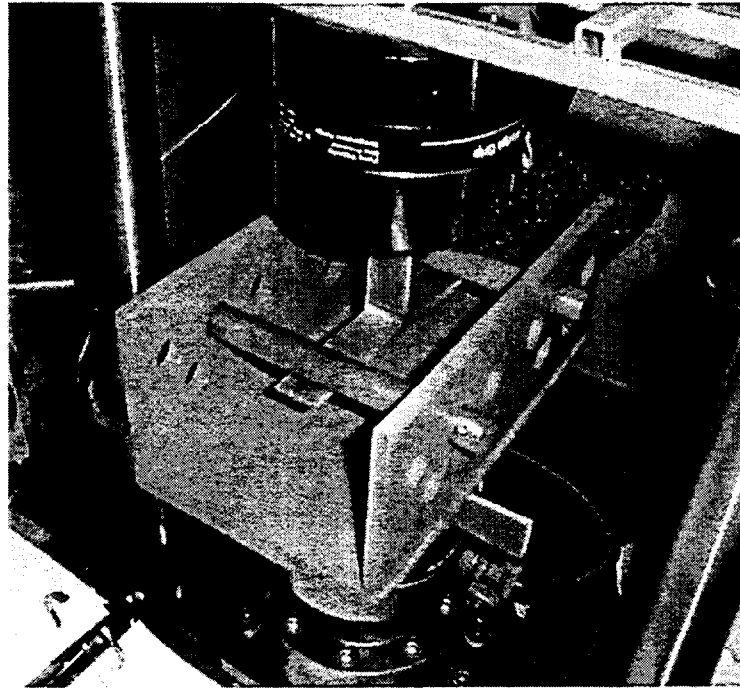
Figure 30. Thin flanged stiffener pull-off test with jig.

I-Beam Testing

I-beams were tested in four point bending fatigue with the Instron 8501 testing machine (Fig. 31). To transmit the large bending moments, and to localize failure to the center gage section, a series of load pads and stiffeners were bonded to the beams prior to testing per Mandell and Samborsky [47]. In Figure 32, the number of and location of the additional composite material used to reinforce the beams for testing is illustrated. Reinforcing the I-beam geometries as such was labor and time intensive. Stiffeners and pads were carefully trimmed, bonded, secured, and then cured for each I-beam under investigation. These secondary procedures motivated a test that would generate as much
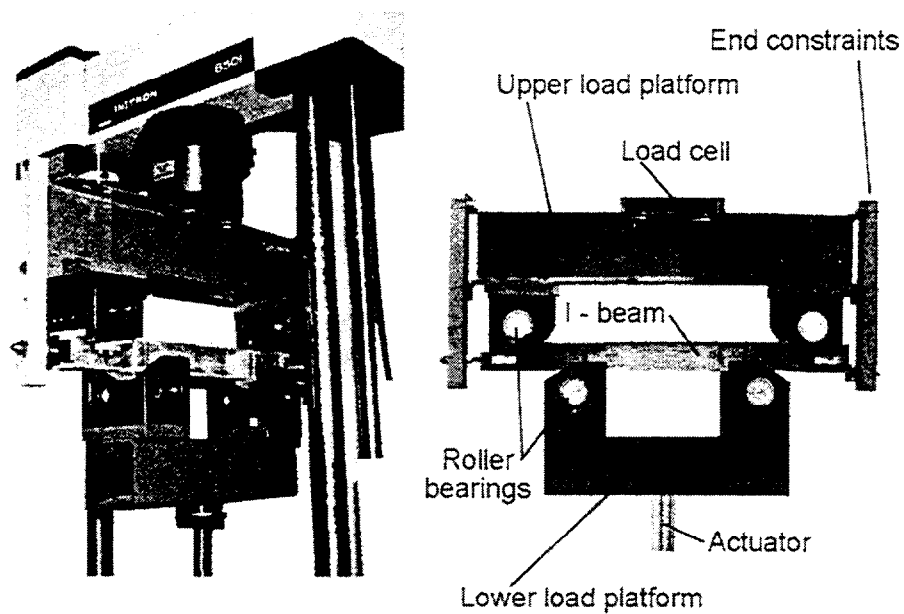
Figure 31. Composite I-beam testing apparatus.
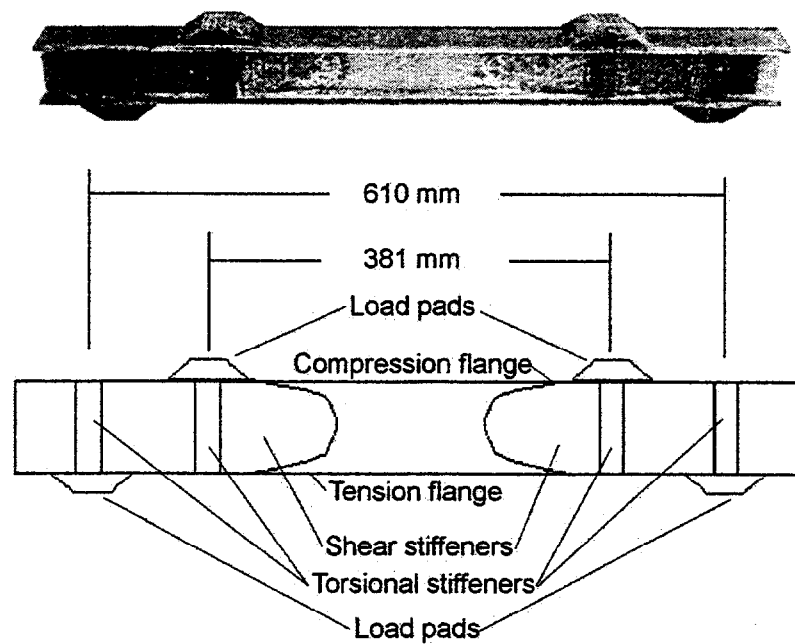
Figure 32. I-beam test geometry and stiffener locations.

67

useful data as possible. Hence, fatigue testing was chosen. Fatigue tests with an R value of 0.1 performed at 5 Hz allowed for observation of delamination initiation as well as fatigue cycle lifetime. The Instron 8501 required the retrofit of a four point bending jig to allow for the I-beam testing [47]. With the hydraulic grips removed, a W18x150 I-beam with 51 mm diameter roller bearing supports was mounted to the top half of the testing machine, while a 127 x 127 x 6.35 mm rectangular, hollow, structural section with roller bearings was located in the lower half. This jig allowed for four point bending fatigue with a support span of 610 mm on the upper I-beam and 381 mm on the lower rectangular section. End constraints of square tubing were also used to eliminate lateral translation of the I-beam while being fatigued in the fixture.

Root Specimen Testing

The root specimen geometry was mechanically tested in static tension and fatigue. Tensile tests were performed on a Baldwin 890 kN, hydraulic universal testing machine (Fig. 33). Specimens were necked down away from the insert to a width of 89 mm for gripping purposes. The insert end of the sample used a 19.1 mm diameter, grade 8 bolt to transmit tensile loads. The gage length of these specimens was 533 mm. Root specimens were loaded to failure and the ultimate loads were monitored with an internal pressure transducer. Root fatigue specimens were tested on an MTS 880, 245 kN, servo-hydraulic testing machine. Instron 8800 electronics were used to monitor load and fatigue life. Fatigue samples were secured with 203 mm wide grips at the end opposing the insert and did not require necking. Insert ends for the hand lay-up and RTM root specimens were

secured with 19.1 mm diameter bolts and gage lengths were 552 mm. Samples were

tensile fatigue tested at an R value of 0.1 with a maximum load of 89 kN.
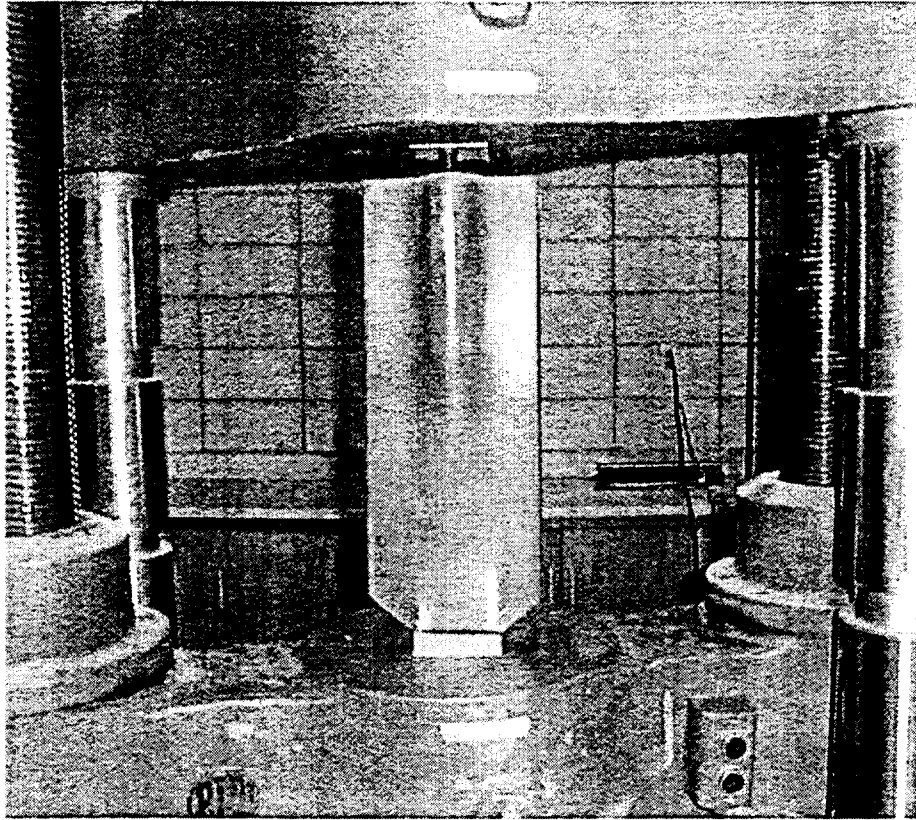
Figure 33. Root static tensile testing with Baldwin 890 kN testing machine.

Statistical Comparison Methods

The variety of geometries and tests in the current study generated a substantial

amount of mechanical property data with which to compare hand lay-up and RTM.

Consequently, a standardized method of determining significant differences in structural

performance according to process was necessary. Modern statistical evaluation

techniques were used to accomplish this task. A total of four statistical tests were used to

compare pairs or larger sets of property data for significant differences. Statistical

methods allowed for the documentation of significant differences between hand lay-up and RTM for each set of testing, fabric, and lay-up combinations. The terminology used to describe the statistical results found in the next chapter are [49]:

- Normality: likelihood that a sample follows a normal, bell-shaped, Gaussian distribution.

- P Value: probability of being wrong when asserting that a difference exists. Small P values (<0.05) suggest a difference, while P values approaching 1 suggest no difference.

- Equal Variance: hypothesis that samples were drawn from populations with similar variability and deviation.

- T-Test: parametrical test used to determine if there is a difference between two groups that is greater than what can be attributed to random sampling variation.

- Mann-Whitney Rank Sum Test: nonparametric test to find whether two samples are not drawn from populations with different medians when normality or equal variance are not present in samples.

- One-Way ANOVA: used to explore whether two or more different experimental groups are from similar populations when the samples are normally distributed and of equal variability.

- Kruskal-Wallis ANOVA on Ranks: nonparametric test to compare several experimental samples for population similarity when normality and equal variance are not present.

With the experimental methods summarized, the results for physical property and mechanical behavior can be reviewed for the hand lay-up and resin transfer molding manufacturing processes.

CHAPTER 4

EXPERIMENTAL RESULTS AND DISCUSSION

RTM and Hand Lay-up Physical Property Comparisons

Evaluation of variations in laminate thickness, fiber content, cycle time, and porosity for hand lay-up and RTM composites were the focus of the physical property comparisons. These experiments were performed for all the geometries under investigation to determine what effects processing would have on strength to weight ratio, manufacturing time, repeatability, and defect quantity. This section concludes with a study of the RTM molds used in the manufacture of the five geometries. The advantages and limitations of each mold are summarized and discussed at length.

Thickness, Fiber Content, and Weight

Thickness and fiber volume content are parameters that significantly contribute to the strength to weight ratios of composites [1,4,6,7]. The strength to weight ratio of individual components and the thickness of the bondlines used to join them will determine the overall structural performance of a given blade versus its weight. This is important to wind turbine blade manufacturing, as well as to other composites fabrications. In turbine blade applications, increased weight results in higher system costs. Thus, a process's ability to reduce thickness and improve fiber volume content in

flat plates and substructures will improve a turbine's performance and reduce its cost. In addition, minimizing or eliminating the number of bondlines for turbine components can increase performance while reducing unnecessary weight and labor. Fewer bonds will also reduce the number of expensive bonding jigs that need to be constructed and maintained. These variables were studied for flat plate and more complex geometries.

Flat Plates. In Tables 14 – 15, the thicknesses and fiber volumes for the laminates used in mechanical testing are summarized. The data shown in these tables were gathered from approximately 33 specimens taken from at least two plates for each lay-up, fabric, and process combination. A complete listing of the flat plate, mechanical test specimen thicknesses can be found in Appendix A. All VARTM laminates were manufactured from the same mold and therefore have almost identical thicknesses. Hand lay-up did not have this advantage and in an effort to determine thickness variability for hand lay-up fabrications, two operators processed each of the plate types. This practice attempted to remove any bias the individual operator's experience might have on the thickness of hand lay-up laminates.

The results of Table 14 show the average thickness, range, and standard deviation for the flat plates studied. Both hand lay-up and VARTM plate thicknesses were gathered and tabulated. Reviewing this table shows that reductions in average thickness and range were improved for all VARTM laminates over the hand lay-up baseline. The [0/±45/0]s lay-ups experienced some thickness decrease (0.01 mm for laminates with D155 fabric and 0.25 mm for A130), while thickness reductions were more substantial in the thicker [0/0/±45/0]s laminates (1.5 mm for D155 and 1.2 mm for A130).

Table 14. Thickness results for flat plate laminates.

Lay-up	Fabric	Process	Mean Thickness (S.D.) mm	Thickness max. mm	Thickness min. mm	Range mm
[0/±45/0]s	D155 / DB120	VARTM	3.25 (0.09)	3.43	3.07	0.36
		HL	3.26 (0.17)	3.68	3.07	0.61
		VARTM*	3.74 (0.21)	4.04	3.25	0.79
[0/±45/0]s	A130 / DB120	VARTM	3.09 (0.08)	3.23	2.95	0.28
		HL	3.34 (0.14)	3.58	3.08	0.50
[0/0/±45/0]s	D155 / DB120	VARTM	3.27 (0.10)	3.48	3.02	0.46
		HL	4.84 (0.23)	5.34	4.39	0.95
[0/0/±45/0]s	A130 / DB120	VARTM	3.34 (0.12)	3.57	3.15	0.42
		HL	4.11 (0.32)	5.21	3.62	1.59

VARTM - Vacuum-Assisted Resin Transfer Molding
HL - Hand Lay-up
S.D. - Standard Deviation
* Cure without injection port ventilation, see text.

Table 15. Fiber content results for flat plate laminates.

Lay-up	Fabric	Process	Mean Fiber Volume (S.D.) %	Fiber Volume min. %	Fiber Volume max. %	Range %
[0/±45/0]s	D155 / DB120	VARTM	34.4 (1.6)	32.7	36.1	3.3
		HL	34.3 (3.2)	30.4	36.1	5.6
		VARTM*	29.9 (4.0)	27.1	34.4	7.3
[0/±45/0]s	A130 / DB120	VARTM	32.2 (1.1)	31.2	33.2	2.0
		HL	30.5 (2.1)	28.7	32.3	3.6
[0/0/±45/0]s	D155 / DB120	VARTM	48.9 (2.6)	46.3	52.3	6.0
		HL	33.0 (3.4)	29.8	36.7	6.9
[0/0/±45/0]s	A130 / DB120	VARTM	40.6 (2.6)	38.3	42.7	4.3
		HL	33.5 (5.3)	26.2	37.8	11.6

These average thickness findings for hand lay-up and RTM result in notable strength to weight ratio differences in the current MSU composite blade design for the AOC 15/50 turbine. Increases in blade skin weight were predicted for the configuration with the largest difference, the D155 / DB120 fabric, [0/0/±45/0]s lay-up. In both hand lay-up and RTM composites, the glass reinforcement provides the majority of the material's strength. Thus, for the same amount of reinforcement material, thickness remains the primary deciding factor for this laminate's strength to weight ratio. For the [0/0/±45/0]s composite, hand lay-up yielded an averaged 1.5 mm or 15% thicker composite when compared with VARTM. If this lay-up was used in the MSU blade skin design, a difference of 9.5 kg or 15.5% would exist between the hand lay-up and RTM manufactured parts. These results were for a single blade skin and even greater reductions in blade weight would be observed as all the blade components were joined. This prediction demonstrates that seemingly small variations in thickness can have a substantial effect on turbine blade weight due to its notable length and girth.

During the fabrication of the VARTM components, an interesting side result was discovered. In the first round of VARTM moldings, the mold fill port was plugged off to prevent excessive resin from escaping from the mold at the completion of every injection. Later injections where the mold was allowed to drain revealed that the glass surfaces actually deflected a notable amount due to resin pressure. Allowing the mold to drain was found to significantly reduce laminate thickness and thickness variability. These results are shown for [0/±45/0]s laminates with D155 and DB120 fabrics in Table 14. Note that average thickness was increased by 0.5 mm and standard deviations doubled for

VARTM flat plates where glass was used as a molding material and the mold was not allowed to vent during cure. This behavior was first noted by Hedley, continues to be a problem when interested in monitoring flow fronts, and should be avoided if possible in future VARTM and RTM moldings [33].

The results of Table 14 were correlated to fiber volume and presented in Table 15. Since the fiber volume results are directly related to the thickness data of Table 15, the trends of both groups were similar. Average fiber volumes and their variations were improved for all VARTM laminates when compared to hand lay-up, with the more noteworthy differences being found for [0/0/±45/0]s flat plates.

Graphical representations of Tables 14 and 15 are found in Figures 34 and 35. In each figure, the average thicknesses and fiber volumes are shown along with their respective maximum and minimum values. The average values of Figures 34 and 35 present a clear contrast of the thickness and fiber volume differences between laminates manufactured by hand lay-up and RTM. It can also be noted that the range of measured thicknesses and fiber contents for all RTM laminates were significantly less than those recorded for the same composites manufactured by the hand lay-up process. Statistical analysis techniques were used to compare the sets of data. This comparative technique substantiated the trend that can be observed in Figures 34 and 35. No significant difference was detected for [0/±45/0]s plates with D155 fabric, while all the other laminates showed statistical differences between hand lay-up and VARTM. A complete summary of the statistical comparisons is found in Appendix D.
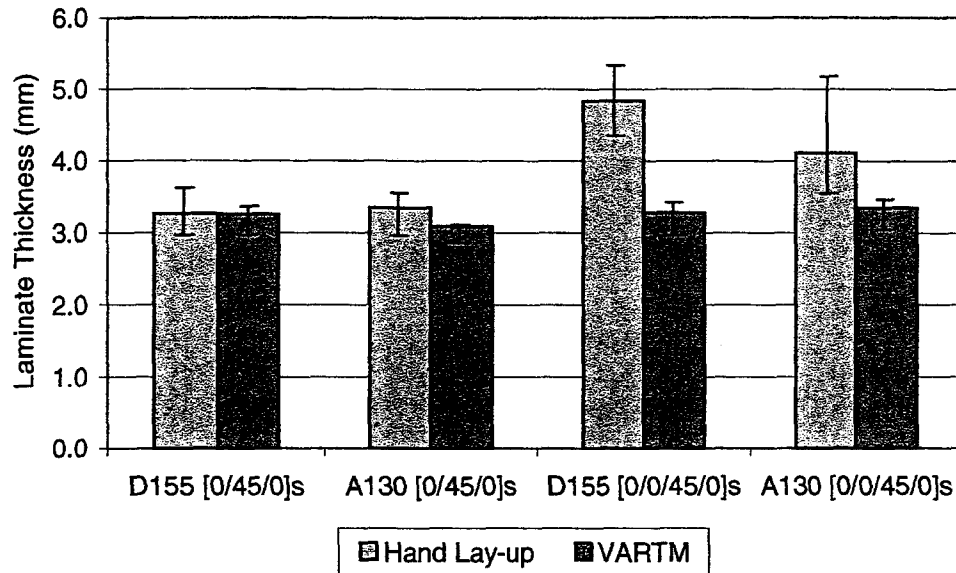
Figure 34. Average flat plate thicknesses with maximum and minimum values.
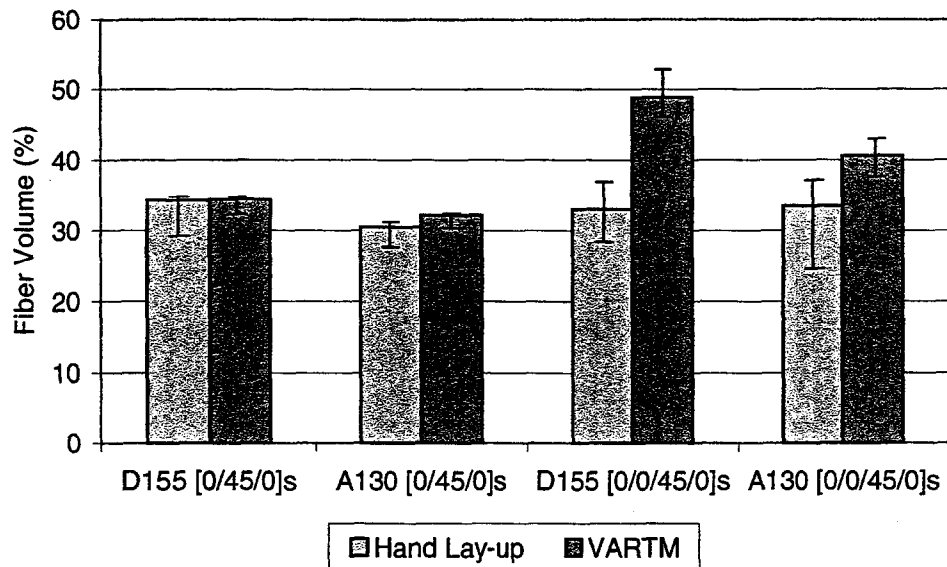
Figure 35. Average flat plate fiber volumes with maximum and minimum values.

In addition to comparing thickness and fiber volume individually, it was useful to present their combined results graphically. Figures 36 and 37 are examples of such correlations. In Figure 36, the ranges of thicknesses and fiber volumes for hand lay-up and VARTM are presented. The data points used in finding the individual curves of this figure were found from composite matrix burn-off tests following ASTM Standard D2584. The fiber volume content data collected can be found in Appendix E. Overall curves were then made and the ranges of thickness and fiber volume were illustrated for each process. It can be seen from Figure 36 that VARTM averages nearly the same thickness for all fabric and lay-up combinations as was first presented in Table 14. The range between maximum and minimum values is similar for all VARTM laminate types and it is notably smaller than the ranges found for hand lay-up plates. Another noteworthy finding in Figure 36 is the hand lay-up fiber volume threshold (Labeled "HL Vf Threshold" in Fig. 36). Maximum fiber volumes between the four laminates appear to vary between 33 and 37%. The information from this figure suggests that there exists a natural attainable fiber volume from this method of hand lay-up and that this value is approximately 35%.

The fiber volume and thickness data are presented again in Figure 37, along with calculated fiber volume vs. thickness equations for the four flat plate laminates. Linear equations were found best suited for the results of the [0/±45/0]s laminates, while [0/0/±45/0]s laminates required quadratic correlations to best fit their broader range of data. These equations were necessary in this study to find the fiber volumes for laminates
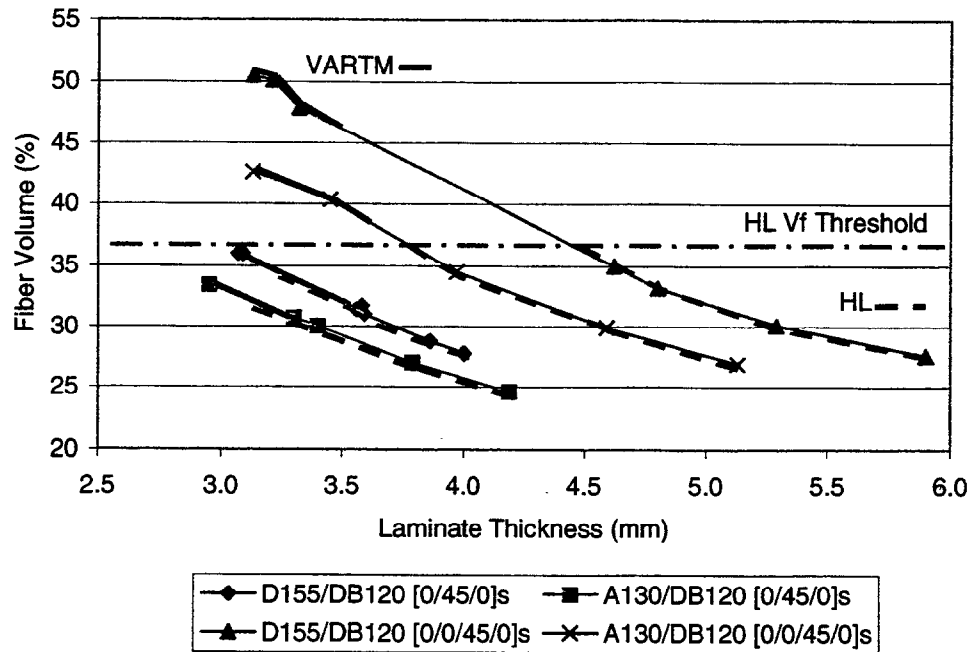
Figure 36. Flat plate fiber volume versus thickness with process ranges.
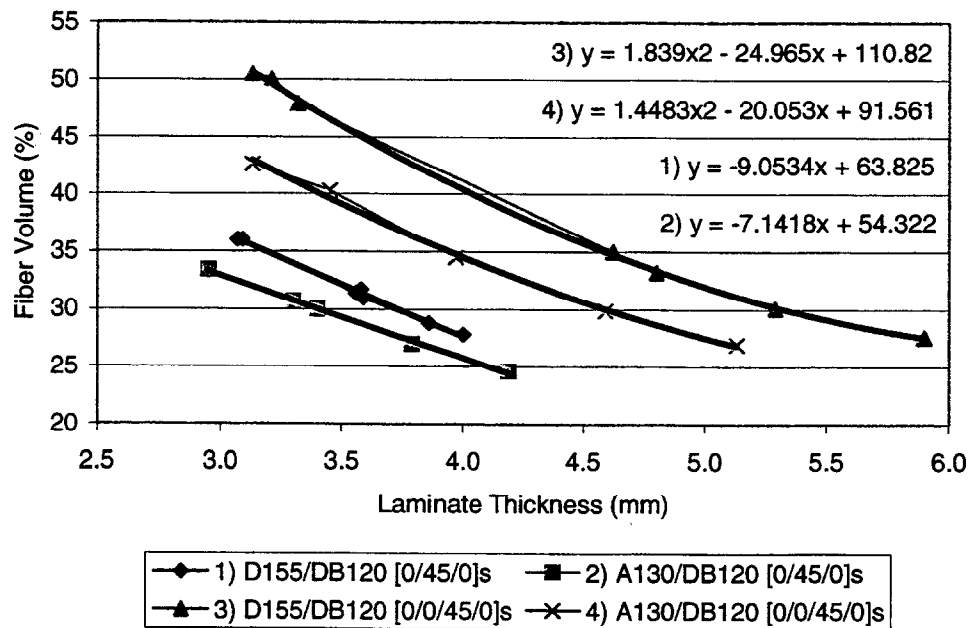
Figure 37. Flat plate fiber volume versus thickness with equations.

of thickness not tested by the matrix burn-off method. They are presented here for future work with these fabrics and lay-ups, and for further research beyond the laminate thicknesses studied in this work. Having access to these equations prior to manufacture could allow designers to prepare RTM molds that accurately yield laminates of a desired fiber volume. This information would eliminate the need to follow an iterative process of making laminates and then revamping tools to adjust the desired fiber volume. However, the equations of Figure 37 are valid only for laminates of identical fabric types and fabric proportions. Fabric architecture and lay-up schedule have different effects upon consolidation of a laminate's reinforcement. Consequently, a database of fiber volumes for a variety of laminates and their thicknesses, is needed to assist composites designers. The matrix burn-off of hand lay-up samples provided additional information for the MSU fatigue database fiber volume equations. Hand lay-up samples of [0/±45/0]s lay-up and D155/DB120 fabric were thicker than had been previously tested for the database, and were added to original data collected by Samborsky [50]. The complete fiber volume versus thickness data set for D155/DB120 [0/±45/0]s laminates are found in Figure 38.

Substructures. Thin flanged T-stiffeners, thick flanged T-stiffeners, I-beams, and root specimens were analyzed for the effects of laminate thickness, bondline thickness, and reinforcement transition radii on substructure weight. In Appendix C, laminate thicknesses, fiber volumes, and equations relating the two are given for these complex substructures. The number of samples fabricated for these cases was significantly less than the number of specimens available for flat plate mechanical testing. Consequently, the amount of matrix burn-off specimens and observed fiber volume deviations were
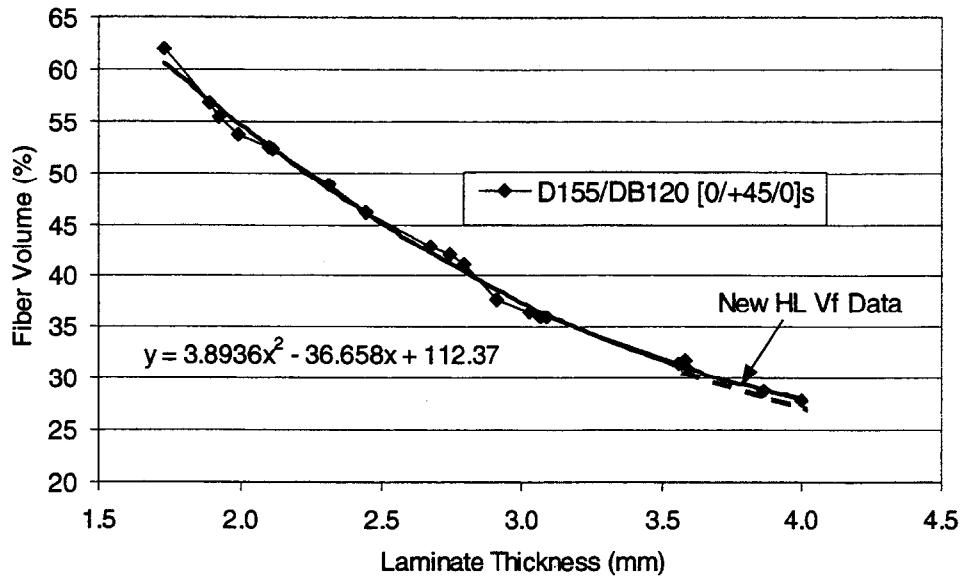
Figure 38. Fiber volume data set for MSU fatigue database laminates.

smaller than noted for the flat plate investigation. Despite the limited results, the matrix

burn-off data played an important role in predicting fiber volume contents in the current

work, and would benefit future designs using any of the fabric and lay-up combinations

shown in Appendix C.

Hand lay-up laminates proved to be consistently thicker for the complex

geometries and thus, increased predicted blade weight over the RTM substructures. Yet

when considering the issue of blade weight, it was found that the greatest contributing

factors were reinforcement transition radius and bondline thickness for three-dimensional

structures. These two effects introduced measurable differences in specimen weights that

were previously unobserved in the flat plate investigations. These issues were quantified

for the composite substructures and differences in specimen weight were determined for

geometries manufactured by the hand lay-up and RTM processes.

In Figures 39 and 40 the cross sections of hand lay-up and RTM thin flanged T-stiffeners are illustrated. From these cross sectional specimens bondline thicknesses, web to flange radii and sample areas were found. The hand lay-up T-stiffener shown in Figure 39 resulted in bond thicknesses ranging between 0.3 – 2.3 mm and a transition radius of 6 mm for hand lay-ups of this geometry. It can be seen from this figure the reinforcement's inability to conform to the mold's 1.8 mm transition radius. At the web to flange transition, the fabric lay-up pulled away from the mold, as discussed earlier in the RTM tool section, resulting in the 6 mm average transition radius. This effect observed for the stiffener reinforcement contributed to the irregularity of the cross section which increased bondline thicknesses and ultimately, the sample's weight.

Examining Figure 40 demonstrates that bondline and transition radius tolerances were much tighter for the RTM thin flanged T-stiffeners. The RTM specimens were manufactured and co-cured in a single step as opposed to the secondary operations necessary for the hand lay-up samples. This advantage could minimize the amount of secondary bonding required in full-scale turbine blades. The use of a closed mold for RTM'd T-stiffeners resulted in a geometry with a tighter and more consistent transition radius (1.8 mm) than observed for hand laid-up samples. Minimizing web to flange radii and eliminating secondary bonds resulted in a reduction of the cross sectional area and the weight for RTM T-stiffeners when compared to the same samples manufactured by hand lay-up.

Total Area: 1592 mm^2
Bond Area: 214 mm^2
Mass: 2.5 kg/m

Max. Bond Thickness: 2.3 mm

Transition Radius: 6 mm

38 mm
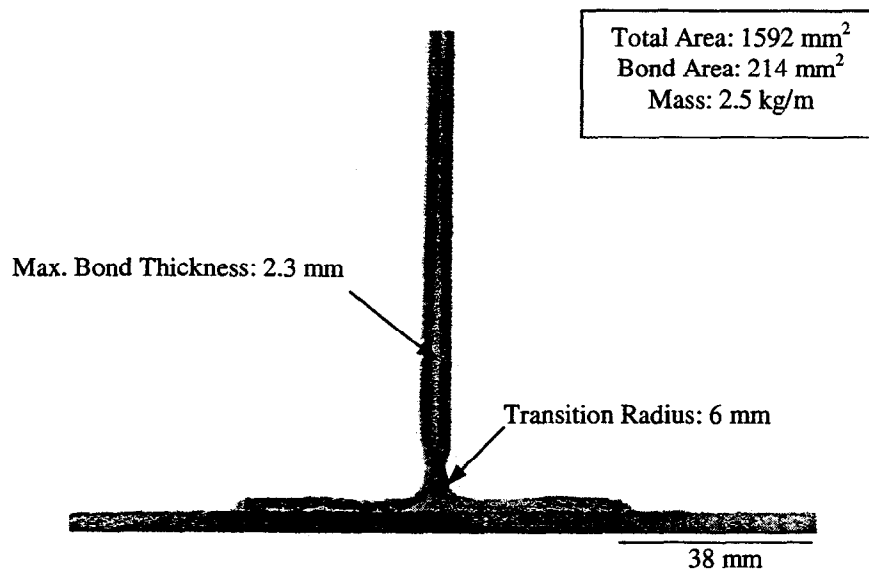
Figure 39. Hand lay-up thin-flanged T-stiffener cross-section.

Total Area: 1206 mm^2
Mass: 1.9 kg/m

Transition Radius: 1.8 mm

38 mm
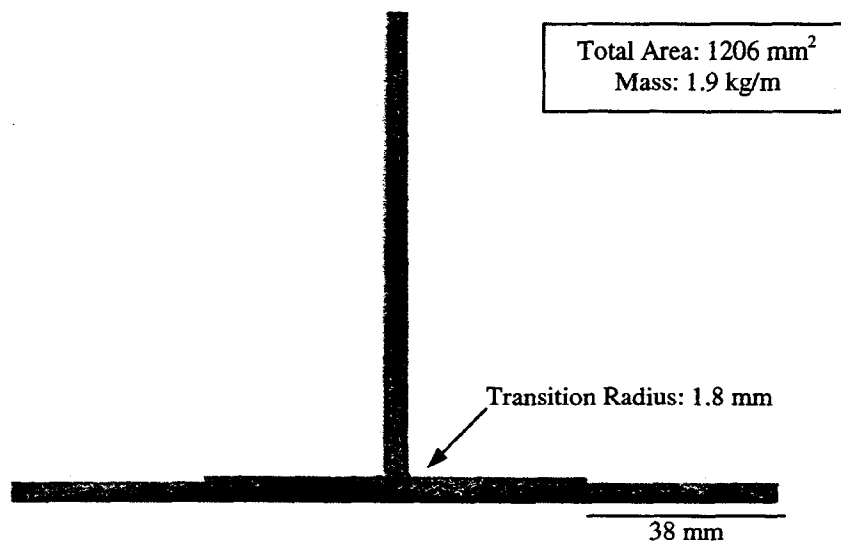
Figure 40. RTM thin-flanged T-stiffener cross-section.

Standard digital image analysis techniques were used to calculate the cross sectional areas of the RTM and hand lay-up samples. The average cross sectional area of the hand lay-up geometry was found to be 1592 mm^2 as compared to the RTM specimen area of 1206 mm^2. The area contributed by secondary bonding materials was also found for the hand lay-up sample. Bond material comprised 214 mm^2 of the hand lay-up sample's area or approximately 13% of the cross section. The difference between total hand lay-up T-stiffener cross section and RTM stiffener area was 386 mm^2 or 24%.

The differences in cross sectional area yielded a significant distinction between hand lay-up and RTM full-scale, thin flanged T-stiffener weights. First, specimen mass per unit length was calculated for the stiffeners according to process. Assuming a composite of 30% fiber volume and thus a density of 1.57 g/cm^3, the masses per meter of hand lay-up and RTM T-stiffeners were found to be 2.5 and 1.9 kg/m, respectively. Multiplying these values by the MSU composite blade stiffener length of 6 meters (Table b, Figure 1) resulted in full-length stiffener weights of 14.9 kg with hand lay-up and 11.3 kg by RTM. This reduction in mass of 3.6 kg (24%) would be observed twice in a hypothetical RTM composite turbine blade of constant cross-section, as this geometry configuration appears at both airfoil surfaces.

Illustrated in Figures 41 and 42 are the cross-sections of hand lay-up and RTM thick flanged T-stiffeners. For this geometry, hand lay-up bondlines were found to vary between 0.2 and 2.2 mm in thickness. Transition radii conformed well to the 6 mm mold radius for both processes investigated.
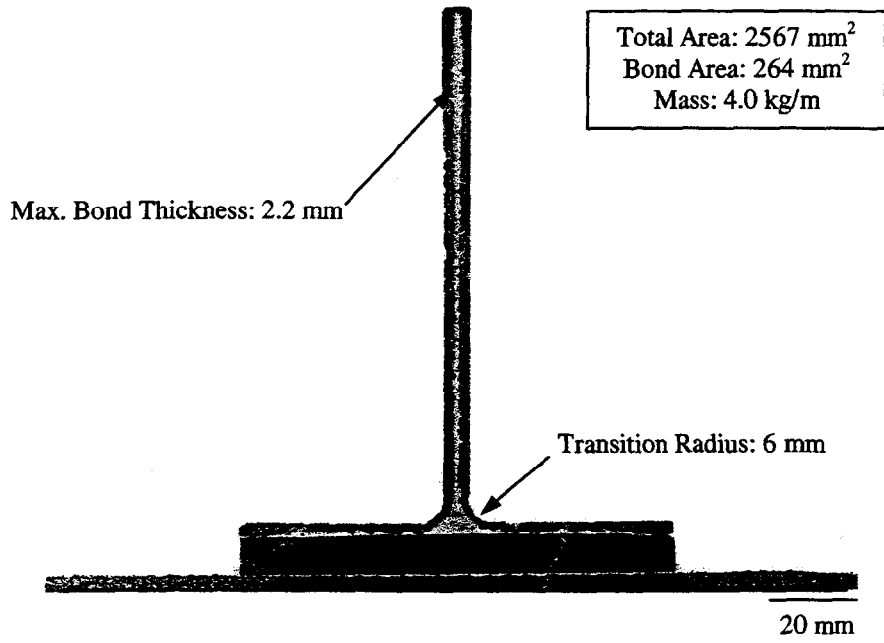
Figure 41. Hand lay-up thick flanged T-stiffener cross-section.
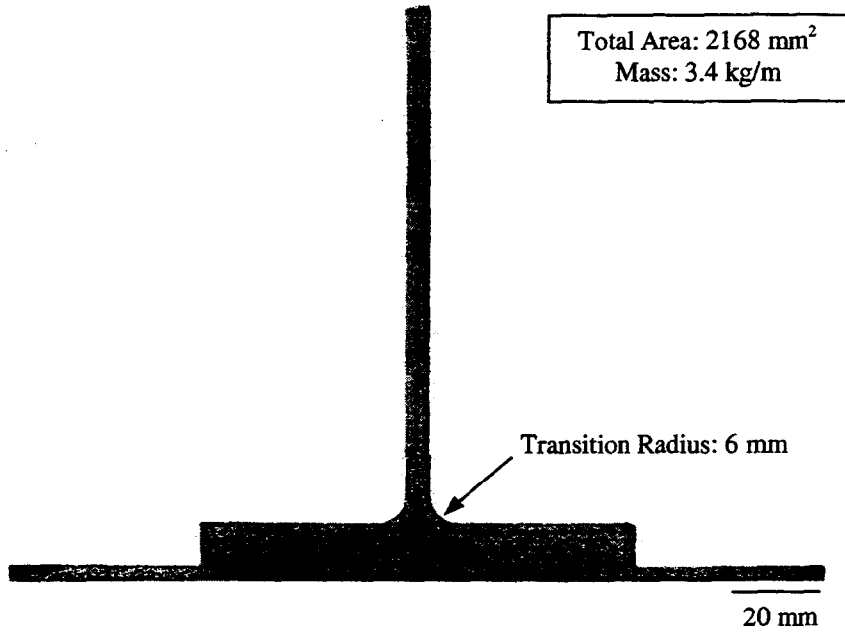
Figure 42. RTM thick flanged T-stiffener cross-section.

The cross-sectional areas of the thick flanged T-stiffeners were 2567 mm^2 for hand lay-up and 2168 mm^2 for RTM specimens. In the hand lay-up geometry, bond material was 139 mm^2 or 10% of the total cross-sectional area. This percentage of bond material is significantly reduced when compared to the thin flanged case and can be attributed to the mold's 6 mm transition radius that better suits hand lay-up. Differences in area between processes were still significant and measured to be 399 mm^2 or 16%. The areas of these stiffener specimens resulted in masses of 3.4 and 4.0 kg/m for laminates of 30% fiber content manufactured by RTM or hand lay-up, respectively. If the thick flanged T-stiffeners are extrapolated to the 6 meter spar length, differences in mass between components would be 3.8 kg or 16 %, according to process. While a greater transition radius was successful in reducing the amount of secondary bonding material required to join irregular geometries, RTM exceeded hand lay-up in minimizing substructure area and weight.

Shown in Figures 43 and 44 are the I-beam cross-sections for hand lay-up and RTM specimens. As was previously observed for the thin flanged T-stiffener geometry, hand lay-up did not conform to the tool's 1.8 mm. Again, it was observed that the reinforcement adopted the greater 6 mm radius. This resulted in bondline thicknesses ranging between 0.4 and 2.6 mm for the hand lay-up I-beam specimen. RTM specimens were co-cured and found to have transition radii matching the mold at 1.8 mm.

For the I-beam geometry, hand lay-up generated a cross-sectional area of 1020 mm^2 while RTM yielded an area of 595 mm^2. The hand lay-up area contained 139 mm^2 of bond material or 14% of the overall cross-section. Differences observed between

Total Area: 1020 mm^2
Bond Area: 139 mm^2
Mass: 1.6 kg/m

Max. Bond Thickness: 2.6 mm

Transition Radii: 6 mm

10 mm
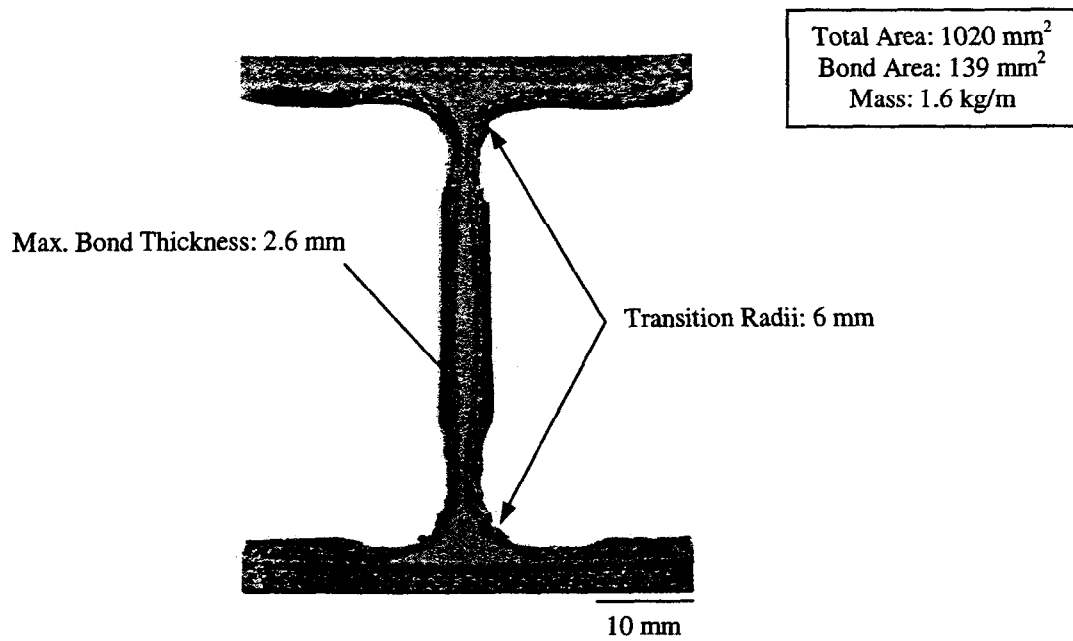
Figure 43. Hand lay-up I-beam cross-section.

Total Area: 595 mm^2
Mass: 0.9 kg/m

Transition Radii: 1.8 mm

10 mm
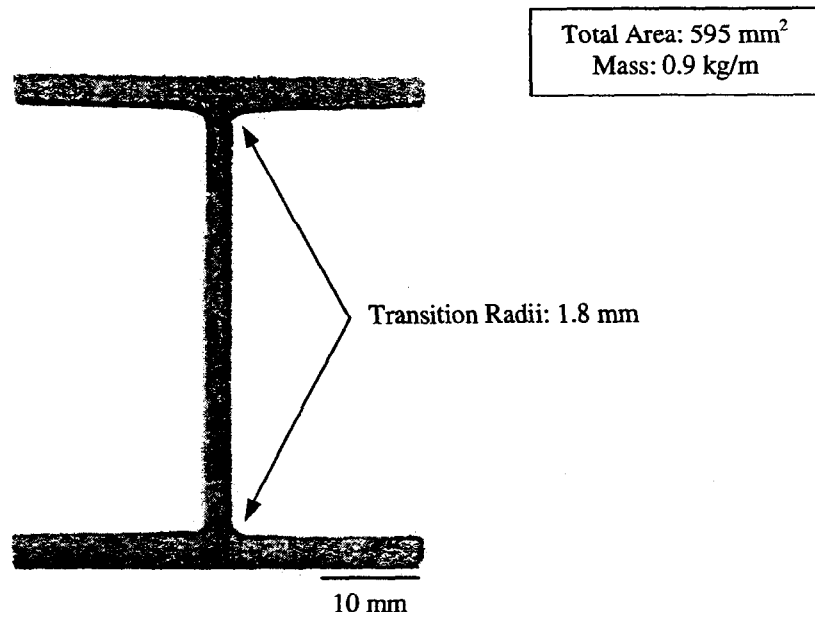
Figure 44. RTM I-beam cross-section.

I-beam specimen areas according to process were 425 mm^2 or 42%, the greatest difference observed for the goemetries under investigation. The unit masses for I-beams manufactured by hand lay-up and by RTM were calculated and these values were found to be 1.6 and 0.9 kg/m, respectively. When extending this geometry over the 6 meter spar span of the current blade design, a 4.0 kg or 41% mass difference was observed. These findings illustrate the importance manufacturing process selection has on dimensional control and subsequent substructure weight differences.

Root specimens were investigated for fiber volume versus thickness relations and component weight for estimating the properties of a complete hub to blade joint. Differences in weight for the substructures already discussed were noteworthy because their centers of mass were located at distances of at least 4 meters from the rotating turbine hub. Reducing mass for full-scale T-stiffeners and I-beams could lower the polar or rotating inertia of a wind turbine, increase its efficiency, and decrease turbine support structure weights. However, the centroidal mass of a root connection is only a fraction of a meter away from the turbine's rotating hub. Variations in mass at this short distance from a blade's center of rotation would have less of an effect on the inertia and efficiency of a turbine compared to structures along the blade span. Hence, investigating the weight behavior of the other three-dimensional geometries was of greater importance and exploring the benefits processing might have on the complete root to hub joint weight is left for future research.

The weights of individual root specimens were used in projecting the approximate weight of the complete root assembly. This information was anticipated to be useful in making predictions of full-scale composite turbine blade weight. Single root specimens were weighed and that information was extrapolated for the entire joint. Single specimens had a mass of 3.85 kg with 0.85 kg being contributed by the steel insert. The MSU composite blade design for the AOC 15/50 turbine consists of 10 such inserts, and the total mass of the current root joint design was estimated at 38.5 kg. Significant differences were not found between hand lay-up and RTM root weights nor were they explored in depth by the rationale previously discussed.

Suggesting the actual weight savings that can be accomplished with RTM for the MSU composite turbine blade is difficult. The substructure mass analyses presented a straightforward method for comparing the hand lay-up and RTM processes while making reasonable approximations on the weight savings for actual turbine blade components. It should be noted that the geometries of this evaluation were primarily of uniform cross-section and that they simplify the weight savings calculations for full-scale blades. The turbine blade design has a twisted, tapered geometry that is more complicated than the constant cross-sections studied herein. As a result, the weight differences between hand lay-up and RTM substructures in the MSU composite blade design might differ slightly from the current findings. The focus of this study was to identify and quantify the variables that affect blade component strength and weight. Thickness, fiber volume, transition radius, and bondline thickness were found to be the greatest contributors and their effects on blade component weight have already been discussed. The RTM process

was found to outperform hand lay-up for all these parameters that contribute to substructure weight. And when process effects are extrapolated for full-scale blade substructures, it is observed that RTM reduces weight, labor, and cost while improving turbine performance when compared to hand lay-up.

Fabrication Cycle Times

Process cycle times are important to turbine blade fabrications because they help to establish the cost and volume output of the parts manufactured. Methods that have a higher degree of automation will yield parts of greater consistency while reducing the cost of labor involved. In addition, automation can reduce the total time in manufacturing and increase the number of blades fabricated in a workday. As a result, it was important in this work to review and evaluate cycle times for the hand lay-up and RTM of the five substructures under investigation.

In Table 16, examples of the steps taken in hand lay-up and RTM fabrications are given. For each geometry studied, comparative tables were compiled and are presented in Appendix D. For each task in the hand lay-up or RTM operations, times were recorded from three different substructure fabrications and averaged. Overall fabrication times could then be summarized and compared between geometry and process. The individual hand lay-up and RTM processing steps of Table 16 include:

- Fabric Cutting: time required to extract reinforcement lay-ups from fabric rolls.

- Hand Lay-ups: the wet process of manually permeating resin into fabric reinforcements using rollers and brushes on an open mold.

- **RTM Lay-up**: the dry lay-up of fabric schedule, addition of gasket materials, and combination of tool components for a closed mold.

- **RTM Injection Preparation**: time required to close mold, secure clamping devices, start-up RTM injector, and attach injection line(s).

- **RTM Resin Injection**: time duration between resin entering an RTM mold and the shutting down of the injection equipment.

- **Hand Lay-up Clean-up**: removal of resin from beakers, rollers, squeegees, and brushes using acetone solvent. This step also includes the disposal of excess resin.

- **RTM Clean-up**: disposal of excess resin and removal of resin from beakers, injection lines, and RTM device using solvent.

- **Part Removal**: time commitment to demold the laminate(s). For RTM specimens this includes removing injection lines, clamping devices, and in some cases, seals.

- **Mold Cleaning**: removal of cured resin flash from the hand lay-up or RTM tool. This operation also includes drilling out ports for post-RTM injections.

- **Secondary Bonding**: time required to apply bonding materials to mating surfaces of hand lay-up, three-dimensional structures. This value of Table 16 does not include the required two hours cure time at 60°C.

Table 16. Hand lay-up and RTM thin flanged T-stiffener fabrication times.

Hand Lay-up	
Fabric cutting	24 min
Web lay-ups	21 min
Flange lay-up	18 min
Skin lay-up	6 min
Clean up	10 min
Part removal	14 min
Mold cleaning	30 min
Secondary bonding	41 min
Fabrication Time	164 min

RTM	
Fabric cutting	24 min
Fabric lay-up	20 min
Injection preparation	23 (R) – 5 (S) min
Resin injection	8 - 29 min
Clean up	12 min
Part removal	15 min
Mold cleaning	10 min
Fabrication Time (R)	112 - 133 min
Fabrication Time (S)	94 - 115 min

(R) – Radius RTM injection
(S) – Spartan RTM molding

The individual fabrication steps found in Table 16 for hand lay-up and RTM did not include the start up and shut-down time associated with each individual task of the operations. For example, when recording the time required to cut fabric for a flat plate laminate used in this study, the time involved in rolling out the fabric, locating cutting utensils, returning cutting supplies, and reeling fabric back onto the roll was not included. This method allowed for the best approximation of the efficient operations found in an industrial setting. It should also be noted that populations were not large enough to justify presenting their standard deviations and therefore, only the average values for the individual time steps and the resultant cycle times were calculated. A summary of the resultant fabrication times for all of the substructures manufactured in this study is presented in Table 17.

The fabrication times and time savings between hand lay-up, RTM with the Radius injector, and RTM using the Spartan equipment are shown in Table 17. Both RTM cycle times were recorded due to a significant difference found in injection preparation time. For example, in Table 16, injection preparation times differed between RTM machines by as much as 17 minutes. This distinction in injection preparation speed was inherent to the type of injection device used. As previously mentioned in the Experimental Methods Chapter, the design of each RTM injector had different strengths and weaknesses. While the Radius RTM injector was one of the best available options for a constant pressure device outfitted with data acquisition, one drawback was that it was labor intensive in injection preparation and clean-up. On the other hand, the Spartan RTM machine was simpler to start-up and shut-down and thus is more likely to be found

Table 17. Hand lay-up and RTM specimen fabrication time summary.

Geometry	Process	Fabrication Time min	Time Saved with RTM (S) min	Time Saved with RTM (S) %
[0/±45/0]s Flat plate	HL	83	10	14
	RTM (R)	90	17	23
	RTM (S)	73	--	--
[0/0/±45/0]s Flat plate	HL	99	28	39
	RTM (R)	88	17	24
	RTM (S)	71	--	--
Thin Flanged T-stiffener	HL	116	45	63
	RTM (R)	87	16	23
	RTM (S)	71	--	--
Thick Flanged T-stiffener	HL	164	59	56
	RTM (R)	123	18	17
	RTM (S)	105	--	--
I-beam	HL	175	61	54
	RTM (R)	132	18	16
	RTM (S)	114	--	--
Root specimen	HL	133	14	12
	RTM (R)	135	16	13
	RTM (S)	119	--	--

HL - Hand Lay-up
RTM (R) - Resin transfer molding with Radius injector.
RTM (S) - Resin transfer molding with Spartan equipment.

on a factory floor. This difference in processing time for the geometries studied was duly noted and summarized in Table 17.

It should be noted that for the cycle times of Table 17, each geometry RTM'd with the Spartan equipment was considerably quicker in fabrication time when compared to hand lay-up. It may also be observed from this table that the differences in fabrication times between hand lay-up and RTM increased with the increasing complexity of the part being manufactured. For example, [0/±45/0]s flat plates were completed 10 minutes or

14% faster when the RTM process was employed, whereas the difference in fabrication times was 59 minutes or 56% for thick flanged T-stiffeners between processes.

The only case where a complex geometry did not benefit greatly from the automation of RTM was for the root specimen scenario. This affect can be attributed to the steel insert, the complicated preform, and the complex mold configuration used to manufacture this laminate. Both hand lay-up and RTM productions of this geometry included a support system for the insert. These jigs maintained the insert in relation to the rest of the laminate, such that the root products would have the steel inserts in the identical location even when process was varied. As a result, the RTM tool for the root specimen was significantly more complicated and difficult to prepare than the other substructure molds. A locating bushing, steel bolt, and O-ring seal were required to mate with the ribbed insert and combining all of these components prior to molding resulted in a notable increase in fabrication time. The benefit in processing time with RTM was significant for the root specimen, but the time savings was just a fraction of what was found for other three-dimensional substructures, due to the extensive mold preparation.

With the exception of the root specimen, it is demonstrated in Table 17 that geometries manufactured by RTM will result in a reduction in fabrication time over hand lay-up with increasing part complexity and size. Benefits in fabrication times for turbine components in the industrial setting could be even greater than those listed in Table 17. The results of this table illustrate the advantages of laying up dry preforms and then using RTM injection equipment to automate the composites manufacturing process, as opposed to the wet lay-up of individual layers of reinforcement. The current results also

demonstrate that RTM manufacturing technique advantages would be greater for specimens of increased size and complexity. While the lay-ups and thicknesses mimic the actual MSU composite turbine blade components (Figure 1b), the sample sections of this study were only a small fraction of the total 8 meter length of this blade. Thus, as the complications of wet lay-up are compounded with increasing length and complexity, it can be assumed that industrial manufacturers would observe even greater benefits in cycle time than those of Table 17.

The final topic investigated under the fabrication time study was cure time. There were two cure times measured for the geometries and processes of this study. These were the cure times of the composite laminate, and the cure times of the epoxy adhesive used in secondary bonding operations. Neither of these values were included in the fabrication times of Table 17 as they might strongly bias the results and not allow for comparison of the individual steps taken for each process. The cure times for each geometry with its tool at ambient temperatures were provided in the Experimental Methods chapter. However, when discussing the optimization of the hand lay-up and RTM processes, it is beneficial to refer to the results of Yu and Young [36]. As the authors suggest, cure times for the RTM process can be largely improved at elevated temperatures. These benefits were not explored in the current work due to the large cost and difficulty introduced with heating all of the tools used.

In a production setting, turbine blade fabricators would take advantage of elevated temperatures with closed, RTM molds to maximize part output. For example, if a manufacturer produced the thick flanged T-stiffeners of Table 17 using hand lay-up,

cycle times would be 164 minutes in addition to the 4-8 hours cure time. Unlike RTM, it is inefficient and difficult to heat an open mold and consequently, requires a lengthy cure time. Thus, only one part per day can be fabricated for each given tool using hand lay-up. RTM with elevated temperatures and pre-manufactured preforms on the other hand, could have cycle times on the order of minutes, with curing being done immediately after initial gelling in the mold. Adopting this modern RTM methodology would result in many more parts per mold per workday than the amount possible with the hand lay-up manufacturing technique.

Secondary bonding operations resulted in increased hand lay-up processing times when compared to their RTM counterparts. For most RTM applications entire components or large substructures can be injected and co-cured in one step. This is not the case for most hand lay-up assemblies, however. Because open molds are required, only flat or simple components can be wet laid-up. As a result, larger structures are built up from simpler pieces, and bonded together in a secondary operation. This was observed for the T-stiffener and I-beam geometries in this work. The results of Table 17 show the times required to manufacture the individual components and apply adhesive material to join the substructure together. However, the time contributions from secondary bond material cure are not included in these results. Two hours at 60°C was required for the cure of the Hysol epoxy and this was performed for each bonding operation. It also requires mention that for the T-stiffener and I-beam geometries, secondary bonding was completed in two steps. This methodology was necessary to attain proper alignment between components. For example, I-beam webs were mated,

aligned, and cured in the first step. Next, flange caps were bonded and cured to complete the substructure geometry. Thus, these geometries had significantly greater fabrication times due to the time required to secondary bond components and to cure the adhesive material. RTM eliminates the need for these secondary bonding steps in many cases and would not suffer from the potential for misalignment and the four hours of cure time required for adhesive bonding.

Computed Tomography (CT) Porosity Scans

Current methods for finding porosity include taking microscopic images of a composite and its pores or burning off the matrix and trying to determine porosity according to weight differences [52]. In the first process, a laminate is polished and prepared for the microscope. A micrograph approximately 1 x 1 mm is then captured and analyzed using digital image analysis techniques. To determine a representative fiber volume for the entire composite, many such images are gathered, the porosity contents are found, and then the image data are averaged. This process is tedious and is subject to error if insufficient data are collected.

The second method for measuring porosity content involves using the matrix burn-off method. The process begins with the measurement of the mass and volume of a laminate of known density and fiber volume. The specimen is then introduced into an oven where the matrix material is removed. Next, knowing the density of the reinforcement and matrix materials, the discrepancy between weights can be accounted for by pores in the laminate. Finally, the number of pores is calculated and a percent porosity by laminate volume can be found. This process is not as labor intensive as the

previously discussed microscope method, but requires great precision and can have problems yielding accurate results.

The difficulties with these two methods motivated the investigation of an alternative method for measuring porosity in the composites of this study. Hand lay-up and RTM are quite different in pore content, size, and location. As a result, it was necessary to select a method that would yield accurate porosity measurements. Computed Tomography (CT) scan methods were chosen for this task. Previous work with quantifying pores in ice was successful, and it was hoped that similar successes could be observed in measuring porosity introduced by the hand lay-up and RTM processes [53].

A Synergistic Detection Designs CT scanner was available for this study. It would accept composite laminates up to 102 mm in diameter and 305 mm in length. Specimens were secured in the scan area by means of Velcro strap, paraffin wax, and in the case of the flat specimens, wood blocks were used to minimize vibration. Once secured in the CT scanner, the equipment passed X-rays through the rotating specimen and then collected the emitted X-rays. The CT machine generates a digital image according to the densities of the materials the X-rays pass through and the intensity of the X-ray transmissions. Digital image "slices" are taken at a number of preset locations as the CT scanner emits X-rays through 0.5 mm thick sections of the geometry being tested. Collected X-rays were conditioned to develop CT digital images. This cross-section of the specimen could then be examined for porosity content and compared to the images taken from other specimens.

Five specimen types were selected in an attempt to determine porosity for a range of pore contents. Samples were taken from a hand lay-up plate, an RTM plate taken from near the outlet vent, an RTM plate taken near the inlet port, an RTM thin flanged T-stiffener, and an RTM I-beam. In the first attempts to present the validity of CT methods in determining composite porosity, it was found another method would be required to calibrate the procedure. CT image comparisons seemed to be a satisfactory method for differentiating between the pore contents of various specimens. However, porosity levels could be easily manipulated according to the steps taken during reduction of the digital image. As a result, the microscope method was employed as a calibration tool and microscope images were gathered for the hand lay-up and RTM plate specimens. The hand lay-up and RTM-vent specimens had significant levels of porosity observable with the unaided eye and were suspected to provide a good starting point for measuring porosity. The RTM specimen taken from near the laminate's injection port had minimal observable porosity and was used to gauge the accurateness of the predictive CT technique.

Micrographs of the hand lay-up and RTM plates are shown in Figures 45 - 47. In these figures the D155 and DB120 tows, the resin matrix, the individual fiber strands, and the pores are clearly illustrated. A minimum of five images like Figures 45 - 47 were captured and examined for each specimen. From these images, average pore diameter and average porosity were recorded. The pore diameter and porosity findings for the
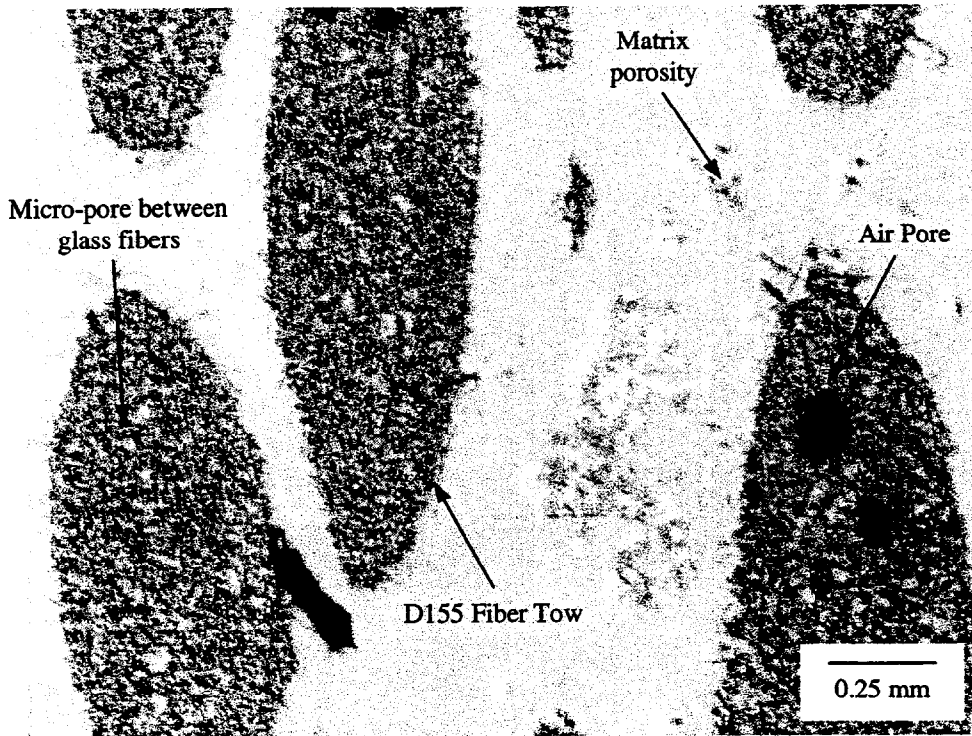
Figure 45. Microscopic view of porous hand lay-up specimen.
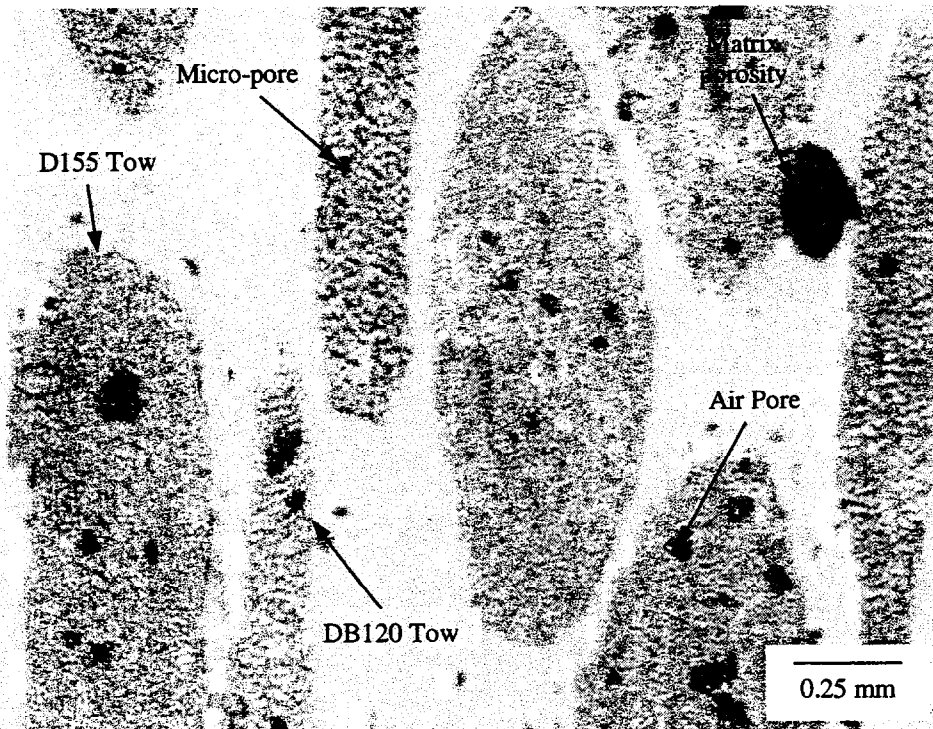
Figure 46. Microscopic view of an RTM specimen near resin vent.

99
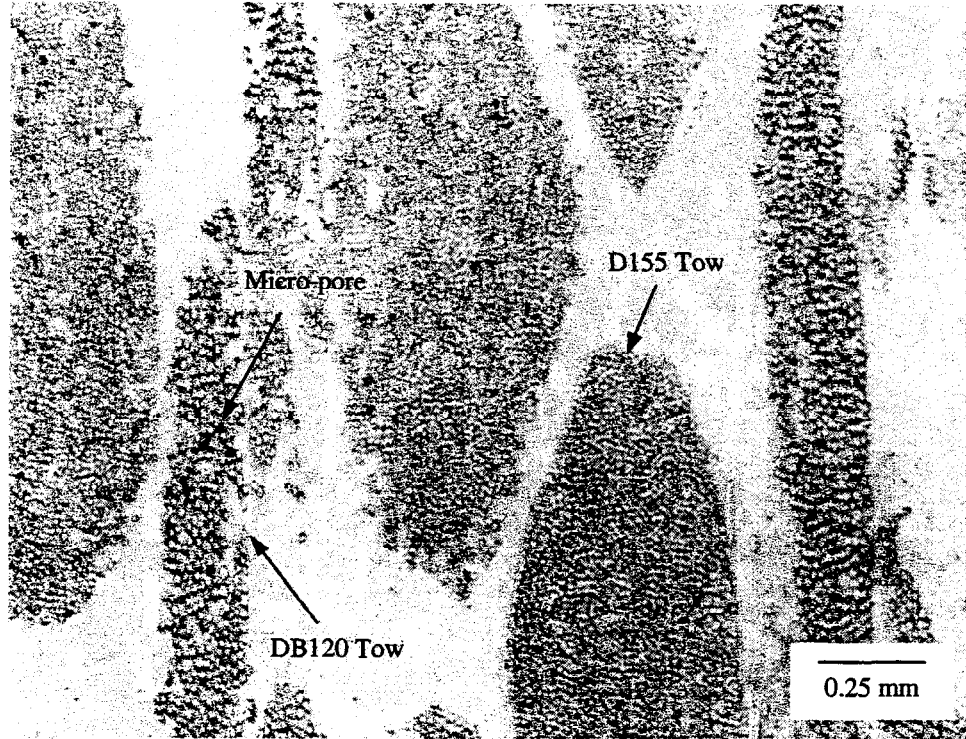
Figure 47. Microscopic view of an RTM specimen near injection port.

hand lay-up and RTM-vent specimens are presented in Table 18. Demonstrated in this

table is the average pore diameter of 0.092 mm for hand lay-up and 0.064 for RTM near a

vent. Sample porosities also revealed that hand lay-up averaged 2.4% porosity while

RTM was approximately 3.3% near its outlet vent. This larger value for RTM was not

alarming, since the majority of the RTM plate that the sample was taken from had

significantly less observable porosity.

Micrograph analysis also included specimens taken from an RTM plate near its

injection port and a VARTM flat plate used in mechanical testing. The RTM-inlet

porosity results were used to evaluate the predictive capabilities of the CT porosity

measurement approach. The VARTM specimens were included in the microscopic study

Table 18. Microscope specimen results.

Lay-up and Fabrics	Process	Specimen Location mm	Avg. Pore Diameter (S.D.) mm	Sample Porosity (%)	Avg. Specimen Porosity (S.D.) %
[0/±45/0]s D155 / DB120	Hand Lay-up	70	0.090 (0.05)	0.7	1.4 (1.0)
				1.2	
				1.0	
				0.7	
				1.4	
				3.7	
				1.3	
		230	0.094 (0.06)	1.4	3.4 (6.4)
				1.3	
				0.6	
				17.9	
				1.3	
				0.6	
				0.5	
	RTM (vent)	70	0.071 (0.03)	4.8	4.1 (1.4)
				3.4	
				6.2	
				3.2	
				3.0	
		230	0.057 (0.01)	3.2	2.4 (0.7)
				2.6	
				2.4	
				1.4	
				2.6	

to find the porosity levels incurred using this manufacturing technique for the purposes of comparisons used in this report.

An example micrograph from the RTM specimens taken near the injection inlet is illustrated in Figure 47. It can be observed from this figure that the sample appears to be nearly void free and that any defects are minor compared to those shown in Figures 45 and 46. The suspected micro-pores for the RTM-inlet specimens were of such small

diameter (< 0.01 mm) that it was not possible to measure or report them accurately. Digital image analysis showed that the average percent porosity for the RTM-inlet microscopic samples was 0.5%. Micrographs of the VARTM specimens were not significantly different than Figure 47. VARTM samples contained only small amounts of porosity, and after digital image analysis, it was found the VARTM specimens used in mechanical testing averaged less than 0.5% porosity.

Once porosity had been calibrated for the hand lay-up and RTM-vent digital images, the CT scan comparisons could begin. Examples of the digital images generated by the CT method are illustrated in Figures 48 and 49 for thin flanged T-stiffener and I-beam geometries. From these figures, the dark colored glass bundles, the gray matrix material, and the air surrounding the specimen can be observed. A similar CT scan for a hand lay-up flat plate where wood blocks have been included to provide support and stability to the specimen is shown in Figure 50. From inspection, it is difficult to determine the porosity content of these cross-sectional images. Thus, digital image analysis techniques were required that would determine what regions of the specimens, on a micro-level, were porous.

An inherent property in CT scanning was the uneveness in intensity of the resultant image. This effect is illustrated in Figure 51 a). The intensity of the image varies according to the amount of material the X-rays must pass through in a single shot. Examining Figure 51 a) demonstrates that either the wood blocks or the width of the flat specimen adversely effected the scan results such that the image appears to be darker towards its center when compared to the lighter ends of the specimen. This nonuniform
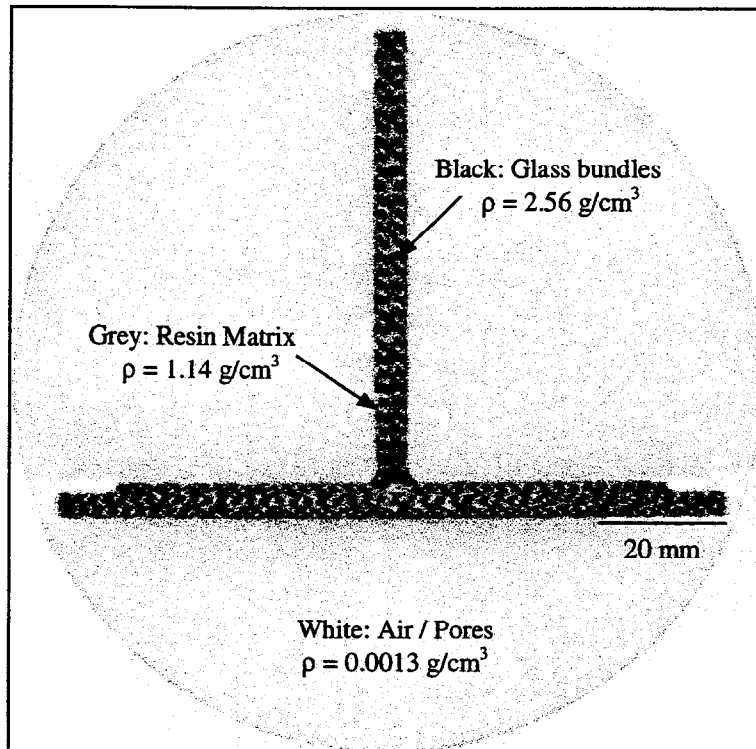
Figure 48. Computed Tomography scan of an RTM T-stiffener.
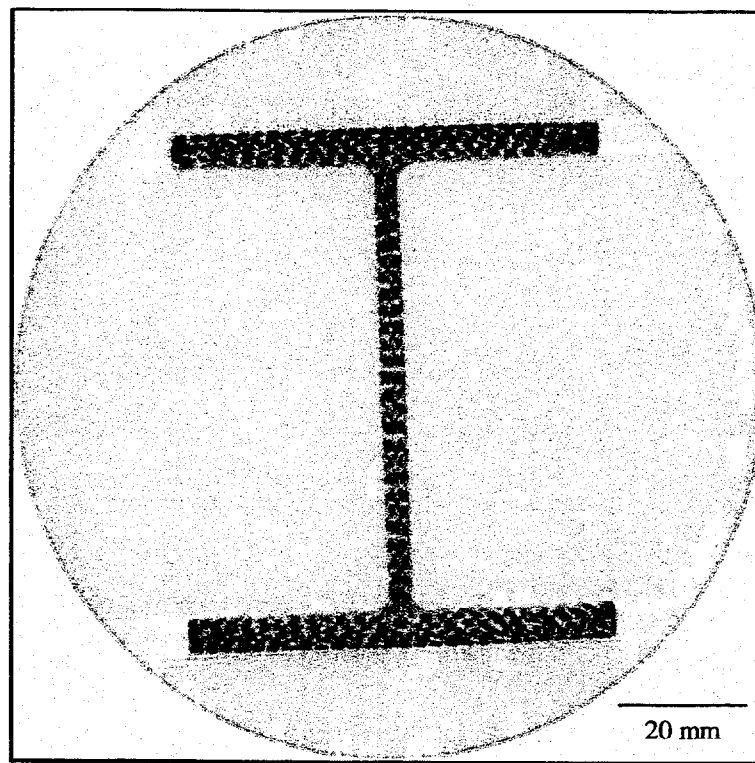
Figure 49. Computed Tomography scan of an RTM I-beam specimen.
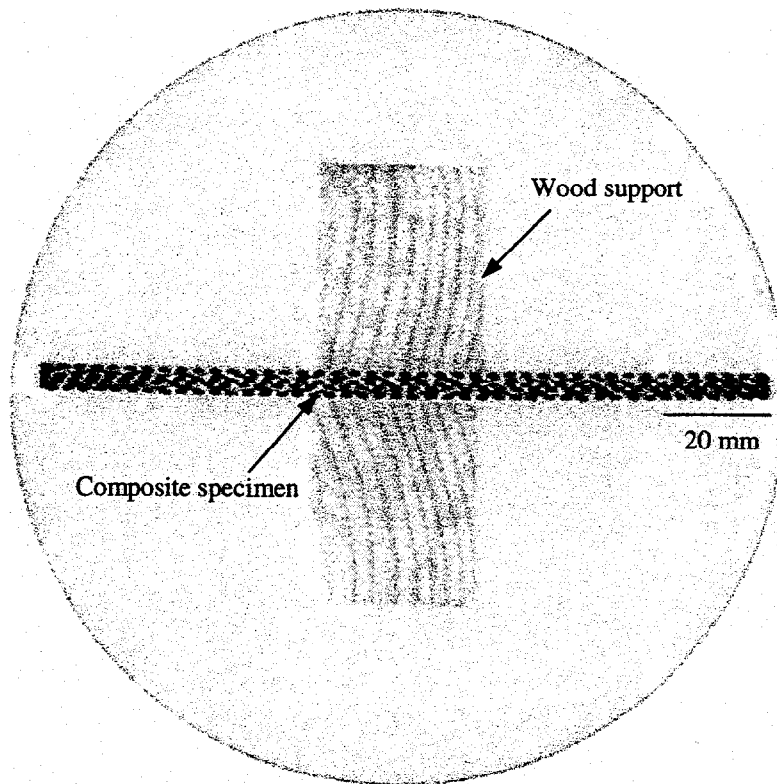
Figure 50. Computed Tomography scan of a flat plate hand lay-up specimen.
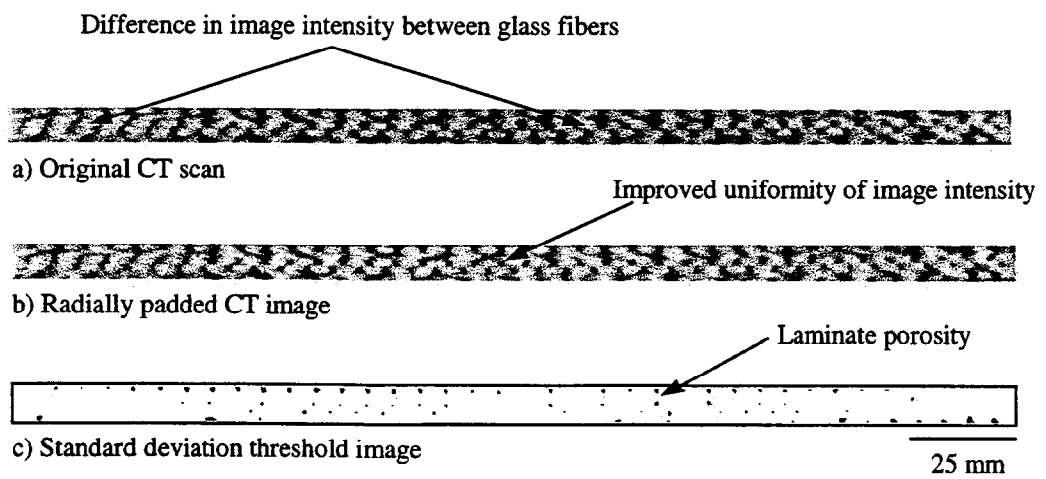
Figure 51. Sequence of digital images between CT scan and porosity measurement.

intensity of the image presents a problem because adjusting the image threshold to measure porosity implies that the center of the sample was the most porous. Visual inspection of the actual sample showed that this was not so, and that at the current state the image would not yield an accurate representation of porosity. Consequently, Edens suggested using a radial padding technique [54]. This procedure adjusts the intensity of the image in a radial pattern and attempts to improve its uniformity. An example of the results observed with the radial padding technique is shown in Figure 51 b). It can be noted from this figure that the image is more uniform in intensity and is more applicable to standard deviation thresholding. The standard deviation threshold was an arbitrary value that determined which portions of the image were of low enough density to be considered porosity. This value was calibrated with the results from the hand lay-up and RTM-vent microscope specimens previously examined. A graphical demonstration of the standard deviation threshold technique is presented in Figure 51 c).

A summary of the results for the CT scan investigation can be found in Table 19. The locations where scans were taken, measured porosity, and pore primary location are shown in this table. The average result of porosity for all specimens scanned was approximately 3% porosity. As noted in Table 19, the porosity measurements between samples did not differ by more than ±1% for any of the samples studied. Since this observation contradicted the micrograph results for the RTM-inlet specimens, further development of the current CT method is necessary.

Improvements in the CT scanning procedure appear to be required. First, previous studies compared materials of only two phases (ice and air), while the current

Table 19. CT scan specimen data.

Geometry	Process	Scan Location (mm)	Suspected Porosity (%)	Locations of lowest density
Flat Plate	Hand Lay-up	20	2	Midregion of plate
		60	3	
		100	3	
		140	3	
		180	2	
		220	3	
		260	3	
Flat Plate	RTM-vent	30	3	Midregion of plate
		70	3	
		110	3	
		150	3	
		190	3	
		230	3	
Flat Plate	RTM-inlet	30	3	Midregion of plate
		70	3	
		110	3	
		150	3	
		190	3	
		230	2	
T-stiffener	RTM	30	3	Midregions of web and flange
		90	3	
		150	3	
		210	3	
I-beam	RTM	70	3	Midregion of web
		150	3	
		230	3	

work attempts to extend CT measurement techniques to materials of three components (glass, matrix, and air). Secondly, the nature of X-ray emission measurement could have hindered the results. As illustrated earlier, CT images tend to vary in intensity according to location and the amount of material that the X-rays must pass through. It could be possible the radial padding does not alleviate the problem completely.

A possible remedy for the concerns with the current CT images would be to utilize smaller specimen sizes and greater scanning resolutions. The specimens of this study were scanned with a resolution of 110 – 120 microns, which was the limit for samples 102 mm in diameter. Higher resolutions for smaller diameter samples might capture the relatively small pores in composite laminates and resolve the current issues with using CT technology for measuring porosity in composites.

Computed Tomography techniques may have other useful applications in composite analysis, as well. The image quality at 110 – 120 microns, while difficult to ascertain porosity from, might be better suited for measuring other properties such as fiber content and delamination damage. CT methods could prove quite beneficial in its ability to determine these properties in a non-destructive manner. Future work could explore these two options extending the usage of CT equipment.

RTM Tooling and Gasket Comparisons

For future research with RTM, it is important to review the advantages and disadvantages of the many molds used in this study. The tools used to evaluate RTM against hand lay-up were of a variety of materials, different seal compositions, and various types of closing devices. The different components of each mold had its own strengths and weaknesses and these are summarized in Table 20. Each criterion for the RTM tools is rated between 1 and 5 in this table; 5 denotes a good performance in this study, while 1 suggests a poor property for RTM moldings. The criteria under review found in Table 20 are defined as follows:

- Ease of manufacture (tool): machinability or manufacturability of the RTM tool surfaces, joints, and gasket allowances.

- Ease of manufacture (part): the tool's capability in fabricating components quickly, consistently, and without a high degree of difficulty.

- Chemical resistance (seal): the degree of inertness of the gasket materials to unsaturated polyester resin and solvents.

- Chemical resistance (mold): the level of resistance against chemical reactivity with the actual tool surfaces.

- Vacuum integrity: ability to deliver a vacuum tight seal consistently and with relative ease.

- Dimensional repeatability: tool's ranking for minimizing the thickness variations between moldings.

- Tool longevity: a tool's lifetime and tolerance to damage during part removal.

- Ambient temperature cure: insulating properties of a tool as it decreases RTM cycle times.

Table 20. Resin transfer molding tool comparisons.

Criteria	Tool Ratings				
	Flat Plate	Thin T	Thick T	I-beam	Root
Ease of manufacture (tool)	3	3	3	1	3
Ease of manufacture (part)	4	3	2	1	4
Chemical resistance (seal)	5	1	1	2	5
Chemical resistance (mold)	5	5	5	5	1
Vacuum integrity	5	1	1	1	3
Dimensional repeatability	4	2	2	3	5
Tool longevity	3	3	3	5	1
Ambient temperature cure	1	1	1	1	5
Overall Ratings	30	19	18	19	27

Ratings: 5 Good - 1 Poor

Compiling the individual criteria of Table 20 demonstrates that the flat plate and root specimen tools had unique advantages over the other RTM tools of this study. The primary benefits of these two tools were vacuum integrity, chemical resistance, and ease of manufacturing. Consequently, in future RTM molds in would be worthwhile to use the materials and devices that enhanced these properties. Namely, it would be advantageous in future RTM tool designs to use toggle type clamps, multiple seals, matched surface seals, and chemical resistant gaskets to improve cycle time and part quality.

Cost is another criterion of RTM tools that has yet to be discussed. The cost criteria were not included in Table 20 due to the fact that, when normalized for part complexity, the capital investment for aluminum, steel, and composite tools was not significantly different between the five tool geometries. This similarity in cost was primarily due to the size and simplicity of the components being fabricated. However, in utility-grade turbine blade manufacturing applications tool choices would be notably different. For example, if large, contoured composite blade skins were to be manufactured from steel or aluminum tools, a computer numerically controlled (CNC) mill would be required to machine out the tool cavities for both closed mold halves. This would be an expensive process that would require a large amount of milling time. A more reasonable alternative might be to manufacture steel reinforced composite tools. This has been the design path of the MSU composite turbine blade project for a variety of reasons. First, the process of tool fabrication is significantly less expensive and time intensive when compared to machining operations on a turbine blade scale. Secondly,

the tool material will have the same coefficient of thermal expansion that the part has and as a result better dimensional tolerances may be achieved. Lastly, the insulating properties of fiberglass could result in quicker cycle times. Drawbacks to using steel reinforced fiberglass tooling were recognized during the course of this study, however. The tooling material is not as damage tolerant or chemically resistant as metal molds. In spite of these two disadvantages, fiberglass tooling is still recommended for large RTM fabrications, where varying cross section and part complexity do not lend towards other composites manufacturing processes.

Flat Plate Mechanical Testing

The flat plate mechanical experiments provided the basic yet essential information on the structural performance of hand lay-up and fiberglass composites. Transverse tension, compression, three-point bending, tension, and fatigue tests were chosen because they define many of the primary structural properties of composites. If manufacturing practices influence these properties, then it would be useful to document the differences for the parameters studied in this research.

Transverse Tension

Transverse tension tests are relatively sensitive to matrix strength, when compared to other composite mechanical tests. Consequently, this test was chosen to determine the effects that process, fabric and lay-up have on matrix-dominated strength properties. The data collected for transverse tensile tests in this study included the stress versus strain history and the ultimate strength values. A graphical representation of the

stress versus strain behavior for the transverse tensile experiments is illustrated in Figure 52. From similar curves for each specimen tested, elastic modulus, initial damage, ultimate strength, and failure strain were documented. The stress vs. strain curve of Figure 52 correlated well with other observations made in the laboratory. The initial damage was readily audible as the 90° plies began cracking. At approximately 2% strain, the 90° layers ceased to produce audible cracks and the 45° plies began to delaminate [55]. While this delamination was not audible, the unaided eye could observe the 45° layer damage in the composite. For transverse tensile tests, it was also observed that the ultimate strength coincided with the failure strain. The ultimate failure occurred as the 45° plies completely delaminated within the gage length. The delaminated 45° layers and the surrounding damage zones are shown in Figure 53.

The final results for all the transverse tensile data collected are shown in Table 21. The results are for the lay-up, fabric, and process variations that were developed under the Testing Matrix section of the Experimental Methods chapter. These lay-up configurations, fabric architectures, and processing techniques of Table 21 were the primary variables for the flat plate mechanical tests to be discussed. For the results of this table, average values and standard deviations are summarized according to manufacturing parameters. Each result type was reviewed separately to determine the influence lay-up schedule, fabric architecture, and manufacturing process had on the transverse tensile properties of flat composite specimens.

The average ultimate transverse tensile strengths and the maximum and minimum values recorded for the transverse experiments are shown in Figure 54. No definitive
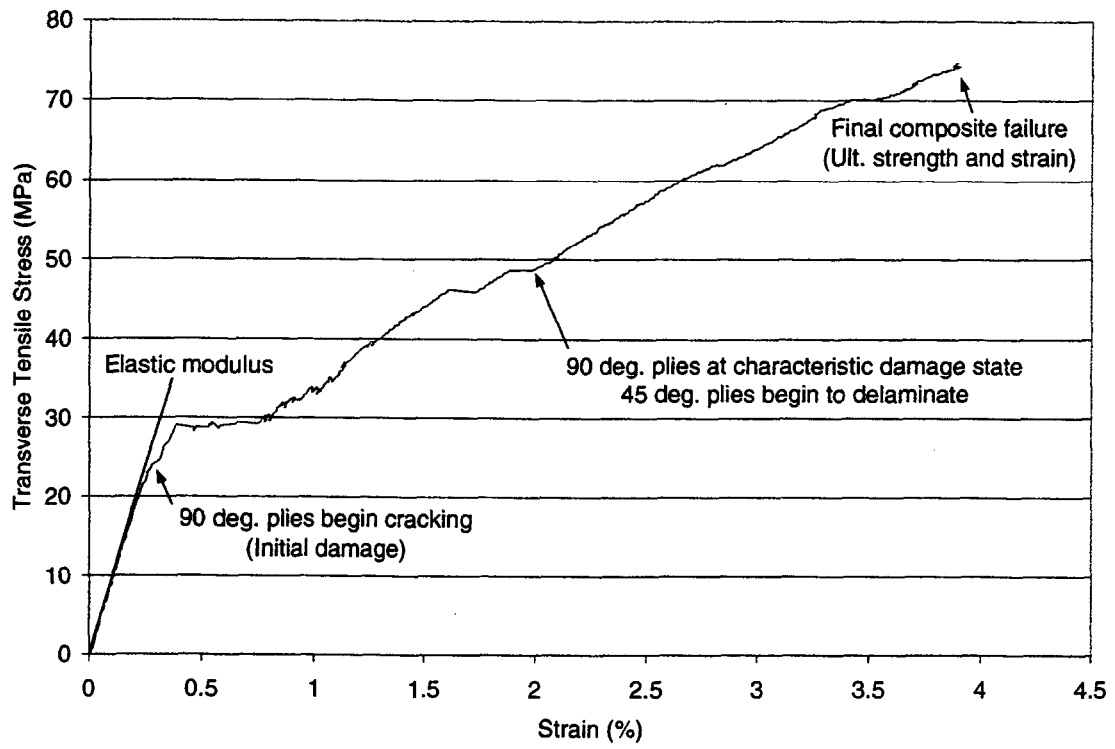
Figure 52. Transverse tensile test example data.
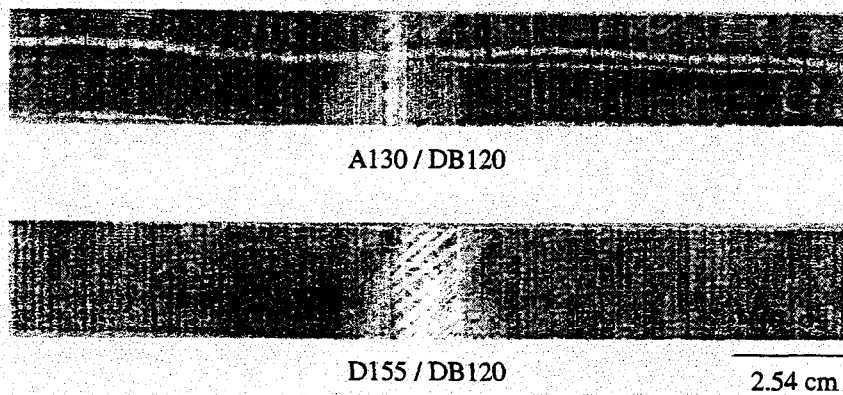
Figure 53. Transverse tension test specimens.

Table 21. Transverse Tensile Test Results

Lay-up	Fabrics	Process	UTTS (S.D.) MPa	TT Modulus (S.D.) GPa	Strain to 1st Fracture (S.D.) %	Strain to Failure (S.D.) %	Data Points
[0/±45/0]s	D155 / DB120	HL	67.4 (6.6)	9.38 (0.63)	0.27 (0.01)	2.7 (0.5)	13
		RTM - R	74.6 (2.3)	9.69 (0.60)	0.30 (0.02)	2.7 (0.2)	16
		RTM - S	74.2 (1.7)	9.01 (0.37)	0.29 (0.01)	3.3 (0.5)	5
		VARTM	77.0 (6.8)	10.04 (0.77)	0.33 (0.03)	3.4 (0.4)	14
	A130 /	HL	65.7 (1.4)	9.51 (0.17)	0.30 (0.02)	NA	4
	DB120	VARTM	85.5 (4.5)	9.74 (0.46)	0.33 (0.03)	NA	6
[0/0/±45/0]s	D155 /	HL	50.0 (6.0)	9.32 (0.64)	0.21 (0.02)	NA	6
	DB120	VARTM	74.5 (2.2)	13.98 (0.72)	0.21 (0.02)	NA	
	A130 /	HL	59.5 (9.3)	9.04 (0.25)	0.27 (0.03)	NA	
	DB120	VARTM	81.6 (2.6)	11.67 (0.35)	0.30 (0.02)	NA	

UTTS - Ultimate Transverse Tensile Strength
TT - Transverse Tensile
NA - Not available
NOTE: Sample thicknesses vary between HL and RTM in accordance with Table 14.

trends were observed for transverse tensile strengths according to fabric or lay-up. When the average values were compared pairwise according to process, the ultimate transverse tensile strengths were greater with VARTM for all combinations of fabrics and lay-ups. Spartan and Radius RTM injected plates were also included in the D155/DB120 [0/±45/0]s laminate comparisons. These specimens were included to record any significant differences between RTM with and without vacuum-assist. Statistical analyses showed that there were no measurable differences between all three types of D155/DB120, [0/±45/0]s RTM samples (Table 22). However, when comparing VARTM and Radius RTM specimens with hand lay-up samples statistical differences were found. Reductions in ultimate transverse tensile strengths were found for the fabric and lay-up combinations in Figure 54, as well. The statistical comparisons of these samples are included in Table 22 and the complete statistical analyses for all mechanical experiments are found in Appendix D. For the four types of composite specimens tested, average transverse tensile strengths were reduced for hand lay-up by between 13% and 33% when compared to VARTM samples.

The effects thickness had on the ultimate transverse tensile strengths were of concern. For the transverse tensile specimens of this study, it was found that their strength was primarily determined by the quantity of 45° layers. The 0° layers do not contribute significantly to transverse strength, and only glass reinforcement at greater angles will benefit transverse properties [50]. By this reasoning, it could be possible that the strength provided by the 45° plies would dominate over any matrix defects found between processes. To investigate this hypothesis, the data from Figure 54 were

114

normalized. This is a fairly frequent procedure performed in composite analyses where the thicknesses of two laminates of different fiber volumes are assumed identical via rule of mixtures. Then the results could be compared for specimens of similar cross-sectional area and structural reinforcement content. In this study, thicknesses were adjusted to yield fiber volume fractions of 30% for all normalized comparisons.

The normalized results for transverse tensile strength are found in Figure 55. While this figure does not represent the true transverse strengths of the samples tested, it does allow for a unique comparison between groups. For example, after normalizing the transverse strength data, it can be seen that the differences between hand lay-up, RTM, and VARTM according to transverse strength were reduced for the laminates of this study. A130/DB120 [0/±45/0]s laminates had a 19% greater average transverse tensile strength for VARTM versus hand lay-up, while the remaining laminates varied in strength between processes by less than 5%.

After reviewing the results for normalized transverse strengths, it follows that matrix differences according to process may have little effect on laminate strength, when the composite material has 45° plies. Transverse tensile strength results could be notably different for laminates where less glass reinforcement supports the transverse loads. Another issue concerning the normalized results, is fiber content selection. For this study it was necessary to select 30% as it represented the average fiber volume finding of Table 15 for hand lay-up flat plate mechanical testing. However, normalizing practices are typically utilized for composite samples varying by only as much as 5% in fiber content. In this study, [0/0/±45/0]s laminates manufactured by VARTM were as high as
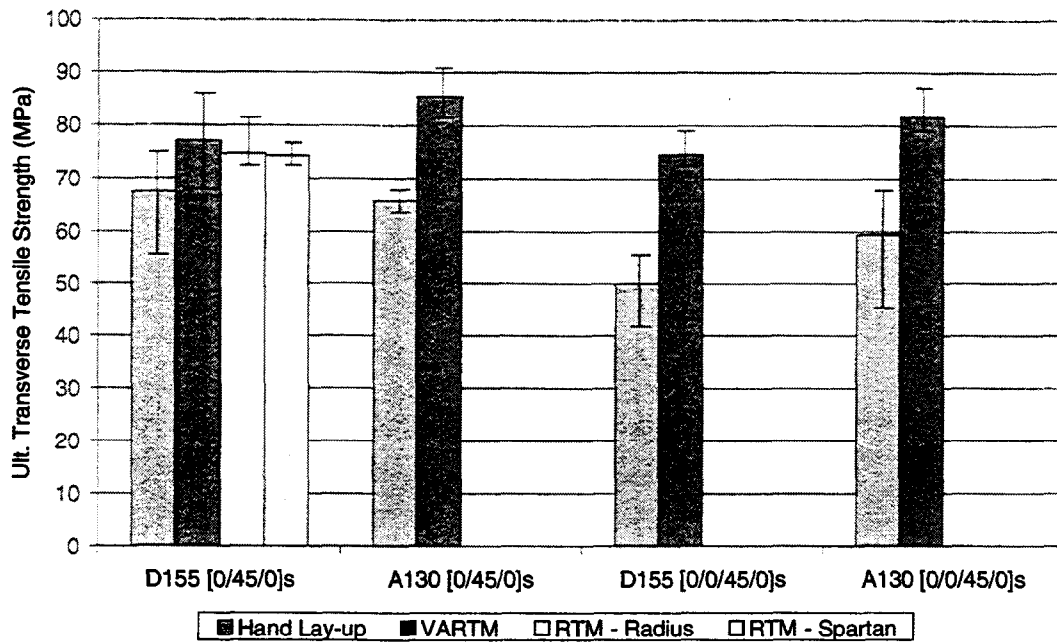
Figure 54. Average ultimate transverse tensile strengths with max. and min. values.
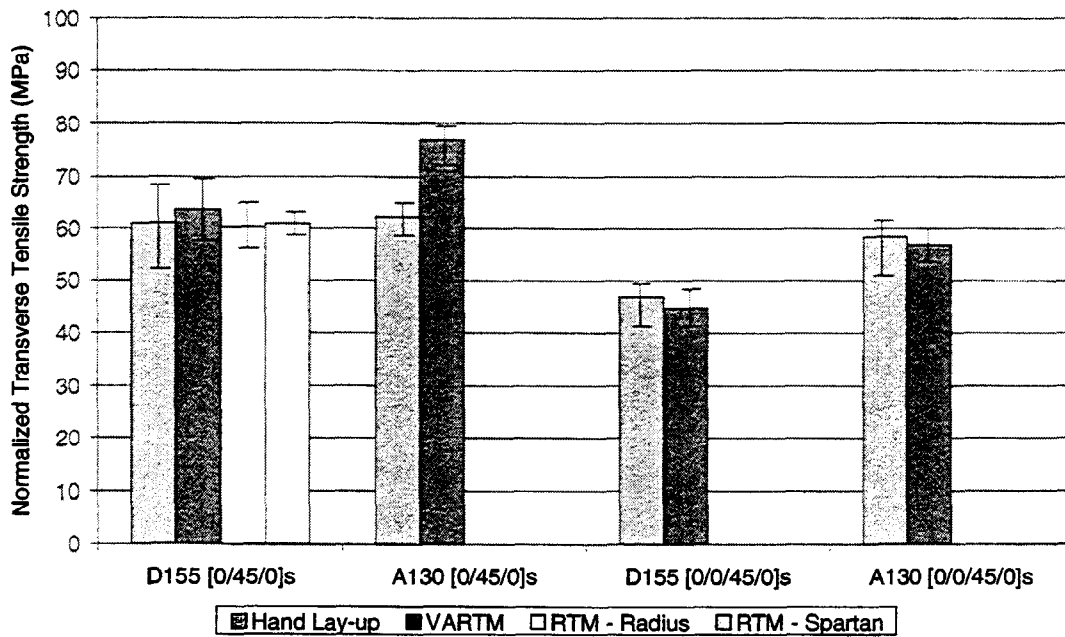
Figure 55. Normalized ultimate transverse tensile strengths ($V_f = 30\%$)

Table 22. Transverse tension results statistical differences.

Laminate Mechanical Property	Lay-up	Zero Degree Fabric	Processes	Normality (P value)	Equal Variance (P value)	Statistical Comparison Method (P value)	Statistical Difference
Ultimate Transverse Tensile Strength	[0/±45/0]s	D155	HL / V	pass (0.353)	fail (0.0003)	ANOVA on Ranks (<0.05)	Yes
			HL / RR	pass (0.353)	fail (0.0003)	ANOVA on Ranks (<0.05)	Yes
			HL / RS	pass (0.353)	fail (0.0003)	ANOVA on Ranks (<0.05)	No
			V / RR	pass (0.715)	fail (0.0009)	t-test (0.467)	No
			V / RS	pass (0.353)	fail (0.0003)	ANOVA on Ranks (<0.05)	No
			RR / RS	pass (0.186)	pass (0.830)	t-test (0.698)	No
		A130	HL / V	pass (0.126)	pass (0.163)	t-test (<0.0001)	Yes
	[0/0/±45/0]s	D155	HL / V	pass (0.329)	pass (0.252)	t-test (<0.0001)	Yes
		A130	HL / V	pass (0.287)	pass (0.480)	t-test (0.0002)	Yes
Normalized Transverse Tensile Strength	[0/±45/0]s	D155	HL / V	pass (0.881)	fail (0.0036)	ANOVA on Ranks (0.164)	No
			HL / RR				
			HL / RS				
			V / RR				
			V / RS				
			RR / RS				
		A130	HL / V	pass (0.594)	pass (0.721)	t-test (<0.0001)	Yes
	[0/0/±45/0]s	D155	HL / V	pass (0.255)	pass (0.365)	t-test (0.158)	No
		A130	HL / V	pass (0.235)	pass (0.454)	t-test (0.401)	No
Transverse Tensile Modulus	[0/±45/0]s	D155	HL / V	pass (0.551)	pass (0.451)	1-Way ANOVA (0.105)	Yes
			HL / RR	pass (0.559)	pass (0.332)	t-test (0.185)	No
			HL / RS	pass (0.726)	pass (0.270)	t-test (0.242)	No
			V / RR	pass (0.551)	pass (0.451)	1-Way ANOVA (0.105)	No
			V / RS	pass (0.551)	pass (0.451)	1-Way ANOVA (0.105)	Yes
			RR / RS	pass (0.551)	pass (0.451)	1-Way ANOVA (0.105)	No
		A130	HL / V	pass (0.106)	pass (0.293)	t-test (0.363)	No
	[0/0/±45/0]s	D155	HL / V	pass (0.294)	pass (0.543)	t-test (<0.0001)	Yes
		A130	HL / V	pass (0.058)	pass (0.302)	t-test (<0.0001)	Yes

HL-Hand Lay-up   V-VARTM
RR-Radius RTM   RS-Spartan RTM

117

41% and 49% in fiber volume and varied from their hand lay-up counter parts by as much as 7 - 16% in fiber content. To address these concerns, normalized comparisons could be repeated at a higher fiber volume or another normalizing technique could be developed.

In Figure 56, the moduli for the transverse tensile specimens were compared. These averages of Table 21 show that significant differences occur for the thicker, [0/0/±45/0]s laminates. While there were statistical differences between hand lay-up and RTM for D155/DB120, [0/±45/0]s specimens, these distinctions were small (P > 0.1). Comparing average transverse tensile moduli between hand lay-up and VARTM manufactured samples showed 2 – 6 % differences for the 6 layer laminates and 23 – 34% differences for 8 ply composites. It was also of interest to note that the moduli of Figure 56 were nearly identical for the [0/±45/0]s laminates and all hand lay-up specimens. The differences in transverse tensile moduli for the 8 ply laminates were clearly due to the significant differences in fiber volume contents between the two types of manufactured specimens.

Initial damage is noted in Figure 52 where the experimental data begins to take on nonlinear behavior. This was also observed in the laboratory as audible and visual cracks initiated in the transverse specimens. The average strain to first fracture values for all the transverse tensile specimens tested are presented in Figure 57. From examining this figure it can be observed that under all cases RTM and VARTM laminates had initial fractural strain values of equal or greater value than those found for hand lay-up. Actual distinctions in average strain to initial damage between hand lay-up and VARTM were
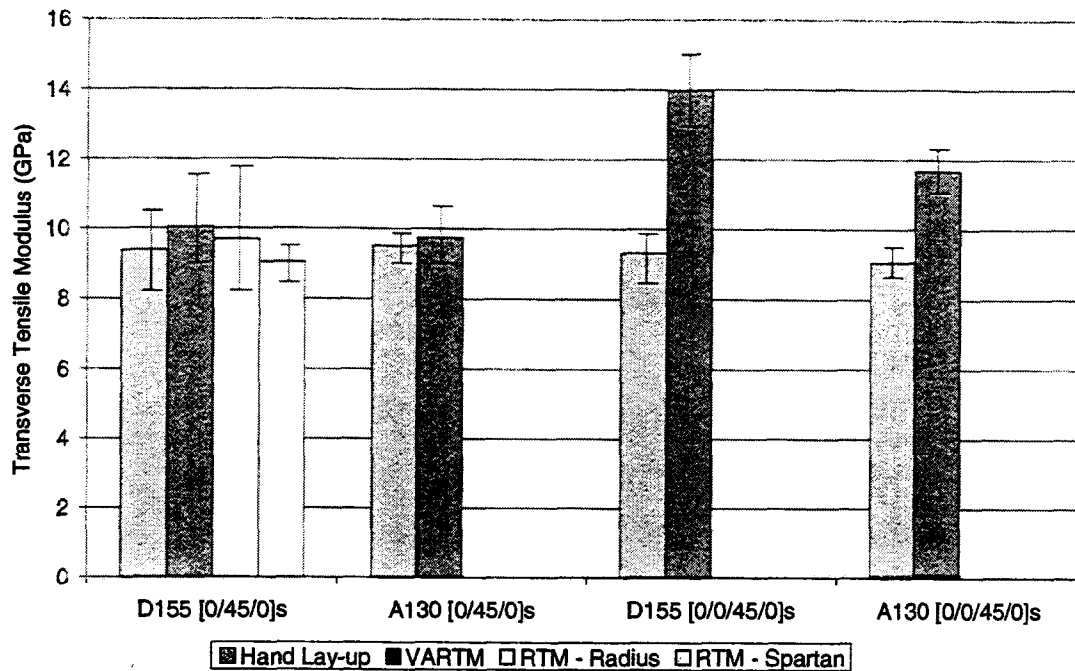
Figure 56. Transverse tensile moduli results with maximum and minimum values.
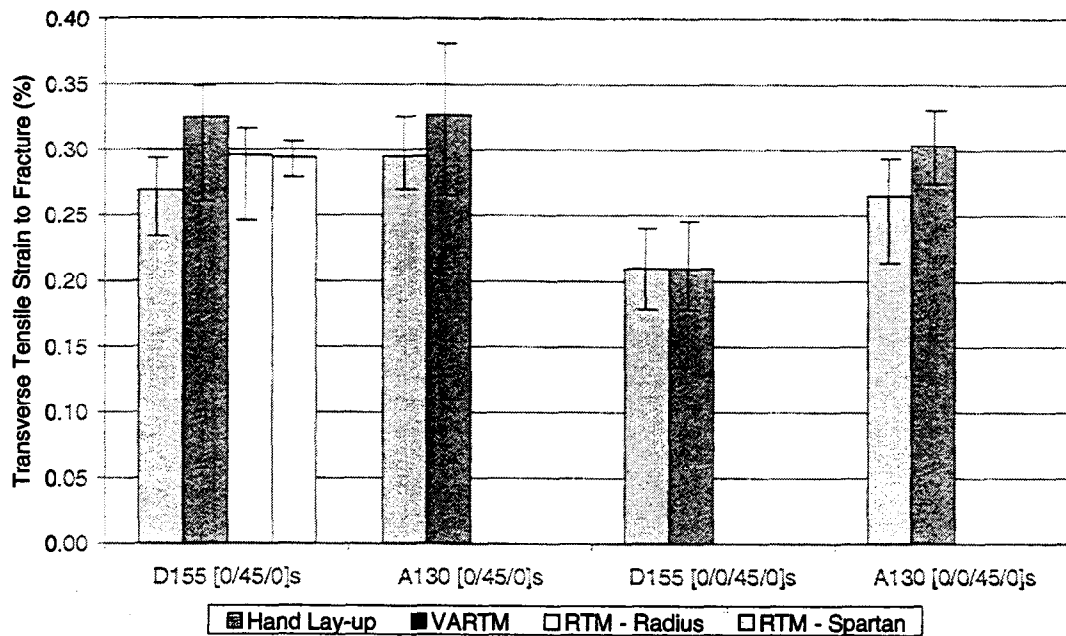
Figure 57. Transverse tensile strain to first fracture.

119

found to be 9 –18% for 6 layer specimens and 0 – 10% for 8 ply samples. Statistical analyses showed that the only significant differences between VARTM and hand lay-up were for D155/DB120 [0/±45/0]s and A130/DB120 [0/0/±45/0]s laminates. The initial fracture is a fairly random occurrence, and may require further investigation for the transverse specimens [56].

During the first round of transverse testing, damaging the extensometer was a concern. Loads over 4.4 kN would have enough strain energy stored to potentially damage the extensometer device at failure. As a result, D155/DB120 [0/±45/0]s laminates were chosen to determine failure strains, as they consistently failed at loads less than 4.4 kN. The ultimate failure strains for transverse specimens manufactured by hand lay-up and RTM are presented in Table 23. The average, maximum, and minimum values of this table show that a high level of variability was found for this fracture property, as well. No statistical differences were found between VARTM versus Spartan-RTM and hand lay-up vs. Radius-RTM. However, no conclusions can be drawn on what effects process may have on strain to failure due to the variability of this fracture property.

To conclude the review of transverse tensile performance, the stress and strain curves of selected fabric and lay-up types were compared. While these curves illustrate the behavior seen in Figure 52 for the other lay-up and fabric combinations, they did not present much new information. However, they are available in Appendix A for completeness.

Table 23. Transverse tensile failure strains for D155/DB120 [0/+45/0]s laminates.

Sample No.	Strain at laminate failure (%)			
	D155/DB120 [0/±45/0]s			
	HL	RTM - S	RTM - R	VARTM
R3				
1	2.9	3.4	2.3	3.6
2	2.2	3.9	2.3	2.5
3	2.5	2.6	2.8	3.3
4	2.4	3.3	2.8	3.2
5	2.9	3.3	2.6	3.9
R2				
1	3.6	--	2.8	3.3
2	3.2	--	2.8	3.4
3	2.1	--	2.8	3.7
Average	2.7	3.3	2.7	3.4
Std. Dev.	0.5	0.5	0.2	0.4

Compression

The compression experiments of hand lay-up and RTM laminates in this study used short gage lengths to eliminate specimen buckling. As a result, extensometer data could not be collected because the extensometer device was larger than the specimen test gage section. Only ultimate compressive strengths were recorded from the Instron digital equipment. Example specimens of the compression mechanical testing are shown in Figure 58.

Ultimate compressive strength results are presented in Figure 59. The strong effects that fabric architecture had on compressive strength are demonstrated in this figure. For both lay-up schedules, the ultimate strengths of laminates manufactured with A130 fabric were approximately half of the composites processed with D155 fabric. This was touched upon earlier in the Manufacturing Materials section of the Experimental
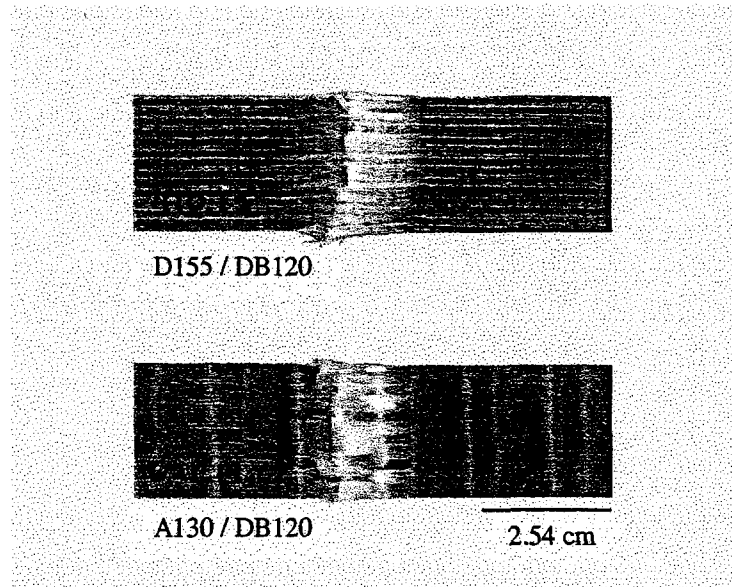
Figure 58. Compression test specimens.
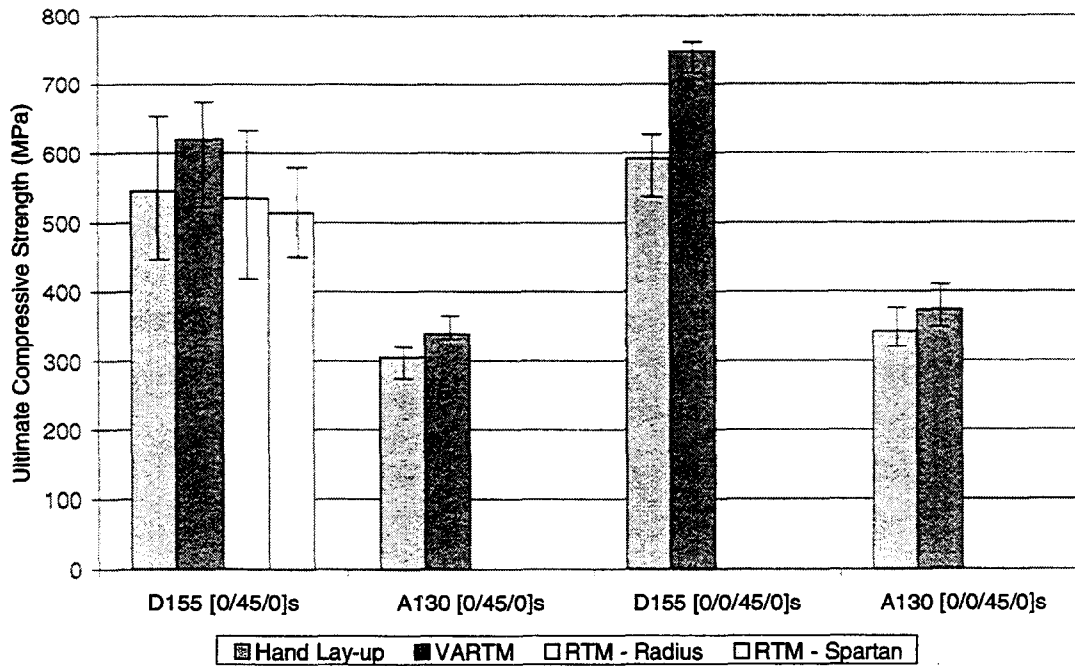
Figure 59. Average ultimate compressive strengths.

Methods chapter. The A130 fabric has a weave type architecture and the glass fibers are not as straight as in the D155 reinforcement. This weave architecture does not resist the bundle buckling condition as well and results in the significant differences in compressive strength, as seen in Figure 59. An additional contributor to the lower results for A130 laminates was the fabric's weight. This fabric was measurably lower in weight when compared to the D155 reinforcement and consequently has a lesser amount of unidirectional glass material. This reduction in unidirectional structural reinforcement also contributes to the differences in compressive strength observed in Figure 59.

The average values of ultimate compressive strength for VARTM laminates proved greater than those of hand lay-up composites for all fabrics and lay-ups explored. Differences in average ultimate compressive strength varied between 8 and 21% for the specimens of this study. Statistical differences were found between VARTM and hand lay-up laminate strengths for all cases except those of the A130/DB120 [0/0/±45/0]s laminate configurations. It should be mentioned that, when statistical comparisons were made between the standard (not vacuum assisted) RTM injected specimens and the hand lay-up samples, no significant differences were found in average compressive strength.

The results of Figure 59 were also normalized and these findings are shown in Figure 60. The average value differences and the statistical comparisons of Appendix D show that the practical differences between [0/±45/0]s laminates manufactured by hand lay-up and RTM were small. Compressive strengths for these specimens differed by 5% or less between the two processes. The [0/0/±45/0]s laminates were also reviewed and it was found that normalizing techniques did not apply well to these specimens. The
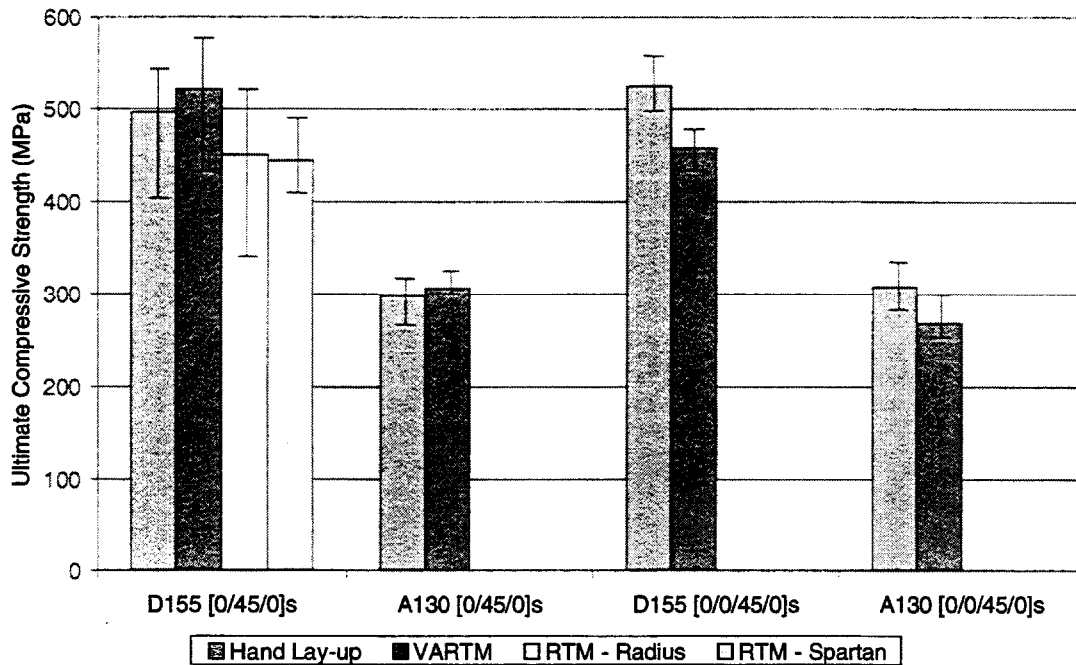
Figure 60. Normalized average ultimate compressive strengths (V_f = 30 %).

[0/0/±45/0]s laminates had differences in fiber volume as high as 16% and were normalized to the average hand lay-up fiber content. In following these steps, the normalized compressive strengths for VARTM samples were lower when compared to the hand lay-up specimens. This behavior might be explained by the effects thickness had on resisting buckling or that the normalizing technique does not work well beyond its typical 5% fiber content range.

Three-Point Bending

In the three-point bending test an extensometer cannot be used. However, the Lebow load cell used in series with the Instron equipment did allow the collection of load versus crosshead displacement data. Example bending test results for [0/±45/0]s and

[0/0/±45/0]s laminates are found in Figures 61 and 62, respectively. The reduced bending strengths of A130 composites, due to the reinforcement's poor resistance to compression, is illustrated in these figures. The difference in ultimate bending load and test deflection for [0/±45/0]s laminates of varying fabric types is shown in Figure 61. It was seen earlier for the compression specimens that ultimate compressive strengths would be reduced by half in cases where A130 fabrics were used for unidirectional reinforcement instead of D155 fabrics. Examination of Figure 61 reveals that this correlates to a 25% reduction in ultimate bending load and a 24% decrease in ultimate specimen deflection for VARTM laminates where the only difference is the use of D155 or A130 fabrics. Greater differences in ultimate bending load and deflection were found for the higher percentage 0° fabric, [0/0/±45/0]s composites of Figure 62. The reduction in ultimate three-point bending load for these VARTM'd specimens was 38%, while the difference in failure deflection was 40% between samples manufactured with D155 and A130 fabrics.

The load versus deflection data from the three-point bending tests were useful in distinguishing samples of different fabrics. The bend test data were also used to determine the effects that processing might have in this set of experiments. It was observed that the choice of reinforcement materials had a stronger effect on strength than the choice between the hand lay-up and RTM processes. Bend test samples of A130/DB120 and D155/DB120 fabrics are illustrated in Figures 63 and 64. It can clearly be seen in these figures that the failures of the compression and tension surfaces were quite different depending on which fabric was used. Shown in Figure 63 are the
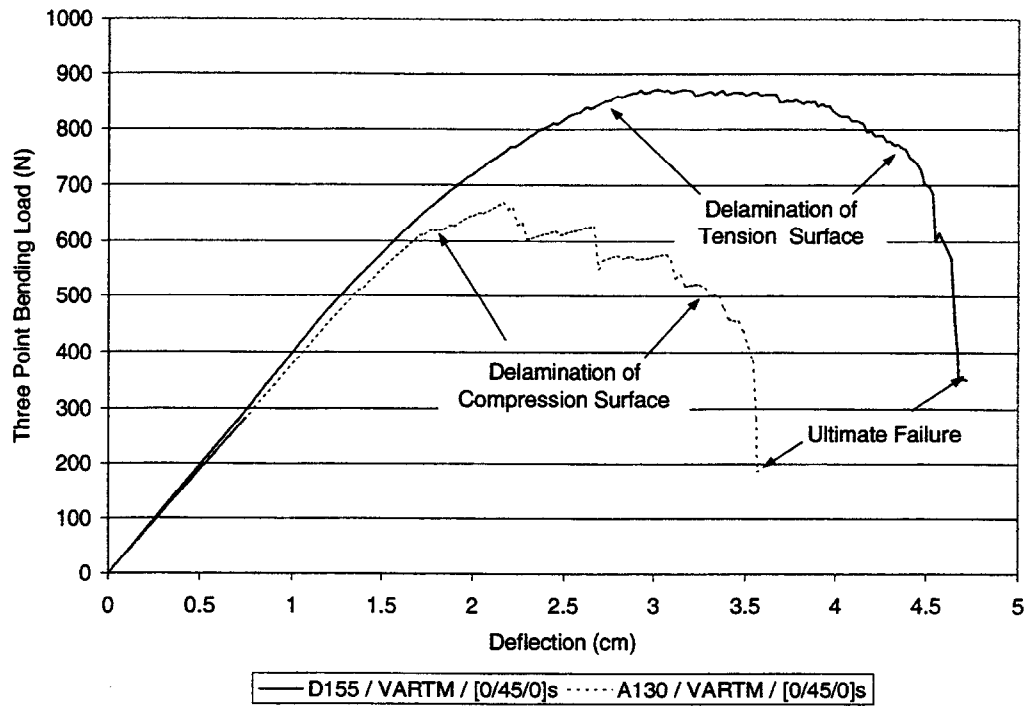
Figure 61. Example data from three-point bend testing of [0/±45/0]s laminates.
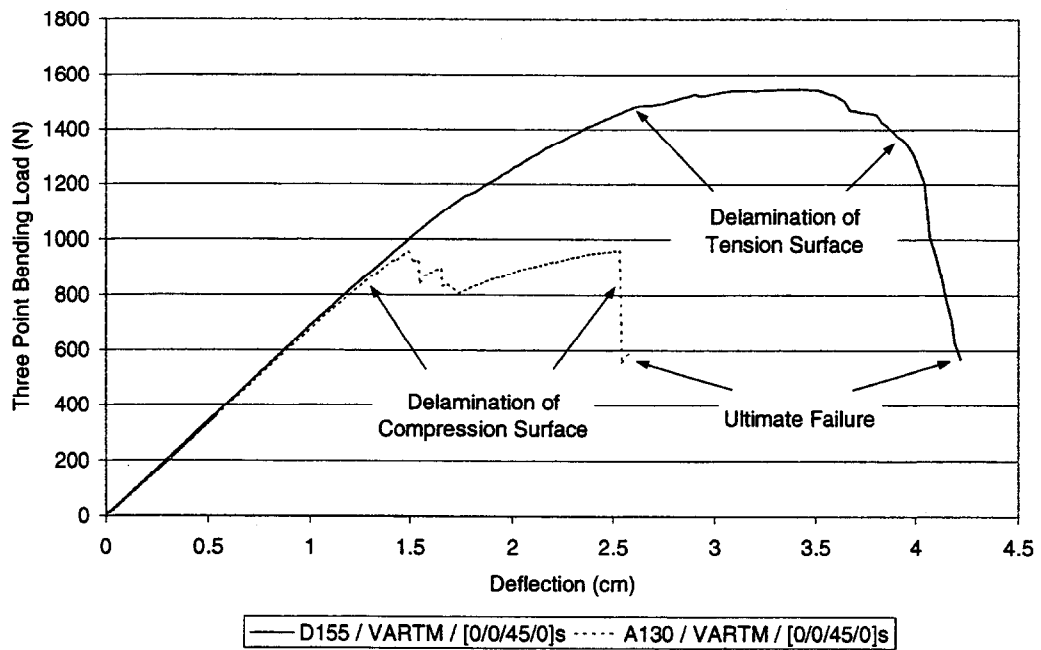
Figure 62. Example data from three-point bend testing of [0/0/±45/0]s laminates.
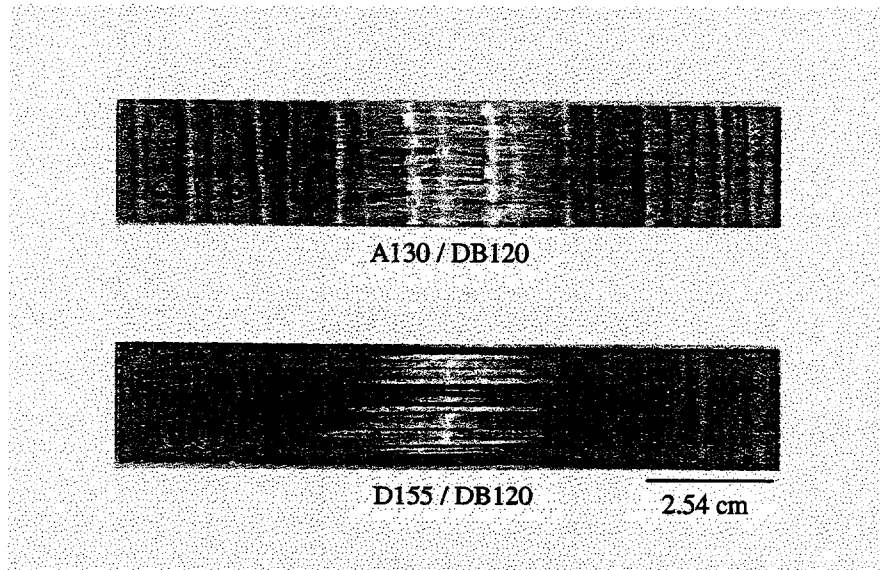
Figure 63. Bending test specimens – compression surface.
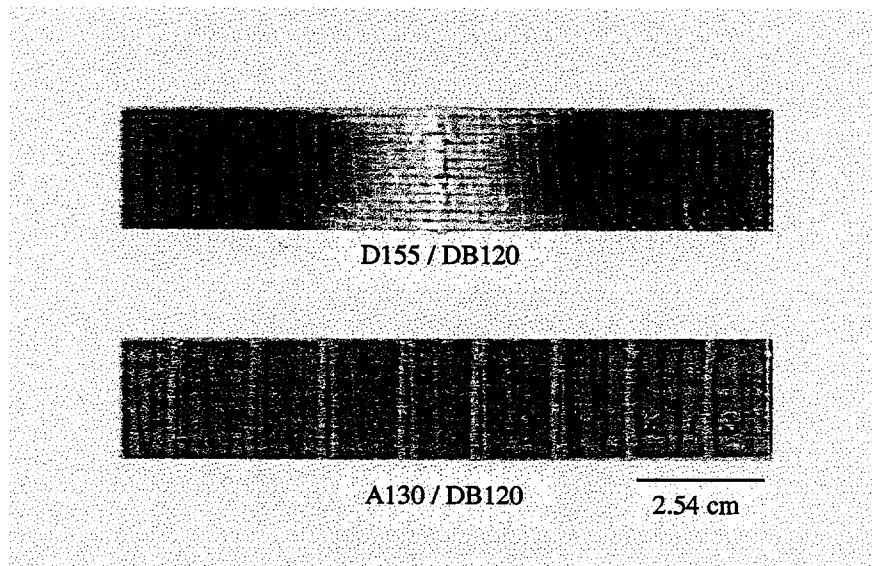
Figure 64. Bending test specimens – tension surface.

compression surfaces of the bend specimens. Comparing the A130 specimen to the D155 sample demonstrates the notably large delamination zone for bending test laminates of A130 fabric. The D155 sample of Figure 63 has a fiber reinforcement that is not of a weave-type architecture and consequently sustains a higher bending load, while also producing greater delamination resistance. The tension surfaces of the three-point bending samples are shown in Figure 64. It can be noted from this figure that no delamination was observed on the tension surface of the A130 specimens. This correlates to the early failure of the compression side of these samples. Since the A130 laminates fail at relatively low loads due to the buckling of the compression surface, the tension side will not see the greater loads required for failure. Composites of A130 reinforcement are notably stronger in tension than compression, and this behavior explains the mechanical failures of the these laminates observed during the bending tests. The D155 laminates do not suffer from a reduced compressive strength and as a result, they experience significantly greater ultimate bending strengths and tension surface delaminations, as illustrated in Figure 64.

The thickness, stiffness, maximum stress, and flexural modulus data from the three-point bending tests are shown in Table 24. Thickness was included in this table due to its significant role in the mechanical strengths of the bending specimens. The thickness of the laminates had strong effects on moments of inertia and consequently, the stiffness, maximum strength, and flexural modulus of the composites subject to three-point bending loads. The specimen stiffness data were included in Table 24 due to the limited amount of stress data that was feasible to collect. The only stress that was

Table 24. Three-point bending test comparisons.

Lay-up	Fabrics	Process	Average Thickness (S.D.) mm	Average Stiffness (S.D.) N/cm	Average Max. Stress (S.D.) MPa	Flexural Modulus (S.D.) GPa	Data Points
[0/±45/0]s	D155 / DB120	HL	3.32 (0.21)	484 (47)	675 (22)	25.1 (1.0)	10
		RTM - R	3.07 (0.08)	425 (16)	698 (18)	27.7 (1.3)	
		RTM - S	3.20 (0.16)	458 (72)	686 (43)	27.1 (1.0)	
		VARTM	3.15 (0.17)	443 (48)	694 (25)	27.0 (2.7)	
	A130 / DB120	HL	3.44 (0.11)	461 (31)	486 (36)	20.7 (1.3)	5
		VARTM	3.13 (0.07)	393 (15)	475 (54)	25.0 (2.7)	
[0/0/±45/0]s	D155 / DB120	HL	4.68 (0.16)	1512 (81)	797 (35)	20.8 (1.5)	5
		VARTM	3.24 (0.04)	722 (25)	1042 (33)	40.0 (0.9)	
	A130 / DB120	HL	4.07 (0.15)	1001 (125)	615 (28)	27.2 (1.6)	
		VARTM	3.28 (0.05)	683 (29)	629 (17)	36.1 (1.4)	

approximated for the bending test specimens was the average ultimate strength. This was accomplished with the standard equation used for small displacement tests ($\sigma_{max} = Mc/I$). However, this equation has limited validity as the bending specimen reaches large non-linear behavior at failure. As a result, the maximum stress equation was employed as a comparative technique between fabrics, lay-ups, and processes, and was not intended to be used in finding the actual maximum strength of the three-point bending specimens.

Approximations in maximum bending strength allowed for the comparisons shown in Figure 65. In this figure the average, maximum, and minimum values of bending strength are presented for the variety of fabrics, lay-ups, and processes examined. The average strength values for the D155 laminates were found to be 32% higher for the [0/±45/0]s lay-ups and 40% higher for the [0/0/±45/0]s schedules when compared to A130 laminates. Differences between the hand lay-up and VARTM processes were less than 3% or less for 6 ply laminates and 2 – 24% for composites of 8 layers. When evaluating bending test specimens statistically, differences between the hand lay-up and VARTM processes were found only for the D155/DB120 [0/0/±45/0]s composites. All other samples showed no significant differences between average strengths for specimens of varying manufacturing techniques.

The bending stiffness properties of the hand lay-up and RTM specimens tested in this study are illustrated in Figure 66. It was found that thickness had a strong influence on this mechanical property. Statistical analyses showed no significant difference between D155/DB120 [0/±45/0]s laminates manufactured by hand lay-up and RTM. The remaining sets of samples were compared, and hand lay-up specimens proved to be stiffer
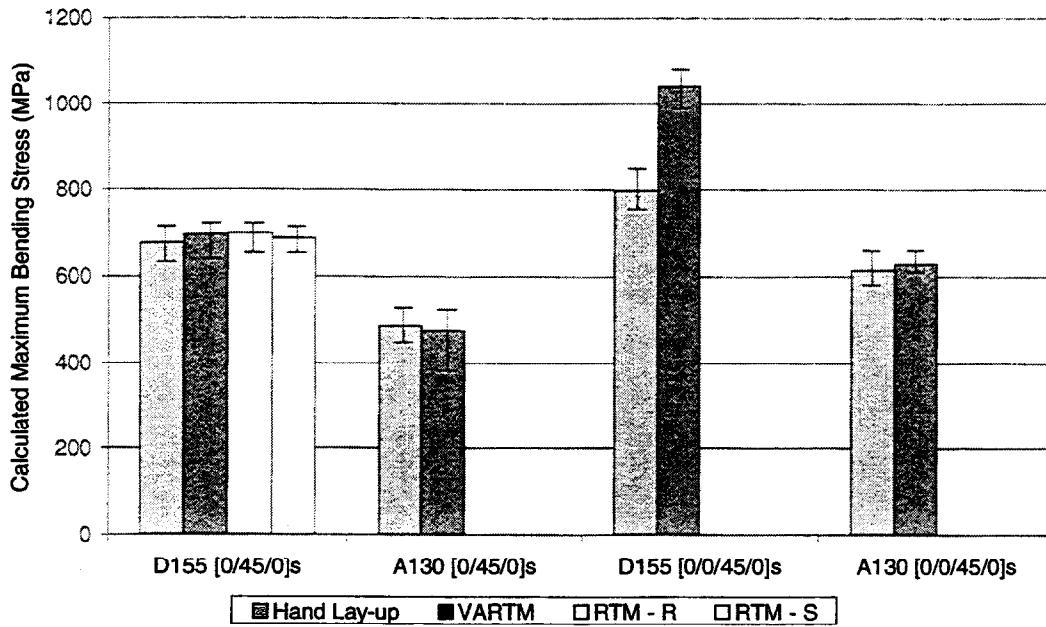
Figure 65. Calculated maximum bending stress comparisons.
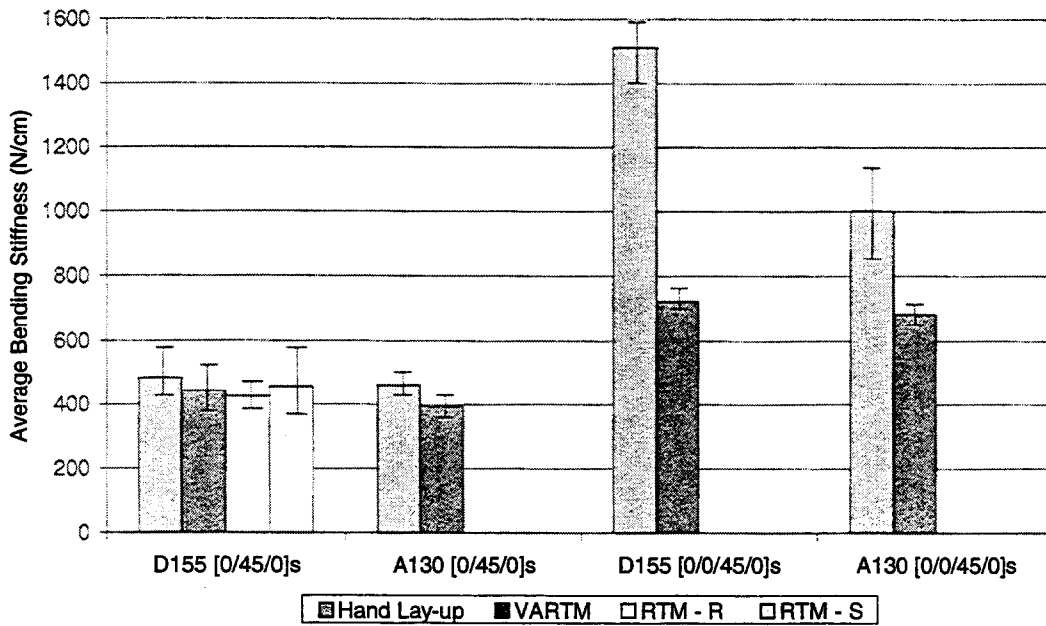
Figure 66. Average three-point bending stiffness.

than their VARTM counterparts. It was observed that this was not due to improved interaction of the matrix and reinforcement with hand lay-up processing. Rather, the specimens were considerably thicker and consequently, stiffer. For example, the [0/0/±45/0]s bending specimens manufactured by hand lay-up versus VARTM were thicker by 0.8 - 1.5 mm, and this resulted in differences in bending specimen stiffness by up to 52% for the D155 composites and up to 32% for the A130 laminates. These improvements in bending stiffness for hand lay-up samples over VARTM specimens were clearly due to increases in the moment of inertia of the test cross-section as opposed to improvements in the actual material subjected to testing.

Flexural modulus was another property provided by the three-point bending test. The average values for the flexural modulus results of this study are shown in Figure 67. The averages in bending modulus were found to be significantly greater for all VARTM manufactured laminates when compared to hand lay-up. Differences in average flexural modulus were between 7 – 17% for the [0/±45/0]s laminates and 10 – 48% for the [0/0/±45/0]s composites. The significant differences in flexural modulus between samples manufactured by VARTM versus hand lay-up are primarily due to the improvements in fiber volume content made possible by the RTM process. RTM was noted to maintain nearly identical specimen thicknesses throughout this study. It was noted earlier under the Physical Property Comparisons that for all the laminate types used in this study, hand lay-up yielded specimens that were significantly thicker than the samples manufactured by VARTM. These measurable differences in thickness and fiber content contribute to the differences in flexural modulus, shown in Figure 67. It can also
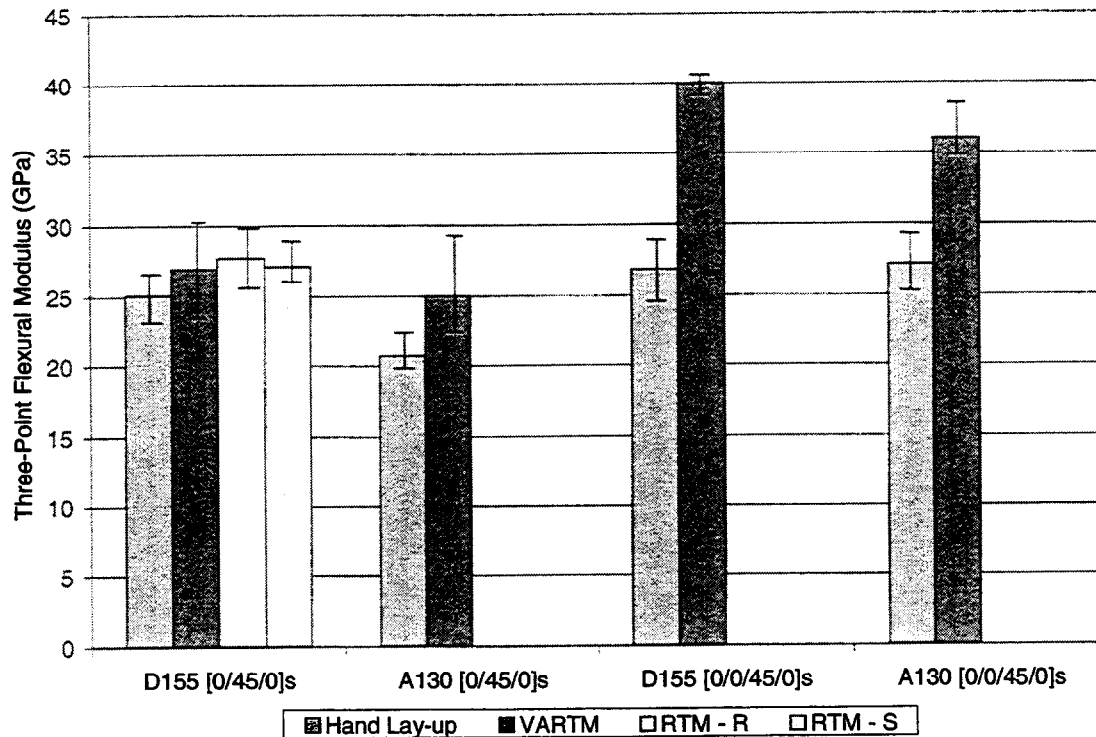
Figure 67. Three-point bending moduli results.

be observed that as the difference in fiber content increases, so does the difference in

flexural modulus between hand lay-up and VARTM manufactured specimens.

Longitudinal Tension

Longitudinal tensile specimen data were collected with an extensometer until

slightly past initial damage. The high loads in these tests were sufficient to damage the

extensometer as energy was released at failure. To avoid this hazard, the Instron digital

instrumentation was used to record ultimate failure strengths instead. An example of the

data gathered with the use of the extensometer can be found in Figure 68. The points of

interest are labeled for the tensile tests. These are initial damage strain, elastic modulus, and ultimate tensile strength.

Typical tensile specimens tested in this study are illustrated in Figure 69. Shown in this figure are the dogbone geometries and the additional tab material of these specimens. Both of these features helped to ensure specimen gage section failures.

The tensile test results found during the course of this study are summarized in Table 25. This table contains the average and standard deviation values for ultimate tensile strength, tensile modulus, and initial fracture strain of the specimens tested. It is worth noting that for the tensile experiments, only VARTM and hand lay-up samples were fabricated, tested, and then compared. The reason that only these two processes were tested was due to the labor intensive operations of routering the dogbone shape and secondary bonding the tab material. The additional time involved in including standard RTM specimens did not seem justified for a test that was not suspected to have a strong relation to manufacturing technique. As a result, VARTM (using Radius equipment) and hand lay-up specimens were used exclusively in this study.

The average ultimate tensile strengths and their maximum and minimum recorded values are shown in Figure 70. Lay-up schedule affected the laminate tensile strength according to unidirectional fabric content. The [0/0/±45/0]s specimens contained 75% unidirectional fabric while [0/±45/0]s samples had only 67% of their volume containing 0° reinforcements. These differences in unidirectional material content resulted in improved strength for VARTM composites of [0/0/±45/0]s lay-up over [0/±45/0]s by 28% for A130 and 31% for D155. Fabric type also appears to have a significant effect on
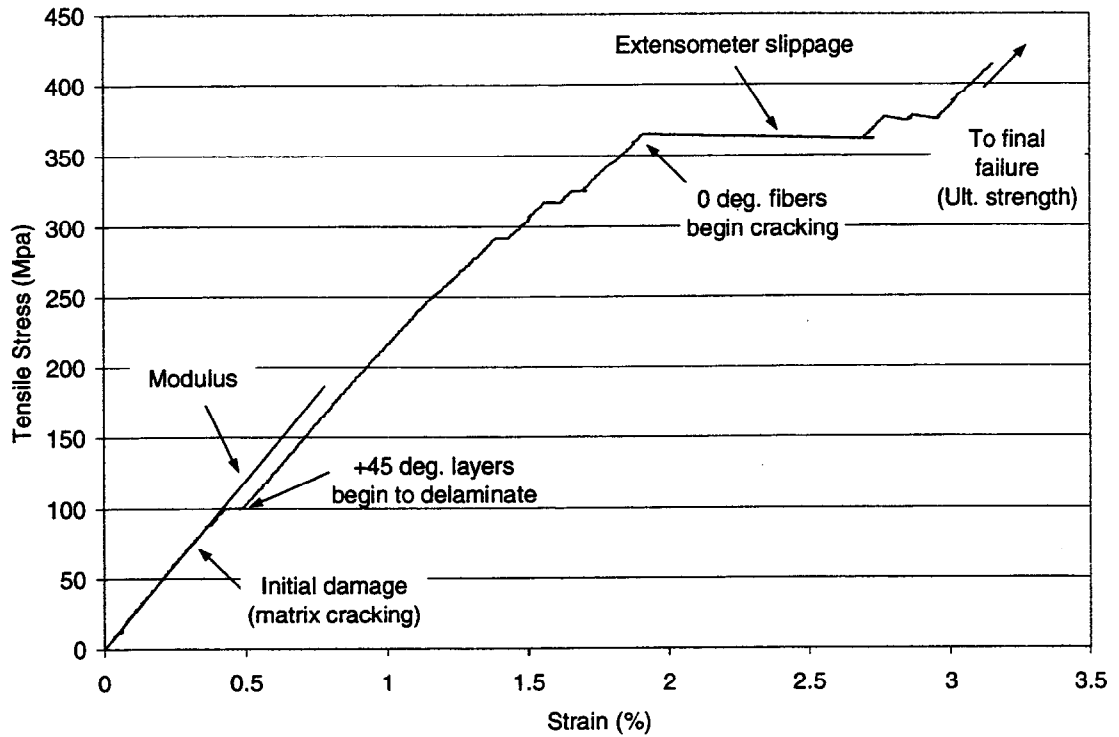
Figure 68. Tensile test data example.
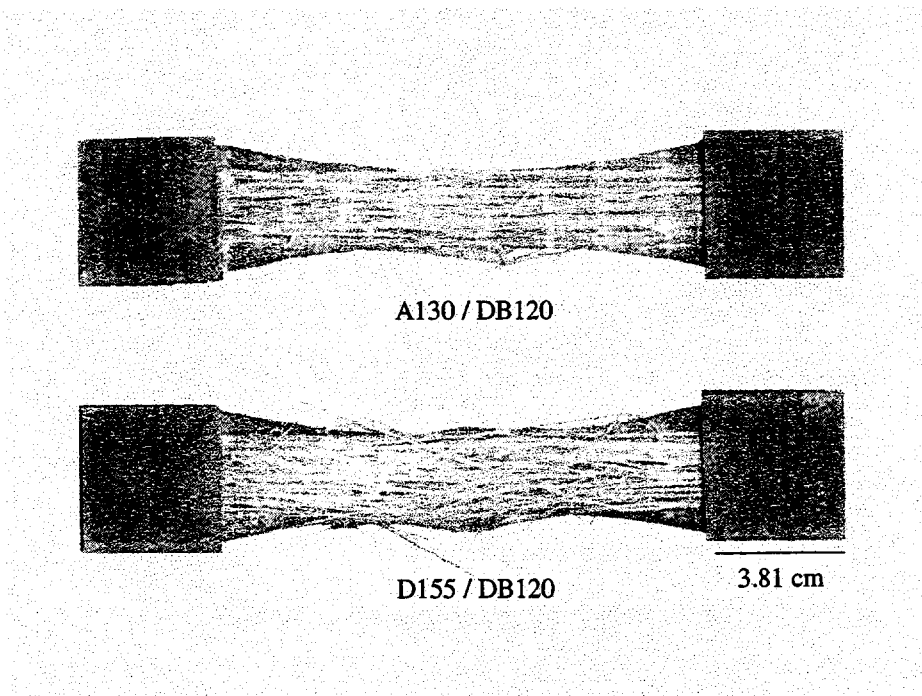
Figure 69. Tensile test specimens.

Table 25. Longitudinal tensile testing results.

Lay-up	Fabrics	Process	UTS (S.D.) MPa	Tensile Modulus (S.D.) GPa	Strain to 1st Fracture (S.D.) %	Data Points
[0/±45/0]s	D155 /	HL	639.5 (37.2)	24.9 (1.0)	1.22 (0.17)	5
	DB120	VARTM	646.8 (7.9)	24.1 (0.5)	1.18 (0.48)	
	A130 /	HL	488.9 (37.0)	20.9 (1.3)	1.60 (0.13)	
	DB120	VARTM	545.1 (5.7)	21.9 (0.8)	1.55 (0.53)	
[0/0/±45/0]s	D155 /	HL	635.8 (39.1)	24.5 (1.3)	1.01 (0.24)	5
	DB120	VARTM	932.8 (29.2)	34.4 (1.3)	0.92 (0.13)	
	A130 /	HL	610.9 (26.1)	23.9 (0.5)	1.41 (0.23)	
	DB120	VARTM	752.7 (24.3)	28.1 (1.6)	1.42 (0.06)	

UTS - Ultimate Tensile Strength
NOTE: Sample thicknesses vary between HL and VARTM in accordance with Table 14.

ultimate tensile strength. Reductions were again found for unidirectional material type. Reductions in tensile strength between 16% and 19% were observed when comparing VARTM with D155 unidirectional fabrics versus A130 fabrics. These differences in strength can be accounted for by a combination of the lower content of unidirectional material and the inherent lower strength of A130 laminates when compared to similar specimens with D155 fabric [50]. Moving on to process comparisons, differences in ultimate tensile strength between hand lay-up and VARTM laminates were 1 – 10% for 6 layer samples and 19 – 32% for 8 layer specimens. Statistical tests showed no measurable differences between VARTM and hand lay-up for [0/±45/0]s samples, while significant differences were found for composites of [0/0/±45/0]s lay-up.

Normalizing the data of Figure 70 reduced the differences between process for all the specimens tested. The normalized tensile strength data are presented in Figure 71. The differences in average normalized compressive strength were 4% or less for all laminate types tested. With the exception of the A130/DB120 [0/0/±45/0]s specimens, all the sample types yielded no statistical differences according to process. Even the normalized results for A130/DB120 [0/0/±45/0]s laminates were not strong in their measured differences (statistical P value = 0.03). These normalized investigations show that the differences in processing between hand lay-up and RTM will not have measurable differences in ultimate tensile strength.

The results for average tensile moduli are shown in Figure 72. Fabric types and unidirectional fabric content had the similar effects on moduli as observed for ultimate tensile strength. The tensile specimen results shown in Figure 72 suggest that moduli are
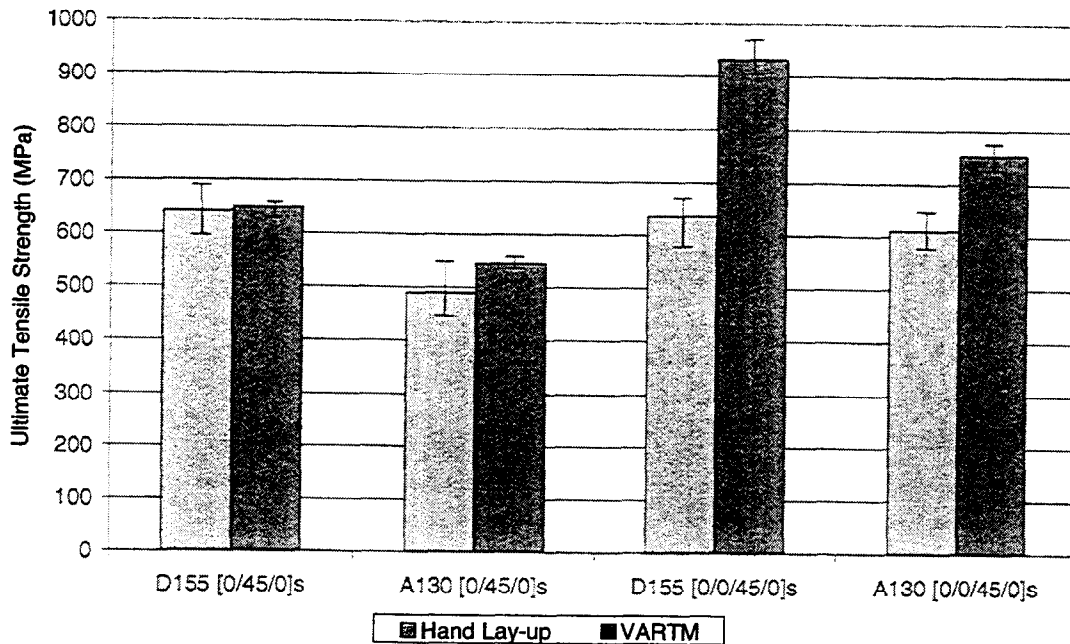
Figure 70. Average ultimate tensile strength with maximum and minimum values.
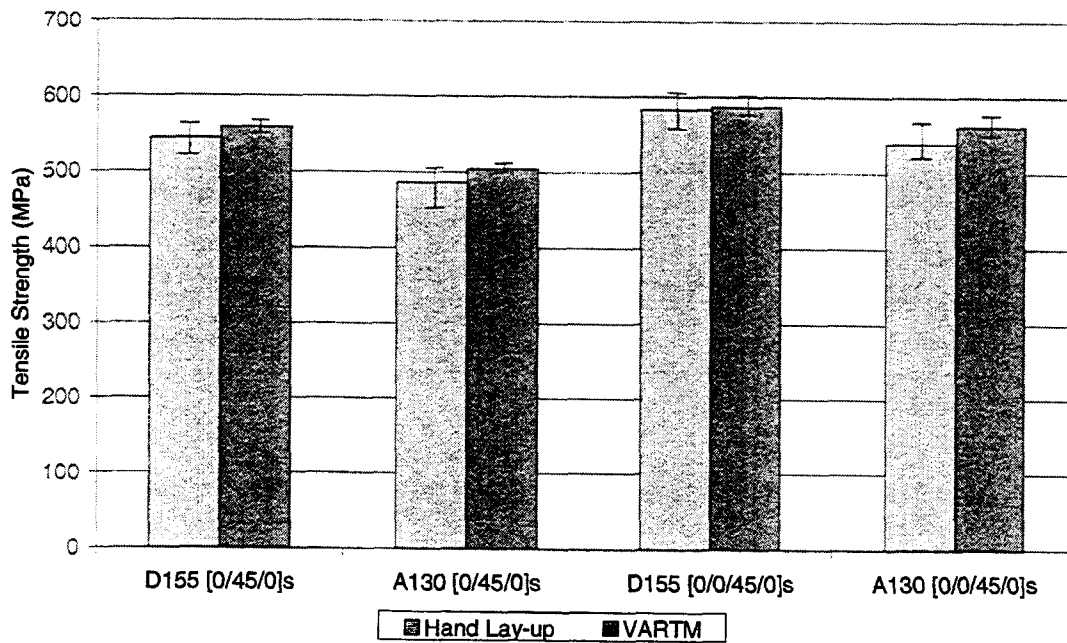
Figure 71. Normalized average ultimate tensile strengths.

reduced for composites with A130 reinforcement, when compared to those with D155 fabric. These reductions in moduli were found to be 9% between [0/±45/0]s laminates and 18% between [0/0/±45/0]s composites. The percentage of 0° degree reinforcement also improved tensile moduli as it improved ultimate tensile strength earlier. When processes were compared, no statistical differences were found for [0/±45/0]s laminates, while [0/0/±45/0]s composites had measurable distinctions. These eight ply laminates saw reductions between 14 and 26% in tensile modulus with A130 reinforcement.

Normalization for modulus was not shown here but yields the same conclusions as with the tensile strength results. That is, process has little effect on normalized longitudinal tensile modulus. These results underscore the observation that while processing does not affect normalized laminate strengths and stiffnesses in fiber dominated directions, hand lay-up will be detrimental in other areas, such as weight and fiber content.

The strains at initial damage for tensile specimens were also recorded and their average, maximum, and minimum values are shown in Figure 73. Statistical analyses of these groups of data showed no differences between any of the fabric and lay-up combinations. While it was useful to find the average of damage onset, this investigation implied that the variability associated with initial tensile damage was too great to distinguish between the hand lay-up and RTM processes.
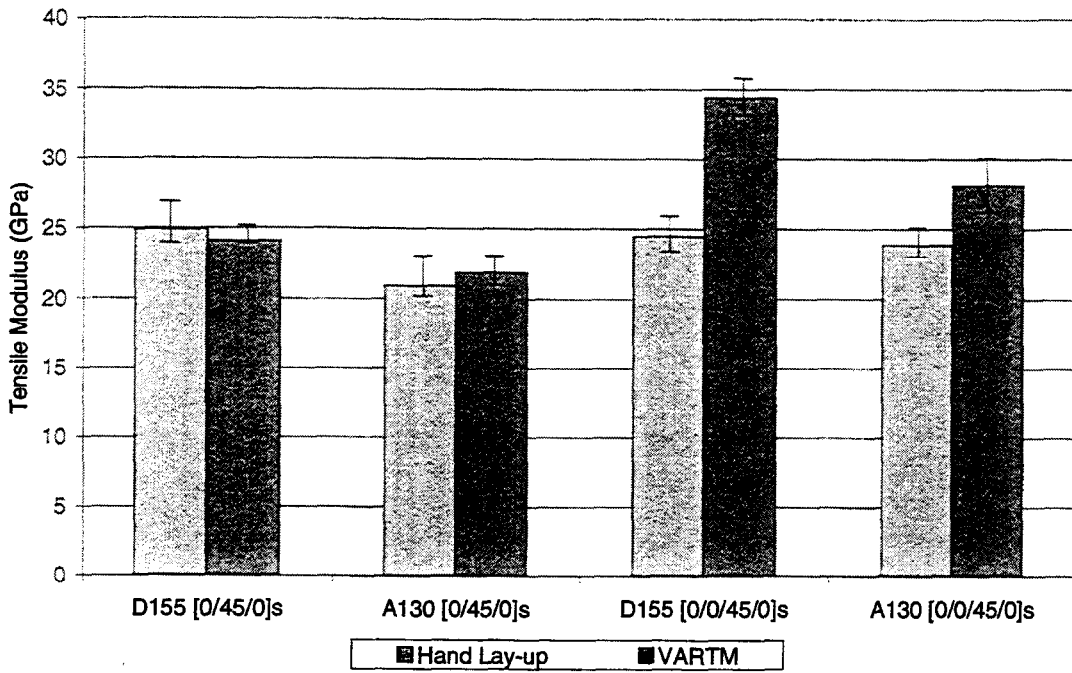
Figure 72. Tensile modulus results.
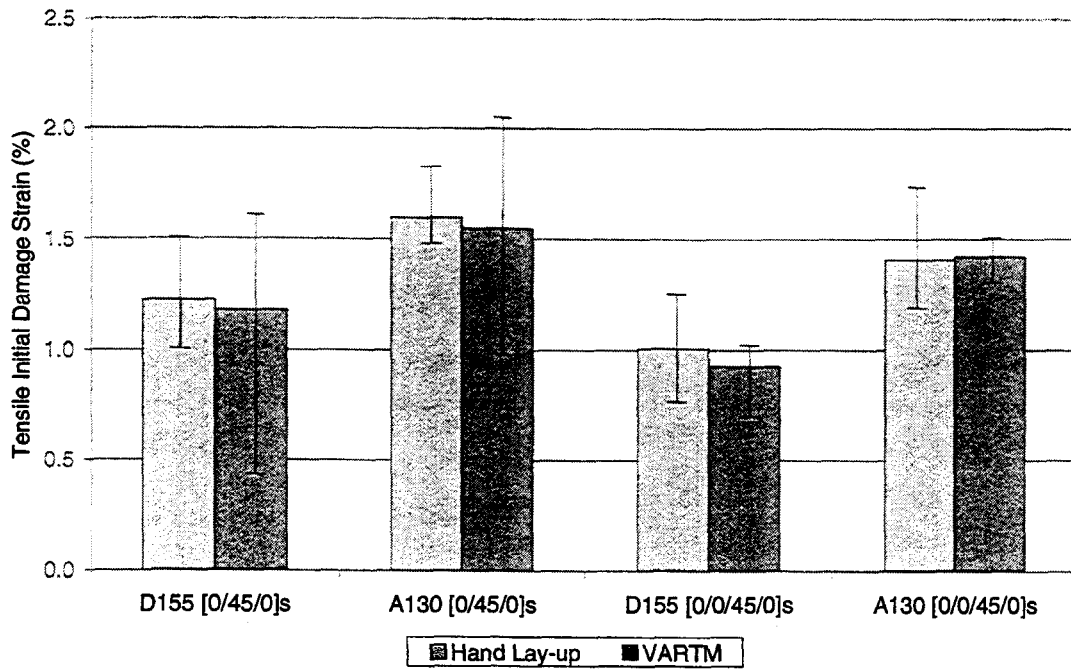
Figure 73. Tensile initial damage strain results.

Fatigue

The fatigue tests of this study were performed under reversed tension and compression loading (R = -1) to represent severe fatigue loading of the turbine blade. This test required short gage lengths and as a result, extensometer data were not collected. The information collected were specimen stress and fatigue lifetime from the Instron digital readout. Tested fatigue specimens are illustrated in Figure 74. Fatigue specimens were not complicated to prepare, but did require many hours to test. Due to this time commitment, only the [0/±45/0]s laminates of D155/DB120 and A130/DB120 fabrics were investigated.
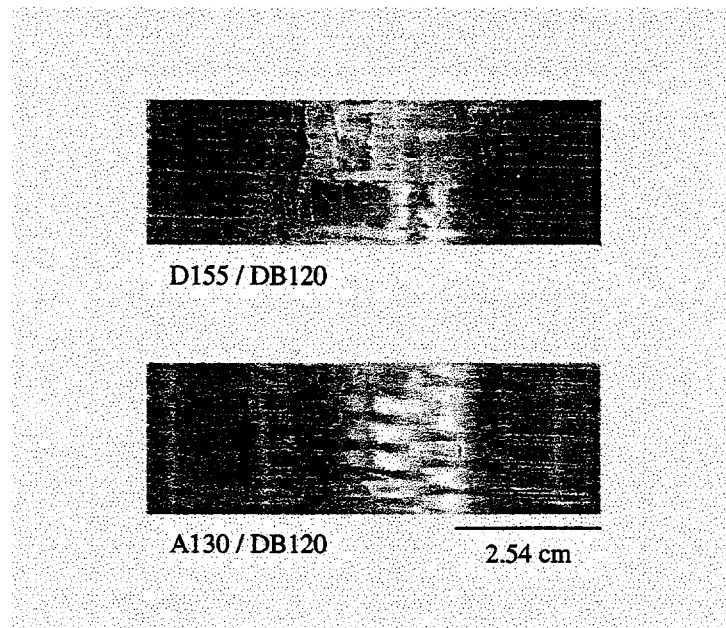
Figure 74. Fatigue test specimens.

A summary of the fatigue testing data is given in Table 26. The test stresses shown in this table were chosen to achieve a target fatigue lifetime of approximately 100,000 cycles. During testing, the Instron machine operated in load control to apply

±172 MPa stresses to the D155 samples and ±138 MPa stresses to the A130 specimens. The D155/DB120 (R= -1) fatigue specimens were nearly identical in thickness and showed no statistical difference (P = 0.7). On the other hand, the A130/DB120 samples had over a 0.6 mm difference in thickness that significantly effected the fatigue results. The average fatigue lifetime for VARTM A130/DB120 specimens was more than five times greater than the life found for the hand lay-up samples. This significant drop in fatigue life for hand lay-up laminates could have been attributed to thickness and loading criteria. With the notably greater thickness measured for the A130 hand lay-up samples an equally greater load was required to stress the specimens to the same levels of their VARTM counterparts. The increased loading scheme for the hand lay-up specimens may have unfairly biased them against VARTM and required further investigation.

To address this issue, the A130/DB120 specimens were retested under constant loads. Matrix material should contribute very little to the structural performance of these specimens and as a result it is fair to apply specimens of identical reinforcement content to similar loads. The constant load chosen was approximately 10 kN and tests of this type resulted in fatigue lifetimes of 435k and 280k for hand lay-up and VARTM, respectively. At first glance the average values suggest a notable difference, yet a statistical treatment of the complete fatigue data suggests little difference between the two sample groups (P > 0.1). Therefore, the results of the fatigue specimen study show that composite applications will not see a difference in fatigue performance for [0/±45/0]s laminates manufactured by either VARTM or hand lay-up.

Table 26. Fatigure data summary.

Lay-up and Fabrics	Process	Sample No.	Average Thickness (S.D.) mm	Test Stress MPa	Fatigue Cycles	Average Fatigue Life (S.D.) cycles
[0/±45/0]s	HL	702.34	3.11 (0.10)	±172	62257	139,890 (113,397)
		702.35			364201	
		702.36			105255	
		702.37			70566	
		702.38			95787	
		702.39			141276	
D155 / DB120	VARTM	622.34	3.18 (0.07)	±172	46707	115,740 (68,957)
		622.35			88727	
		622.36			95102	
		622.37			70028	
		622.38			232841	
		622.39			161036	
[0/±45/0]s	HL	705.34	3.69 (0.27)	±138	47302	51,140 (38,453)
		705.35			48328	
		705.36			123583	
		705.37			48209	
		705.38			11396	
		705.39			28021	
A130 / DB120	VARTM	619.34	3.06 (0.06)	±138	470659	280,132 (115,979)
		619.35			255852	
		619.36			235153	
		619.37			364006	
		619.38			189096	
		619.39			166027	

Lay-up and Fabrics	Process	Sample No.	Average Thickness (S.D.) mm	Test Stress MPa	Fatigue Cycles	Average Fatigue Life (S.D.) cycles
[0/±45/0]s	HL	705.40	3.50 (0.26)	±121	612132	434,952 (184,254)
		705.41			553304	
		705.42			632739	
		705.43			318823	
		705.44			228950	
		705.45			263763	
A130 / DB120	VARTM	619.34	3.06 (0.06)	±138	470659	280,132 (115,979)
		619.35			255852	
		619.36			235153	
		619.37			364006	
		619.38			189096	
		619.39			166027	

RTM Flat Plate Washout Observations

The flat plates that the mechanical test specimens were collected from were manufactured with RTM flow rates and injection pressures that yielded reasonable cycle times. However, a production environment would require that injections be optimized such that specimens can be injected as quickly as possible without washing-out or distorting the fabric reinforcement. Washout and distortion are a consequence of the resin flow displacing the fiber reinforcement during injection. In this study, the general trends in washout onset were documented for the laminates of the flat plate mechanical testing matrix. "Onset of washout" is defined for the purposes of this study as the lowest (averaged) injection pressure where displacement of the fibers is first noticeable to the unaided eye during RTM. The results of this washout study demonstrate at what ultimate parameters future flat plate specimens could be manufactured. In addition, this information compliments RTM flow modeling applications like the work performed by Rossell [45].

The washout experiments began with selecting all of the fabric and lay-up combinations used in the mechanical testing study. The Radius RTM equipment and data acquisition system were used to determine and record the approximate pressures for fiber washout. An aluminum top was substituted with the glass plates for safety at elevated pressures. A series of plates were then injected for each fabric and lay-up combination and pressures were recorded. While the values collected might appear to be strict pressures for the onset of washout, many factors contribute to fabric distortion. Washout behavior is notably variable in nature even for identical RTM situations. As a result, the

washout investigation results show the average injection pressures that will most likely washout the glass reinforcements. The influence of pressure gradients (versus absolute pressure), fabric types, matrix viscosity, etc. would need to be investigated at length for a more complete study of the fiber washout phenomenon.

The results for the current washout investigation are summarized in Table 27. For the results of washout injection pressures, average values, a range of values, or the maximum tested values are presented. Pressures denoted with a plus sign were either the maximum values tested or the maximum attainable with the current RTM equipment. A number of trends in flat plate washout behavior is noted in Table 27. Fabric architecture appears to be an important parameter in washout onset. For all the lay-ups used in the mechanical testing study, laminates with unidirectional D155 material required significantly greater injection pressures for washout when compared to the same flat plates utilizing A130 unidirectional reinforcement. Injections where resin is fed into the outer end of a flat plate required significantly less pressure for washout than for injections where resin entered near the center of the mold. This observation held true for all fabric and lay-up combinations explored. Increased fiber content also increased the resin pressure required to achieve fabric washout. This behavior seemed intuitive since greater fiber volumes will have greater frictional forces securing the reinforcement in place. VARTM was also introduced for [0/±45/0]s A130/DB120 laminates to determine the influence vacuum assist might have on washout behavior. The results of Table 27 show that the injection pressure required to initiate washout in VARTM specimens is notably less than an identical specimen injected by RTM. It requires mention that utilizing

Table 27. RTM flat plate washout
results.

Fabrics	Lay-up	Process	Fiber Volume (%)	Injection Location	Washout Inject Press. (kPa)
D155 / DB120	[0/45/0]s	RTM	34	end	483 - 538
				center	724+
	[0/0/45/0]s		49	end	483+
				center	724+
A130 / DB120	[0/45/0]s	RTM	32	end	179
				center	400+
	[0/0/45/0]s		41	end	510
				center	400+
	[0/45/0]s	VARTM	32	end	103 - 172
UC1018/V	[0/45/0]s	VARTM	NA	end	207

Note: + sign denotes washout did not occur at or below value
shown.

injection pressures less than those shown in Table 27 will result in a laminate with no

observable fabric distortion.

Thin Flanged T-stiffener Testing

Thin flanged T-stiffener specimens were tested with the Instron 8562 and a

stiffener pull-off jig. Small loads were required to delaminate the stiffener to skin

interface, and as a result the Lebow 2.2 kN load cell was used in series with the Instron

machine. Specimen deflection was measured against increasing pull-off load with this

equipment. An example of the data collected is shown in Figure 75. The initial damage,

stiffener stiffness, and maximum load properties recorded for the stiffener specimens are

illustrated in this figure. Failure modes were observed and recorded for the variety of T-

stiffeners tested. The results for all of the above properties are summarized in Table 28.
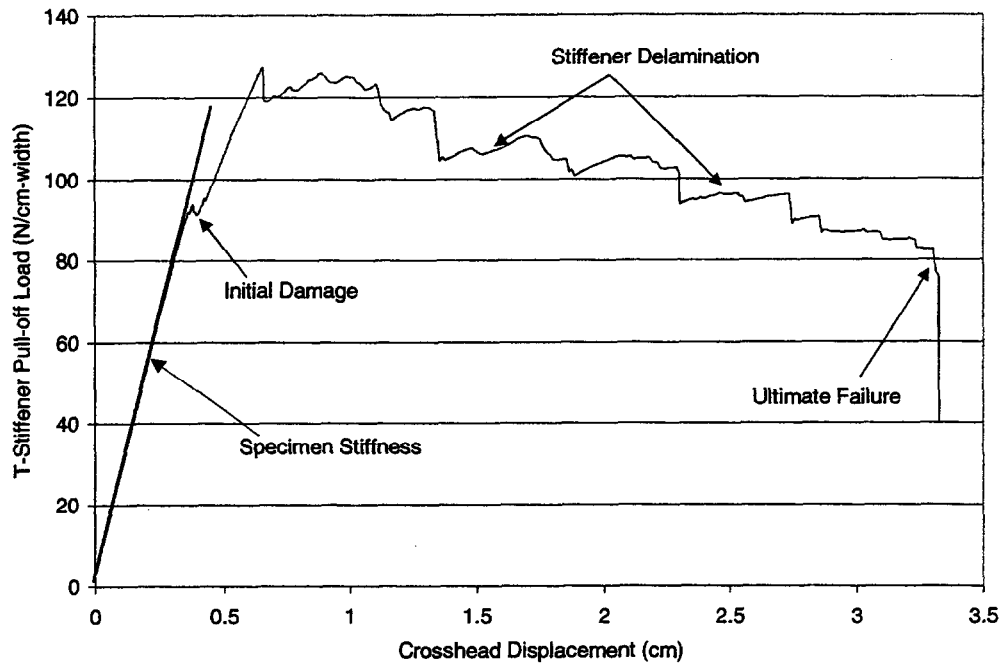
Figure 75. Example curve of T-stiffener pull-off test data.

CC - Co-cured
SB - Secondary Bonded
SB(3) - Bonded from three parts
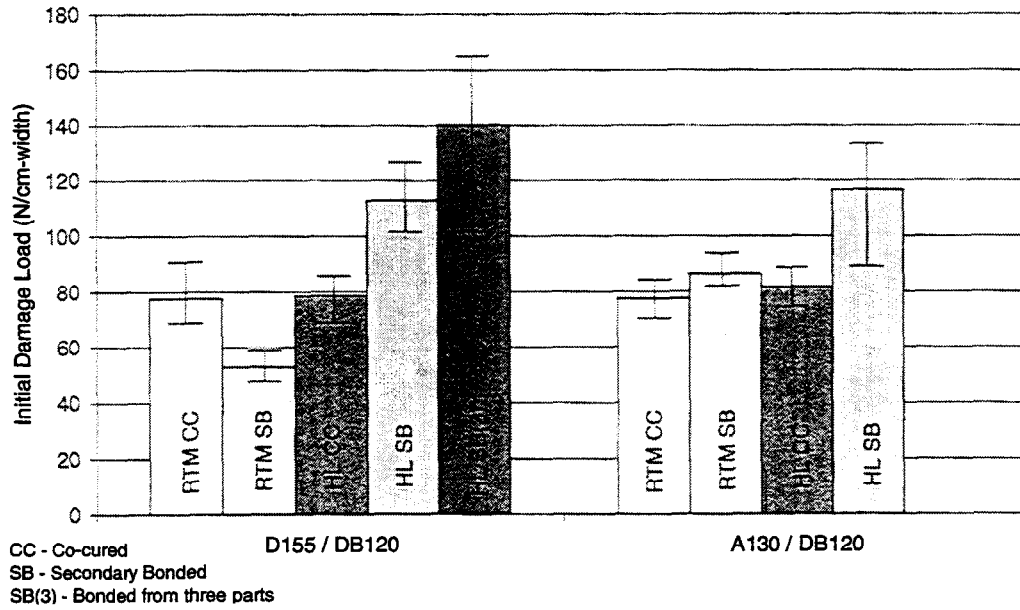
Figure 76. Thin flanged T-stiffener initial damage loads.

Table 28. Test Results for Thin Flanged T-Stiffeners

Fabric	Process	Bond Type	Avg. Web Thickness mm	Avg. Skin Thickness mm	Initial Damage Load (S.D.) N/cm	Maximum Load (S.D.) N/cm-width	Average Pull-Off Stiffness N/cm^2	Failure Mode	Data Points
D155 / DB120	RTM	Co-Cured	4.7	4.0	77.6 (8.9)	144.3 (2.9)	383.1	pull off	6
		Co-Cured *	4.4	4.6	85.5 (15.3)	132.7 (3.9)	NA		11
		Secondary	4.8	3.6	52.7 (3.8)	131.1 (9.9)	290.6		6
		Secondary *	4.6	4.3	87.7 (7.6)	132.3 (9.2)	NA		12
	HL	Co-Cured	4.3	4.6	78.6 (3.8)	111.4 (4.6)	364.7	skin compress	6
		Secondary	4.8	4.4	113.0 (8.9)	159.6 (5.5)	549.1	pull off	6
		Sec. (3 parts)	5.3	4.5	140.3 (25.8)	192.6 (6.6)	590.8		9
A130 / DB120	RTM	Co-Cured	4.7	3.2	77.4 (4.6)	111.6 (1.8)	244.4	pull off	6
		Secondary	4.7	3.4	86.7 (3.4)	124.8 (3.6)	264.7	skin compress	
	HL	Co-Cured	4.7	3.7	81.9 (4.1)	142.7 (4.8)	322.1	tensile pull-out	
		Secondary	4.7	5.0	116.7 (17.9)	139.8 (5.5)	608.0	pull off	

* Results presented in Reference 46.
NA - Information not available

The initial damage results from Table 28 can be examined independently in Figure 76. The damage results for the different T-stiffener specimens according to fabric architecture and interface bond type are shown in this figure. For samples of A130 and D155 unidirectional reinforcement, initial damage in pull-off test occurred at similar loads. Statistical comparisons showed that unidirectional reinforcement type does not appear to influence pull-off strength. Next, it can be noted that when comparing RTM samples, bond interface does not play a significant role in initial damage load. The pull-off loads for D155 T-stiffeners tested by Haugen [46] also showed comparable independence for thin bondlines, and his results were statistically similar to the current findings.

A discrepancy between the RTM secondary bonded and co-cured T-stiffeners can be observed in Figure 76 when comparing average initial damage loads. The initial damage load for the RTM secondary bonded specimens was significantly less than those found for similar T-stiffeners of alternative processing and bond type. This was found to be a problem introduced as a result of the RTM mold. In the manufacture of the T-stiffeners, flexible gasket / spacers were required that allowed skin and web thicknesses to vary. Originally, it was suspected that the variations in thickness would be minimal, however, the results for specimen thicknesses at a variety of locations show otherwise (Appendix B). Comparing laminate thickness and initial damage load implies that specimen mass and moment of inertia play an instrumental role in mechanical performance and that tighter manufacturing tolerances should be followed in the future.

The first modified hand lay-up technique (where T-stiffeners were forced to fit into an RTM tool) shows little difference in initial damage loads when compared to similar RTM specimens. Statistical analysis reinforced this observation for stiffeners of different fabric types. Process selection and porosity content seemed to have little effect on initial damage load for thin flanged T-stiffeners, as well. The second modified hand lay-up and true hand lay-up techniques did show significant differences in initial damage load when compared to the other RTM and hand lay-up specimens. The processing of the latter two hand lay-up specimens yielded samples of greater cross-sectional area than the previous T-stiffeners. The greater cross-section increased mass and moment inertia of the specimens and resulted in the greater initial damage loads observed in Figure 76.

Parameters affecting initial damage similarly influenced maximum pull-off loads. The maximum pull-off loads in Figure 77 seem to be independent of unidirectional reinforcement (either A130 or D155). Ultimate pull-off loads appear to be governed by cross-sectional area, as a review of Figure 77 and Appendix B will show. Hand lay-up processing yielded D155/DB120 T-stiffeners of the greatest amount of mass and as a result had the largest pull-off loads of the specimens tested.

Pull-off stiffnesses were also calculated for the stiffeners of this study. The stiffness value corresponds to the load required per unit width to deflect the specimen. The range of values where pull-off stiffness data is collected is illustrated in Figure 75. Thin flanged T-stiffener pull-off stiffness results are illustrated in Figure 78. Unidirectional fabric reinforcement had little influence on the stiffness property. Again, it appears that process and specimen size were the dominate influences in stiffness
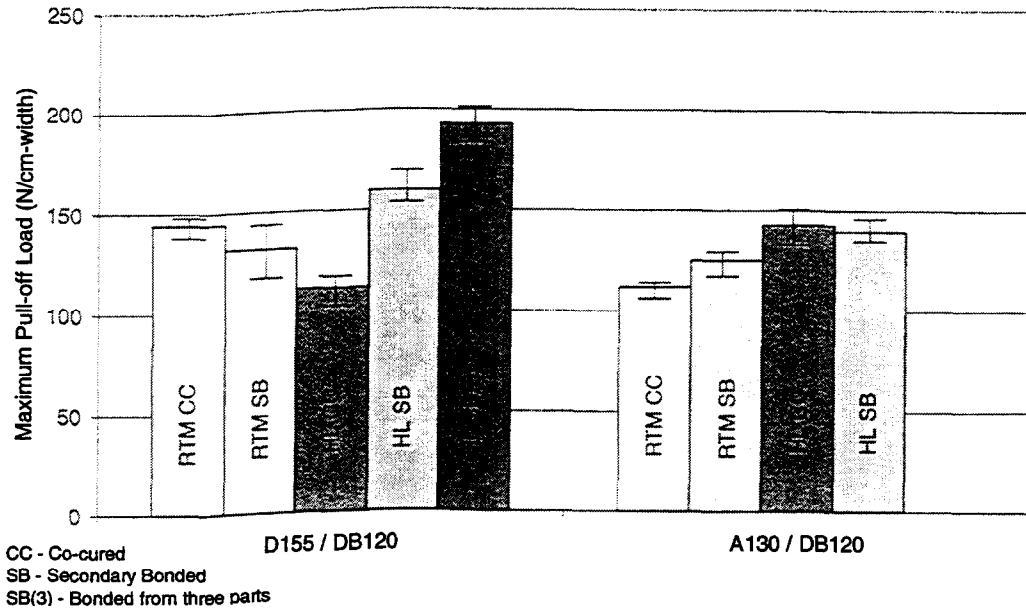
Figure 77. Thin flanged T-stiffener maximum pull-off loads.
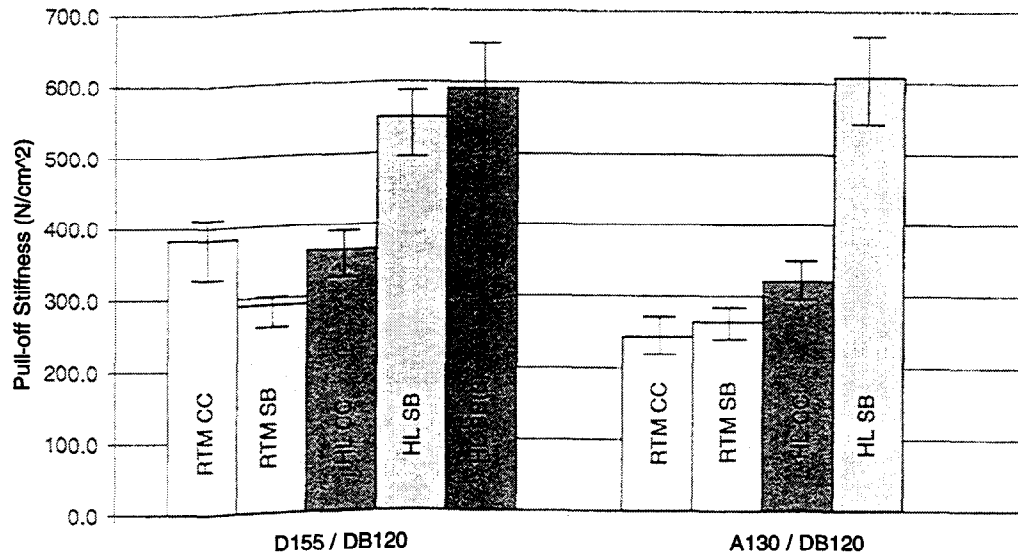
Figure 78. Thin flanged T-stiffener stiffnesses.

results. All specimens manufactured with hand lay-up and secondarily bonded together were significantly greater in specimen pull-off stiffness when compared to the same samples manufactured by RTM, as a consequence of the greater moment of inertia. Variability in stiffness between the RTM co-cured, RTM secondary bonded, and hand lay-up co-cured specimens correlated with variances between specimen web and skin thicknesses.

Review of the stiffener results showed that relying exclusively on pull-off load data may not have been the best approach for evaluating the parameters of this complicated substructure. For the specimens of the flat plate mechanical testing study, normalization techniques were available that allowed for reliable comparisons between samples of slight variances. Yet, the normalization techniques used in the flat plate study are not applicable to more complicated geometries. In an effort to normalize the effects dimensional differences had in the T-stiffener results, a skin stress analysis was performed.

Stiffener skin stresses were calculated at a location near the flange tip to compare specimens in a normalized manner. The location chosen was at the surface of the T-specimen skin, just before it interfaces with the stiffener. This point was selected because a simple mechanics of materials approach could be used at this location and more convoluted methods like FEA could be avoided. Skin stress in this area was calculated with three-point bending, simply supported equations. The results for these skin stress calculations are shown in Figure 79.
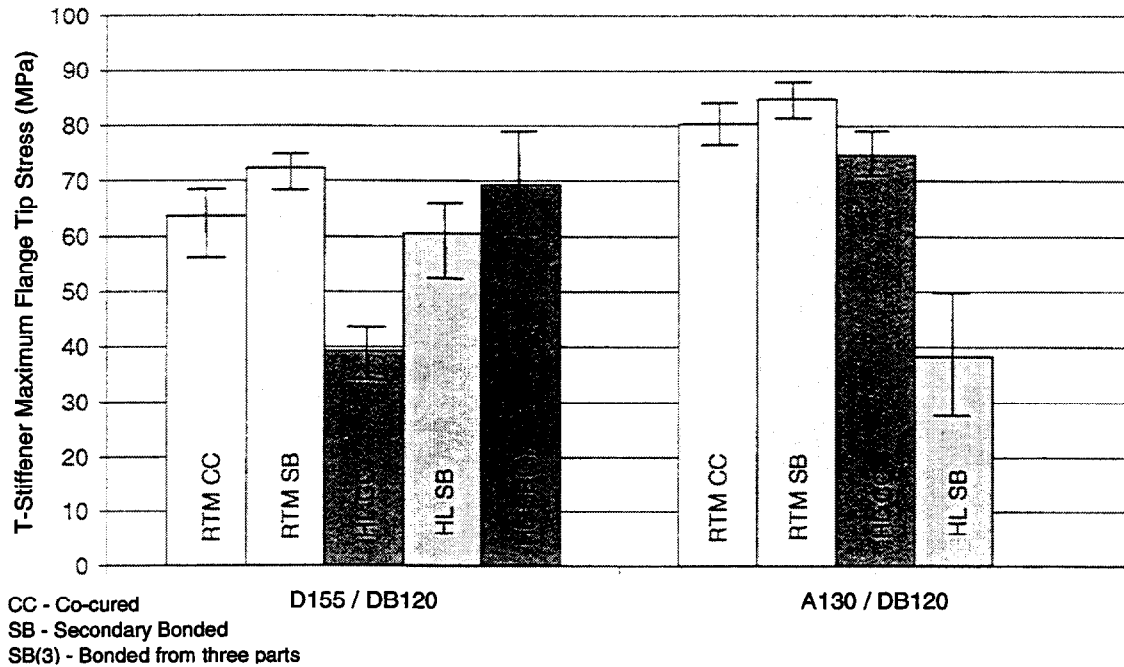
Figure 79. Thin flanged T-stiffener skin stress at flange tip.

RTM specimens supported greater flange tip stresses at T-stiffener maximum load when compared to hand lay-up, as shown in Figure 79. For example, the T-stiffeners manufactured with RTM, D155/DB120 fabrics, and co-cured experienced a 38% increase in flange tip stress when compared to hand lay-up. The same RTM samples that were secondary bonded together were 4 – 16% stronger than the same T-stiffeners manufactured by hand lay-up. It also appears that bond interface and moment of inertia play a role in skin surface stress. Examination of the D155/DB120 specimen results in Figure 79 shows that the use of secondary bond material and the increase in moment of inertia increased the flange tip skin stress in the T-stiffener samples. This behavior was noted for the A130/DB120 specimens manufactured by RTM, but was not repeated for

the same samples manufactured by hand lay-up. This was due to the large difference in skin thicknesses (> 1.5 mm) used to calculate flange tip stress for the co-cured and secondary bonded hand lay-up samples.

The skin stress analysis near the flange tip demonstrates another method for comparing composite substructures. Results from the stress calculations show that this approach normalizes the effects of thickness variation, to a certain extent. In future analyses of complicated geometries a stress and strain method of comparison may prove better in determining the effects dimensional tolerance, bondline thickness, and process have on composite structure mechanical performance.

An interesting discovery made during the course of the stiffener pull-off testing was failure mode. Failure mode was found to be a property that was influenced by all three of the process, fabric, and bond parameters. Previous research demonstrated that RTM T-stiffeners manufactured with polyester resin and glass reinforcement and having the dimensions illustrated in Appendix B, would fail in skin stiffener pull-off [46]. This failure mode is illustrated in Figure 80. This type of skin stiffener specimen had initial damage in the interface near the web. Delamination of the specimen continued until the entire stiffener was removed from the skin. Nearly 75% of the T-stiffener specimens tested in this study failed in this manner. For example, all D155/DB120 T-stiffeners manufactured by RTM and all D155/DB120 T-stiffeners manufactured hand lay-up and secondary bonded failed in stiffener pull-off.

The observation that was of interest was that two additional failure modes were found for specimens of different thickness, fabric, and process. The second failure mode
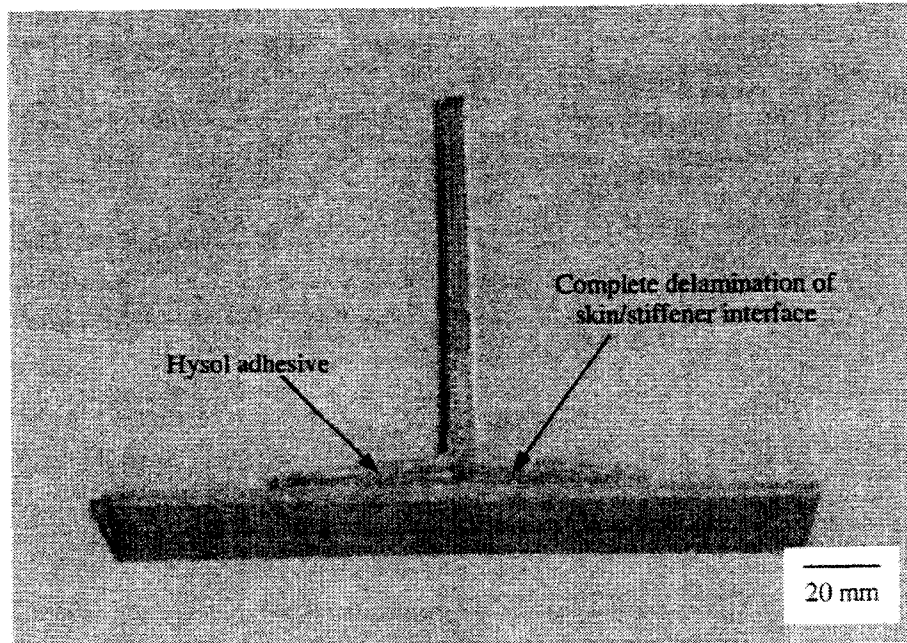
Figure 80. Stiffener pull-off failure mode.
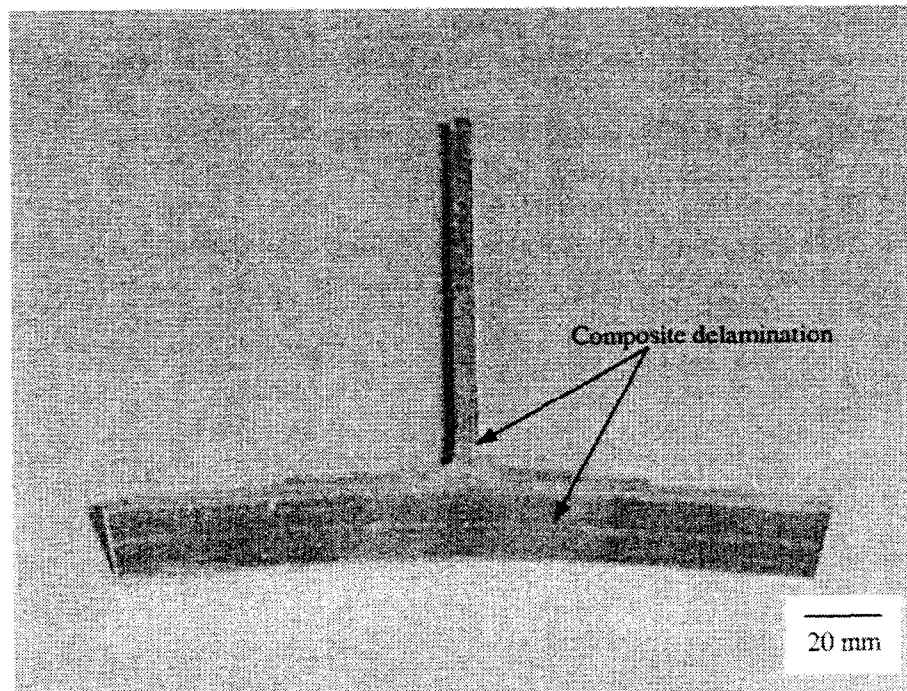
Figure 81. Stiffener tensile pull-out failure mode.

observed was tensile pull-out. The tensile pull-out failure mode is illustrated in Figure 81. In this damage scenario, failure initiates in a similar manner to stiffener pull-off. However, the stiffener is never entirely removed from the skin. Rather, the skin and stiffener are pulled past the simple supports and out of the jig all together. T-stiffeners manufactured by hand lay-up with A130 unidirectional material and co-cured failed in tensile pull-out.

The third failure mode observed during T-stiffener mechanical testing was skin compression. This failure mode is shown in Figure 82. The skin compression failure initiated with damage in the skin interface near the web, yet significant delamination did not propagate. Instead, the skin failed in compression at this location. Co-cured hand lay-up stiffeners with D155/DB120 fabrics and secondary bonded RTM stiffeners with A130/DB120 fabrics demonstrated the skin compression failure mode.
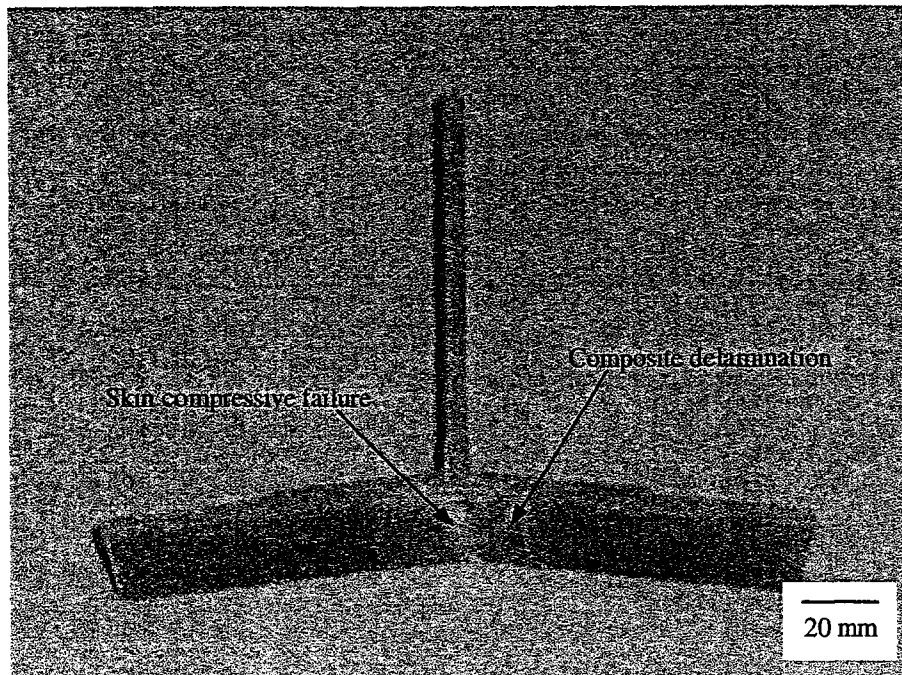
Figure 82. Stiffener skin compression failure mode.

These findings demonstrate that thin flanged T-stiffener failure mode can vary according to manufacturing process and fabric type employed. Current examinations of failure mode versus cross-sectional area did not yield any correlations between the two, but cannot be ruled out at this time. It is uncertain what effect processing could have on stiffener pull-off failure mode, and future work is required to address this interesting phenomenon.

Thick Flanged T-stiffener Mechanical Testing

The four thick flanged T-stiffeners of the experimental matrix were manufactured and prepped for testing. However, the thin flanged T-stiffener results and time limitations precluded the testing of these specimens. The thin flanged stiffener results showed that fabric and process contributed to the structural performance of the samples only in their influences on cross-sectional area. Mass and moment of inertia were the strongest influences on the mechanical performance of the thin flanged T-stiffeners. Reviewing these results suggests that the same would hold true for mechanical testing of thick flanged T-stiffeners. These specimens could shed further light on the issue of failure mode. Future work could include the testing of thick flanged T-stiffeners with varying reinforcement types and manufacturing processes.

I-beam Specimen Mechanical Testing

The eight I-beams of the experimental matrix were manufactured but not tested for structural performance. This was due to problems that arose in manufacturing hand

lay-up I-beams of the lay-up and the size suggested from previous work [47]. Referring

back to Figures 43 and 44 shows the vast difference in cross-sectional area between the

two specimens. The three-point bending and stiffener pull-off tests demonstrated that

area and mass overwhelmed the effects process might have in mechanical performance.

It was suspected that this would also be the case for I-beam specimens where the largest

differences in cross-sectional area were observed. Secondly, the hand lay-up beams were

not feasible to manufacture under the current conditions. The suggested web lay-up of

[±45/0/±45]s performed well in RTM manufacturing due to its symmetry. However, the

hand lay-up methodology required the web and flanges to be fabricated as individual C-

channels. These C-channels were unsymetrical in their lay-ups and were warped

significantly during post-cure due to the behavior of the 45° reinforcements. This

warpage was measured in each hand lay-up C-channel as an 8° rotation for a 762 mm

specimen length. These manufacturing difficulties underscore the influence of

processing on structural components. The observations on hand lay-up beam fabrication

suggest that another program to study assembly influences needs to be conducted.

Root Specimen Mechanical Testing

The primary focus of the root specimen study was to better understand the

technology of fabricating resin transfer molded structures from composite tooling. While

there is some literature on this type of manufacturing [57], the amount of information is

limited. It would be beneficial for future developments to explore the details of molding

RTM components from a tool cavity made from a hand lay-up template. This research

could prove quite useful in the effort to manufacture large turbine blade structures from this flexible and cost-effective tooling method.

In addition to advancing composite RTM tool molding technology, it was of interest to compare the mechanical performance of RTM root specimens against the same samples manufactured by hand lay-up. This portion of the root study explored whether process effected steel insert to laminate interaction, and will be discussed shortly.

The root specimen was an innovative design that combines a shear loaded, mounting insert in a composite laminate. This MSU Composites Technology Team design for a root specimen required investigation to determine the feasibility of manufacturing a complete turbine blade to hub connection. In addition to the root research areas just mentioned, there were minimum requirements of the root specimens that required investigation. These investigations included the following:

- Satisfy a tensile and compressive load of 98 kN. This is the load subjected on a series of specimens during the maximum wind condition of 214 km/h as determined by the FEA performed by McKittrick [3].

- Process specimens with good interaction between laminate and steel insert. Poor interactions would result in premature mechanical failure of the specimen.

- Attain consistent fiber volume throughout the RTM root specimens. This requirement minimizes the likelihood of stress concentrations and matrix rich regions that could initiate cracks.

- Sustain a reasonable fatigue lifetime. While this had not been predetermined, specimens were fatigue tested at loads approximating the maximum wind condition and the number of cycles that the root samples could survive was recorded.

In the first round developments with the composite root specimen, attempts were made to adequately wet-out the reinforcement in the cavity of the RTM tool. This composite RTM mold from Headwaters Composites, Inc. was manufactured from a hand lay-up template. It was unclear how the identical lay-up of the template would perform in an RTM application, however, this appeared to be a good starting point and was chosen for the first three RTM root specimen moldings. Complete information concerning the lay-up schedules, manufacturing notes, and ultimate loads of the specimens tested in all three rounds of the root specimen research are listed in Table 29. Specimens R101 and R102 were attempts to manufacture an RTM root sample with the identical fabrics and lay-up as the original template. It was discovered that in this RTM application the A130 fabric inhibited complete wet-out of the part, and as a result large dry regions were observed in these laminates (Fig. 83). The last sample manufactured under the first round investigation was of D155 and DB120 fabrics and the original template lay-up. D155 fabric facilitated complete wet-out of the root component and was thus chosen as the unidirectional fabric to be used in the subsequent root investigations.

Static tensile test loads and failure modes of the first round root specimens are listed in Table 29. The average for these three tests was found to be 232 kN or 2.3 times the maximum wind condition load. These values showed promise that the design would perform well as a means to mate the turbine blade to the hub. It was observed that two of the root specimens failed as the insert was pulled out of the laminate, while one specimen failed in the composite near the grip. The specimen that experienced grip failure was

160

Table 29. Root specimen manufacturing and testing data.

Current lay-up: Skin   [±45/02/±45]s
                 Surface [±45/0/±45/02/±45]s

Static Tensile Tests

Sample No.	Process	Zero Fabric	Lay-up Schedule	Notes on Manufacturing	Ultimate Load (kN) [1]	Comments
R101		A130	[±45/02/±45/02/±45]s	Poor wet out	243.8	insert pull-out
R102	RTM	A130	[±45/02/±45/02/±45]s ply drops	Poor wet out	213.6	composite failure
R103		D155		Low Vf about insert	241.1	insert pull-out
R201	VARTM	D155	[±45/0/±45/02/±45]s ply drops	Low Vf about insert	230.6	good bonding w/ insert
R104				Low Vf / Super 77 / 3"-12"	240.3	
R106			[±45/0/±45/02/±45]s ply drops	9"-12" strips	198.0	
R107	RTM	D155		Spartan / wash-out / 9"-12"	240.0	composite failure
R108				9"-12" strips	177.2	
R109			Current w/ skin: [±45/03/±45]s	Spartan / High Vf at insert	254.1	two tests / bolt failure / yield
R110			Current	Spartan	252.4	bolt failure / no insert yield
R301	HL	D155	[±45/0/±45/02/±45]s ply drops	No insert tip / 9"-12"	213.5	composite failure
R303				9"-12" strips	181.3	

Fatigue Tests

Sample No.	Process	Fabric	Lay-up Schedule	Notes on Manufacturing	Fatigue cycles (cycles)	Comments
R105 [2]			[±45/0/±45/02/±45]s ply drops	Low Vf / 3"-12" strips		
R111 [2]						
R112					120,317	R: 0.1, 89/9 kN, no damage
R113 [2]	RTM	D155	Current			
R114 [2]						
R115 [2]						
R116 [2]						
R302 [2]	HL	D155	[±45/0/±45/02/±45]s ply drops	9"-12" strips		

[1] - 98 kN is the root specimen design limit load.

[2] - Manufactured but not tested.

161
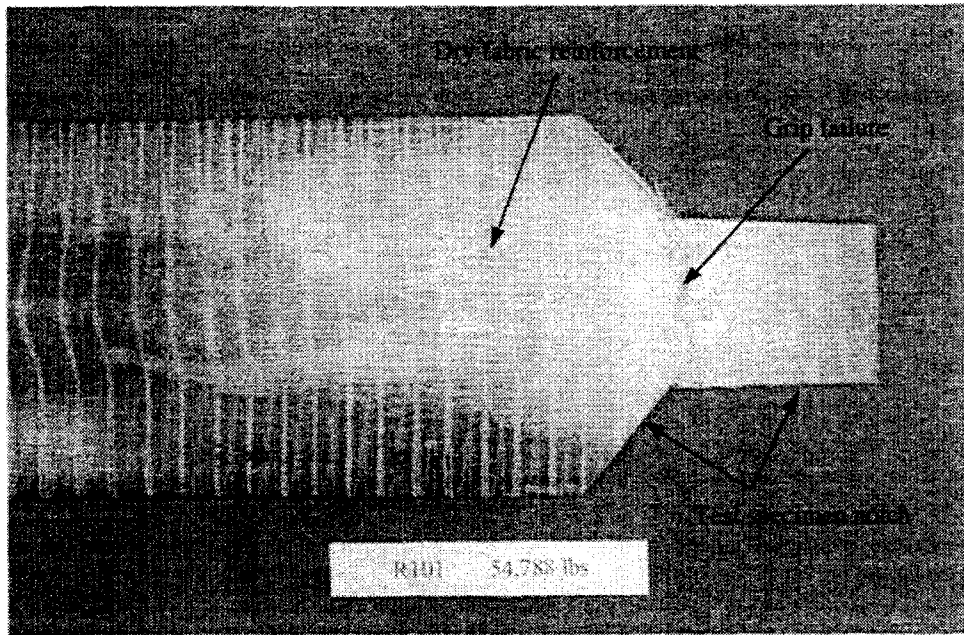
Figure 83. Poor wet out of root specimen R101 with A130/DB120 fabrics.
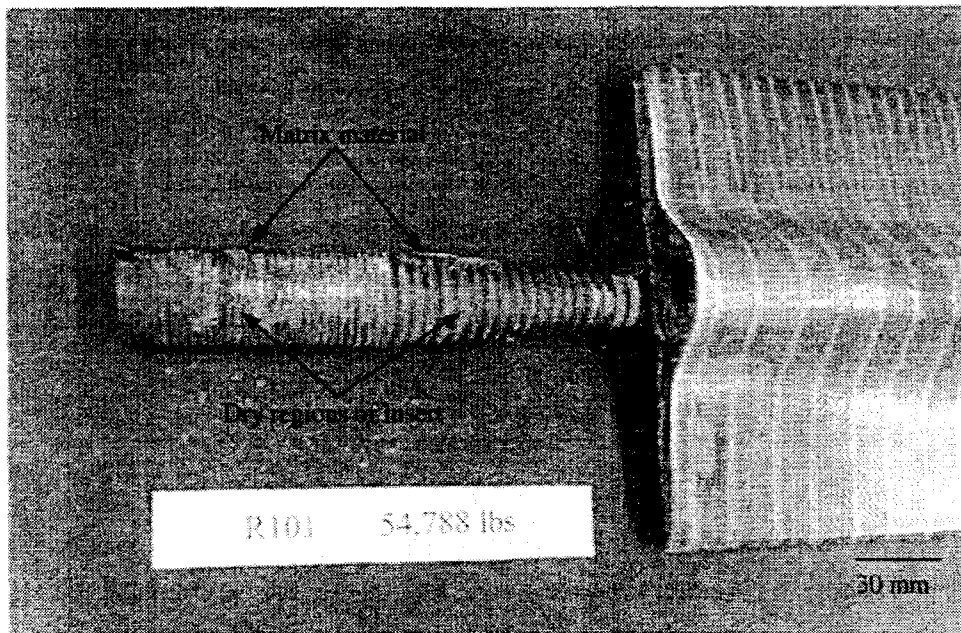
Figure 84. Root specimen R101 and dry steel insert after tensile testing.

poorly wet-out with resin, and consequently it was suspected that the predominate failure mode for root specimens identical to those of round one will be insert pull-out.

The mechanical testing of the round one root specimens demonstrated that the design would meet the maximum load requirement of this study. However, it was found that these specimens did not meet the minimum requirements of insert to laminate interaction and fiber volume distribution. Shown in Figure 84 is root specimen R101 where the insert has been removed during testing. The damage in this specimen through its width illustrates the amount of delamination generated and subsequent energy released during failure (Fig. 85). This failure behavior showed that there was a substantial amount of resistance in removing the insert. However, reviewing the removed insert illustrates little composite / steel rib bonding (Fig. 84). The insert for specimen R101 shows little matrix material and no glass fiber remaining attached to the insert. This demonstrates that composite / insert surface contact was limited. Additional investigations into the root specimen might explore how to improve the interface and achieve better interaction with the polyester matrix and glass reinforcement.

The first round root specimens were also examined for the distribution of fiber volume. No matrix burn-offs were performed on these specimens, yet they were sectioned to gather a visual representation of the distribution of fabric and matrix. Shown in Figure 86 is a sectioned sample of root R103. It was found from these cross-sections that the hand lay-up template was relatively low in fiber volume about the fabric darts. As a result when the same lay-up was used in an RTM application, the injection pressures were sufficient to compress the low volumes of fabric about the sides of the insert. This

behavior resulted in the resin rich regions as shown in Figure 86. These matrix rich regions may have limited the insert interaction with the laminate and could have provided starter cracks during testing. Both possibilities are undesirable and the second round of the root specimen experiments attempted to resolve these issues.

The second round objectives of the root specimen study included increasing the fiber volume about the steel insert and manufacturing hand lay-up samples for process comparisons. During this portion of the root study six RTM specimens and three hand lay-up laminates were manufactured. The first RTM specimen was an attempt to apply vacuum assist on the composite root tool. Composite molds can yield reliable vacuum seals under most circumstances. However, the complicated root tool geometry, including a locator for the steel insert, made vacuum sealing rather difficult. The mold had two seals and required a substantial effort to guarantee consistent vacuum integrity. The inner silicone seal mated well between the tool surfaces, but lost its ability to sustain a vacuum whenever glass fibers overlapped the sealing surfaces. The outer neoprene seal was adjusted on a number of occasions in an attempt to secure a vacuum, but these efforts were also unsuccessful. As a result, specimen R201, the attempt at a vacuum assisted RTM injection yielded a part of marginal quality. The vacuum assist effects were noted to draw in more voids than observed with the standard RTM process. Due to these difficulties with the VARTM process applied to the root mold, the remainder of the RTM specimens studied under the root investigation were manufactured without vacuum assistance.
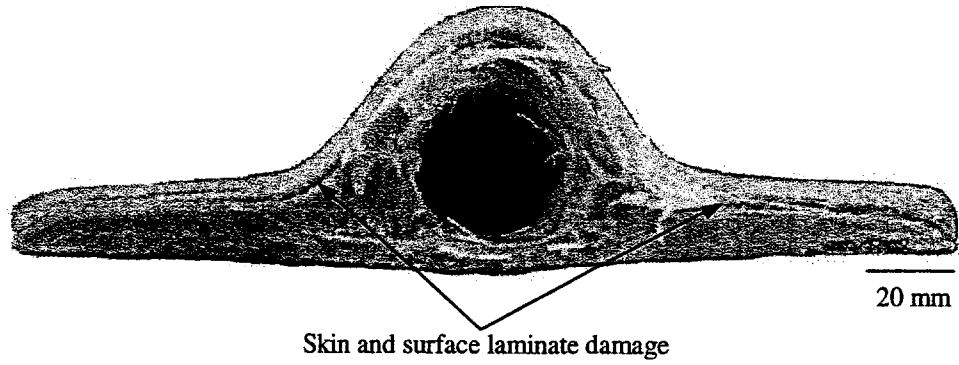
Figure 85. Static tensile test damage through root specimen width.
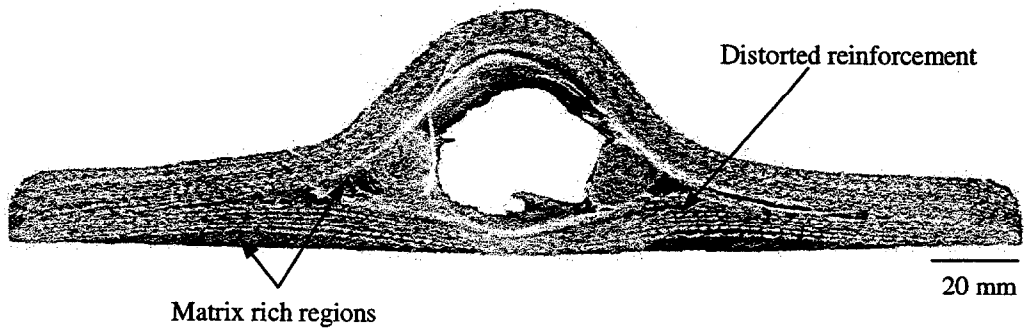
Figure 86. Cross-section of root specimen R201 and resin rich regions near insert.
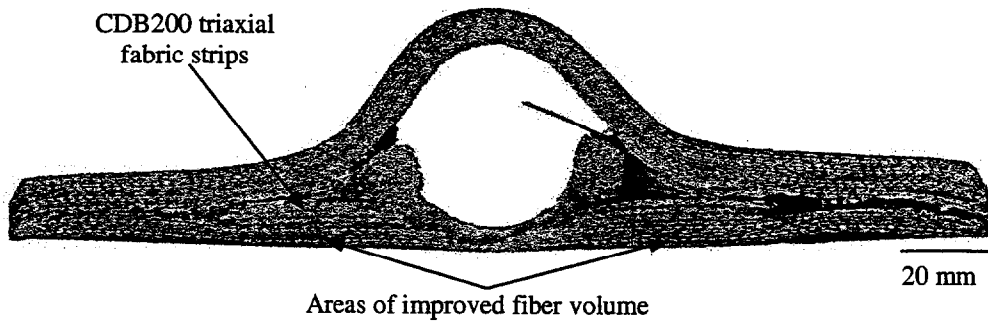
Figure 87. Cross-section of root specimen R104, with higher fiber content at insert.

The remaining five RTM specimens fabricated under the second round root study addressed the low fiber volume noted around the steel insert (Fig. 87). The simplest option for increasing fiber volume on each side of the insert was to add additional glass reinforcement. Modifying the tool surface would have eliminated the need for added material in the RTM'd root specimens, but this would have been the most time consuming and costly solution to the problem. Hence, adding strips of 38 mm wide, CDB200 triaxial reinforcement was the option chosen to address the matrix rich regions of the root design in Figure 86. The specifications for the second round RTM root specimens, as well as a few details on the adjustments made to increase the fiber volume in locations near the insert are provided in Table 29. Illustrated in Figure 87 is a cross section of specimen R106 where the addition of triaxial reinforcement is shown to remedy the fiber volume concern previously noted. Matrix burn-offs were not feasible in these regions because the lay-up and geometry varied in three dimensions and would likely yield suspect fiber volume data. As a result, visual inspection techniques were used for observing composite fiber volumes in complex regions.

Through the course of the second round root study, three hand lay-up specimens were also manufactured. The identical lay-up used to manufacture the RTM roots was used for these specimens. The hand lay-up root samples were fabricated to compare any measurable differences in mechanical strength according to process. During processing, it was found that wetting out the laminate around the steel insert was difficult. The reinforcement had the tendency to pull away from the insert's surface and required

notable amounts of resin for effective wet-out. This raised the concern that perhaps hand lay-up would not force reinforcement against the turbine blade mounting insert as well as in molding procedures. Thus, this issue of whether hand lay-up would generate a steel to laminate interface comparable to that of RTM was noticed and then tested.

Five RTM specimens and two hand lay-up root samples were tested in the second round of mechanical testing. The ultimate loads and failure modes of these specimens were listed in Table 29. The average insert pull-out loads for the RTM specimens were comparable to the values found for the first iteration tests. The ultimate tensile loads for hand laid-up root samples were also found to be within a small margin of the results for the RTM roots. These maximum load comparisons are shown in Table 30. Also listed in this table are the grip location stresses for each specimen. As will soon be discussed, the grip area was of interest during this segment of the root investigations, and it was useful to determine that there was no measurable difference between the pull-out load and grip stress for hand lay-up and RTM root specimens.

Table 30. Root grip stress comparisons.

	Maximum Load (kN)		Maximum Stress (MPa)	
Lay-up Description	Hand Lay-up	RTM	Hand Lay-up	RTM
D155 / DB120	213.5	240.3	247.4	255.0
Surface: [±45/0/±45/02/±45]s pd	181.3	198.0	243.1	215.6
Skin: [±45/0/±45]s	--	240.0	--	262.6
6 layers triax under taper	--	177.2	--	194.1
Average	197.4	213.9	245.3	231.8

The adjustments in lay-up between the first and second root specimen experiments yielded a quite different failure mode during static mechanical testing. In round one, the predominate failure mode was insert pull-out. Increasing the fiber volume about the insert resulted in specimens that were most likely to fail in the laminate near the grip. This failure behavior was observed for five of the seven specimens tested in round two. A laminate grip failure for root specimen R301 is shown in Figure 88. Failures in this area were unexpected and to explore this behavior, matrix burn-offs were performed on the flat grip regions of the hand lay-up and RTM specimens.

The corners of both hand lay-up and RTM specimens required notching to fit into the static tensile testing apparatus. This provided material to obtain fiber volume data from. The root specimen fiber volume data is collected with the matrix burn-off results for the prior geometries in Appendix E. Average fiber volumes for hand lay-up and RTM specimens in the testing grip area were found to be 29% and 26%, respectively. While the average hand lay-up fiber volume was within the range found for flat plates, the fiber volume of the RTM root specimens was under the minimum acceptable fiber volume for the process of 30%. RTM fiber volumes below the 30% threshold do not yield composites of comparable strength to other processes and are likely to washout the reinforcement during processing. Consequently, only fiber volumes above 30% are typically used for RTM structure designs. Since, it was found that the RTM root specimens were below this acceptable fiber volume at the tensile grip location, it was necessary to explore improving its fiber content in a third round of the root experiment study.

168

Although five of the seven mechanical tests resulted in laminate failure, there is significant evidence that the fiber volume issues concerning the insert were resolved. First, visual inspection showed that a better distribution of reinforcement was achieved and matrix rich regions were minimized (Fig. 87). Secondly, the two specimens of round two that did not fail near the grips, failed by insert pull-out. The insert pull-out of specimen R201 is shown in Figure 89. The insert of this specimen illustrates that improving fiber content near the insert did in fact improve laminate / insert contact. Noted in Figure 89 are the areas where reinforcement and matrix were removed along with the insert. This interaction requires notably more energy to achieve failure. As a result, it was desirable to incorporate this level of interaction between insert and laminate. These specimens that did fail by insert pull-out demonstrate that the efforts of the second iteration root experiments were successful.

The objective of the last round of root specimen investigations was to achieve overall improvement in the fiber content of RTM roots, while still maintaining good wet-out of the laminate. Eight RTM specimens were manufactured with additional skin and surface laminate plies. The additional reinforcement improved fiber content, while the number of specimens provided ample testing possibilities.

The final design lay-ups for the root specimen were [±45/0/0/±45]s for the skin side of the laminate and [±45/0/±45/0/0/±45]s for the laminate that contours over the insert surface. The complete lay-up of the root specimen also included the steel insert, the triaxial fabric ahead and alongside the insert, and two rolled-up fabric darts. Two RTM specimens with this prescribed lay-up were statically tested in tension during round
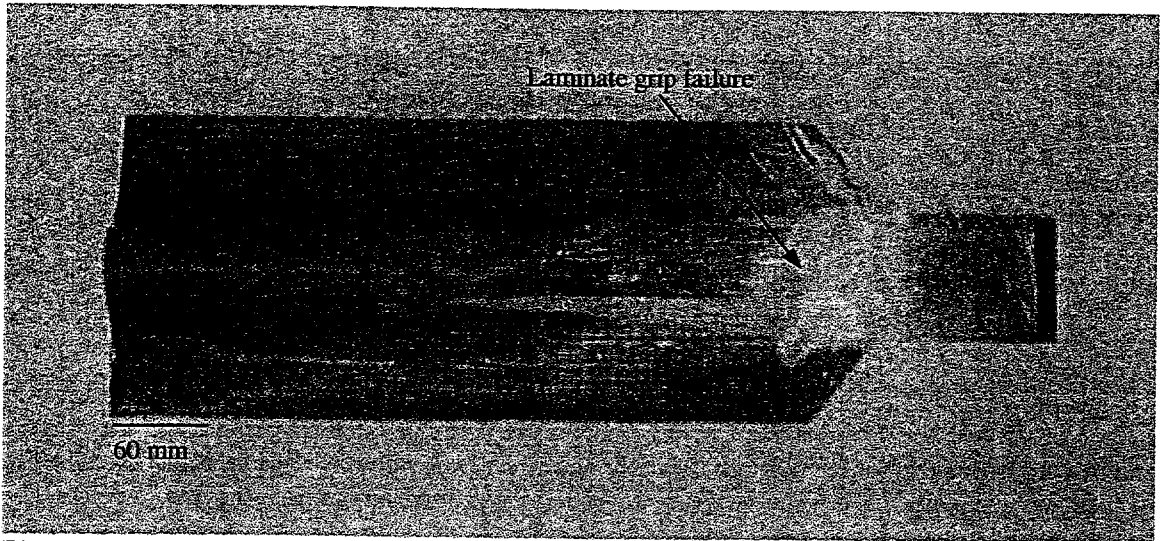
Figure 88. Root tensile test grip failure of specimen R301.
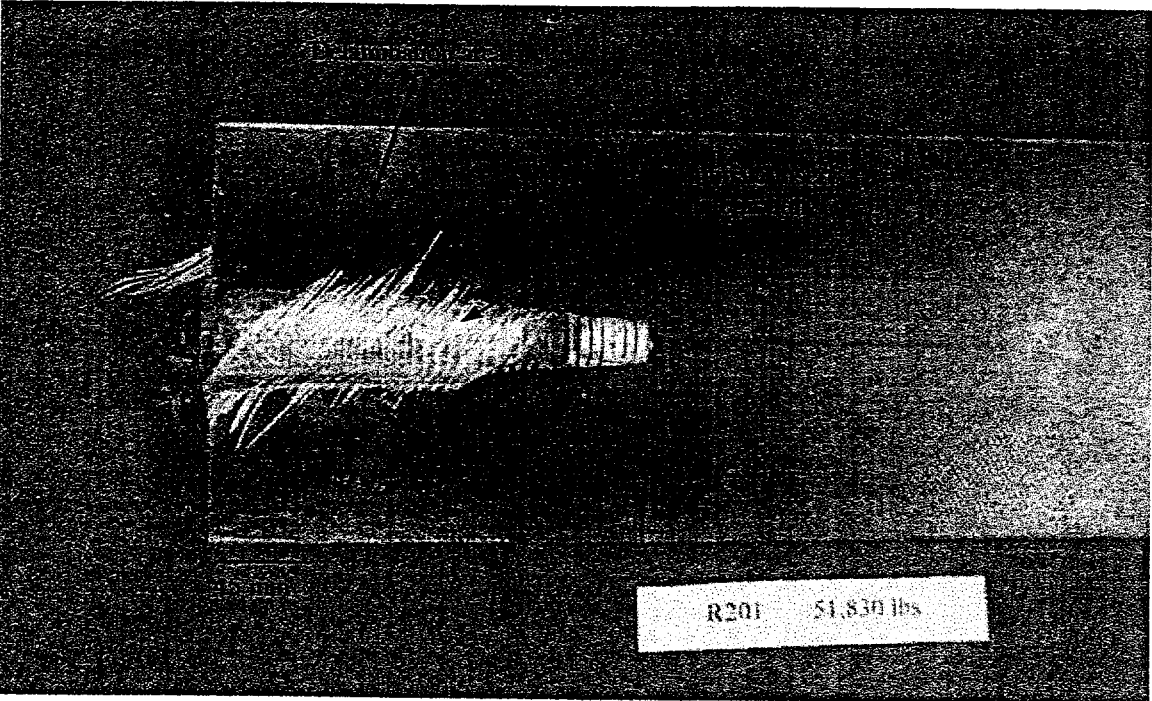
Figure 89. Insert and laminate interaction of specimen R201.

three. The average ultimate load for these specimens was 254 kN, the highest average load of all the root samples tested. In addition, the tensile tests demonstrated that the failure of the latest root specimens would be for the hub attachment bolts. Delamination and cracking was observed near the grip during testing. However, ultimate failure occurred in the 19.1 mm diameter mounting bolts. With a failure load 2.6 times the maximum load required under extreme wind conditions and a static strength that surpasses the mechanical performance of the attaching bolts, it was determined that the final root design exceeds the structural requirements.

It was found that the insert to laminate interaction and fiber volume requirements were met, as well. Although insert pull-out was not observed for the static test specimens, the results of the second round root study demonstrated that interactions were evident. The interactions between steel and composite had potential for improvement as fiber volumes were further increased with the additional skin and surface plies. Thus, the interaction between laminate and insert had been maximized with the available manufacturing techniques. The fiber volumes of the third round specimens also met the required criteria. RTM root specimen fiber contents averaged about 33% at the grip location. This was above the minimum RTM fiber volume threshold, and within the acceptable range.

The final requirement to be satisfied was fatigue performance. The R112 specimen was chosen randomly as the first fatigue candidate to be fatigue tested. These tests were selected for an R value of 0.1 with loads alternating between 89 kN and 9 kN. Under this testing scenario, specimen R112 experienced 120,317 fatigue cycles and four

broken insert mounting apparatuses. As was observed during the static tests, the insert bolts were weaker than the root specimens. This was especially evident for the fatigue test. Consequently, the testing procedure involved fatiguing the specimen until mounting apparatus failure, recording the number of cycles, replacing mounting hardware, and then continuing the experiment. This methodology was followed to find the 120,317 fatigue cycle results of specimen R112. After this number of cycles the unbroken root sample was removed from the testing equipment and sectioned to determine what damage was evident. Shown in Figure 90 is a cross section of the insert and laminate of root specimen R112. It can be observed from this figure that there were a few cracks generated during the sectioning process, however no visible damage was apparent in this section after its fatigue testing.
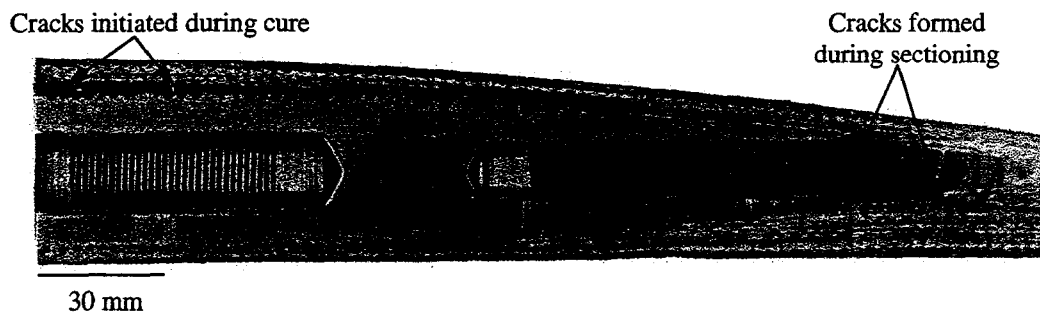
Figure 90. Fatigue specimen, R112 cross-section with steel insert.

The 120,317 cycles this specimen survived in fatigue corresponds to an actual hub insert being loaded to 214 km/h, 11 times a day over a thirty-year blade lifespan. This clearly demonstrates that the current root specimen design far exceeds its fatigue requirements and that the hub to blade joint design is notably robust.

A final note concerning the root specimen: hand lay-up versus RTM comparisons were limited for this group of experiments. The reason behind the limited work with hand lay-up is that the process would not be a serious candidate for manufacturing a complete root mount. Hand lay-up worked adequately on processing a single specimen and the ultimate loads hand lay-up root samples supported were comparable to those of RTM specimens. However, processing a complete, oval root section with ten inserts using hand lay-up, would most likely be beyond its abilities. Hand lay-up works well for laminates of flat or limited curvature, but would experience a series of difficulties for more complex geometries. For example, in a complete root joint the hand lay-up process would introduce complications with fabric lay-up, the wetting out of an oval cross section, keeping the resin in place, securing the large fabric over complex contours, and wet lay-up of small sections of reinforcement for transitions. A process like RTM addresses many of these concerns. An RTM mold for the root assembly would be able to secure complex, dry, preform reinforcements while also incorporating the mounting inserts as an integral part of the mold. These features of RTM eliminate the cumbersome wet lay-ups of individual fabric layers and the difficulty with supporting them during processing with hand lay-up. As a result of these observations, it did not seem worthwhile to explore the hand lay-up process as it showed little usefulness in fabricating the complete root attachment.

CHAPTER 5

CONCLUSIONS AND FUTURE WORK

Resin Transfer molding yields laminates of lower weight, higher fiber volume fraction, faster production capabilities, less dimensional variation, and little or no change in most critical strength properties. Compressive strengths showed significant improvement for RTM. Vacuum assisted RTM shows capability to reduce porosity to well below that of hand lay-up.

Detailed physical and mechanical investigation results are presented below for the five geometries that were researched. Finally, the future work items suggested by this study of hand lay-up and RTM are provided.

Physical Property Study Results

Flat Plate Thickness and Fiber Volume

- Reductions in average thickness and standard deviation were found for all VARTM laminates when compared to the hand lay-up baseline. Reductions in thickness for VARTM samples were between 0.01 – 1.5 mm for the specimens of this study, while reductions in standard deviation were between 0.06 – 0.2 mm.

- These reductions in average thickness could result in significant shedding of blade skin weight (1.5 mm less material correlates to an approximate 16% reduction in weight per hypothetical skin).

- The findings for better dimensional control with RTM suggest that this process is well suited for achieving the smooth aerodynamic surfaces, the tight tolerances between substructure assemblies, and the aggressive airfoil designs desired for modern turbine blades.

- Glass RTM mold surfaces may be beneficial in monitoring flow fronts, but are easily deflected under normal RTM injection pressures. Mold reinforcement and post-injection venting assist in minimizing glass deflections.

- The majority of the fabric and lay-up combinations investigated in this study showed significant statistical differences in fiber volume and average thickness. Only the D155/DB120 [0/+45/0]s flat plate laminates manufactured by hand lay-up and RTM showed no statistical differences in fiber volume and average thickness.

- The flat plate research demonstrated a maximum attainable fiber volume fraction of approximately 35% for hand lay-up laminates. Physical property research also showed that RTM fiber contents are controlled by the reinforcement types and molding assemblies. The RTM process is possible of achieving fiber volume contents in excess of 70%, in certain applications [7].

- Thickness to fiber volume correlations for composite materials can be beneficial to future designers and are recorded for the flat plate and three-dimensional substructures explored in this study.

Substructure Thickness and Fiber Volume

- Thickness of substructure laminates varied similar to the findings for flat plates, but the greatest increases in cross-sectional area were due to transition radii and bond thicknesses.

- Transition radii of 2 mm and less were attainable with RTM, while the sharpest radius found for hand lay-up components was 6 mm.

- Transition radii and bond line thicknesses for hand laid-up substructures resulted in cross-sectional area increases of 10 - 42%, when compared to the same geometries manufactured by RTM.

- Significant reductions in weight would be observed for turbine blade substructures if RTM were substituted as the manufacturing process of choice.

- Small variations in root specimen weight are suspected to have little effect on blade rotational inertia and turbine efficiency.

Fabrication Times

- For all of the geometries researched, reductions in cycle times were observed for RTM fabrications when compared to hand lay-up (10 – 60 minutes time savings).

- The addition of a root insert in a composite laminate complicated mold fabrication and use. This was found to decrease the benefits the RTM process had on reducing cycle time.

- Fabrication time reductions with RTM were greater as part complexity and size increased, when compared to hand lay-up. For example, flat plate specimens experienced a 14% difference in fabrication time according to process, while I-beam cycle times varied by approximately 54%.

- Cure time was detrimental to hand lay-up manufacturing speed. RTM moldings can be elevated in temperature and co-cured, whereas hand lay-up operations are more difficult to heat during cure. Complex hand lay-up geometries also require secondary bonding and bond material curing.

- The ability to elevate resin temperatures can greatly decrease cycle times in an RTM production environment. Resins at elevated temperatures permeate preforms faster during injection and cross-link more quickly after mold fill than the same RTM injections performed at ambient temperatures.

CT Scan Results

- At the present time, there exists a need for a convenient and accurate means to measure porosity in composite materials.

- Computed Tomography (CT) scanning technology was identified as a viable means for measuring laminate porosity. During this study, it was found that calibration of the digital images generated by CT methods with another porosity measuring process was required.

- Microscopic inspection was chosen to calibrate the CT technique. Micrographs showed average porosities of 2.4% for hand lay-up, 3.2% for RTM at the vent, 0.5% for RTM near the inlet port, and less than 0.5% for VARTM.

- The current CT porosity measurements found that the average pore contents for hand lay-up flat plates, RTM flat plates, RTM T-stiffeners, and RTM I-beams were all approximately 3%. This result suggests that that the CT method needs further refinement.

176

RTM Mold Review

- Reviewing the molds of this study found that tools with toggle clamps, multiple chemically inert seals, and matched mating surfaces would reduce cycle time and increase part quality.

- For full-scale blade RTM components, steel reinforced composite tooling is recommended. This tool design is the most cost and time effective, in addition to being able to take advantage of the previously mentioned benefits.

Flat Plate Testing

Transverse Tension

- Thickness variations according to processing method were found to bias strength results for flat plate testing. As a result, normalizing techniques were introduced to compare samples at an identical fiber volume (30% for this study).

- The fiber volume contents of the [0/0/±45/0]s laminates exceeded the 5% range typically allowed for linear thickness normalizing. The significant differences in fiber content complicated process comparisons for the eight ply laminates.

- Improvements in ultimate transverse tensile strength (UTTS) were between 13% and 33% for the VARTM specimens of this study, when compared to hand lay-up samples.

- Most fabric and lay-up combinations did not show significant differences in UTTS according to process. Statistical differences were observed only for the normalized UTTS results of the A130/DB120 [0/±45/0]s specimens.

- Significant differences in transverse tensile modulus were found for the [0/0/±45/0]s flat plates according to process (23 – 34% difference between hand lay-up and VARTM). Differences in average transverse modulus between processes were 2 – 6% for the [0/±45/0]s specimens.

- The range of data found for transverse initial damage strain was broad for all specimen types tested. However, statistical improvements in the onset of initial fracture were observed for D155/DB120 [0/±45/0]s and A130/DB120 [0/0/±45/0]s composites.

- Transverse strain to failure data was also scattered and did not demonstrate significant differences according to process.

Compression

- Ultimate compressive strengths (UCS) for laminates using D155 unidirectional material were 50% greater than those strengths found for composites with A130 material. This agreed with previous experimental findings by Samborsky [50].

- For the specimen types utilized in this study, VARTM averaged 7% to 21% greater UCS when compared to similar samples manufactured by hand lay-up.

- The [0/±45/0]s laminates of this study did not show any statistical differences in normalized UCS. The [0/0/±45/0]s hand lay-up specimens demonstrated a greater normalized UCS over their VARTM counterparts. This behavior was explained by the greater thicknesses introduced by hand lay-up processing and the resultant improvements in buckling resistance.

Three-Point Bending

- Fabric type played a significant role in three-point bending ultimate load. Laminates with A130 reinforcement failed at forces 25 - 38% below those for identical laminates with D155 unidirectional fabric.

- The bending specimen failure behavior was also noted to vary according to fabric type. Samples with A130 fabric were observed to delaminate entirely on the compression side of the specimen. Similar laminates using D155 reinforcement showed signs of damage on both surfaces of the specimen, with the majority of the delamination occurring on the tensile side of the specimen.

- A 24% increase in calculated ultimate bending strength was found for D155/DB120 [0/0/±45/0]s specimens using small displacement approximations. No statistical difference was found between the other specimen types.

- An increase in average bending stiffness was observed for all hand lay-up laminates. This was accounted for by the improvements in moment of inertia due to increased laminate thicknesses.

- Improvements in laminate fiber content with RTM versus hand lay-up were found to increase flexural modulus. Results of the three-point bending tests show improvements in bending modulus of 7 – 17% for the [0/±45/0]s samples and 10 – 48% for the [0/0/±45/0]s specimens, manufactured by RTM.

Longitudinal Tension

- Flat plate laminates with A130 fabric yielded ultimate axial tensile strengths (UTS) 16 – 19% below the ultimate strengths found for the same lay-ups using D155 reinforcement. These findings agree with previous composites mechanical strength research [50].

- The UTS did not demonstrate distinctions between process for the [0/±45/0]s lay-ups tested. UTS did distinguish between hand lay-up and VARTM for [0/0/±45/0]s flat plates, however.

- Normalized UTS results showed a statistical difference between methods of manufacture for A130/DB120 [0/0/±45/0]s laminates only. Even the difference for this set of samples was small, however, with a resultant P value of 0.03.

- For the two lay-ups explored in this study, laminates with A130 fabric experienced a 9 – 18% reduction in longitudinal tensile modulus, when compared to similar samples with D155 fabric.

- No statistical differences in longitudinal tensile moduli were observed between [0/±45/0]s flat plate composites manufactured by hand lay-up and VARTM. Significant differences in moduli were noted between manufacturing methods for [0/0/±45/0]s specimens.

Fatigue

- Differences in average fatigue life were not significant between hand lay-up and VARTM specimens of [0/±45/0]s lay-up.

- The greater thicknesses of the hand lay-up A130/DB120 [0/±45/0]s specimens unfairly biased the first attempt at fatigue cycle results (similar stress loading correlated to significantly higher forces for hand lay-up specimens).

- The second round fatigue life measurements for the A130/DB120 hand lay-up and VARTM samples, where identical testing forces were employed, showed no statistical difference between processes.

A summary of the percent differences in average mechanical properties between hand lay-up and VARTM for all the flat plate specimens tested in this study is presented in Table 31:

Table 31. Summary of flat plate mechanical property comparisons in average values between VARTM and hand lay-up

| Mechanical Property | Percent difference between VARTM and hand lay-up (%) | | | |
| | [0/±45/0]s | | [0/0/±45/0]s | |
	D155	A130	D155	A130
Ultimate transverse tensile strength	13	23	32	27
Normalized ult. transverse strength	5	19	--	--
Transverse tensile modulus	6	2	34	23
Transverse strain at initial damage	18	9	0	10
Transverse strain to failure	21	--	--	--
Ultimate compressive strength	12	10	21	8
Normalized ult. comp. strength	5	3	--	--
Three point bending maximum stress	3	(2)	24	2
Flexural modulus	7	17	48	10
Ultimate tensile strength	1	10	32	19
Normalized ultimate tensile strength	3	4	1	4
Tensile modulus	(3)	5	26	14
Fatigue life (R: -1)	nd	nd	--	--

( ) - denotes hand lay-up outperformed VARTM
nd - no measurable difference between fatigue lifetimes

RTM Flat Plate Washout

- Fabric washout injection pressures data are useful to the composites manufacturer. Employing injection pressures slightly less than those required for washout will optimize the cycle speeds for the RTM process.

- Fabric architecture was an important parameter in the washout study. Laminates that included D155 unidirectional washed out at greater injection pressures than samples with A130 fabric, for a variety of lay-ups and injection locations.

- RTM injections where resin is fed into the perimeter of the mold should be avoided to minimize fabric washout. The findings of the current washout study show that the pressure required to washout identical reinforcements is less when injected from an end as opposed to the center of the reinforcement.

- Increased fiber content was found to improve a lay-up schedule's resistance to fabric washout.

- For the limited tests conducted, vacuum-assist effects introduced to the RTM process appear to reduce the injection pressure required to washout reinforcement.

Thin Flanged T-stiffener Mechanical Testing

- Unidirectional fabric type, bond interface, and material processing seemed to have little influence on initial damage, stiffness, and maximum pull-off load properties of the T-stiffeners tested.

- Typical hand lay-up fabrications resulted in specimens of greater moment of inertia when compared to similar samples manufactured by RTM and had increased performance under mechanical loading.

- Thickness variations presented a problem for the thin flanged T-stiffener specimens studied. Compressible gasket/spacer materials in the T-mold did not yield identical dimensions between specimens and adversely effected structural performance.

- A variety of failure modes were observed for the T-stiffener pull-off tests. This was attributed to the unique dimensions and processing of each sample tested.

Thick Flanged T-stiffener and I-beam Testing

- The thick flanged T-specimens were not mechanically tested. However, the thin flanged T-stiffener results have already demonstrated that differences in geometry and moment of inertia would be the determining factors for mechanical strength.

- I-beams of the current lay-up schedule manufactured by the hand lay-up process would be complicated to test mechanically. The I-beams were excessively massive, difficult to assemble, and were not similar in moment of inertia when compared to the RTM beams. Comparing dissimilar specimens would not further the current process evaluations, and consequently, I-beams were excluded from mechanical testing.

Root Specimen Mechanical Testing

- Research experiments with the root specimen attempted to illustrate some important issues with composite tooling and to develop a laminate architecture that would be beneficial to the complete root joint developments.

- The requirements the final root insert design had to meet were:

  - Support ultimate load of 98 kN under maximum wind load condition [3].
  - Demonstrate good interaction between mounting insert and root laminate.
  - Maintain fairly consistent fiber volume throughout root specimen.
  - Sustain a reasonable fatigue life at cycle loads approximating the maximum wind condition.

- First round results demonstrated that low fiber volumes existed about the insert, D155 fabric worked best for wetting-out the root samples, ultimate failure loads were 2.3 times the maximum wind load condition, and failure modes were predominately insert pull-out.

- The second round of root research focused on improving fiber volume near the steel insert and comparing root specimens according to process. A total of nine samples were manufactured for these studies.

  - Vacuum-assisted RTM was attempted on a number of samples, yet was unsuccessful due to the limited vacuum integrity of the root tool.

  - Visual inspection demonstrated that the 38 mm wide strips of triaxial reinforcement were adequate in addressing the previous concerns with insert area fiber volume.

  - The second round static tensile tests of the root specimens showed that the ultimate loads of RTM samples would be 2.3 times the maximum wind load condition and that the failure mode would be delamination near the testing grip.

  - No significant differences were found between hand lay-up and VARTM according to root ultimate tensile load or maximum testing grip stress.

  - Fiber volumes at the root testing grip were found to be 29% and 26% for hand lay-up and RTM, respectively.

  - A 26% fiber volume for RTM specimens was unacceptable. RTM parts are typically manufactured with fiber contents above and beyond 30% [6].

- The third round root investigations strove to improve the overall fiber content of RTM specimens and to determine the current laminate's fatigue strength.

  - A total of eight specimens were manufactured and two of the RTM roots were tested statically. Ultimate failure loads were 2.6 times the maximum wind condition loading. Some delamination was observed near the laminate grip, but ultimate failure was observed in the 19.1 mm testing bolt and not in the composite specimen.

  - Additional plies in the skin and surface laminates improved RTM root fiber volume. Matrix burn-off tests near the grip showed that the average fiber content was 33%.

  - A root fatigue test with an R value of 0.1 and a maximum load of 89 kN yielded a fatigue life of 120,317 cycles. Four bolt support apparatuses failed during the course of the fatigue test. In addition, the specimen was sectioned after testing and no delamination damage was found.

  - The root fatigue results, yielding a 120,317 cycle lifetime, is equivalent to a root specimen seeing the 214 km/h maximum wind load condition, 11 times a day for a 30 year blade lifetime. This information strongly suggests a high level of fatigue resistance for the current root design.

  - All manufactured specimens surpassed the wind turbine blade's design limit load, and the third round of testing demonstrated that the weak link at the hub joint will be the blade mounting fasteners.

- Hand lay-up root specimens were not as aggressively pursued as in the experiments for the previous geometries. This was due to the limited applicability of hand lay-up to a complete turbine blade root structure.

Future Work

Flat Plates

- Further investigations into alternative warp, unidirectional fabrics may yield a reinforcement that significantly outperforms the current A130 fabric for laminate compressive and bending properties in turbine blade applications.

- Comparisons in fatigue performance between hand lay-up and RTM flat plates should be expanded with further variations in fiber volume, lay-up, and fabric type.

- Minimizing the use of gaskets that also serve as spacing materials would be beneficial to future resin transfer moldings. Combination gasket/spacers are poor in dimensional repeatability, can undesirably effect fiber volume, and contribute to complications with maintaining vacuum integrity.

- The current VARTM flat plate mold could benefit from an additional O-ring seal. Modern vacuum-assisted RTM molds take advantage of multiple seals to guarantee vacuum integrity. An additional seal would ease manufacturing and improve the quality of composite flat plates.

- CT methods should be applied to smaller sample sizes and scanned at higher resolutions. This might resolve the issues with CT imaging that were raised in this work.

- Computed Tomography methods might be instrumental in other areas of composite analysis. Particularly, the issues of crack propagation and fiber content might be benefited by this non-destructive test method.

Substructures

- Current work was primarily directed towards constant cross-section specimens. Future work could include research on the varying cross-sections of current turbine blade designs in an effort to approximate weight savings more accurately.

- The use of spray adhesives in fabricating reinforcement preforms needs investigation. It was observed that some preforming strategy is required for complex substructures and spray adhesives may prove successful, if they do not adversely affect the mechanical performance of fiberglass composites.

- Substructures could also be used to explore the advanced features of RTM with the Radius injector. Elevated injection and tool temperatures were not explored in the current work, but could be included in further research.

- Additional research into thick versus thin subassemblies should be conducted. Future work in comparing manufacturing techniques could help to separate geometrical effects versus material performance. This is especially needed for laminates that are flexurally loaded.

- Hand lay-up I-beams should be assembled and tested. The assembly challenges and structural performance of hand lay-up I-beams should be noted and compared to similar beams manufactured by RTM.

Full-Scale Turbine Blade

- Cost can be one of the primary determining factors in selecting the RTM process for wind turbine blade fabrication. It would be informative to explore the role cost plays in subassembly and full-scale turbine blade manufacturing.

- Polyester secondary bond performance could be tested – this would set the standards for bonding polyester to polyester in areas on the wind turbine blade, i.e. the leading edge tabs.

- Experiments with molded syntactic foam cores might illustrate the advantages of a tailorable (thickness and weight) core material over conventional balsa wood core.

- Specimens of a complete root connection assembly require investigation. This critical structure design could also benefit from research into insert/fiberglass interaction, manufacturing laminates of great thickness in a continuous cross-section, and the strength of blade components containing such a large amount of concentrated mass.

- The data acquisition feature of resin flow position sensing was not tested in the current manufacturing evaluation. Yet, the use of this equipment could prove very useful in RTM developments with full-scale blades. The Radius resin position sensors would assist in monitoring flow fronts in composite tools where flow fronts cannot be observed through the mold surfaces.

REFERENCES CITED

1. Mallick, P.K., *Fiber-Reinforced Composites*, Marcel Dekker, Inc., New York, 1988.

2. *Owens Corning Fiber Pricing vs. Weight Performance List*, www.owenscorning.com/owens/composites/, 1999.

3. Cairns, D.S., et al., "Design/Manufacturing Synthesis of a Composite Blade for the AOC 15/50 Wind Turbine," *Proceedings of 37th AIAA Aerospace Sciences Meeting and Exhibit, 1999 ASME Wind Energy Symposium*, Reno, NV, 11-14 January, 1999, AIAA/ASME, NY, 1999, 58-65.

4. Potter, K., *An Introduction to Composite Products*, Chapman & Hall, UK, 1997.

5. Mandell, J.F., Sutherland, H.J. and Samborsky, D.D., " Effects of Materials Parameters and Design Details on the Fatigue of Composite Materials for Wind Turbine Blades," *Proceedings of 1999 European Wind Energy Conference and Exhibition*, Nice, France, 1-5 March, 1999, WIP-Munich, Germany, 1999.

6. Schwartz, M.M., *Composite Materials – Processing, Fabrication, and Applications*, Prentice Hall PTR, New Jersey, 1997, Vol. 2.

7. Swanson, S.R., Introduction to Design and Analysis with Advanced Composite Materials, Prentice Hall, New Jersey, 1997, 16.

8. Cairns, D.S., Humbert, D.R., and Mandell, J.F., "Modeling of Resin Transfer Molding of Composite Materials with Oriented Unidirectional Plies," *Composites: Part A 30 (1999)*, Elsevier Science Limited, Great Britain, 1999, 375-383.

9. Lekakou, C. and Bader, M.G., "Mathematical Modeling of Macro- and Micro-Infiltration in Resin Transfer Molding (RTM)," *Composites: Part A 29A (1998)*, Elsevier Science Limited, Great Britain, 1997.

10. Patel, N. and Lee, L.J., "Effect of Capillary Pressure on Mold Filling and Fiber Wetting in Liquid Composite Molding," *Proceedings of ASM/ESD 10th Annual Advanced Composites Conference*, Dearborn, MI, USA, 7-10 November, 1994, ASM/ESD, Materials Park, OH, 325-333.

11. Parnas, R.S., et al., "The Interaction Between Microscopic and Macroscopic Flow in RTM Preforms," *Composite Structures*, 1994, 27(1-2), 93-107.

12. Fontana, Q.P.V., "Viscosity: Thermal History Treatment in RTM Process Modelling," *Composites Part A 29A (1998)*, Elsevier Science Limited, Great Britain, 1997.

13. Young, W-B. and Lai, C-L., "Analysis of Edge Effects in Resin Transfer Molding," *Composites Part A 28A (1998)*, Elsevier Science Limited, Great Britain, 1997, 817-822.

14. Lai, C-L., Khomami, B. and Kardos, J.L., "Accurate Permeability Characterization of Preforms in Polymer Matrix Composite Fabrication Processes," *Polymer Composites*, June 1997, Vol. 18, No. 3, 368-377.

15. Friedman, H.L., et al., "Forced In-Plane Flow Through Complex Deformable Structures: Influence of an Imposed Curve," *Polymer Composites*, October 1997, Vol. 18, No. 5, 663-671.

16. Lundstrom, T.S., "Bubble Transport Through Constricted Capillary Tubes With Application to Resin Transfer Molding," *Polymer Composites*, December 1996, Vol. 17, No. 6, 770-779.

17. Summerscales, J., "Manufacturing Defects in Fiber-Reinforced Plastic Composites," *Insight*, 1994, 36(12), 936-942.

18. Hayward, J.S. and Harris, B., "Effect of Process Variables on the Quality of RTM Moldings," *SAMPE Journal*, 1990, 26, 39-46.

19. Hayward, J.S. and Harris, B., "The Effect of Vacuum Assistance in Resin Transfer Molding," *Composites Manufacturing*, 1990, 1, 161-166.

20. Chan, A.W. and Morgan, R.J., "Tow Impregnation During Resin Transfer Molding of Bidirectional Nonwoven Fabrics," *Polymer Composites*, 1993, 14(4), 335-340.

21. Lowe, J.R., Owen, M.J. and Rudd, C.D., "Void Formation in Resin Transfer Molding," *Proceedings of ICAC 95*, Nottingham, 1995, Institute of Materials, London.

22. Springer, G.S., "A Model of the Curing Process of Epoxy Matrix Composites," *Proceedings of ICCM 4*, Tokyo, October 1982, North Holland Publishing Co., Amsterdam, Vol. 1, 23-25.

23. Loos, A.C. and Springer, G.S., "Curing of Epoxy Matrix Composites," *Journal of Composite Materials*, 1983, 17(2), 135-169.

24. Kardos, J.L., et al., "Void Formation and Transport During Composite Laminate Processing," *ASTM STP*, 1983, 797, 96-109.

25. Kardos, J.L., Dave, R. and Dudukovic, M.P., "Void Growth and Resin Transport During Processing of Thermosetting Matrix Composites," *Advances in Polymer Science*, 1986, 80(4), 101-123.

26. Kardos, J.L., Dave, R. and Dudukovic, M.P., "Voids in Composites," *Manufacturing International*, 1988, (IV), 41-48, *Proceedings of Manufacturing Science of Composites, ASME*, Atlanta, April 1988.

27. Holmberg, J.A. and Berglund L.A., "Manufacturing and Performance of RTM U-Beams," *Composites Part A 28A (1998)*, Elsevier Science Limited, Great Britain, 1997, 513-521.

28. Branco, C.M., et al., "A Comparative Study of the Fatigue Behavior of GRP Hand Lay-up and Pultruded Phenolic Composites," *Int. J. Fatigue Vol. 18*, No. 4, Elsevier Science Limited, Great Britain, 1996, 255-263.

29. Holmberg, J.A. and Berglund L.A., "Micromechanisms of Delamination Failure in RTM U-Beams," *Composites Part A 28A (1998)*, Elsevier Science Limited, Great Britain, 1997, 709-717.

30. Hinrichs, R.J., "Quality Control", *Engineered Materials Handbook Volume 1, Composites*, Dostal, C.A. ed., ASM International, 1987.

31. ANSYS (Revision 5.4), *Engineering Analysis System*, Swanson Analysis Systems Inc., Houston, Pennsylvannia.

32. Simacek, P., Sozer, E.M., and Advani, S.G., Liquid Injection Molding Simulation (Revision 4.0), *User's Manual*, University of Delaware Center for Composite Materials, Newark, Delaware, February, 1998.

33. Hedley, C.W., "Mold Filling Parameters in Resin Transfer Molding of Composites," *Master's Thesis*, Montana State University-Bozeman, 1994.

34. Pearce, N.R.L, et al., "An Investigation into the Effects of Fabric Architecture on the Processing and Properties of Fiber Reinforced Composites Produced by Resin Transfer Molding," *Composites: Part A 29A (1998)*, Elsevier Science Limited, Great Britain, 1997.

35. Pearce, N.R.L., et al., "Optimization of Reinforcement Fabrics for the Resin Transfer Molding of High Fiber Volume Fraction Composites," *Proceedings of 17th International Conference, SAMPE European Chapter*, Basel CH. 28-30, May 1996.

36. Yu, H-W., Young, W-B., "Optimal Design of Process Parameters for Resin Transfer Molding", *Journal of Composite Materials*, Vol. 31, No. 11, Technomic Publishing Co., 1997.

37. Pearce, N.R.L., et al., "A Study of the Effects of Convergent Flow Fronts on the Properties of Fiber Reinforced Composites Produced by RTM," *Composites Part A 29A (1998)*, Elsevier Science Limited, Great Britain, 1997.

38. Lundstrom, T.S., et al., "Void Formation in RTM," *Proceedings of SPI Composite Institutes 47th Annual Conference, Cincinatti, 1992*, SPI, New York.

39. Bowles, K.J. and Frimpong, S., "Void Effects on the Interlaminar Shear Strength of Unidirectional Graphite Fiber-Reinforced Composites, *Journal of Composite Materials*, 1992, 26, 1487-1509.

40. Judd, N.C.W. and Wright, W.W., "Voids and their Effects on the Mechanical Properties of Composites – an Appraisal," *SAMPE Journal*, 1978.

41. Ghiorse, S.R., "Effect of Void Content on the Mechanical Properties of Carbon/Epoxy Laminates," *SAMPE Quarterly*, 1993.

42. Stone, D.E.W. and Clarke, B., "Ultrasonic Attenuation as a Measure of Void Content in Carbon-Fiber Reinforced Plastics," *Non-Destructive Testing*, 1975.

43. Shenoi, R.A. and Wellicome, J.F., "Composite Materials in Marine Structures Volume 1: Fundamental Concepts," *Cambridge University Press*, Cambridge, UK, 1993.

44. Varna, J., et al., "Effect of Voids on Failure Mechanisms in RTM Laminates," *Composite Science and Technology*, 1995, 53, 241-249.

45. Rosell, S.M., *Interim Master's Thesis Work (to be published)*, Montana State University-Bozeman, 1999.

46. Haugen, D.J., "Fracture of Skin-Stiffener Intersections in Composite Wind Turbine Blade Structures," *Master's Thesis*, Montana State University-Bozeman, 1998.

47. Mandell, J.F., et al., "Fatigue of Composite Material Beam Elements Representative of Wind Turbine Blade Substructure," *NREL/SR-500-24379*, National Renewable Energy Laboratory, Golden, CO, November, 1998.

48. Mandell, J.F. and Samborsky, D.D., "DOE/MSU Composite Material Fatigue Database: Test Methods, Materials, and Analysis," *Contractor Report SAND97-3002*, Sandia National Laboratories, Albuquerque, NM, 1997.

49. Fox, E., et al., SigmaStat Statistical Software for Windows (Revision 1.0), *User's Manual*, Jandel Scientific, CA, 1994.

50. Samborsky, D.D., *Interim Master's Thesis Work (to be published)*, Montana State University-Bozeman, 1999.

51. Hedley, C.W., CEO of Headwaters Composites, *personal communication*, June, 1999.

52. Hull, D. and Clyne, T.W., *An Introduction to Composite Materials*, Cambridge University Press, Great Britain, 1996.

53. Kawamura, T., "Nondestructive, Three-Dimensional Density Measurements of Ice Core Samples by X Ray Computed Tomography," *Journal of Geophysical Research*, Vol. 95, August, 1990.

54. Edens, M., Post-Doctorate Research Engineer – MSU, *private communication*, July, 1999.

55. Reifsnider, K.L., *Fatigue of Composite Materials*, Elsevier Science Publishing Company, Inc., New York, 1991, 30-38.

56. Broek, D., *Elementary Engineering Fracture Mechanics (Third Edition)*, Martinus Nijhoff Publishers, Netherlands, 1983.

57. *Composite Mold Fabrication Guide*, Glas-Craft/RTM Systems Inc., 1998.

APPENDICES

APPENDIX A

Flat Plate Experimental Data and Results

FP410 Mechanical Testing   RTM   [0/+45/0]s   D155 / DB120

Transverse Tension

Sample No.	Thickness (mm)	Width (mm)	Modulus (GPa)	First Fracture (% strain)	Ultimate Fail (lbs)
410.01	3.00	27.81	9.81	0.27	1468
410.02	3.05	27.61	10.16	0.26	1480
410.03	3.00	27.53	9.72	0.30	1551
410.04	3.05	27.58	10.24	0.29	1468
410.05	3.10	27.58	10.01	0.29	1525
410.06	3.00	27.74	9.34	0.31	1500

Compression

Sample No.	Thickness (mm)	Width (mm)	Modulus (GPa)	First Fracture (% strain)	Ultimate Fail (lbs)
410.12	3.07	27.76	--	--	12100
410.13	3.18	27.43	--	--	11110
410.14	3.20	27.89	--	--	11440
410.15	3.23	27.66	--	--	10810
410.16	3.23	27.53	--	--	10940

FP411 Mechanical Testing   RTM   [0/+45/0]s   D155 / DB 120

Transverse Tension

Sample No.	Thickness (mm)	Width (mm)	Modulus (GPa)	First Fracture (% strain)	Ultimate Fail (lbs)
411.01	3.12	26.83	9.95	0.29	1395
411.02	2.93	26.88	10.36	0.29	1312
411.03	2.97	26.91	10.09	0.31	1415
411.04	3.13	26.87	10.07	0.31	1393
411.05	3.00	26.95	10.06	0.30	1310
411.06	3.04	26.76	9.34	0.30	1352
411.07	3.00	26.96	9.41	0.30	1339
411.08	3.04	26.85	9.85	0.29	1384

Compression

Sample No.	Thickness (mm)	Width (mm)	Modulus (GPa)	First Fracture (% strain)	Ultimate Fail (lbs)
411.17	3.21	26.31	--	--	8980
411.18	3.25	26.63	--	--	8936
411.19	3.29	26.74	--	--	8939
411.20	3.28	26.42	--	--	8744
411.21	3.08	26.87	--	--	8450
411.22	3.14	26.87	--	--	8687
411.23	3.11	26.76	--	--	8437
411.24	3.18	26.89	--	--	8732

FP620 Mechanical Testing   VARTM   [0/0/+45/0]s   D155 / DB120

Transverse Tension

Sample No.	Thickness (mm)	Width (mm)	Modulus (GPa)	First Fracture (% strain)	Ultimate Fail (lbs)
620.01	3.38	27.56	13.29	0.21	1502
620.02	3.12	27.36	14.31	0.19	1482
620.03	3.05	27.23	14.43	0.15	1414
620.04	3.28	27.46	13.48	0.17	1459
620.05	3.30	27.36	13.32	0.16	1530
620.06	3.02	27.46	15.04	0.16	1390

Compression

620.12	3.23	27.36	--	--	14850
620.13	3.25	27.25	--	--	15130
620.14	3.30	27.36	--	--	15300
620.15	3.25	27.36	--	--	15190
620.16	3.23	27.28	--	--	14110

Tension

620.17	3.44	21.75	32.8	1.03	15180
620.18	3.34	21.66	34.8	1.00	15211
620.19	3.20	21.60	36.1	0.94	14880
620.20	3.41	21.74	33.6	0.69	15140
620.21	3.30	21.71	34.6	0.95	15580

FP621 Mechanical Testing   VARTM   [0/0/+45/0]s   A130 / DB120

Transverse Tension

Sample No.	Thickness (mm)	Width (mm)	Modulus (GPa)	First Fracture (% strain)	Ultimate Fail (lbs)
621.01	3.20	27.53	11.36	0.28	1564
621.02	3.23	27.51	11.46	0.28	1624
621.03	3.18	27.51	11.87	0.27	1562
621.04	3.15	27.51	11.83	0.26	1677
621.05	3.20	27.41	12.20	0.26	1600
621.06	3.20	27.46	11.32	0.29	1630

Compression

621.12	3.35	27.51	--	--	7374
621.13	3.38	27.38	--	--	7300
621.14	3.33	27.41	--	--	7827
621.15	3.25	27.25	--	--	8150
621.16	3.18	27.18	--	--	7121

Tension

621.17	3.35	21.49	30.0	1.44	12390
621.18	3.50	21.73	28.3	1.45	12440
621.19	3.34	21.45	27.4	1.48	12300
621.20	3.36	21.45	29.2	1.32	12630
621.21	3.55	21.44	25.8	1.42	12315

FP702 Mechanical Testing   HL   [0/+45/0]s   D155 / DB120

Transverse Tension

Sample No.	Thickness (mm)	Width (mm)	Modulus (GPa)	First Fracture (% strain)	Ultimate Fail (lbs)
702.01	3.68	27.76	10.43	0.26	1343
702.02	3.38	28.14	9.40	0.24	1321
702.03	3.33	28.09	10.00	0.25	1244
702.04	3.56	28.02	9.98	0.27	1277
702.05	3.28	27.94	8.99	0.26	1310
702.06					

Compression

702.12	3.25	28.02	--	--	11450
702.13	3.15	28.02	--	--	12680
702.14	3.12	28.02	--	--	12790
702.15	3.07	27.79	--	--	12250
702.16	3.12	27.41	--	--	12510

Tension

702.17	3.33	21.64	24.1	1.46	9990
702.18	3.10	21.71	26.6	1.25	10370
702.19	3.10	21.67	25.1	1.12	9824
702.20	3.32	21.70	24.2	1.25	9538
702.21	3.10	21.67	24.5	1.02	9896

FP705 Mechanical Testing   HL   [0/+45/0]s   A130 / DB120

Transverse Tension

Sample No.	Thickness (mm)	Width (mm)	Modulus (GPa)	First Fracture (% strain)	Ultimate Fail (lbs)
705.01	3.20	28.04	9.44	0.27	1318
705.02	3.15	28.07	9.47	0.30	1284
705.03	3.18	28.09	--	--	--
705.04	3.28	28.17	9.36	0.30	1351
705.05	3.25	27.97	9.49	0.27	1383
705.06					

Compression

705.12	3.30	27.81	--	--	6509
705.13	3.35	28.19	--	--	6559
705.14	3.28	28.30	--	--	6683
705.15	3.30	28.24	--	--	5782
705.16	3.45	28.07	--	--	6570

Tension

705.17	3.53	21.47	21.3	1.57	8338
705.18	3.51	21.60	20.2	1.68	7603
705.19	3.40	21.90	19.7	1.78	7968
705.20	3.10	22.18	23.0	1.50	8471
705.21	3.44	21.60	20.3	1.47	8096

FP714 Mechanical Testing   HL   [0/0/+45/0]s   D155 / DB120

Transverse Tension

Sample No.	Thickness (mm)	Width (mm)	Modulus (GPa)	First Fracture (% strain)	Ultimate Fail (lbs)
714.01	5.28	27.91	8.45	0.22	1398
714.02	4.67	28.19	9.46	0.19	1631
714.03	4.70	28.27	9.92	0.21	1570
714.04	4.70	28.14	9.86	0.17	1607
714.05	4.70	28.14	9.63	0.24	1595
714.06	5.31	28.22	8.60	0.24	1428

Compression

714.12	4.39	28.27	--	--	17260
714.13	4.55	28.22	--	--	16760
714.14	4.67	28.14	--	--	18560
714.15	4.88	28.12	--	--	17130
714.16	5.05	28.30	--	--	18350

Tension

714.17	4.90	21.46	24.7	0.74	14720
714.18	4.72	21.47	24.7	1.26	15220
714.19	4.61	21.45	26.4	1.01	14300
714.20	4.80	21.58	23.6	1.23	15580
714.21	5.34	21.54	23.0	0.80	14860

FP710 Mechanical Testing   HL   [0/0/+45/0]s   A130 / DB120

Transverse Tension

Sample No.	Thickness (mm)	Width (mm)	Modulus (GPa)	First Fracture (% strain)	Ultimate Fail (lbs)
710.01	4.01	28.24	9.36	0.28	1707
710.02	4.06	28.14	9.22	0.23	1738
710.03	5.16	28.07	8.83	0.25	1446
710.04	4.22	28.35	8.84	0.22	1692
710.05	4.06	28.30	9.20	0.27	1624
710.06	5.21	28.22	8.76	0.22	1709

Compression

710.12	4.24	27.94	--	--	8794
710.13	3.99	28.07	--	--	9606
710.14	4.29	28.14	--	--	9278
710.15	4.17	27.31	--	--	7995
710.16	3.89	28.02	--	--	8501

Tension

710.17	3.79	21.60	23.3	1.79	11520
710.18	3.96	21.61	23.9	1.20	11900
710.19	4.23	21.85	23.7	1.31	12040
710.20	4.04	21.60	24.6	1.28	12590
710.21	4.24	21.84	23.8	1.46	12240

Transverse Tensile Mechanical Testing (Round 2)

[0/+45/0]s   D155 / DB120   0.1 in/min   5 points/sec (5 Hz) sampling

tensile test #4

FP622 - Radius VARTM

Sample No.	Thickness (mm)	Width (mm)	Modulus (GPa)	First Fracture (% strain)	Ultimate Fail (lbs)
622.01	3.04	27.83	9.29	0.33	1636
622.02	3.05	28.03	9.07	0.33	1603
622.03	3.05	27.75	9.31	0.35	1593
Average	3.05	27.89	9.19	0.34	1598
Std Dev.	0.00	0.20	0.17	0.01	7

FP411 - Radius RTM

Sample No.	Thickness (mm)	Width (mm)	Modulus (GPa)	First Fracture (% strain)	Ultimate Fail (lbs)
411.01	3.01	27.58	9.70	0.29	1355
411.02	3.00	27.65	10.03	0.31	1404
411.03	3.01	27.73	9.62	0.29	1343
Average	3.01	27.69	9.83	0.30	1374
Std Dev.	0.01	0.06	0.29	0.01	43

FP412 - Spartan RTM   ** specimens not fully cured and 45 stitching in weft direction

Sample No.	Thickness (mm)	Width (mm)	Modulus (GPa)	First Fracture (% strain)	Ultimate Fail (lbs)
412.01	3.02	27.31	--	--	747
412.02	3.05	27.30	--	--	739
412.03	3.00	27.44	--	--	818
412.04	2.97	27.45	--	--	776
412.05	3.12	27.92	--	--	--
412.06	2.93	27.81	--	--	--
Average	3.01	27.58	--	--	778
Std Dev.	0.07	0.27	--	--	40

FP704 - Hand Lay-up

Sample No.	Thickness (mm)	Width (mm)	Modulus (GPa)	First Fracture (% strain)	Ultimate Fail (lbs)
704.01	3.46	27.63	9.08	0.26	1451
704.02	3.49	27.81	9.78	0.27	1567
704.03	3.43	27.52	9.86	0.25	1458
Average	3.46	27.67	9.82	0.26	1513
Std Dev.	0.04	0.21	0.06	0.01	77

Transverse Tensile Mechanical Testing (Round 3)

[0/+45/0]s   D155 / DB120   0.1 in/min   5 points/sec (5 Hz) sampling
                                                            tensile test #4

FP622 - Radius VARTM

Sample No.	Thickness (mm)	Width (mm)	Modulus (GPa)	First Fracture (% strain)	Ultimate Fail (lbs)
622.20	3.01	26.61	9.73	0.35	1486
622.21	3.01	26.68	9.48	0.35	1477
622.22	2.98	26.50	9.53	0.34	1414
622.23	3.00	26.42	9.74	0.36	1422
622.24	2.99	26.38	9.52	0.33	1463
Average	3.00	26.52	9.6	0.35	1452
Std Dev.	0.01	0.13	0.1	0.01	33

FP411 - Radius RTM

Sample No.	Thickness (mm)	Width (mm)	Modulus (GPa)	First Fracture (% strain)	Ultimate Fail (lbs)
411.20	2.99	26.37	10.31	0.31	1338
411.21	2.99	26.04	9.56	0.32	1407
411.22	3.02	26.36	9.38	0.28	1360
411.23	3.01	26.23	9.04	0.29	1321
411.24	3.05	26.60	8.11	0.25	1317
Average	3.01	26.32	9.3	0.29	1349
Std Dev.	0.02	0.21	0.8	0.03	37

FP413 - Spartan RTM

Sample No.	Thickness (mm)	Width (mm)	Modulus (GPa)	First Fracture (% strain)	Ultimate Fail (lbs)
413.20	3.08	26.86	8.88	0.30	1428
413.21	3.08	26.96	8.58	0.28	1394
413.22	3.05	25.71	9.48	0.31	1291
413.23	3.08	26.99	8.83	0.28	1355
413.24	3.06	25.54	9.30	0.30	1291
Average	3.07	26.41	9.0	0.29	1352
Std Dev.	0.01	0.72	0.4	0.01	61

FP704 - Hand Lay-up

Sample No.	Thickness (mm)	Width (mm)	Modulus (GPa)	First Fracture (% strain)	Ultimate Fail (lbs)
704.20	3.26	26.19	8.46	0.29	1418
704.21	3.31	26.16	8.94	0.25	1443
704.22	3.29	26.08	8.31	0.28	1373
704.23	3.30	26.30	9.22	0.27	1445
704.24	3.25	25.91	9.49	0.27	1419
Average	3.28	26.13	8.9	0.27	1420
Std Dev.	0.03	0.15	0.5	0.01	29

Compression Mechanical Testing (Round 2)

[0/+45/0]s lay-up   D155 / DB120 fabrics   0.5 in/sec   0.5" gauge

FP622 - Radius VARTM

Sample No.	Thickness (mm)	Width (mm)	Area (mm^2)	Ultimate Fail (lbs)	Comments
622.12	3.05	27.52	83.9	11410	
622.13	3.06	27.47	84.1	11060	
622.14	3.05	27.04	82.5	12440	
622.15	3.09	27.32	84.4	11050	
622.16	3.10	27.72	85.9	10940	
622.17	3.11	27.66	86.0	11700	

FP411 - Radius RTM

Sample No.	Thickness (mm)	Width (mm)	Area (mm^2)	Ultimate Fail (lbs)	Comments
411.12	3.23	27.15	87.7	11190	
411.13	3.27	27.25	89.1	11710	
411.14	3.25	27.45	89.2	11650	
411.15	3.22	27.49	88.5	11750	
411.16	3.15	27.43	86.4	10620	
411.17	3.10	27.37	84.8	10820	

FP412 - Spartan RTM

Sample No.	Thickness (mm)	Width (mm)	Area (mm^2)	Ultimate Fail (lbs)	Comments
412.12	3.35	26.69	89.4	9556	
412.13	3.37	27.27	91.9	9362	
412.14	3.45	27.72	95.6	9678	
412.15	3.40	27.87	94.8	11260	
412.16	3.30	27.94	92.2	10430	
412.17	3.22	27.78	89.5	10770	

FP704 - Hand Lay-up

Sample No.	Thickness (mm)	Width (mm)	Area (mm^2)	Ultimate Fail (lbs)	Comments
704.12	3.97	25.59	101.6	10880	
704.13	3.77	26.14	98.5	10010	
704.14	3.54	27.51	97.4	11050	
704.15	3.50	27.51	96.3	11250	
704.16	3.47	27.70	96.1	11550	
704.17	3.50	27.66	96.8	10690	

Compression Mechanical Testing (Round 3)

[0/+45/0]s lay-up   D155 / DB 120 fabrics   0.5 in/sec   0.5" gauge

FP622 - Radius VARTM

Sample No.	Thickness (mm)	Width (mm)	Area (mm^2)	Ultimate Fail (lbs)	Comments
622.30	3.05	26.46	80.7	11390	
622.31	2.97	26.42	78.5	12100	
622.32	2.96	26.48	78.4	11970	
622.33	3.03	26.51	80.3	10880	
622.34	3.10	26.11	80.9	9429	

FP411 - Radius RTM

Sample No.	Thickness (mm)	Width (mm)	Area (mm^2)	Ultimate Fail (lbs)	Comments
411.30	3.01	26.76	80.5	7503	
411.31	3.00	26.59	79.8	9390	
411.32	3.08	26.13	80.5	7805	
411.33	3.03	25.94	78.6	7713	
411.34	3.06	26.40	80.8	8629	

FP413 - Spartan RTM

Sample No.	Thickness (mm)	Width (mm)	Area (mm^2)	Ultimate Fail (lbs)	Comments
413.30	3.04	26.40	80.3	9165	
413.31	3.11	26.62	82.8	10120	
413.32	3.17	26.40	83.7	10790	
413.33	2.97	26.38	78.3		
413.34	2.97	26.56	78.9	10300	

FP704 - Hand Lay-up

Sample No.	Thickness (mm)	Width (mm)	Area (mm^2)	Ultimate Fail (lbs)	Comments
704.30	3.35	25.49	85.4	10630	
704.31	3.45	26.04	89.8	10220	
704.32	3.61	26.43	95.4	11680	
704.33	3.39	26.09	88.4	8829	
704.34	3.45	26.46	91.3	11760	

Three Point Bending Mechanical Testing (RTM)

FP615 - VARTM D155 [0/+45/0]s 0.5 in/min Flex test #11

Sample No.	Thickness (mm)	Width (mm)	Area (mm^2)	Stiffness (N/cm)	Max. Load (lbs)	Max. Stress (MPa)
615.07	3.25	27.71	90.1	437.4	220	636.8
615.08	3.28	27.99	91.7	472.0	237	668.4
615.09	3.35	27.99	93.9	518.0	249	670.8
615.10	3.43	27.81	95.4	522.5	254	658.5
615.11	3.20	27.91	89.3	458.0	231	685.2
Average	3.30	27.88	92.1	481.6	238	664

FP619 - VARTM A130 [0/+45/0]s

Sample No.	Thickness (mm)	Width (mm)	Area (mm^2)	Stiffness (N/cm)	Max. Load (lbs)	Max. Stress (MPa)
619.07	3.10	27.33	84.7	389.5	151	487.4
619.08	3.18	27.48	87.4	408.8	169	515.5
619.09	3.23	27.51	88.9	409.1	131	386.9
619.10	3.07	27.43	84.2	372.0	142	465.6
619.11	3.07	27.20	83.5	388.5	157	519.2
Average	3.13	27.39	85.7	393.6	150	475

FP620 - VARTM D155 [0/0/+45/0]s

Sample No.	Thickness (mm)	Width (mm)	Area (mm^2)	Stiffness (N/cm)	Max. Load (lbs)	Max. Stress (MPa)
620.07	3.20	27.18	87.0	693.8	348	1059.9
620.08	3.28	27.28	89.5	740.8	342	987.8
620.09	3.25	27.36	88.9	757.0	366	1073.6
620.10	3.25	27.33	88.8	713.7	357	1048.4
620.11	3.20	27.38	87.6	709.2	344	1040.1
Average	3.24	27.31	88.4	722.9	351	1042

FP621 - VARTM A130 [0/0/+45/0]s

Sample No.	Thickness (mm)	Width (mm)	Area (mm^2)	Stiffness (N/cm)	Max. Load (lbs)	Max. Stress (MPa)
621.07	3.25	27.48	89.3	706.3	222	648.4
621.08	3.35	27.46	92.0	710.5	224	616.2
621.09	3.30	27.48	90.7	694.5	216	611.9
621.10	3.23	27.31	88.2	646.5	217	645.6
621.11	3.28	27.48	90.1	658.3	218	625.1
Average	3.28	27.44	90.1	683.2	219	629

FP410 - RTM D155 [0/+45/0]s Radius

Sample No.	Thickness (mm)	Width (mm)	Area (mm^2)	Stiffness (N/cm)	Max. Load (lbs)	Max. Stress (MPa)
410.07	3.18	27.33	86.9	436.1	215	659.5
410.08	3.15	27.64	87.1	442.9	212	655.3
410.09	3.10	27.58	85.5	440.0	213	681.3
410.10	3.10	27.79	86.1	436.7	217	688.8
410.11	3.10	27.84	86.3	435.9	209	662.2
Average	3.13	27.64	86.4	438.3	213	669

FP412 - RTM D155 [0/+45/0]s Spartan

Sample No.	Thickness (mm)	Width (mm)	Area (mm^2)	Stiffness (N/cm)	Max. Load (lbs)	Max. Stress (MPa)
412.09	3.29	27.43	90.2	524.6	248	708.1
412.10	3.35	27.73	92.9	529.9	260	708.3
412.11	3.26	27.65	90.1	500.0	246	709.7
412.12	3.19	27.61	88.1	461.4	236	712.1
412.13	3.41	27.84	94.9	579.1	274	717.5
412.14	3.46	27.75	96.0	600.0	280	711
Average	3.33	27.72	92.4	534.1	259	4

Three Point Bending Mechanical Testing (Hand Lay-up)

FP702 - Hand Lay-up D155 [0/+45/0]s

Sample No.	Thickness (mm)	Width (mm)	Area (mm^2)	Stiffness (N/cm)	Ultimate Fail (lbs)	Max. Stress (MPa)
702.07	3.20	27.99	89.6	452.8	214	632.9
702.08	3.10	27.94	86.6	421.1	211	666.2
702.09	3.12	28.07	87.6	430.3	217	673.2
702.10	3.35	28.09	94.1	480.4	236	634.6
702.11	3.51	28.12	98.7	579.8	266	650.9
Average	3.26	28.04	91.3	472.9	229	652
Std Dev.	0.17	0.07	5.0	64.0	23	18

FP705 - Hand Lay-up A130 [0/+45/0]s

Sample No.	Thickness (mm)	Width (mm)	Area (mm^2)	Stiffness (N/cm)	Ultimate Fail (lbs)	Max. Stress (MPa)
705.07	3.30	27.20	89.8	436.4	171	489.4
705.08	3.58	28.40	101.7	505.0	190	442.5
705.09	3.38	27.86	94.2	428.4	202	538.0
705.10	3.53	27.99	98.8	477.3	204	495.8
705.11	3.43	28.24	96.9	459.2	181	461.8
Average	3.44	27.94	96.3	461.2	190	486
Std Dev.	0.11	0.46	4.5	31.1	14	36

FP714 - Hand Lay-up D155 [0/0/+45/0]s

Sample No.	Thickness (mm)	Width (mm)	Area (mm^2)	Stiffness (N/cm)	Ultimate Fail (lbs)	Max. Stress (MPa)
714.07	4.70	27.89	131.1	1502.0	578	795.3
714.08	4.52	28.35	128.1	1415.5	577	844.5
714.09	4.70	28.42	133.6	1567.7	583	787.2
714.10	4.93	28.35	139.8	1618.4	608	748.0
714.11	4.57	27.69	126.5	1460.2	552	809.2
Average	4.68	28.14	131.8	1512.7	580	797
Std Dev.	0.16	0.33	5.2	81.4	20	35

FP710 - Hand Lay-up A130 [0/0/+45/0]s

Sample No.	Thickness (mm)	Width (mm)	Area (mm^2)	Stiffness (N/cm)	Ultimate Fail (lbs)	Max. Stress (MPa)
710.07	3.91	27.84	108.9	946.6	309	615.4
710.08	4.17	28.09	117.1	1037.8	357	619.6
710.09	4.27	28.30	120.8	1171.8	363	596.4
710.10	4.04	27.97	113.0	1020.8	315	584.9
710.11	3.94	27.64	108.9	829.2	333	657.9
Average	4.07	27.97	113.7	1001.2	335	615
Std Dev.	0.15	0.25	5.2	125.9	24	28

Three Point Bending Mechanical Testing (Round 2)

FP622 - VARTM D155 [0/+45/0]s   5 Hz sampling   6.5" specimen

0.5 in/min   Flex test #11

Sample No.	Thickness (mm)	Width (mm)	Area (mm^2)	Stiffness (N/cm)	Max. Load (lbs)	Max. Stress (MPa)
622.25	3.02	26.10	78.8	398.0	197	701.6
622.26	2.96	26.40	78.1	406.0	200.4	734.5
622.27	2.94	26.30	77.3	392.0	195	727.2
622.28	3.05	25.80	78.7	410.1	203	717.0
622.29	3.01	26.50	79.8	415.2	210	741.5
Average	3.00	26.22	78.5	404.3	201	724
Std Dev.	0.05	0.28	0.9	9.3	6	16

FP411 - RTM D155 [0/+45/0]s Radius

Sample No.	Thickness (mm)	Width (mm)	Area (mm^2)	Stiffness (N/cm)	Max. Load (lbs)	Max. Stress (MPa)
411.25	3.01	26.48	79.7	409.1	204	720.8
411.26	3.02	26.46	79.9	417.2	209	734.2
411.27	2.99	26.51	79.3	396.2	201	719.0
411.28	3.00	26.68	80.0	411.8	210	741.4
411.29	3.08	26.51	81.7	422.1	213	718.0
Average	3.02	26.53	80.1	411.3	207	727
Std Dev.	0.04	0.09	0.9	9.8	5	11

FP413 - RTM D155 [0/+45/0]s Spartan

Sample No.	Thickness (mm)	Width (mm)	Area (mm^2)	Stiffness (N/cm)	Max. Load (lbs)	Max. Stress (MPa)
413.25	2.96	26.31	77.9	378.0	191	702.4
413.26	3.00	26.36	79.1	387.9	187	668.2
413.27	3.08	25.78	79.4	393.1	198	686.3
413.28	3.21	25.59	82.1	426.3	205	659.1
413.29	2.99	26.31	78.7	395.9	164	591.1
Average	3.07	26.01	79.8	400.8	189	661
Std Dev.	0.10	0.38	1.6	17.3	18	43

FP704 - Hand Lay-up D155 [0/+45/0]s

Sample No.	Thickness (mm)	Width (mm)	Area (mm^2)	Stiffness (N/cm)	Max. Load (lbs)	Max. Stress (MPa)
704.25	3.36	25.88	87.0	487.0	239	693.4
704.26	3.31	25.90	85.7	477.8	232	693.1
704.27	3.31	26.09	86.4	480.8	240	711.8
704.28	3.42	25.97	88.8	499.0	250	697.7
704.29	3.54	25.89	91.7	533.3	265	692.4
Average	3.39	25.95	87.9	495.6	245	698
Std Dev.	0.10	0.09	2.4	22.6	13	8

Fatigue Mechanical Testing

[0/+45/0]s lay-up   R: -1   Specimen Size: 1" x 3.25"
D155 @ ±25000 psi   A130 @ ±20000 psi   6 Hz test cycling

FP622 - VARTM D155

Sample No	Test No.	Test Machine	Thickness (mm)	Width (mm)	Area (mm^2)	Max. Load (lbs)	Fatigue Cycles (cycles)
622.34	4342	8501	3.08	27.29	84.1	3257	46707
622.35	4352	8501	3.16	27.36	86.5	3350	88727
622.36	4347	8572	3.24	27.63	89.5	3469	95102
622.37	4344	8501	3.25	27.55	89.5	3470	70028
622.38	4349	8572	3.23	27.60	89.1	3454	232841
622.39	4346	8572	3.14	27.67	86.9	3367	161036
Average			3.18	27.52	87.6	3395	115740

FP619 - VARTM A130

Sample No	Test No.	Test Machine	Thickness (mm)	Width (mm)	Area (mm^2)	Max. Load (lbs)	Fatigue Cycles (cycles)
619.35	4354	8501	2.95	27.41	80.9	2507	470659
619.36	4358	8572	3.03	27.41	83.1	2575	255852
619.37	4355	8572	3.09	27.44	84.8	2628	235153
619.38	4360	8572	3.12	27.26	85.1	2637	364006
619.39	4363	8501	3.08	27.32	84.1	2609	189096
619.71	4364	8572	3.06	27.21	83.3	2581	166027
Average			3.06	27.34	83.5	2589	280132

FP702 - Hand Lay-up D155

Sample No	Test No.	Test Machine	Thickness (mm)	Width (mm)	Area (mm^2)	Max. Load (lbs)	Fatigue Cycles (cycles)
702.34	4343	8501	3.06	27.26	83.4	3232	62257
702.35	4345	8572	3.02	27.98	84.5	3274	364201
702.36	4350	8501	3.02	27.53	83.1	3222	105255
702.37	4353	8572	3.10	27.96	86.7	3359	70566
702.38	4348	8501	3.15	27.45	86.5	3351	95787
702.39	4351	8501	3.29	27.97	92.0	3566	141276
Average			3.11	27.69	86.0	3334	139890

FP705 - Hand Lay-up A130

Sample No	Test No.	Test Machine	Thickness (mm)	Width (mm)	Area (mm^2)	Max. Load (lbs)	Fatigue Cycles (cycles)
705.34	4357	8501	3.34	27.38	91.4	2835	47302
705.35	4365	8572	3.47	27.24	94.5	2930	48328
705.36	4362	8572	3.62	27.30	98.8	3064	123583
705.37	4356	8572	3.76	27.44	103.2	3198	48209
705.38	4359	8501	3.91	27.50	107.5	3333	11396
705.39	4361	8501	4.05	27.45	111.2	3446	28021
Average			3.69	27.39	101.1	3134	51140

FP705 - Hand Lay-up A130 (Round 2)

Sample No	Test No.	Test Machine	Thickness (mm)	Width (mm)	Area (mm^2)	Max. Load (lbs)	Fatigue Cycles (cycles)
705.40			3.51	24.54	86.1		612132
705.41			3.87	24.60	95.2		553304
705.42		8501	3.21	24.61	79.0	± 2317	632739
705.43			3.27	24.49	80.1		318823
705.44			3.72	24.58	91.4		228950
705.45			3.39	24.55	83.2		263763
Average			3.50	24.56	85.8		434952

510 x 810mm Flat Plate Testing
Transverse Tensile Stress and Strain Comparisons for D155 [0/±45/0]s Laminates

Legend: HL 704 — VARTM 622 — RTM-R 411 — RTM-S 413
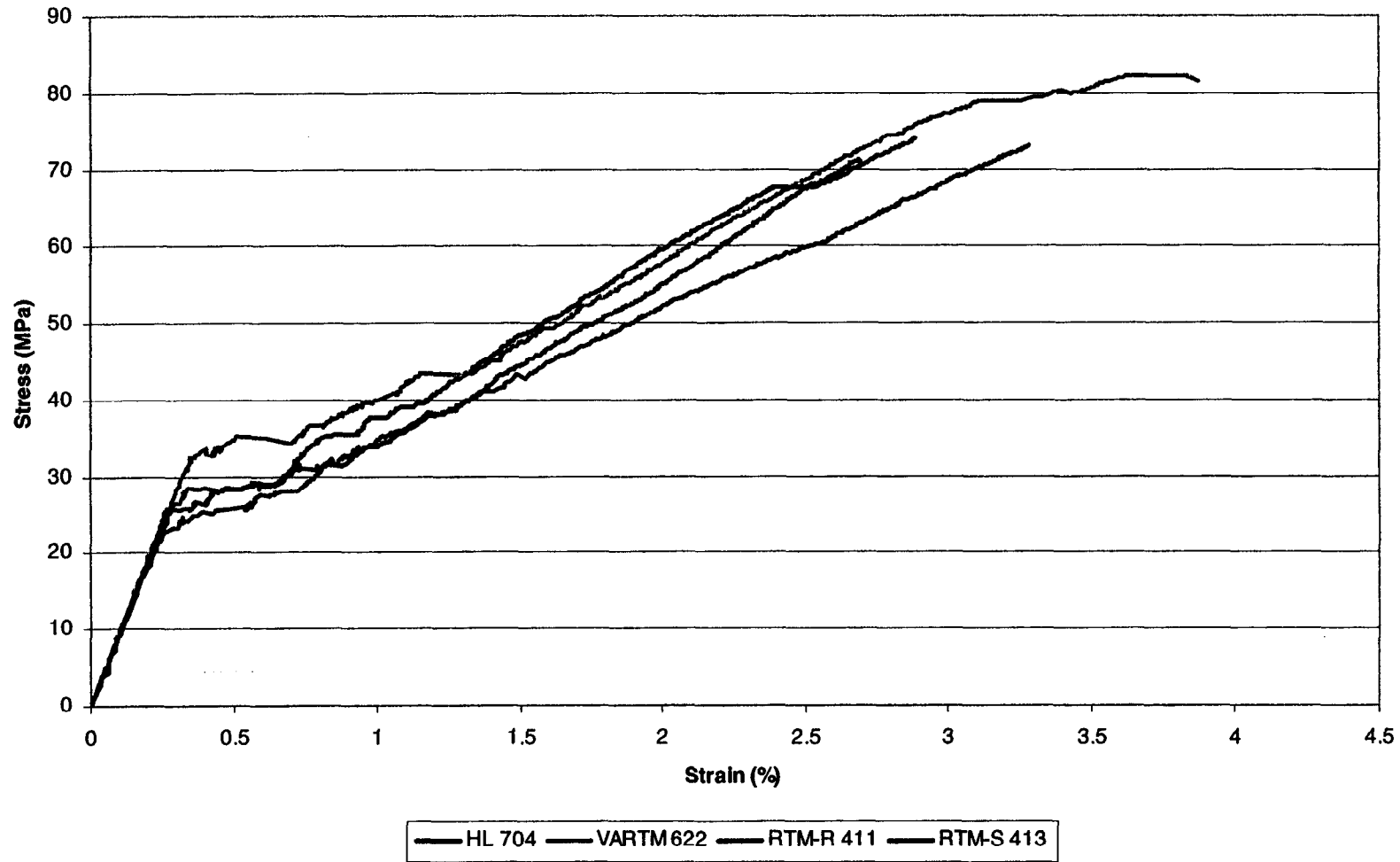
510 x 810mm Flat Plate Comparisons
Transverse Tensile Stress and Strain Comparisons
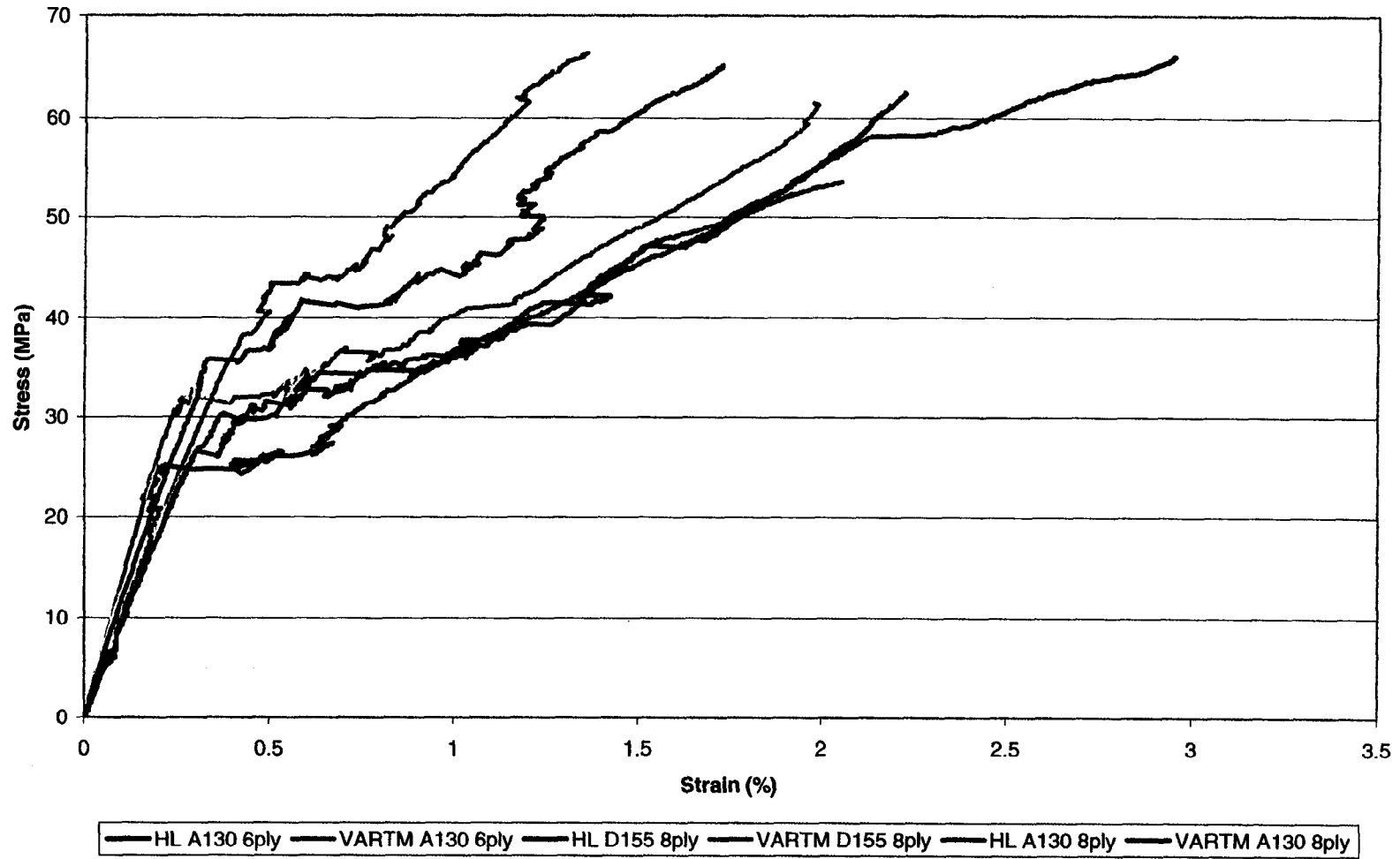
APPENDIX B

T-Stiffener Experimental Data and Results

Load

Loading
Grips →

Units in cm

9.8

Test fixture support
Dia. =1.92
Spacing =12.7

Radius = 0.18

15.9

Thin flanged T-stiffener testing jig [46]

Load

Loading
Grips →

Units in cm

11.5

Test fixture support
Dia. =1.92
Spacing =12.7

Radius =0.635

1.0

Flange

Skin

12.7
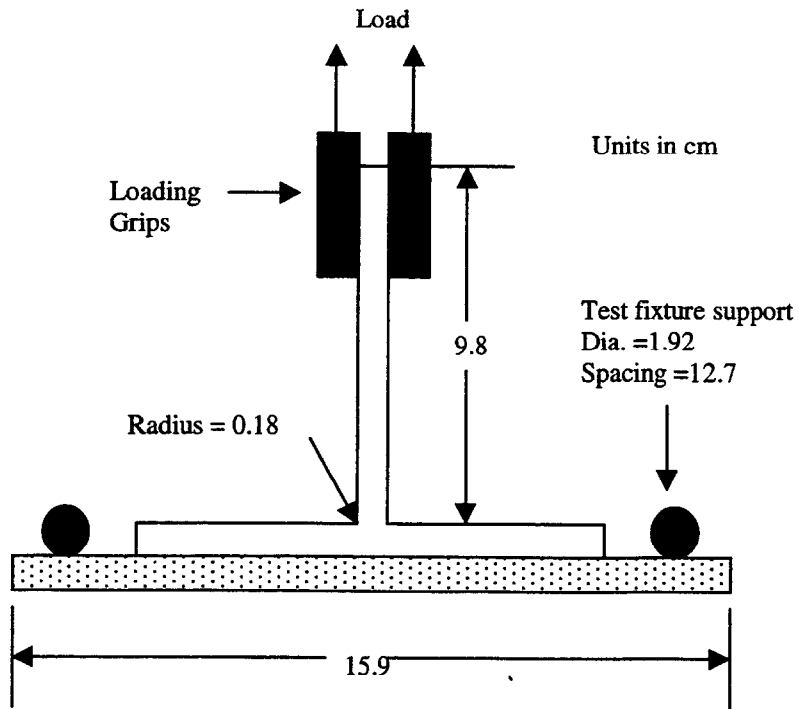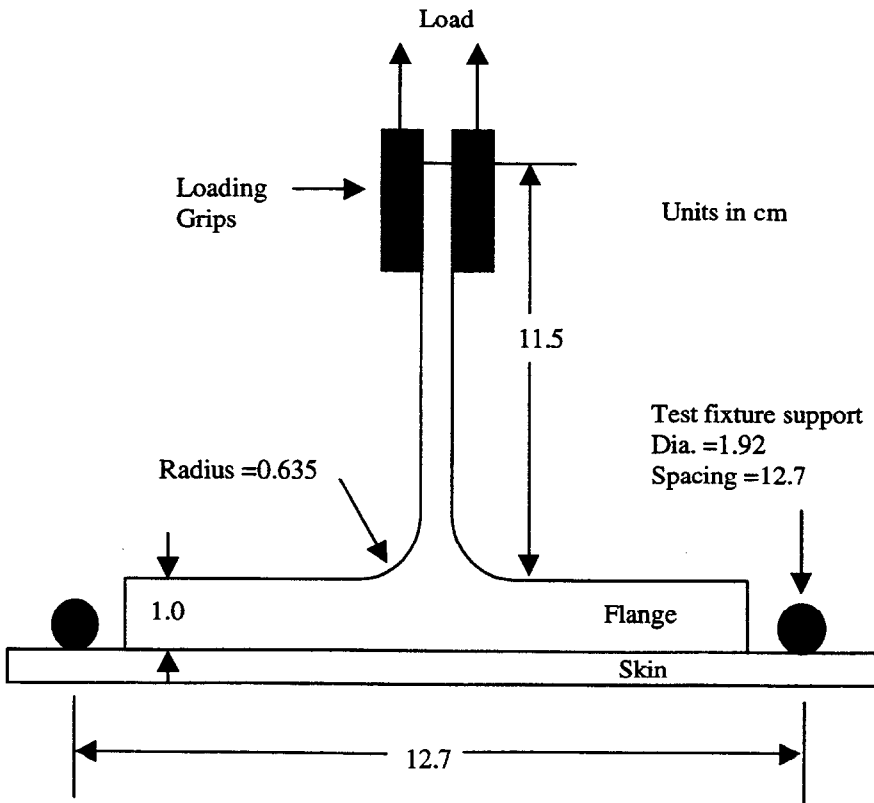
Thick flanged T-stiffener jig [46]

RTM Thin Flanged T-stiffeners
Dimensions and Testing

Tensile Test Method #18
0.5 in/min
5 points/sec (5 Hz) sampling
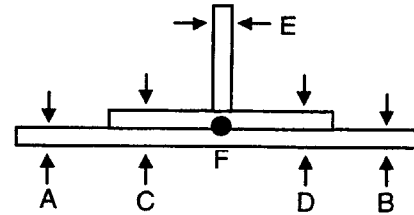
Sample 110 - RTM, D155/DB120 fabrics, Co-cured
Sample 114 - RTM, A130/DB120 fabrics, Co-cured
Sample 112 - RTM, D155/DB120 fabrics, Secondary bonded
Sample 116 - RTM, A130/DB120 fabrics, Secondary bonded

| Sample No. | Skin Thickness (mm) | | Skin & Flange Th. | | Web Th. | Sample Th. | Max. Load |
	A	B	C	D	E	F	(lbs)
110.01	4.03	4.07	5.57	5.54	4.75	29.58	94.1
110.02	4.08	4.03	5.51	5.56	4.72	29.01	94.8
110.03	4.07	3.94	5.44	5.43	4.71	33.80	106.2
110.04	4.04	3.94	5.53	5.43	4.73	29.97	98.5
110.05	4.00	4.05	5.53	5.47	4.73	30.09	98.9
110.06	4.07	4.03	5.51	5.49	4.72	29.53	97.4
114.01	3.15	3.08	4.62	4.64	4.73	30.78	76.6
114.02	3.19	3.06	4.62	4.62	4.69	31.60	80.3
114.03	3.17	3.07	4.62	4.60	4.73	29.50	72.2
114.04	3.17	3.05	4.62	4.58	4.70	30.29	75.5
114.05	3.19	3.06	4.62	4.58	4.69	29.76	75.3
114.06	3.15	3.07	4.65	4.64	4.71	31.45	80.3
112.01	3.61	3.45	5.14	5.28	4.79	30.50	79.8
112.02	3.62	3.51	5.33	5.34	4.73	29.95	84.5
112.03	3.62	3.46	5.25	5.26	4.75	29.91	87.3
112.04	3.64	3.52	5.26	5.26	4.74	30.30	93.6
112.05	3.61	3.45	5.19	5.25	4.75	29.09	95.1
112.06	3.62	3.46	5.11	5.22	4.78	29.32	86.7
116.01	3.42	3.18	4.89	5.07	4.70	29.66	84.5
116.02	3.25	3.46	5.06	5.02	4.70	29.52	84.4
116.03	3.16	3.37	4.90	4.88	4.70	30.80	82.0
116.04	3.26	3.47	5.23	5.09	4.72	29.48	85.0
116.05	3.29	3.46	5.01	5.11	4.72	30.42	84.8
116.06	3.20	3.40	4.89	4.96	4.70	30.11	83.7

Hand Lay-up Thin Flanged T-stiffeners
Dimensions and Testing

Tensile Test Method #18
0.5 in/min
5 points/sec (5 Hz) sampling
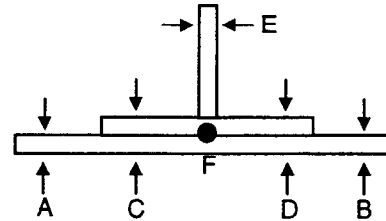
No. 301 - D155/DB120 fabrics, Co-cured   No. 305 - A130/DB120 fabrics, Sec. Bonded
No. 306 - A130/DB120 fabrics, Co-cured   No. 307 - D155/DB120 fabrics, Sec. Bonded(3)
No. 303 - D155/DB120 fabrics, Secondary Bonded

| Sample No. | Skin Thickness (mm) | | Skin & Flange Th. | | Web Th. | Sample Th. | Max. Load |
	A	B	C	D	E	F	(lbs)
301.01	4.62	4.61	6.37	6.06	4.20	31.40	76.5
301.02	4.45	4.53	5.94	6.37	4.25	28.84	75.7
301.03	4.59	4.64	6.06	6.38	4.26	29.97	70.9
301.04	4.57	4.62	6.04	6.41	4.32	29.96	78.1
301.05	4.49	4.53	5.91	6.30	4.23	30.63	77.9
301.06	4.47	4.38	5.88	6.27	4.30	30.03	73.4
306.01	3.72	3.72	5.25	5.25	4.75	30.56	95.8
306.02	3.70	3.71	5.22	5.25	4.75	29.36	90.0
306.03	3.72	3.75	5.25	5.25	4.79	29.95	95.6
306.04	3.71	3.71	5.25	5.27	4.75	30.74	100.1
306.05	3.74	3.74	5.28	5.28	4.73	31.05	104.9
306.06	3.73	3.74	5.25	5.26	4.72	28.82	92.8
303.01	4.30	4.44	7.95	7.78	4.83	29.06	100.3
303.02	4.33	4.41	8.04	7.81	4.82	29.73	112.6
303.03	4.34	4.46	7.41	7.67	4.82	28.98	104.8
303.04	4.34	4.41	7.66	7.58	4.88	30.66	107.2
303.05	4.51	4.54	8.04	7.82	4.89	29.62	104.1
303.06	4.37	4.29	7.69	7.96	4.84	29.19	106.6
305.01	5.13	5.00	7.78	7.95	4.75	31.38	92.2
305.02	5.25	4.91	7.75	7.95	4.73	30.70	95.6
305.03	5.00	4.85	8.06	7.88	4.72	30.26	95.9
305.04	5.09	4.80	7.89	7.88	4.74	30.84	101.2
305.05	5.14	5.03	7.98	8.12	4.72	30.26	98.5
305.06	5.27	5.05	7.83	7.86	4.75	28.86	89.4
307.01	4.47	5.51	7.76	7.76	5.40	30.32	136.6
307.02	4.56	4.49	7.58	7.64	5.15	29.59	132.5
307.03	4.36	4.58	5.56	7.50	5.43	32.85	150.9
307.04	4.69	4.35	7.50	7.40	5.38	29.92	131.2
307.05	4.45	4.44	7.51	7.49	5.32	29.38	121.6
307.06	4.60	4.33	7.60	7.42	5.32	29.98	128.7
307.07	4.53	4.48	7.53	7.52	5.22	29.98	129.0
307.08	4.25	4.34	7.72	7.64	5.36	29.73	136.3
307.09	4.25	4.34	7.53	7.65	5.34	31.60	134.8

Thin Flanged T-stiffener Tolerance Summaries

Lay-up	Fabric	Process	Bond Type	Location	Mean Thickness (mm)	Std. Dev. (mm)	Thickness	
							max (mm)	min (mm)
[±45/02/+45]s	D155 DB120	RTM	CC	Skin	4.03	0.050	4.08	3.94
				Web	4.73	0.010	4.75	4.71
			SB	Skin	3.55	0.080	3.64	3.45
				Web	4.76	0.020	4.79	4.73
		Hand Lay-up	CC	Skin	4.54	0.080	4.64	4.38
				Web	4.26	0.040	4.32	4.20
			SB	Skin	4.4	0.080	4.54	4.29
				Web	4.85	0.030	4.89	4.82
			SB(3)	Skin	4.42	0.140	4.69	4.25
				Web	5.32	0.090	5.38	5.22
	A130 DB120	RTM	CC	Skin	3.12	0.060	3.19	3.05
				Web	4.71	0.020	4.73	4.69
			SB	Skin	3.33	0.120	3.47	3.16
				Web	4.71	0.010	4.72	4.70
		Hand Lay-up	CC	Skin	3.72	0.020	3.75	3.70
				Web	4.75	0.020	4.79	4.72
			SB	Skin	5.04	0.150	5.27	4.80
				Web	4.74	0.010	4.75	4.72

Thin Flanged T-stiffener Fiber Volume Summaries

Lay-up	Fabric	Process	Bond Type	Location	Mean Vf (%)	Std. Dev. (%)	Fiber Volume	
							min (%)	max (%)
[±45/02/+45]s	D155 DB120	RTM	CC	Skin	35.19	0.47	34.70	36.08
				Web	30.41	0.05	30.32	30.48
			SB	Skin	40.82	1.08	39.57	42.16
				Web	30.30	0.09	30.18	30.40
		Hand Lay-up	CC	Skin	31.32	0.46	30.79	32.29
				Web	33.17	0.34	32.71	33.65
			SB	Skin	32.21	0.53	31.30	32.94
				Web	30.00	0.09	29.87	30.08
			SB(3)	Skin	31.52	0.84	29.78	32.64
				Web	N/A	-	-	-
	A130 DB120	RTM	CC	Skin	41.61	0.75	40.66	42.50
				Web	27.75	0.08	27.66	27.83
			SB	Skin	39.00	1.40	37.30	41.05
				Web	27.76	0.04	27.70	27.79
		Hand Lay-up	CC	Skin	34.64	0.15	34.39	34.88
				Web	27.59	0.10	27.43	27.70
			SB	Skin	26.71	0.35	26.27	27.39
				Web	27.64	0.06	27.58	27.7

RTM: Resin Transfer Molding
SB: Secondary bonded in two parts
SB(3): Secondary bonded in three parts
CC: Co-Cured

Note: data obtained from six samples in each case.

APPENDIX C

I-Beam and Root Specimen Experimental Data and Results

Root specimen manufacturing and testing data.

Current lay-up: Skin   [±45/02/±45]s
Surface [±45/0/±45/02/±45]s

Static Tensile Tests

Sample No.	Process	Zero Fabric	Lay-up Schedule	Notes on Manufacturing	Ultimate Load (kN)[1]	Comments
R101	RTM	A130	[±45/02/±45/02/±45]s	Poor wet out	243.7	insert pull-out
R102	RTM	A130	[±45/02/±45/02/±45]s ply drops	Poor wet out	213.5	composite failure
R103		D155		Low Vf about insert	241.0	insert pull-out
R201	VARTM	D155	[±45/0/±45/02/±45]s ply drops	Low Vf about insert	230.5	good bonding w/ insert
R104	RTM	D155	[±45/0/±45/02/±45]s ply drops	Low Vf / Super 77 / 3"-12"	240.2	
R106				9"-12" strips	197.9	composite failure
R107				Spartan / wash-out / 9"-12"	239.8	
R108				9"-12" strips	177.1	
R109			Current w/ skin: [±45/03/±45]s	Spartan / High Vf at insert	254.0	two tests / bolt failure / yield
R110			Current	Spartan	252.3	bolt failure / no insert yield
R301	HL	D155	[±45/0/±45/02/±45]s ply drops	No insert tip / 9"-12"	213.4	composite failure
R303				9"-12" strips	181.3	

Fatigue Tests

Sample No.	Process	Fabric	Lay-up Schedule	Notes on Manufacturing	Fatigue cycles (cycles)	Comments
R105[2]	RTM	D155	[±45/0/±45/02/±45]s ply drops	Low Vf / 3"-12" strips		
R111[2]						
R112					535.2	R: 0.1, 20/2k, no damage
R113[2]			Current			
R114[2]						
R115[2]						
R116[2]						
R302*	HL	D155	[±45/0/±45/02/±45]s ply drops	9"-12" strips		

[1] -98 kN is the root specimen design limit load.

[2] -Manufactured but not tested

APPENDIX D

Statistical Comparison Results

Transverse tension results statistical differences.

Laminate Mechanical Property	Lay-up	Zero Degree Fabric	Processes	Normality (P value)	Equal Variance (P value)	Statistical Comparison Method (P value)	Statistical Difference
Ultimate Transverse Tensile Strength	[0/±45/0]s	D155	HL / V	pass (0.353)	fail (0.0003)	ANOVA on Ranks (<0.05)	Yes
			HL / RR	pass (0.353)	fail (0.0003)	ANOVA on Ranks (<0.05)	Yes
			HL / RS	pass (0.353)	fail (0.0003)	ANOVA on Ranks (<0.05)	No
			V / RR	pass (0.715)	fail (0.0009)	t-test (0.467)	No
			V / RS	pass (0.353)	fail (0.0003)	ANOVA on Ranks (<0.05)	No
			RR / RS	pass (0.186)	pass (0.830)	t-test (0.698)	No
		A130	HL / V	pass (0.126)	pass (0.163)	t-test (<0.0001)	Yes
	[0/0/±45/0]s	D155	HL / V	pass (0.329)	pass (0.252)	t-test (<0.0001)	Yes
		A130	HL / V	pass (0.287)	pass (0.480)	t-test (0.0002)	Yes
Normalized Transverse Tensile Strength	[0/±45/0]s	D155	HL / V	pass (0.881)	fail (0.0036)	ANOVA on Ranks (0.164)	No
			HL / RR				
			HL / RS				
			V / RR				
			V / RS				
			RR / RS				
		A130	HL / V	pass (0.594)	pass (0.721)	t-test (<0.0001)	Yes
	[0/0/±45/0]s	D155	HL / V	pass (0.255)	pass (0.365)	t-test (0.158)	No
		A130	HL / V	pass (0.235)	pass (0.454)	t-test (0.401)	No
Transverse Tensile Modulus	[0/±45/0]s	D155	HL / V	pass (0.551)	pass (0.451)	1-Way ANOVA (0.105)	Yes
			HL / RR	pass (0.559)	pass (0.332)	t-test (0.185)	No
			HL / RS	pass (0.726)	pass (0.270)	t-test (0.242)	No
			V / RR	pass (0.551)	pass (0.451)	1-Way ANOVA (0.105)	No
			V / RS	pass (0.551)	pass (0.451)	1-Way ANOVA (0.105)	Yes
			RR / RS	pass (0.551)	pass (0.451)	1-Way ANOVA (0.105)	No
		A130	HL / V	pass (0.106)	pass (0.293)	t-test (0.363)	No
	[0/0/±45/0]s	D155	HL / V	pass (0.294)	pass (0.543)	t-test (<0.0001)	Yes
		A130	HL / V	pass (0.058)	pass (0.302)	t-test (<0.0001)	Yes

HL - Hand Lay-up
RR - Radius RTM
V - VARTM
RS - Spartan RTM

Transverse tension results statistical differences.

Laminate Mechanical Property	Lay-up	Zero Degree Fabric	Processes	Normality (P value)	Equal Variance (P value)	Statistical Comparison Method (P value)	Statistical Difference
Transverse Tensile Strain at Initial Damage	[0/±45/0]s	D155	HL / V	fail (0.028)	--	ANOVA on Ranks (<0.05)	Yes
			HL / RR	fail (0.028)	--	ANOVA on Ranks (<0.05)	Yes
			HL / RS	fail (0.028)	--	ANOVA on Ranks (<0.05)	No
			V / RR	fail (0.0002)	--	M-W Rank Sum(0.001)	Yes
			V / RS	fail (0.028)	--	ANOVA on Ranks (<0.05)	No
			RR / RS	pass (.113)	pass (.471)	t-test (0.843)	No
		A130	HL / V	pass (0.338)	pass (0.316)	t-test (0.137)	No
	[0/0/±45/0]s	D155	HL / V	pass (0.308)	pass (1.0)	t-test (1.0)	No
		A130	HL / V	pass (0.556)	pass (0.871)	t-test (0.019)	Yes
Transverse Tensile Strain to Failure	[0/±45/0]s	D155	HL / V	pass (0.231)	pass (0.682)	1-Way ANOVA (0.003)	Yes
			HL / RR				No
			HL / RS				Yes
			V / RR				Yes
			V / RS				No
			RR / RS				Yes

HL - Hand Lay-up   V- VARTM

RR - Radius RTM   RS - Spartan RTM

Compression and Bending test results statistical differences.

Laminate Mechanical Property	Lay-up	Zero Degree Fabric	Processes	Normality (P value)	Equal Variance (P value)	Statistical Comparison Method (P value)	Statistical Difference
Ultimate Compressive Strength	[0/±45/0]s	D155	HL / V	pass (0.650)	pass (0.475)	1-Way ANOVA (<0.05)	Yes
			HL / RR	pass (0.736)	pass (0.588)	t-test (0.663)	No
			HL / RS	pass (0.650)	pass (0.475)	1-Way ANOVA (<0.05)	No
			V / RR	pass (0.650)	pass (0.475)	1-Way ANOVA (<0.05)	Yes
			V / RS	pass (0.650)	pass (0.475)	1-Way ANOVA (<0.05)	Yes
			RR / RS	pass (0.121)	pass (0.559)	t-test (0.380)	No
		A130	HL / V	pass (0.459)	pass (0.506)	t-test (0.005)	Yes
	[0/0/±45/0]s	D155	HL / V	pass (0.882)	pass (0.237)	t-test (<0.001)	Yes
		A130	HL / V	pass (0.558)	pass (0.956)	t-test (0.087)	No
Normalized Ultimate Compressive Strength	[0/±45/0]s	D155	HL / V	pass (0.136)	pass (0.228)	1-Way ANOVA (<0.001)	No
			HL / RR	pass (0.136)	pass (0.228)	1-Way ANOVA (<0.001)	Yes
			HL / RS	pass (0.136)	pass (0.228)	1-Way ANOVA (<0.001)	Yes
			V / RR	pass (0.136)	pass (0.228)	1-Way ANOVA (<0.001)	Yes
			V / RS	pass (0.136)	pass (0.228)	1-Way ANOVA (<0.001)	Yes
			RR / RS	pass (0.136)	pass (0.228)	1-Way ANOVA (<0.001)	No
		A130	HL / V	pass (0.235)	pass (0.466)	t-test (0.360)	No
	[0/0/±45/0]s	D155	HL / V	pass (0.618)	pass (0.620)	t-test (<0.005)	Yes
		A130	HL / V	pass (0.448)	pass (0.533)	t-test (0.007)	Yes
Bending Strength	[0/±45/0]s	D155	HL / V	fail (<0.0001)	--	ANOVA on Ranks (0.137)	No
			HL / RR	fail (<0.0001)	--	ANOVA on Ranks (0.137)	No
			HL / RS	fail (<0.0001)	--	ANOVA on Ranks (0.137)	No
			V / RR	fail (<0.0001)	--	ANOVA on Ranks (0.137)	No
			V / RS	fail (<0.0001)	--	ANOVA on Ranks (0.137)	No
			RR / RS	fail (<0.0001)	--	ANOVA on Ranks (0.137)	No
		A130	HL / V	pass (0.75)	pass (0.55)	t-test (0.73)	No
	[0/0/±45/0]s	D155	HL / V	pass (0.38)	pass (0.85)	t-test (<0.001)	Yes
		A130	HL / V	pass (0.81)	pass (0.42)	t-test (0.35)	No

Tension and fatigue test results statistical differences.

Laminate Mechanical Property	Lay-up	Zero Degree Fabric	Processes	Normality (P value)	Equal Variance (P value)	Statistical Comparison Method (P value)	Statistical Difference
Tensile Strength	[0/±45/0]s	D155	HL / V	fail (0.002)	--	M-W Rank Sum (1.0)	No
		A130	HL / V	fail (0.02)	--	M-W Rank Sum (0.95)	No
	[0/0/±45/0]s	D155	HL / V	pass (0.51)	pass (0.63)	T-test (<0.001)	Yes
		A130	HL / V	pass (0.18)	pass (0.86)	T-test (<0.001)	Yes
Normalized Ultimate Tensile Strength	[0/±45/0]s	D155	HL / V	fail (<0.001)	--	M-W Rank Sum (0.27)	No
		A130	HL / V	pass (0.10)	fail (0.01)	M-W Rank Sum (0.095)	No
	[0/0/±45/0]s	D155	HL / V	pass (0.17)	pass (0.18)	T-test (0.7)	No
		A130	HL / V	pass (0.11)	pass (0.24)	T-test (0.03)	Yes
Tensile Modulus	[0/±45/0]s	D155	HL / V	fail (<0.001)	--	M-W Rank Sum (0.34)	No
		A130	HL / V	pass (0.30)	pass (0.57)	T-test (0.2)	No
	[0/0/±45/0]s	D155	HL / V	pass (0.50)	pass (0.44)	T-test (<0.001)	Yes
		A130	HL / V	pass (0.52)	fail (0.04)	M-W Rank Sum (0.008)	Yes
Tensile Initial Damage	[0/±45/0]s	D155	HL / V	fail (<0.001)	--	M-W Rank Sum (0.43)	No
		A130	HL / V	pass (0.72)	pass (0.09)	T-test (0.85)	No
	[0/0/±45/0]s	D155	HL / V	pass (0.27)	pass (0.05)	T-test (0.50)	No
		A130	HL / V	fail (0.04)	--	M-W Rank Sum (0.55)	No
Fatigue	[0/±45/0]s	D155	HL / V	fail (0.03)	--	M-W Rank Sum (0.7)	No
		A130	HL / V	fail (0.02)	--	M-W Rank Sum (0.02)	Yes
		A130	HL / V	pass (0.61)	pass (0.05)	T-test (0.11)	No

APPENDIX E

Fiber Volume and Fabrication Time Records

Flat Plate Fiber Volume Data

D155 / DB120 [0/45/0]s		A130/ DB120 [0/45/0]s		D155 / DB120 [0/0/45/0]s		A130 / DB120 [0/0/45/0]s	
thickness (mm)	Vf (%)	thickness (mm)	Vf (%)	thickness (mm)	Vf (%)	thickness (mm)	Vf (%)
1.73	62	2.95	33.4	3.13	50.5	3.13	42.6
1.89	56.8	3.3	30.7	3.21	50.1	3.45	40.3
1.92	55.4	3.4	30	3.32	47.9	3.97	34.5
1.99	53.7	3.79	27	4.62	35	4.59	29.9
2.1	52.5	4.19	24.6	4.8	33.2	5.13	26.9
2.11	52.3			5.29	30.1		
2.31	48.9			5.9	27.6		
2.44	46.2						
2.67	42.9						
2.74	42.1						
2.79	41.1						
2.91	37.7						
3.03	36.5						
3.07	36						
3.09	36						
3.56	31.4						
3.58	31.7						
3.59	31						
3.86	28.8						
4	27.8						

Fiber volume calculations data

Sample No.	Part	Fabric	Location	Lay-up	Width	Thickness	Length	Vol(cm^3)	Fiber wt. (after burn)	Fiber Vol. (cm^3)	% Vf
LTA.1	Little T	A130	SKIN	[+-45/02/+-45]s	35.00	3.00	60.28	6.33	7.00	2.73	43.20
LTA.2			WEB		36.61	4.67	62.00	10.60	7.60	2.97	28.01
LTA.3			WEB		35.71	4.78	42.60	7.27	5.10	1.99	27.40
LTD.1		D155	SKIN		34.51	3.55	56.43	6.91	7.20	2.81	40.68
LTD.2			SKIN		32.51	4.44	59.23	8.55	6.90	2.70	31.53
LTD.3			WEB		32.30	4.80	59.90	9.29	7.20	2.81	30.28
IWD.1	I-Beam	D155	WEB	[+-45/0/+-45]s	28.18	3.41	56.78	5.46	4.20	1.64	30.07
IWD.2					26.16	3.28	60.13	5.16	3.90	1.52	29.53
IWU.1		U1018			28.05	3.21	54.95	4.95	4.10	1.60	32.37
IWU.2					27.98	3.10	52.10	4.52	3.90	1.52	33.71
IWA.1		A130			27.75	3.47	54.50	5.25	3.60	1.41	26.80
IWA.2					28.26	3.32	57.56	5.40	3.90	1.52	28.21
IFD.1		D155	FLANGE	[0/+-45/0]s	19.71	5.80	53.15	6.08	4.40	1.72	28.29
IFD.2					19.95	4.50	52.40	4.70	4.30	1.68	35.71
IFD.3					19.81	4.05	53.30	4.28	4.40	1.72	40.19
IFU.1		U1018			20.00	5.04	52.70	5.31	4.80	1.88	35.30
IFU.2					20.70	4.80	52.41	5.21	4.80	1.88	36.01
IFU.3					19.82	4.25	59.08	4.98	5.40	2.11	42.39
IFA.1		A130			21.10	4.30	61.26	5.56	4.90	1.91	34.44
IFA.2					19.60	4.90	57.81	5.55	4.10	1.60	28.85
R301	Root 1	D155	GRIP		32.80	9.30	43.48	13.26	9.70	3.79	28.57
R201A					27.62	10.62	45.49	13.34	9.00	3.52	26.35
R201B					33.35	11.09	43.84	16.21	10.50	4.10	25.30
IWD.3	I-Beam	D155	WEB	[+-45/0/+-45]s		3.28					29.50
IWD.4						3.36					29.1
IWD.5						3.28					29.5
R112A	Root 2	D155	GRIP			10.52					33.7
R112B						11.47					31.26

Note: Dimensions in mm unless stated otherwise.

221

I-Beam Composite Fiber Volumes
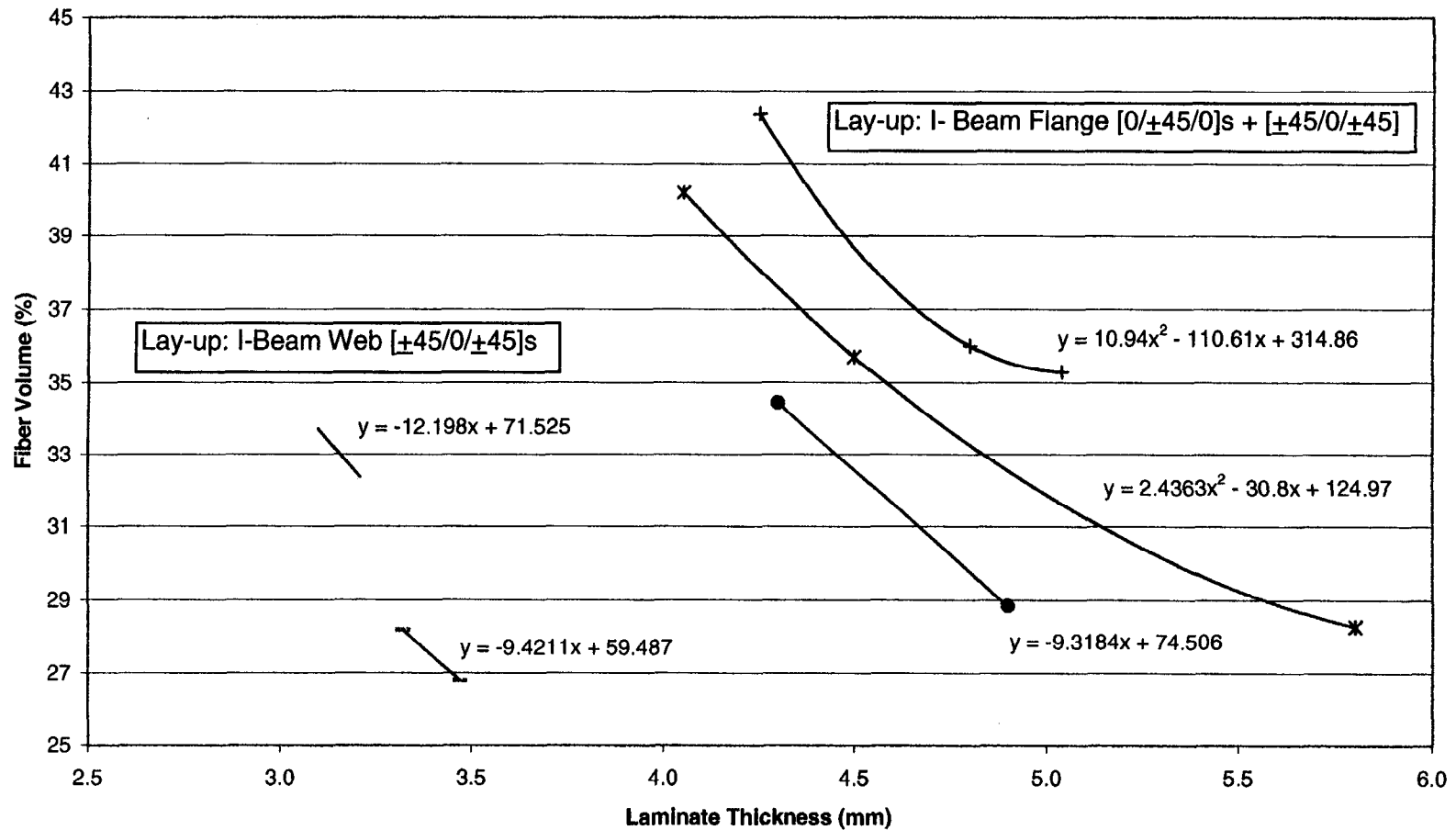
Thin Flanged T-Stiffener and Root Composite Fiber Volumes

$y = 2.8158x^2 - 30.741x + 110.07$

$y = 4.0754x^2 - 42.524x + 140.36$

T-stiffener web and skins: [±45/02/±45]s

Root 2: [±45/0/±45/02/±45]s + [±45/02/±45]s

$y = -2.5684x + 60.72$

$y = 0.4489x^2 - 10.893x + 91.013$

Root 1: [±45/0/±45/0/±45]s + [±45/0/±45]s

Fiber Volume (%)

Laminate Thickness (mm)

◆ Thin T - D155 ■ Thin T - A130 ∴ Root 1 ✕ Root 2
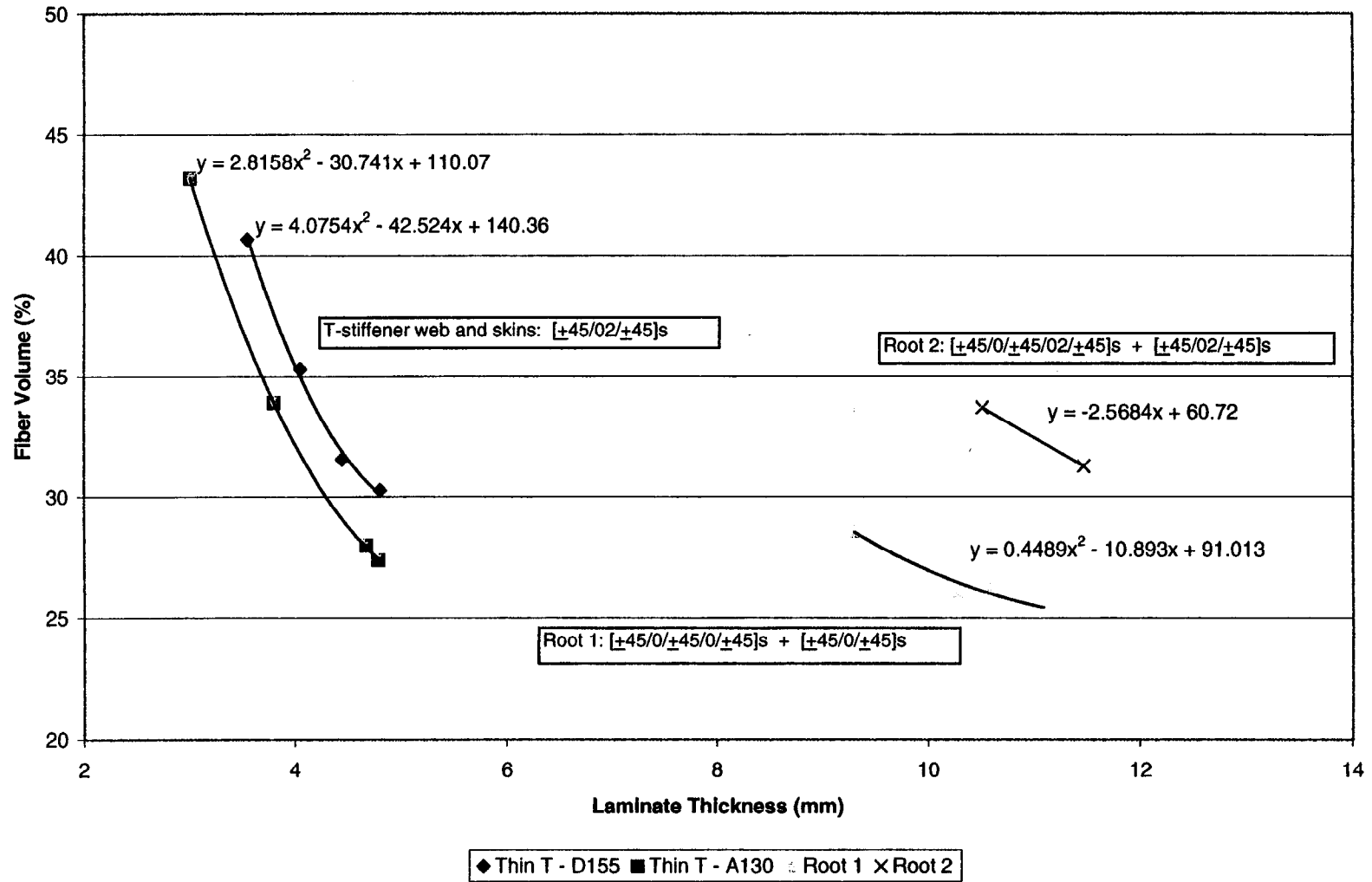
510 x 810 mm [0/+45/0]s Flat Plate Fabrication Time

Resin volume: 1250 - 1650 mL   Pour and mix resin: 4 min

Hand Lay-up	
Fabric cutting	9 min
Wet lay-up	44 min
Clean up	10 min
Part removal	5 min
Mold cleaning	15 min
Fabrication Time	83 min

RTM	
Fabric cutting	9 min
Fabric lay-up	7 min
Injection preparation*	22 min
Resin injection	8 - 30 min
Clean up	12 min
Part removal	7 min
Mold cleaning	14 min
Fabrication Time (R)	79 - 101 min
Fabrication Time (S)	62 - 84 min

* Injection preparation times averaged 5 minutes for Spartan RTM machine.

510 x 810 mm [0/0/+45/0]s Flat Plate Fabrication Time

Resin volume: 1050 - 1350 mL

Hand Lay-up	
Fabric cutting	12 min
Wet lay-up	57 min
Clean up	10 min
Part removal	5 min
Mold cleaning	15 min
Fabrication Time	99 min

RTM	
Fabric cutting	12 min
Fabric lay-up	8 min
Injection preparation*	22 min
Resin injection	12 - 22 min
Clean up	12 min
Part removal	7 min
Mold cleaning	14 min
Fabrication Time (R)	83 - 93 min
Fabrication Time (S)	66 - 76 min

Thin Flanged T-Stiffener Fabrication Time

Resin volume: 550 - 700 mL

Hand Lay-up	
Fabric cutting	13 min
Web lay-ups	19 min
Skin lay-up	5 min
Clean up	10 min
Part removal	10 min
Mold cleaning	31 min
Secondary bonding	28 min
Fabrication Time	116 min

RTM	
Fabric cutting	13 min
Fabric lay-up	12 min
Injection preparation*	21 min
Resin injection	5 - 12 min
Clean up	12 min
Part removal	12 min
Mold cleaning	8 min
Fabrication Time (R)	83 - 90 min
Fabrication Time (S)	67 - 74 min

Thick Flanged T-Stiffener Fabrication Time
Resin volume: 950 - 1350 mL

Hand Lay-up	
Fabric cutting	24 min
Web lay-ups	21 min
Flange lay-up	18 min
Skin lay-up	6 min
Clean up	10 min
Part removal	14 min
Mold cleaning	30 min
Secondary bonding	41 min
Fabrication Time	164 min

RTM	
Fabric cutting	24 min
Fabric lay-up	20 min
Injection preparation*	23 min
Resin injection	8 - 29 min
Clean up	12 min
Part removal	15 min
Mold cleaning	10 min
Fabrication Time (R)	112 - 133 min
Fabrication Time (S)	94 - 115 min

I-beam Fabrication Time
Resin volume: 750 - 1000 mL

Hand Lay-up	
Fabric cutting	15 min
Web lay-ups	30 min
Flange lay-ups	8 min
Clean up	10 min
Part removal	18 min
Mold cleaning	20 min
Secondary bonding	74 min
Fabrication Time	175 min

RTM	
Fabric cutting	15 min
Fabric lay-up	30 min
Injection preparation*	23 min
Resin injection	9 - 21 min
Clean up	12 min
Part removal	19 min
Mold cleaning	18 min
Fabrication Time (R)	126 - 138 min
Fabrication Time (S)	108 - 120 min

Root Insert Fabrication Time
Resin volume: 1750 - 2000 mL

Hand Lay-up	
Fabric cutting	34 min
Wet lay-up	60 - 80 min
Clean up	10 min
Part removal	11 min
Mold cleaning	8 min
Fabrication Time	123 - 143 min

RTM	
Fabric cutting	34 min
Fabric lay-up	25 min
Injection preparation*	21 min
Resin injection	15 - 30 min
Clean up	12 min
Part removal	10 min
Mold cleaning	10 min
Fabrication Time (R)	127 - 142 min
Fabrication Time (S)	111 - 126 min

225

DISTRIBUTION

T. Almeida
TPI Inc.
225 Alexander Road
Portsmouth RI 02871

H. Ashley
Dept. of Aeronautics & Astro Mech. Engr.
Stanford University
Stanford CA 94305

C. P. Butterfield
NREL
1617 Cole Boulevard
Golden CO 80401

G. Bywaters
Northern Power Technology Co.
Box 999
Waitsfield VT 05673

J. Cadogan
US Dept. of Energy, EE-12
Office of Geothermal & Wind Technology
1000 Independence Avenue SW
Washington DC 20585

D. Cairns
Montana State University
Mechanical & Industrial Engineering Dept.
Bozeman MT 59717

S. Calvert
US Department of Energy, EE-12
Office of Geothermal & Wind Technology
1000 Independence Avenue SW
Washington DC 20585

J. Chapman
OEM Development Corp.
840 Summer St.
Boston MA 02127-1533

R. N. Clark
USDA
Agricultural Research Service
PO Drawer 10
Bushland TX 79012

J. Cohen
Princeton Economic Research Inc.
1700 Rockville Pike
Suite 550
Rockville MD 20852

C. Coleman
Northern Power Technology Co.
PO Box 999
Waitsfield VT 05673

K. J. Deering
The Wind Turbine Company
515 116th Avenue NE
No. 263
Bellevue WA 98004

A. J. Eggers Jr.
RANN Inc.
744 San Antonio Road
Suite 26
Palo Alto CA 94303

P. R. Goldman, Director
Office of Geothermal & Wind Technology
US Department of Energy, EE-12
1000 Independence Avenue SW
Washington DC 20585

C. Hansen
Windward Engineering
4661 Holly Lane
Salt Lake City UT 84117

C. Hiel
W. Brandt Goldsworthy & assoc.
23930-40 Madison Street
Torrance CA 90505

S. Hock
Wind Energy Program
NREL
1617 Cole Boulevard
Golden CO 80401

K. Jackson
Dynamic Design
123 C Street
Davis CA 5616

G. James
University of Houston
Dept. of Mechanical Engineering
4800 Calhoun
Houston TX 77204-4792

M. Kramer
Foam Matrix Inc.
PO Box 6394
Malibu CA 90264

D. Malcolm
Global Energy Concepts, LLC
5729 Lakeview Drive NE
Suite 100
Kirkland WA 98033

J. F. Mandell
Montana State University
Chemical Engineering Department
302 Cableigh Hall
Bozeman MT 59717

T. McCoy
Global Energy Concepts, LLC
5729 Lakeview Drive NE
Suite100
Kirkland WA 98033

P. Migliore
NREL
1617 Cole Boulevard
Golden CO 80401

W. Musial
NREL
1617 Cole Boulevard
Golden CO 80401

NWTC Library   (5)
NREL
1617 Cole Boulevard
Golden CO 80401

V. Nelson
Alternative Energy Institute
West Texas A&M University
WT Box 60248
Canyon TX 79016

G. Nix
NREL
1617 Cole Boulevard
Golden CO 80401

L. Pratsch
Office of Geothermal & Wind Technology
US Department of Energy, EE-12
1000 Independence Avenue SW
Washington DC 20585

D. Sanchez
US Department of Energy
Albuquerque Operations Office
PO Box 5400
Albuquerque NM 87185

L. Schienbein
CWT Technologies Inc.
4006 S. Morain Loop
Kennewick WA 99337

R. Sherwin
Atlantic Orient
PO Box 1097
Norwich VT 05055

Brian Smith
NREL
1617 Cole Boulevard
Golden CO 80401

K. Starcher
AEI
West Texas State University
WT PO Box 60248
Canyon TX 79016

F. S. Stoddard
Dynamic Design
PO Box 1373
Amherst MA 01004

A. Swift
Dept. of Mech. & Industrial Engineering
University of Texas at El Paso
El Paso TX 79968

R. W. Thresher
NREL
1617 Cole Boulevard
Golden CO 80401

W. A. Vachon
W. A. Vachon & Associates
PO Box 149
Manchester MA 01944

B. Vick
USDA
Agricultural Research Service
PO Drawer 10
Bushland TX 79012

L. Wendell
2328 Enterprise Drive
Richland WA 99352

S. R. Winterstein
Civil Engineering Department
Stanford University
Stanford CA 94305

M. Zuteck
MDZ Consulting
931 Grove Street
Kemah TX 77565

MS 0555	B. Hansche, 9122
MS 0557	T. J. Baca, 9125
MS 0557	T. G. Carne, 9124
MS 0708	H. M. Dodd, 6214 (25)
MS 0708	T. D. Ashwill, 6214 (10)
MS 0708	D. E. Berg, 6214
MS 0708	P. L. Jones, 6214
MS 0708	D. L. Laird, 6214
MS 0708	M. A. Rumsey, 6214
NS 0708	H. J. Sutherland, 6214
MS 0708	P. S. Veers, 6214
MS 0835	W. Wolfe, 9111
MS 0847	D. W. Lobitz, 9125
MS 0847	D. R. Martinez, 9124
MS 0847	K. E. Metzinger, 9133
MS 0958	T. R. Guess, 1472
MS 0958	M. Donnelly, 1472
MS 9018	Central Technical Files, 8940-2
MS 0899	Technical Library, 9616 (2)
MS 0612	Review & Approval Desk, 9612, for DOE/OSTI